Ageing, driving and effective temperatures: from "soft rheology" to glassy dynamics

Suzanne Fielding

Doctor of Philosophy
University of Edinburgh
2000

To my family

Acknowledgements

First thanks must go to my supervisor, Peter Sollich, for his constant flow of useful suggestions, his unflagging moral support, and his endless good humour in the face of my confused ramblings. Many thanks also to Martin Evans for supervising the "spin chain" work once Peter had left Edinburgh, and for providing much needed words of encouragement at the "writing-up" stage. Thanks are also due to Mike Cates for his significant contribution to the development of the SGR model (before my arrival in Edinburgh), for organising a superb "glassy rheology" summer school during the second year of my PhD, for many interesting discussions, for his comments on the final script of the thesis, and for his generosity in the Old Bell.

Further from home, I'm very grateful to Tom McLeish for supervising the "dynamic dilution" work, and for his hospitality during an enjoyable week spent at the polymer IRC in Leeds. I'm also grateful to Armand Ajdari, Caroline Derec, Mike Evans, Matthias Fuchs, David Head, François Lequeux, Ignacio Pagonabarraga, George Petikidis and Peter Pusey for interesting discussions.

Particularly heartfelt thanks to everyone who helped initiate me into the joys of trying to get a computer to do anything remotely resembling what you want it to do: Richard Blythe, Andy Jackson, Viv Kendon, Liz McIvor, and Owen O'Loan to name but a few of those I've pestered. I'd also like to take this opportunity to thank my undergraduate tutor, John Chalker, and my school Physics teacher, Peter Sudlow – without their superb teaching and endlessly patient encouragement over past few years I'd never have embarked on this PhD.

Finally, and of course most importantly, thanks to all my friends (in Edinburgh and elsewhere), and to my family, for (amongst everything else) their unfailing ability to make those "bad PhD moments" seem not so bad after all.

Abstract

This thesis studies non-equilibrium dynamics in disordered "glassy" systems, focusing particularly on the response of such systems to external driving and loading. Its primary motivation is a body of experimental data suggesting that glassy dynamics underlie the mechanical properties (rheology) of a wide variety of disordered soft materials (*e.g.* foams, dense emulsions and dense colloidal suspensions): typically, such materials show pronounced non-linearity in their stress response to slow steady shear (often with a yield stress in the limit of zero shear) and a loss modulus which curves upwards slightly at low frequencies (in apparent violation of linear response theory). In what follows, we show that two very simple models of glassy dynamics – a trap model, and a kinetically constrained spin chain – can, when rheologically driven, broadly capture this behaviour. We also show that they predict *ageing* at small loads, in qualitative agreement with the results of recent ageing experiments. Beyond this rheological motivation, we also use the models to study more general concepts of glassy dynamics, such as the use of fluctuation-dissipation theorems (FDTs) for defining effective non-equilibrium temperatures.

As a preliminary step, we extend the existing rheological formalism to include ageing materials in which time-translational invariance (TTI) is lost. Within this generalized framework, we then analyze the rheologically driven trap model – the "soft glassy rheology" (SGR) model – which considers an ensemble of elastic elements undergoing activated local yielding dynamics, with distributed yield thresholds, governed by a noise temperature x. (Between yields, each element follows affinely the applied shear.) We review the model's exact constitutive solution and discuss its mapping, in the undriven limit, to Bouchaud's trap model. We exploit this mapping to demonstrate the existence (in linear rheology at least) of an ageing glass phase ($x < 1$), in which the relaxation time is always of order the sample age.

We then use this solution to study the model's strain-controlled rheology. For $x < 1$, the linear spectra depend on frequency *times* the system's age. The loss modulus rises as frequency is lowered, explaining the apparent experimental violation of linear response

theory. The linear stress relaxation function decays on a time-scale of order the system's age. The oscillatory and step response functions are related by Fourier transform (a result which is not automatic for non-TTI systems). For $x > 1$, true ageing is lost, but for $x \gtrsim 1$ we see "long transients" during the approach to equilibrium. In equilibrium, the linear spectra are weak power laws of frequency.

Under shear start-up we find (for $x < 1$) an age-dependent stress overshoot, after which the stress falls to an age-*independent* value: steady shear *interrupts* ageing, and restores a steady state with a relaxation time-scale set by the inverse shear rate. The flow curve is $\sigma(\dot{\gamma}) - \sigma_y \propto \dot{\gamma}^{1-x}$, (where σ is stress and $\dot{\gamma}$ strain rate) with a yield stress σ_y in the limit of zero shear. In contrast, for $1 < x < 2$ we have a power-law fluid, $\sigma(\dot{\gamma}) \sim \dot{\gamma}^{x-1}$; there is no yield stress, although the viscosity is still infinite.

We then study the model's stress-controlled rheology. After a step stress for $1 < x < 2$, the strain is initially linear in stress, with a rate $\dot{\gamma}$ which (due to the infinite "zero-shear" viscosity) appears to be tending to zero in time. However, after a crossover time (which diverges as $\sigma \to 0$) the system approaches a steady non-linear flow regime, with a strain rate given by the flow curve discussed above. For $x < 1$, and below the yield stress, we see ageing; there is no ultimate steady state, and the strain rate tends to zero at long times. Above the yield stress, ageing is interrupted and the system approaches a flow regime, with a constant strain rate as prescribed by the flow curve. We finally study strain response to small oscillatory stress.

In its linear regime at $x \gtrsim 1$, we demonstrate the SGR model to have the same dynamics as the tube model of highly branched polymer melts with a disordered (power law) branching distribution. We exploit this mapping to predict long rheological transients in these melts following preparation by an initial, rapid pre-shear.

We then study FDT in the linear SGR model's ageing regime, and find that there is no unique (observable-independent) FDT temperature. (We do, however, find several non-trivial limiting FDT curves.)

We finally consider a kinetically constrained spin chain which shows slow glassy coarsening at low temperatures. We incorporate non-Hamiltonian driving, to mimic rheological shear. As in the SGR model, we find that driving at constant rate interrupts the low-temperature relaxation process, and restores a non-equilibrium steady state in which the relaxation times is prescribed by the inverse shear rate. We finally consider non-equilibrium FDT in the slow shear limit.

Contents

Chapter 1

Introduction

Glassy systems are characterized by the fact that they relax very slowly at low temperatures, and therefore remain out of equilibrium for long times. A striking experimental consequence of this is the phenomenon of ageing: the time-scale for response to a small external perturbation increases with the system's age (that is, the time one has waited at the low temperature before applying the perturbation), as though the system gets stuck in progressively deeper traps in phase space as time progresses. At long times the dynamics become very sluggish, and the system effectively becomes completely "frozen".

Such phenomena have been the focus of intense research for several decades and have been observed in a wide variety of systems, all of which share the basic glassy features of disorder and frustration: examples include super-cooled liquids ("structural glasses") [Kob00]; spin systems with random inter-spin couplings ("spin glasses") [BCKM98, NS98]; pinned defects such as Bloch walls, vortices in super-conductors, charge density waves, dislocations, *etc.* interacting with randomly placed impurities [Bou00, GL98]; the viscoelastic properties of polymer melts [Str78]; and the structural relaxation of dense colloidal suspensions [VMMWM98].

The primary motivation for this thesis is an accumulating body of data which suggests that glassy dynamics also occur in the *rheology* (mechanical properties) of a wide variety of *disordered soft materials* including foams, dense emulsions, and dense colloidal suspensions. At high concentrations these materials show a "yield stress" σ_y, *i.e.* they can "freeze" into frustrated states of non-zero stress σ (with $0 < \sigma < \sigma_y$), even though the ultimate equilibrium state would be one of zero stress. Furthermore, after preparation by (for example) a rapid pre-shear, they exhibit *ageing* in their response to small mechanical probes: they stiffen over time. In what follows, we show that the qualitative features of this data can be captured within two very simple models of

glassy dynamics: a trap model, and a kinetically constrained spin chain. Because of our rheological motivation, we use driven versions of the models in which a non-Hamiltonian driving term mimics external shear (although in the limit of infinitesimal deformation – linear rheology – we recover purely relaxational dynamics). Due to the simplicity of the chosen models, our results are likely (besides their intended rheological application) to apply generically to dynamics of any glassy system subject to external driving and loading. With this in mind, we also use the models to study more general concepts of glassy dynamics: in particular, we consider violations of the fluctuation-dissipation theorem in the models' non-equilibrium regimes.

1.1 Layout of thesis

The thesis is organized as follows. In chapter 2 we introduce the necessary theoretical concepts of glassy dynamics. We also review the basic principles of rheology, and generalize the existing "time-translationally invariant" (TTI) rheological formalism to include ageing samples in which TTI is lost. (Specifically, we extend the argument list of each response function to include an absolute – ageing – time variable.) In chapter 3 we review the experimental evidence for glassy dynamics in the rheology of disordered soft solids. We also compare our theoretical approach to modelling this data with approaches adopted elsewhere in the literature.

In chapter 4 we describe the first of our two models: the trap model, which considers an ensemble of uncoupled elements exploring a free-energy landscape of traps (with distributed depths) by means of thermal activation. We discuss the existence of a glass transition at a finite temperature $T_g = 1$. For temperatures $T < 1$, *ageing* occurs: the system's apparent relaxation time-scale is always of order its own age. We then introduce the trap model's (rheologically) driven counterpart, the phenomenological "soft glassy rheology" (SGR) model, in which elements (now identified as local, mesoscopic elastic elements in a disordered soft material) are effectively pulled up the sides of their traps (which are now interpreted as the energy barriers inhibiting local "yielding" rearrangements) by external shear. In this context, it is necessary to replace the thermodynamic temperature T with an effective "noise" temperature $x \gg T$, which models in a mean field way interactions between the different regions of the sample. We show that, in its linear rheological regime, the SGR model has the same dynamics as the trap model itself and hence (in this linear regime at least) has a glass phase in which rheological ageing must occur. We review the SGR model's rheology under *non*-ageing conditions, where TTI applies.

We then (in chapters 5 and 6) present the results of our own detailed study of the

SGR model's rheological predictions in its glass phase ($x < 1$). Here, the model has a macroscopic yield stress. Provided this is not exceeded, ageing occurs, with a sample's apparent relaxation time-scale of order its own age (*i.e.* the time since it was prepared by a "quench"[1] into the glass phase). For loads greater than the yield stress, ageing is "interrupted", and the system "shear-thins" to a steady (TTI) flowing liquid state, in which the apparent relaxation time-scale is now set by the inverse shear rate (rather than the age). Outwith the glass phase ($x > 1$) the model has no yield stress, and there is no ageing (even at small loads). However, for $x \gtrsim 1$ we still see interesting "power-law fluid" behaviour (see section 2.2), and long rheological transients as the system very slowly equilibrates following an initial quench.

In chapter 7 we apply concepts of slow dynamics (as developed in chapters 1 to 6) to the rheology of another disordered soft material: the highly branched polymer melt. (Here, the "branching distribution" of the polymer molecule can be considered a type of glassy disorder.) We demonstrate that the tube model, in its application to such highly branched molecules, can (under certain conditions) be approximately mapped onto the SGR model in its linear regime just above the glass transition. The mapping enables us to make rheological predictions for these polymers without any formalism beyond that used in previous chapters. For a melt prepared by a rapid pre-shear, we predict very long rheological "transients" (which experimentally could be very difficult to distinguish from ageing proper) as the system slowly equilibrates.

In chapter 8, we discuss violations of the equilibrium fluctuation-dissipation theorem (FDT) in non-equilibrium situations, and outline the use of modified, non-equilibrium FDTs for defining effective temperatures in the ageing or weakly driven regimes of glassy systems. We study in detail non-equilibrium FDT in the ageing regime of the trap model. Although we obtain several non-trivial "limiting FDT plots", we conclude that in this particular model there exists no sensible non-equilibrium FDT temperature.

In chapter 9, we consider the second of our two models: the kinetically constrained spin chain. We review its slow glassy relaxation process at low temperatures, as solved by previous authors. We then incorporate non-Hamiltonian driving, to mimic rheological shear. Note that, unlike the SGR model, the spin chain is an N body model. It is nonetheless still tractable to analytical study, and is therefore necessarily much more abstract than the SGR model: it is not intended as a realistic rheological model, but merely as an oversimplified description of any driven glassy system. Nonetheless, we find its phenomenology to be (broadly) similar to that of the SGR model. In particular,

[1] See below for a definition of quench, and for a discussion of how this might relate to experimental procedures such as "pre-shear".

we present simulation results showing that (as in the SGR model) external loading can interrupt the chain's low temperature relaxation process, and restore a non-equilibrium steady state in which the relaxation time-scale is set by the inverse "shear" rate. We describe an independent-interval theory for this steady state, and demonstrate it to give excellent agreement with the simulation data. We finally consider non-equilibrium FDT in the weakly driven limit of this spin chain.

Chapter 2

Theoretical background

In this chapter, we review the theoretical formalism needed for the remainder of the thesis: in section 2.1 we introduce glassy dynamics, and provide a formal theoretical definition of ageing; in section 2.2 we review the basic principles of rheology, and extend the existing time-translationally invariant (TTI) rheological formalism to include ageing samples in which TTI is lost.

2.1 Glassy dynamics

Glassy systems are characterized by the fact that they relax very slowly at low temperatures. Typically, the "ergodic" (equilibration) time $\tau_{\rm erg}(T)$ increases dramatically as temperature is lowered and, at some "glass temperature" $T_{\rm g,exp}$, crosses the longest time-scale $\tau_{\rm exp}$ realistically available for any experiment. (See figure 2.1.) The system then falls out of equilibrium and becomes (for all practical purposes) a "glass". In some theoretical glass models, the ergodic time actually *diverges* at a finite temperature $T_{\rm g}$, which marks a strict *glass transition*. Experimentally, however, it is impossible to observe any such true divergence (even if it exists), because one obviously cannot measure $\tau_{\rm erg}(T)$ once it exceeds $\tau_{\rm exp}$ (*i.e.* once $T < T_{\rm g,exp}$).

2.1.1 Phenomenology, ageing and long term memory

Whether or not a true glass transition exists, at low temperatures $T < T_{\rm g,exp}$ the system cannot equilibrate on the time-scale $\tau_{\rm exp}$ of any experiment. Instead it *ages*. In this section, we summarize the experimental hallmarks of ageing, and use them to develop a formal theoretical definition which will allow us to distinguish true ageing from trivial "transient" approaches to equilibrium which can occur in non-ageing systems.

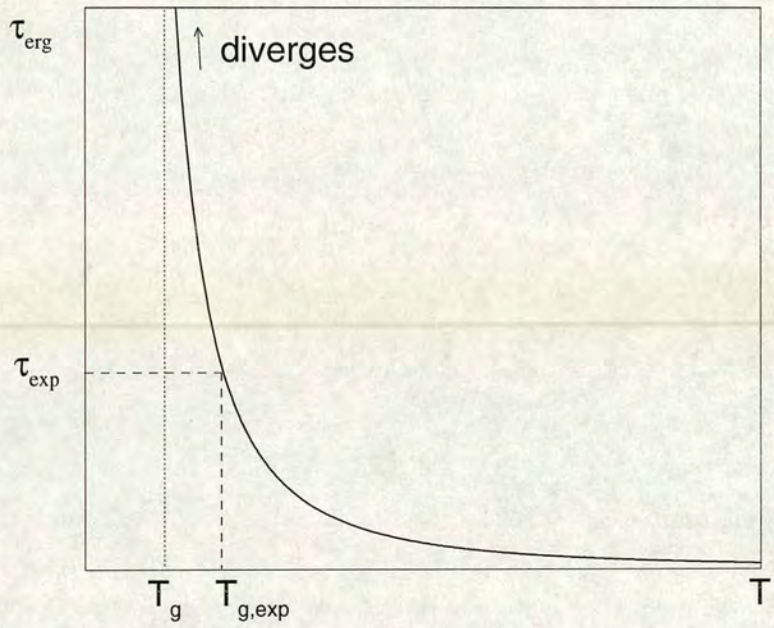

Figure 2.1. Schematic dependence of ergodic time upon temperature, with the experimental and true glass transition temperatures ($T_{\mathrm{g,exp}}$ and T_{g} respectively) marked. In some models, T_{g} is finite. Experimentally, it is impossible to tell whether T_{g} is finite (marking a true glass transition) or zero.

The canonical method for observing ageing is as follows. The system is quenched, in a small "field" h (which may be an actual magnetic field, but which here denotes a generalized field variable), from a high initial temperature $T_{\mathrm{i}} \gg T_{\mathrm{g,exp}}$ to a low temperature $T < T_{\mathrm{g,exp}}$. After some waiting time t_{w}, the field is switched off, and the subsequent relaxation of the (generalized) "magnetization"[1] (m) is measured. Because the system is out of equilibrium, this relaxation depends explicitly on the chosen waiting time t_{w}: time-translational invariance (TTI) has broken down and we have $m = m(t - t_{\mathrm{w}}, t_{\mathrm{w}})$. (In contrast, the dynamics of a steady-state system are invariant under time translations: here $m = m(t - t_{\mathrm{w}})$.)

Of course, TTI would also be transiently lost even in a non ageing system, during the small interval over which the system equilibrates to the new post-quench temperature. The distinguishing feature of non-TTI *ageing* behaviour, however, is that the system remains out of equilibrium on very long time-scales, over which the dynamics become ever more sluggish: more rigorously, *a significant part of the relaxation (of m) takes*

[1] Which may be an actual magnetization, but which here denotes the observable which is conjugate to the field h.

place on time-scales which grow with the age of the system. The interval $t - t_w$ needed to observe a given $[O(1)]$ fraction of the relaxation increases with t_w, and formally (assuming for the purposes of the present discussion that $\tau_{erg}(T)$ is actually infinite) diverges in the limit $t_w \to \infty$. Hence, to see the full extent of the relaxation ($m \to 0$), we must consider a fixed, *finite*, t_w, and a subsequent interval $t - t_w \to \infty$. In other words, encoding the relaxation in the response function $\chi(t-t_w, t_w) = \lim_{h\to 0}[m(t-t_w, t_w)/h]$, we have

$$\lim_{t\to\infty} \chi(t - t_w, t_w) = 0, \tag{2.1}$$

provided t_w *is fixed.* On the other hand, if we took $t_w \to \infty$ first, we could never then see the full extent of the decay in any subsequent interval $\Delta t = t - t_w$, however large. Formally,

$$\lim_{\Delta t\to\infty} \lim_{t_w\to\infty} \chi(\Delta t, t_w) \neq 0, \tag{2.2}$$

because it doesn't allow for that portion of the decay which takes place on time-scales which diverge with the age of the system.

In contrast, in any transient losses of TTI shown by non-ageing systems, the full relaxation is always visible on finite time-scales *however large the age* t_w, and hence

$$\lim_{\Delta t\to\infty} \lim_{t_w\to\infty} \chi(\Delta t, t_w) = 0, \tag{2.3}$$

and the ways 2.1 and 2.3 of observing the decay are equivalent:

$$\lim_{t\to\infty} \chi(t - t_w, t_w) = \lim_{\Delta t\to\infty} \lim_{t_w\to\infty} \chi(\Delta t, t_w). \tag{2.4}$$

With these remarks in mind, we adopt the definition that a system ages if at least one of its response (or correlation) functions violates this equality. Deviations from TTI in other systems are referred to as "transients".

So far, we have assumed for simplicity that the ergodic time is infinite. What happens if the ergodic time is actually finite (but still large)? Here, ageing still occurs, but only for waiting times $t_w \lesssim \tau_{erg}$, after which the system equilibrates. To distinguish this "temporary ageing" from trivial transients, we realize that, in the former case, relaxation time-scales still grow with t_w, although now only until $t_w = O(\tau_{erg})$. On the other hand, in the latter case the time-scales always remain of $O(\tau_0)$, where τ_0 is the underlying characteristic clock on which some basic, elemental process occurs (*e.g.* the single spin-flip time-scale in an Ising system). One can still use equation 2.4 to distinguish the two cases, but must recognize that the limits $t_w \to \infty$ and $\Delta t \to \infty$ actually mean "large but much less than τ_{erg}". Formally, then, the ageing regime is defined by waiting times t_w which obey $\tau_0 \ll t_w \ll \tau_{erg}$. In what follows we assume for

simplicity that $\tau_{\rm erg} = \infty$, unless otherwise stated.

Long term memory

Systems that violate the equality 2.4 are said to have "long term memory" [CK95, BCKM98, CK93]. They can be further subdivided according to the strength of this memory. To illustrate this distinction, imagine applying a (small) field to a system at time t_0 and switching it off again at some later time t_1. The corresponding magnetization at time $t > t_1$ is proportional to $\chi(t - t_1, t_1) - \chi(t - t_0, t_0)$. If this decays to zero at large times t, that is, if

$$\lim_{t\to\infty} [\chi(t - t_1, t_1) - \chi(t - t_0, t_0)] = 0 \tag{2.5}$$

(and equation 2.4 is violated) then we say that the system has "weak long term memory" (WLTM); otherwise it has "strong long term memory"(SLTM). Physically, a system with SLTM will never forget any perturbation, even if it was only applied for a finite time. In contrast, a system with WLTM will ultimately forget any perturbation which was only applied for a finite time: at any time, it is unaffected by perturbations of finite duration which were applied in the distant past.

Ageing time-scales; relaxation spectra

Above, we defined ageing to be the property that a significant part of the relaxation of (at least one of) the system's response or correlation functions takes place on time-scales which grow with the age of the system. In the simplest scenario, there is (at long times $t_{\rm w} \gg \tau_0$) just one such characteristic time-scale, which grows linearly with age. In this case

$$\chi(t - t_{\rm w}, t_{\rm w}) = \chi\left(\frac{t - t_{\rm w}}{t_{\rm w}}\right); \tag{2.6}$$

the evolution of a system of age $t_{\rm w}$ is the same as that of a system of age $2t_{\rm w}$, up to a linear re-scaling of time.

Note that, although there is just one *characteristic* growing time-scale in this example, this need not imply a single exponential decay, $\chi \sim \exp[-(t - t_{\rm w})/\tau(t_{\rm w})]$ with $\tau(t_{\rm w}) = O(t_{\rm w})$. Indeed, in glassy systems one commonly expects a very broad underlying spectrum $P(\tau, t_{\rm w})$, and a corresponding relaxation function

$$\chi(t - t_{\rm w}, t_{\rm w}) = \int d\tau P(\tau, t_{\rm w}) \exp\left(-\frac{t - t_{\rm w}}{\tau}\right) \tag{2.7}$$

which has a broad non-exponential (*e.g.* stretched exponential or power law) decay.

This is still consistent with the single characteristic time-scale implied by 2.6, provided the spectrum $P(\tau, t_w)$ has most of its weight centred on the (diverging) average $\tau = O(t_w)$.

More complicated ageing scenarios are also possible. Commonly, for example, one finds two distinct characteristic time-scales: "fast" (of order the microscopic time τ_0), and "slow" (ageing) of $O(t_w)$. In this case

$$\chi(t - t_w, t_w) = \chi_{st}\left(\frac{t - t_w}{\tau_0}\right) + \chi_{ag}\left(\frac{t - t_w}{t_w}\right) \tag{2.8}$$

and the invariance under scaling by t_w, as referred to above, is only visible after the decay of the fast, "stationary" (TTI) portion χ_{st}. Physically, the intuitive notion for the ageing part of the decay is that the system gets stuck in progressively deeper traps as it attempts to equilibrate to the low temperature regions of phase space. The fast part of the decay is generally attributed to a rapid exploration of the limited region of phase space in one trap. For the example of structural glasses, a real-space interpretation of this scenario is that molecules are trapped in cages formed by their neighbours. On fast time-scales ($O(\tau_0)$) they rattle inside these cages. On longer time-scales they rearrange with respect to their neighbours, and move into different cages; the time-scale for such rearrangements increases with the age, t_w.

The most general ageing scenario for a system with weak long term memory is [CK94]

$$\chi(t - t_w, t_w) = \sum_i \chi_i \left[h_i(t)/h_i(t_w)\right] \tag{2.9}$$

which can have several ageing time-scales (defined by the functions $h_i(t)$) each of which diverges differently with age. Note that if there is just one term in the sum, with $h(t) \sim t/\tau_0$, we recover the simplest ageing scenario of equation 2.6. Likewise a single term with $h(t) = \exp(t/\tau_0)$ gives TTI behaviour. The function

$$h(t) = \exp\left(\frac{\left(\frac{t}{\tau_0}\right)^{1-\mu} - 1}{1 - \mu}\right) \tag{2.10}$$

interpolates between these two limits, and gives "sub-ageing": at short time intervals (compared with the waiting time), $t - t_w \ll t_w$, it gives

$$\frac{h(t)}{h(t_w)} \sim \exp\left(\frac{1 - \mu}{\tau_0}\frac{t - t_w}{t_w^{\mu}}\right) \tag{2.11}$$

with an apparent relaxation time-scale of $O(t_{\rm w}^{\mu})$. In what follows, we adopt the convenient nomenclature that a system shows "full ageing" if it has just one characteristic growing time-scale $O(t_{\rm w}^{\mu})$ with $\mu = 1$, and sub-ageing if $\mu < 1$.

Low temperatures vs. high densities

So far, we have considered systems which become glassy at low temperatures $T < T_{\rm g,exp}$. In many systems, however, the relevant thermodynamic parameter is in fact (inverse) density. For example, in colloidal hard spheres [VMMWM98] (in which there is of course no meaningful energy scale to compare with $k_{\rm B}T$) glassy behaviour is seen for volume fractions exceeding some critical value $\phi = \phi_{\rm g} \sim 0.59$; other examples (of particular relevance to this thesis) include "soft glasses" such as foams and dense emulsions. Naively, one might expect the preparatory quench into the glass phase in such systems to constitute a sudden compression (*e.g.* by centrifugation). In fact more commonly the material is prepared directly in the high density phase, but then "pre-sheared", to ensure that it is in some known fluidized state at some initial time $t_{\rm w} = 0$ (see chapter 3).

2.1.2 Quenched and self-induced disorder

As noted above, the basic ingredient common to all glassy systems is *disorder*. Some glasses (*e.g.* spin glasses) contain quenched [2] disorder, which is present a priori in the underlying Hamiltonian (*e.g.* as random inter-spin couplings), and does not dynamically change over time. In contrast, there is no such quenched disorder in structural glasses: these instead kinetically self-induce their own disorder at low temperatures. Of the theoretical models studied in this thesis, the first (the phenomenological trap model) contains a quenched disorder, via the randomness of its (free) energy landscape. In contrast, the second (the constrained spin chain) induces its own glassiness by means of a simple kinetic constraint.

2.2 Rheology

Rheology is the study of the deformation and flow properties of matter. In this thesis we consider incompressible materials, in which the only possible deformations are volume-preserving extensional or shear strains; we further assume that only pure shear strains

[2] Note that in this thesis (following the example of the glassy literature) we use the word quenched to refer both to a fixed underlying disorder in certain types of glassy system (as in this section), and (as in the previous section) to the rapid procedure used to prepare a system in its glass phase.

arise (figure 2.2). The material's shear stress $\sigma(t)$ at any time t can then be specified in terms of the strain rate history $\dot{\gamma}(t' < t)$ via a constitutive equation (CE)

$$\sigma(t) = \sigma[\dot{\gamma}(t' < t)]. \tag{2.12}$$

(Alternatively, $\gamma(t)$ could be expressed in terms of the stress history: $\gamma(t) = \gamma[\sigma(t' < t)]$.) Note that in general shear strains can also give rise to *normal* stresses [DE86]. However we neglect these in what follows, because the models to be studied below are too simple to address any such tensorial issues.

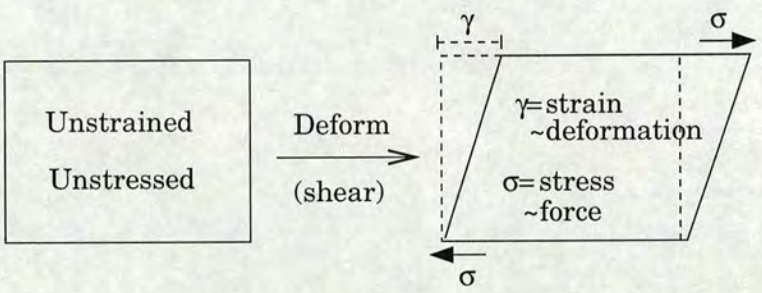

Figure 2.2. Schematic illustration of a sheared material.

A CE such as 2.12 clearly allows an arbitrary dependence of strain (or stress) upon time. In practice, though, many experiments comprise only a simple perturbation (such as a step or oscillatory strain or stress), the response to which can be encoded in a response function (which follows as a special case of the full CE). In the conventional (TTI) rheological formalism, each response function depends only upon a *relative* time variable (*e.g.* for a step perturbation, the time $t - t_w$ since the step was applied at t_w) since the underlying material properties do not change over time. In this thesis, however, we shall study ageing rheology, and therefore need to generalize the existing response functions such that they can now also depend upon an absolute time argument (t_w). This extension in fact allows an arbitrary evolution of the underlying material properties, and therefore applies not only to true ageing, but also to the more trivial transient losses of TTI which any non-ageing system can exhibit during equilibration. With these remarks in mind, we now introduce each (generalized) response function in turn. Throughout, we assume the material to have been prepared in some known state (unstressed and unstrained) at time $t = 0$.

2.2.1 Imposed strain

Step strain

Consider suddenly straining a previously undeformed material by an amount γ_0. Denoting the time of strain application by t_w, the stress response as a function of the subsequent time $t - t_w$ can, in the most general case, be written

$$\sigma(t) = \gamma_0 G(t - t_w, t_w; \gamma_0), \tag{2.13}$$

which defines the stress relaxation modulus $G(t - t_w, t_w; \gamma_0)$. For small deformations, a regime can arise in which $\sigma(t)$ depends linearly upon γ_0. Then we have

$$\sigma(t) = \gamma_0 G(t - t_w, t_w) \tag{2.14}$$

in which the linear stress relaxation modulus

$$G(t - t_w, t_w) = \lim_{\gamma_0 \to 0} G(t - t_w, t_w; \gamma_0). \tag{2.15}$$

In this case, the stress response to an arbitrary strain history can be found by superposing the response to each separate strain increment using the linear CE:

$$\sigma(t) = \int_{t_s}^{t} dt' G(t - t', t') \dot{\gamma}(t') \tag{2.16}$$

in which t_s denotes the time at which shearing was commenced.

In a steady (TTI) state the explicit t_w dependence is lost from equations 2.13 to 2.15: we have

$$\sigma(t) = \gamma_0 G(t - t_w; \gamma_0), \tag{2.17}$$

and (for linear deformations)

$$G(t - t_w) = \lim_{\gamma_0 \to 0} G(t - t_w; \gamma_0). \tag{2.18}$$

Equation 2.16 then becomes

$$\sigma(t) = \int_{t_s}^{t} dt' G(t - t') \dot{\gamma}(t') \tag{2.19}$$

and the stress at any time t now depends only upon the interval $t - t_s$ since the (now arbitrary) time t_s at which straining commenced.

We now briefly describe the behaviour of the linear stress relaxation function, $G(t -$

t_w, t_w). By causality, no stress can arise before the application of the strain, and hence $G(t - t_w, t_w)$ must be zero for $t - t_w < 0$. Upon strain application at $t = t_w$, the stress typically increases very rapidly (almost instantaneously) and then decays as a function of the subsequent time $t - t_w$. The rate of this decay depends upon the underlying properties of the material. In a simple (TTI) Newtonian liquid, the decay is very rapid; for all practical purposes we have $G(t) = \eta\delta(t)$ where η is the viscosity. In contrast in a (TTI) elastic solid the relaxation time-scales are (practically) infinite, and $G(t) = G_0\Theta(t)$. Many soft materials show intermediate "viscoelastic" behaviour, and relax on experimental time-scales; the simplest (TTI) model of such behaviour is the so called Maxwell model, which has a single relaxation time-scale, τ, such that[3] $G(t) = G_0 \exp(-t/\tau)$. This shows solid-like behaviour on time-scales $t - t_w \ll \tau$, but liquid-like response for $t - t_w \gg \tau$.

More commonly, there is a *spectrum* of (stress) relaxation time-scales and (assuming for the moment TTI conditions) we have

$$G(t - t_w) = \int d\tau P(\tau) \exp\left(-\frac{t - t_w}{\tau}\right). \tag{2.20}$$

Often, it is possible to identify a longest ("terminal") relaxation time-scale τ_{max}. However, in many cases to be considered below, this terminal time is infinite. Here, a more realistic measure of the longest relaxation time-scale could be set by

$$\int_{\tau_{max}}^{\infty} d\tau P(\tau) = \epsilon \tag{2.21}$$

such that only a *negligible fraction* (ϵ) of the stress decay takes place upon time-scales larger than τ_{max}.

In a non-TTI material, the relaxation spectrum becomes time-dependent and we have

$$G(t - t_w, t_w) = \int d\tau P(\tau, t_w) \exp\left(-\frac{t - t_w}{\tau}\right). \tag{2.22}$$

As noted in section 2.1.1, in a glassy ageing system one expects a broad relaxation spectrum, centred about some diverging average, say $\langle\tau\rangle = O(t_w)$. In this rheological context, an evolution of $P(\tau, t_w)$ towards larger time constants means that the material gradually stiffens over time, from a liquid-like to a solid-like state.

[3]The Theta function, which is demanded by causality to ensure that G is zero for negative values of its relative time argument, is hereafter assumed in, but omitted from, our expressions for G.

Viscoelastic spectra

Another standard rheological test consists of measuring the stress response to an oscillatory shear strain. For a strain having commenced at time t_s we have

$$\gamma(t) = \Theta(t - t_s)\Re\left[\gamma_0 e^{i(\phi+\omega t)}\right] \tag{2.23}$$

(where $\Re$ denotes real part). Straining is continued up to (at least) a time t, when the stress is measured. For small strain amplitudes, a linear regime can arise in which the stress response can be found by superposition using equation 2.16, or (under TTI conditions) equation 2.19. Assuming for the moment TTI conditions we have

$$\begin{aligned}\sigma(t) &= \Re\left[\gamma_0 i\omega \int_{t_s}^{t} dt' e^{i(\phi+\omega t')} G(t-t') + \gamma_0 e^{i(\phi+\omega t_s)} G(t-t_s)\right] \\ &= \Re\left[\gamma_0 e^{i(\phi+\omega t)} G^*(\omega, t-t_s)\right]\end{aligned} \tag{2.24}$$

in which[4]

$$G^*(\omega, t-t_s) = i\omega \int_0^{t-t_s} dt'' e^{-i\omega t''} G(t'') + e^{-i\omega(t-t_s)} G(t-t_s). \tag{2.25}$$

As the number of cycles becomes very large ($\omega(t-t_s) \gg 1$), transient "switch-on" effects become negligible: the $t - t_s$ dependence is lost, and the stress settles to a steady oscillatory function of time. We can then write

$$\sigma(t) = \Re\left[\gamma_0 e^{i(\phi+\omega t)} G^*(\omega)\right] \tag{2.26}$$

in which the *viscoelastic spectrum* $G^*(\omega)$ is, to within a factor $i\omega$, the Fourier transform of the stress relaxation modulus $G(t)$:

$$G^*(\omega) = i\omega \int_0^{\infty} dt e^{-i\omega t} G(t). \tag{2.27}$$

Traditionally one writes

$$G^*(\omega) = G'(\omega) + iG''(\omega) \tag{2.28}$$

where G', G'' are called respectively the storage and loss moduli of the material, and measure the in-phase (elastic) and out-of-phase (dissipative) response to an applied

[4]The second term on the RHS of equation 2.25 accounts for any stress which arises at time t as a result of any step strain at the switch-on time t_s.

strain. For the simple TTI Maxwell model [in which $G(t) = G_0 \exp(-t/\tau)$] we have

$$G'(\omega) = G_0 \frac{(\omega\tau)^2}{1 + (\omega\tau)^2}, \tag{2.29}$$

and

$$G''(\omega) = G_0 \frac{\omega\tau}{1 + (\omega\tau)^2} \tag{2.30}$$

which are plotted in figure 2.3. For high frequencies $\omega \gg 1/\tau$, the model behaves quasi-elastically: $G' \gg G''$, and most of the stress is in phase with the strain. At low frequencies $\omega \ll 1/\tau$, the response becomes liquid-like: $G'' \gg G'$, and most of the stress is out of phase with the strain, leading to dissipation of energy.

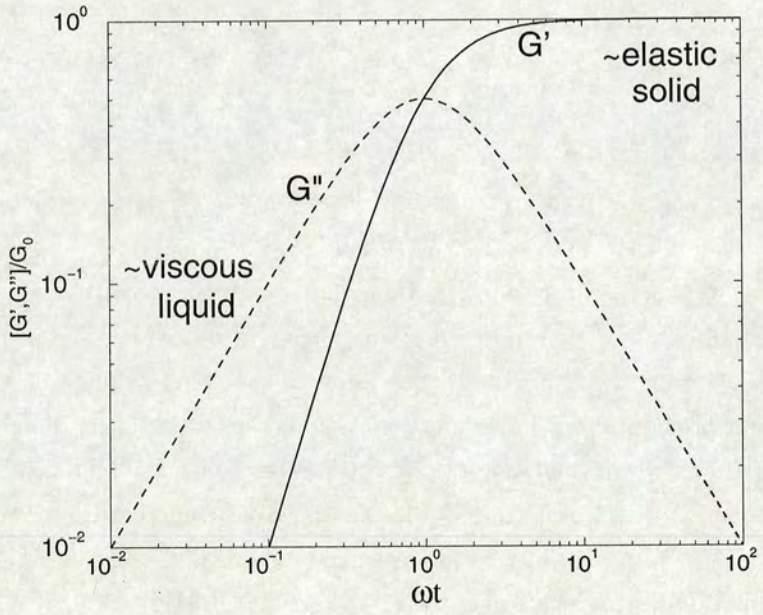

Figure 2.3. Viscoelastic spectra for the simple maxwell model.

For any system, the two components of G^* (real G' and imaginary G'', or, equivalently, amplitude $|G^*|$ and phase, which we denote by δ) are by definition determined by the relationship between strain and stress. At any single time t, for a strain of given known phase ϕ, frequency ω, and amplitude γ_0, this relationship gives

$$\sigma(t) = \gamma_0 |G^*| \cos(\omega t + \phi + \delta). \tag{2.31}$$

As a single equation, this clearly cannot be solved for *two* components $|G^*|$ and δ.

To resolve this problem (in a TTI system at least) one can obviously just observe the strain and stress at two separate times. Most commonly, in fact, one plots the entire steady state strain and stress functions against time, and reads off $|G^*|$ and δ from the amplitude ratio and phase offset between them.

Viscoelastic spectra without TTI

When TTI is lost, the step response functions in the first line of equation 2.24 show absolute time-dependence, and we now have

$$\sigma(t) = \Re\left[\gamma_0 i\omega \int_{t_s}^{t} dt' e^{i(\phi+\omega t')} G(t-t', t') + \gamma_0 e^{i(\phi+\omega t_s)} G(t-t_s, t_s)\right]. \tag{2.32}$$

We are still able unambiguously to define a viscoelastic spectrum G^* by

$$\sigma(t) = \Re\left[\gamma_0 e^{i(\phi+\omega t)} G^*(\omega, t, t-t_s)\right] \tag{2.33}$$

in which

$$G^*(\omega, t, t-t_s) = i\omega \int_{t_s}^{t} dt' e^{-i\omega(t-t')} G(t-t', t') + e^{-i\omega(t-t_s)} G(t-t_s, t_s). \tag{2.34}$$

However, $G^*(\omega, t, t-t_s)$ is now a somewhat cumbersome object since it depends on two time arguments – the sample age t, and the time $t-t_s$ since straining was commenced – as well as frequency. Intuitively, one expects the t dependence to reflect the underlying evolution of the material's properties with age, and the $t-t_s$ dependence to encode (as in the TTI case) more transient switch-on effects. In the TTI case, the many cycle condition $\omega(t-t_s) \gg 1$ eliminated this transient dependence upon $t-t_s$, and furthermore allowed us to relate $G^*(\omega)$ to the Fourier transform of $G(t)$ (see equation 2.27). Corresponding simplifications are certainly not guaranteed in the absence of TTI. However, the transient dependence on t_s *may* become negligible[5] when $\omega(t-t_s) \gg 1$, in which case we have

$$G^*(\omega, t, t-t_s) \to G^*(\omega, t), \tag{2.35}$$

giving a viscoelastic modulus that depends only on the age t. If, in addition, the time evolution of the underlying material properties is negligible on the time-scale of one

[5]For the SGR model discussed in chapters 4 to 6, an additional requirement is that $\omega t_s \gg 1$; see section 5.1.2 below.

oscillation, then $G^*(\omega, t)$ *may* obey the Fourier relation

$$G^*(\omega, t) = i\omega \int_0^\infty dt' e^{-i\omega t'} G(t', t). \tag{2.36}$$

As noted above, to measure G^* in the TTI case one must observe the relation between strain and stress for two separate times (or more commonly for an entire time window). Without TTI, that procedure is not necessarily reliable, since G^* itself varies with time. However, if the variation of G^* is slow on the scale of the oscillation period, this method can still be used to good approximation: G^* at any time t follows from the (roughly constant) relation between the phase and amplitude of σ and γ over a time window of a few cycles, centred upon t. *If*, on the other hand, G^* varies more quickly, then one must use a single measurement time. Here, to obtain two equations of the form of 2.31, which may be solved simultaneously for G^*, one must use two different phase offsets ϕ (*e.g.* a pure sine and a pure cosine strain), and perform a separate experiment for each.

We note finally that it is sometimes useful to extend the definitions of 2.25 and 2.34 to include non-linear (finite amplitude) strain oscillations. Interest in these functions is more limited, however, since, when amplitude dependence is non-trivial, there is no analogue of equation 2.27 or 2.36 relating the step and oscillatory response functions by simple Fourier transform.

Rheological linearity

So far, we have claimed that a regime of linear response can arise in the limit of small strains, $\gamma_0 \ll 1$. We now consider the extent to which this criterion can be made less stringent to include, for example, some steady shear experiments (see next section) in which the overall strain always becomes large at long times.

Formally, linear response theory tells us that the response to any given perturbation will be linear provided that the perturbation does not cause any observable to deviate by more than the intrinsic fluctuations which would occur anyway in a mesoscopically large sample of unperturbed material. In a rheological context, then, one might reasonably expect that linearity will be preserved provided stress can be relaxed as quickly as it develops due to the application of strain. Assuming the material to be characterized by some intrinsic average stress relaxation time-scale τ_s (and, for the moment, that TTI conditions apply, such that τ_s is time-independent), this sets the following condition on the maximal strain which can be applied between any time t and $t + \tau_s$

$$\gamma(t) - \gamma(t - \tau_s) \ll 1 \tag{2.37}$$

(where some underlying strain threshold in the material has been re-scaled to be $O(1)$). This is clearly consistent with the condition $\gamma_0 \ll 1$ given above for step or oscillatory measurements, but also encompasses steady shear with unbounded total strain, provided the strain rate $\dot{\gamma} \ll 1/\tau_s$. This criterion can clearly be rather easily extended to non-TTI systems, by setting $\tau_s = \tau_s(t_w)$, and requiring that $\dot{\gamma}(t_w) \ll 1/\tau_s(t_w)$ for any time t_w.

Shear startup; steady-state flow curve

With the above discussion in mind, we now consider the stress response to strain applied at a small constant rate $\dot{\gamma}$. We consider the TTI case first, and later generalize to non-TTI conditions. We also assume a priori that response is linear; we shall consider the self-consistency of this assumption a posteriori. Within linearity, then, the stress at time t after straining was commenced at a time t_w is given by equation 2.19 as

$$\sigma(t) = \dot{\gamma} \int_0^{t-t_w} dt' G(t'), \tag{2.38}$$

(which we note only depends on the interval $t - t_w$, as it must in this TTI case). If $G(t)$ decays to zero quickly enough that its integral converges, then, as $t - t_w \to \infty$, the stress tends to the finite steady-state limit

$$\sigma_{ss}(\dot{\gamma}) = \dot{\gamma}\eta. \tag{2.39}$$

In this equation, η is the material's zero shear viscosity:

$$\eta = \lim_{\dot{\gamma}\to 0} \left[\frac{\sigma_{ss}(\dot{\gamma})}{\dot{\gamma}}\right] = \int_0^\infty dt G(t); \tag{2.40}$$

it has the dimensions of a modulus times a characteristic stress relaxation time-scale. If we identify this time-scale with that used in the above criterion for linearity (τ_s) we find that, for a material with a finite η and τ_s, our assumption of linearity is self consistent, provided the strain rate $\dot{\gamma} \ll 1/\tau_s$.

In many cases encountered in this thesis, however, $G(t)$ decays so slowly that its integral diverges; examples include $G(t) \to G_\infty \neq 0$ or $G(t) \sim t^{-y}$ with $y < 1$ as $t \to \infty$. The zero-shear viscosity η and overall linear relaxation time-scale τ_s are then both infinite: if linearity were still to apply, the stress would (by equation 2.38) increase without bound at long times $t - t_w \to \infty$. However, we see from the condition 2.37 (which in this context is just $\dot{\gamma}(t - t_w) \ll 1$, since $\tau_s = \infty$) that linearity must in fact

break down[6] once $t - t_w = O(1/\dot{\gamma})$.

In many hard materials, such breakdown of linearity is marked by fracture. Soft materials, however, can restructure themselves non-catastrophically under non-linear shear: for example, they can become "fluidized", and enter a flow regime in which the stress does not now diverge, but tends to a steady state value given by the non-linear relation

$$\sigma_{ss} = \sigma_{ss}(\dot{\gamma}). \tag{2.41}$$

For consistency with the fact that the zero-shear viscosity $\eta = \lim_{\dot{\gamma}\to 0} \sigma(\dot{\gamma})/\dot{\gamma}$ is infinite, this relation must have an infinite slope at the origin; possible candidate functions include

$$\sigma_{ss}(\dot{\gamma}) \sim \dot{\gamma}^n \tag{2.42}$$

with $n < 1$ ("power-law fluid" behaviour) or

$$\sigma_{ss}(\dot{\gamma}) - \sigma_y \sim \dot{\gamma}^n \tag{2.43}$$

("Herschel-Bulkeley", or, for $n = 1$, "Bingham fluid" behaviour) with a finite yield stress in the limit of zero shear: $\sigma_y = \lim_{\dot{\gamma}\to 0} \sigma_{ss}(\dot{\gamma})$.

Note that an equation of the form $\sigma_{ss} = \sigma(\dot{\gamma})$ (*e.g.* 2.39, 2.42 and 2.43) specifying a steady-state relation between stress and strain rate is called a "flow-curve".

Shear-startup without TTI

In materials without TTI, the stress response at time t to straining commenced at t_w in general depends not just on $t - t_w$, but also explicitly upon t_w: equation 2.38 becomes

$$\sigma(t) = \dot{\gamma} \int_{t_w}^{t} dt' G(t - t', t'). \tag{2.44}$$

In this case, it is not obvious that a steady stress could ever be established at long times $t - t_w \to \infty$, since there is in general no sensible definition of steady state in ageing systems. However, in the models to be considered below, we find that ageing can in fact be interrupted, and the material "re-fluidized" by shear: a steady state is restored with a constant stress, as prescribed by a non-linear flow curve of the form of either 2.42 or 2.43.

[6] Only by considering a succession of experiments with progressively smaller $\dot{\gamma} \to 0$ could one see linearity out to arbitrarily long times, $t - t_w \to \infty$.

2.2.2 Imposed stress

Creep compliance

Consider a material subject to a constant load σ_0 for all times $t > t_w$. The strain response can, in the most general case (non TTI and non-linear) be encoded in the creep compliance J, where

$$\gamma(t) = \sigma_0 J(t - t_w, t_w; \sigma_0). \tag{2.45}$$

(As usual, J must, by causality, be zero for $t - t_w < 0$.) In the limit of small stresses, a linear regime may arise in which

$$\gamma(t) = \sigma_0 J(t - t_w, t_w), \tag{2.46}$$

with

$$J(t - t_w, t_w) = \lim_{\sigma_0 \to 0} J(t - t_w, t_w; \sigma_0). \tag{2.47}$$

In a TTI material, the explicit t_w dependences are lost from equations 2.45 to 2.47. For a simple TTI Newtonian fluid, the linear compliance is $J(t) = t/\eta$ where η is the viscosity. For a Maxwell model [for which $G(t) = G_0 \exp(-t/\tau)$], $J(t) = 1/G_0 + t/\eta$ where $\eta = G_0\tau$. In both these cases, there is at long times a limiting strain rate: the materials flow like liquids, with a flow-curve $\sigma_0 = \eta\dot{\gamma}$. In contrast, for an elastic solid we have $J(t) = 1/G_0\Theta(t)$: there is a limiting strain, and zero strain rate. Intermediate between these liquid and solid behaviours is "power law creep" $J(t) \sim t^y$ with $y < 1$ (or logarithmic creep with $y \approx 0$) for which no ultimate steady state exists: the strain rate tends to zero, but at an ever decreasing rate such that there is no limiting strain. The zero-shear viscosity is infinite, and the flow curve must have infinite slope (as in, for example, equation 2.42 or 2.43) in the limit $\dot{\gamma} \to 0^+$.

To determine the time and stress windows over which such linearity holds one can, at any time during the creep, consider the interplay between the rate of intrinsic stress relaxation and the rate of shear-induced stress growth (as outlined on page 18 above). We do not study this in detail here (see section 6.2.1 for a discussion in the context of the SGR model) but note that, even if the stress is small enough for response to be linear at short time intervals, one might still see a crossover to non-linear behaviour at longer times. In fact (see section 6.2.1) the SGR model for $1 < x < 2$ exhibits (for $\sigma_0 \ll 1$) linear power-law creep $\gamma \sim \sigma_0(t - t_w)^{x-1}$ for times $t - t_w \lesssim \sigma_0^{1/(x-1)}$, but at long times becomes fluidized to a steady non-linear flow regime with a flow rate prescribed by the (inverted) flow curve relation $\dot{\gamma} = \sigma_0^{1/(x-1)}$ which has the form of

equation 2.42. We remark finally that, even in its ageing regime $x < 1$ (where a priori one would expect J always to depend explicitly upon t_w) the SGR model can still, for large enough stresses $\sigma > \sigma_y$, show an ultimate steady state of constant stress and strain rate $\sigma - \sigma_y \sim \dot{\gamma}^{1-x}$ (which has the form of equation 2.43): loading can *interrupt* ageing (see section 6.2.1 for details). (For $\sigma < \sigma_y$ and $x < 1$, in contrast, $\dot{\gamma}$ tends to zero at long times: hence, the material can support a non-zero stress, even when the strain rate tends to zero.)

Oscillatory stress

Another standard rheological test consists of measuring the strain response, at some time t, to an oscillatory stress commenced at a switch-on time t_s:

$$\sigma(t) = \Theta(t - t_s)\Re\left[\sigma_0 e^{i(\phi+\omega t)}\right]. \tag{2.48}$$

Arguing along parallel lines to those given above for oscillatory strain, in a TTI material one denotes strain response at time t by

$$\gamma(t) = \Re\left[\sigma_0 e^{i(\phi+\omega t)} J^*(\omega, t - t_s)\right]. \tag{2.49}$$

In the many cycle limit, one expects switch-on transients to become negligible: the strain then settles to a steady oscillatory function, and we have

$$\gamma(t) = \Re\left[\sigma_0 e^{i(\phi+\omega t)} J^*(\omega)\right] \tag{2.50}$$

in which $J^*(\omega)$ is (by analogy with equation 2.27) $i\omega$ times the Fourier transform of the linear creep compliance $J(t)$.

Clearly, the steady-state characterized by equation 2.50 could equally have been established by applying an oscillatory strain (see equation 2.26). Comparing these steady-state equations (2.26 and 2.50), we find the reciprocity relation

$$G^*(\omega)J^*(\omega) = 1. \tag{2.51}$$

For non-TTI systems, a generalized compliance spectrum $J^*(\omega, t, t - t_s)$ can be defined by analogy to the generalized spectrum $G^*(\omega, t, t - t_s)$ of equation 2.34. As for G^*, the many cycle limit $\omega(t - t_s) \gg 1$ *may* eliminate startup dependences upon $t - t_s$, leading to the simpler function $J^*(\omega, t)$ (by analogy with the simplification 2.35). If the underlying evolution of the material is slow on the time-scale of one period, this

may obey

$$J^*(\omega,t) = i\omega \int_0^\infty dt' e^{-i\omega t'} J(t',t) \tag{2.52}$$

(by analogy with equation 2.36). Finally, $G^*(\omega,t)$ and $J^*(\omega,t)$ *may* obey the conventional reciprocal relation

$$G^*(\omega,t)J^*(\omega,t) = 1 \tag{2.53}$$

(which we note above – equation 2.51 – *automatically* holds for the time independent counterparts $G^*(\omega)$ and $J^*(\omega)$ in a TTI system).

To summarize: we have seen that, for TTI systems, $G(t)$ is related to $G^*(\omega)$ (and $J(t)$ to $J^*(\omega)$) by Fourier transform. Furthermore, $G^*(\omega)$ and $J^*(\omega)$ obey the reciprocity relation 2.51. In this TTI case, then, any one of these four functions gives enough information to enable us to calculate the other three. In contrast, in non-TTI systems, these simplifying Fourier transform and reciprocity relations need not hold in general. Below, we shall find they *do* in fact hold for the SGR model, even in its ageing glass phase. They *may* also hold more generally for systems with weak long term memory (which are likely to be the main systems of interest in a rheological context, and of which the SGR model is an example). However, we do not have a rigorous proof for this. Pending such a proof, the relations 2.36, 2.52 and 2.53 remain hypotheses needing explicit verification for any constitutive model.

Chapter 3

Motivation and context of the thesis

In this chapter, we outline the experimental data which suggests the presence of glassy dynamics in the rheology of a wide variety of disordered soft solids; this data forms the primary motivation for much of the work in this thesis. We then set our approach to modelling the data into its proper context by reviewing approaches adopted elsewhere in the literature. Note that we do not make any attempt to review the specific properties of any of the materials to be studied, since we are focusing on the *generic* presence of glassy dynamics, rather than any material-dependent features.

As noted above, because our approach is based upon the incorporation of driving into very simple models of the glass transition, we have also been able to extend our study beyond glassy rheology, to address some more generic issues of glassy dynamics. In particular, we have studied violations of the fluctuation dissipation theorem (FDT) in ageing or weakly driven glassy systems. However we defer a discussion of the theory, motivation and context of this FDT work until the relevant chapter.

3.1 Experimental "soft glassy rheology" (SGR)

3.1.1 Yielding under flow

Many disordered soft materials, such as foams, dense emulsions and dense colloidal suspensions, show qualitative similarities in their low-frequency shear rheology. For example, at concentrations ϕ larger than some critical value ϕ_c, they typically show *yielding* behaviour – *i.e.* for loads less than a yield stress σ_y, they behave as elastic solids, while at larger stresses they flow like liquids. Because of this yielding

phenomenon, mechanical response to flow is highly non-linear, often being fit to the form [Hol93, Dic92, BHW89]

$$\sigma = \sigma_y + a\dot{\gamma}^n \tag{3.1}$$

(Hershel-Bulkeley ($n < 1$) or Bingham fluid ($n = 1$) behaviour; we note that equation 3.1 is of the same form as equation 2.43). At lower concentrations $\phi < \phi_c$, these materials have no yield stress, but can still show non-trivial "power law fluid" behaviour (as given by equation 3.1 with $\sigma_y = 0$; see also equation 2.42). Note that (whatever the value of σ_y) any[1] material obeying equation 3.1 has an infinite viscosity in the limit of zero shear ($\eta = \lim_{\dot{\gamma}\to 0}[\sigma(\dot{\gamma})/\dot{\gamma}] = \infty$) but a finite apparent viscosity $\sigma(\dot{\gamma})/\dot{\gamma}$ under flow: it shear-thins.

The origin of such behaviour is poorly understood[2]. However, it has recently been argued (see *e.g.* [HLMP97, Sol98]) to imply underlying glassy dynamics, which arise as a natural consequence of the structural disorder and metastability which are common to all these materials. At zero shear, the material is effectively "stuck" in very long lived metastable states: for example, the droplets in an emulsion can only explore a very small domain of space under thermal activation; rearrangement of the droplets to states of lower free energy is impeded by energy barriers which are large on the scale of thermal energies. Hence these materials can "freeze" into frustrated states with a non-zero stress $\sigma < \sigma_y$, and never attain the equilibrium state of zero stress. In contrast, under flow the elements' trajectories become strongly modified; elements can rearrange plastically (irreversibly) and the material as a whole becomes "fluidized" (*i.e.* it shear thins).

To substantiate these intuitive ideas, Hébraud *et al.* measured [HLMP97] (using "diffusing wave spectroscopy", or DWS [Pin00]) the time-correlation function for the configuration of particles in a dense emulsion undergoing oscillatory shear. In an elastic sample, this correlation function should echo at the end of every cycle as each scatterer exactly returns to its initial position; any reduction in echo height implies irreversible plastic rearrangements. For the dense emulsions studied, negligible echo decay was seen at small strain amplitudes (consistent with the system being elastic at small loads $\sigma < \sigma_y$). At larger amplitudes the echo showed non-trivial decay; good agreement was obtained between the amplitude needed to give a chosen fractional echo decay, and the "yield strain" (albeit assigned under a somewhat arbitrary criterion) at which non-linearity is first observed in bulk rheological measurements [MBW96]. This clearly

[1] with the exception of the trivial Newtonian fluid, which has $\sigma_y = 0$ and $n = 1$.

[2] In contrast, for crystalline materials, yielding can generally be attributed to elastic bond deformation at low loads, followed by catastrophic fracture, or motion of dislocations at higher loads [WDC85, CAZ94].

supports the claim that the plastic rearrangements probed by the echo measurements are the same as those associated with the yielding of the emulsion as a whole. To summarize, the results of this experiment support the hypothesis that these materials are stuck in long lived glassy states at low loads, but can yield and become fluidized at larger loads.

3.1.2 Anomaly in the loss modulus

In linear or quasi-linear oscillatory shear, the viscoelastic spectra $G'(\omega)$ and $G''(\omega)$ of these glassy materials (foams, dense emulsions *etc.* , as listed above) are typically very weak power laws of frequency [MMSZ94, KPG88, KSA88, MBW95, PRV+96, HR93, MW95], with the loss modulus $G''(\omega)$ curving upwards slightly as frequency is tracked downwards. This behaviour persists to the lowest accessible frequencies (about 10^{-3} to 1Hz depending on the system).

In [Sol98, SLHC97], Sollich *et al.* argued that the dominant dynamical relaxations at such low frequencies are local plastic rearrangements (*e.g.* of droplets or mesoscopic collections of droplets in an emulsion) as probed by Hébraud *et al.* in the DWS experiment[3]. Given this assumption, the fact that the loss modulus $G''(\omega)$ is seen to be non-zero is seemingly at odds with Hébraud's observation of effectively frozen (elastic) behaviour at such linear shear amplitudes. However, Sollich *et al.* also argued that these rearrangement dynamics should *age*, such that G'' (now a function of ω *and* t) should in fact (at any fixed frequency ω) decrease with time as the system becomes (effectively) completely frozen. At long times $t_w \gg 1/\omega$ (which is the regime probed by Hébraud *et al.*, since they effectively performed a steady-state measurement by averaging over very many cycles), G'' should be negligibly small. We now summarize the argument of Sollich *et al.*.

Within linear response theory (for the moment assuming equilibrium conditions), the viscoelastic spectra can be interpreted as a superposition of Maxwell modes, with an underlying distribution of time-scales $P(\tau)$:

$$G'(\omega) = \int d\tau P(\tau) \frac{(\omega\tau)^2}{1+(\omega\tau)^2}, \tag{3.2}$$

[3] At higher frequencies one must also consider less drastic, small local shifts in particle positions, and viscous losses in the fluid films between particles; in the language of glass theory one might call this an "intra-trap" (or "beta") relaxation. We shall however not be concerned with these in what follows.

and

$$G''(\omega) = \int d\tau P(\tau) \frac{\omega\tau}{1+(\omega\tau)^2}, \tag{3.3}$$

where the second factor in each integrand is the standard Maxwell modulus (see equations 2.29 and 2.30). Any individual mode (of time-scale τ) gives rise to a bump ("loss peak") in $G''(\omega)$, and a drop in $G'(\omega)$ as frequency is tracked downwards through $1/\tau$. For inverse frequencies exceeding the longest (terminal) time $\tau_{\max}$, the only significant contribution to $G''(\omega)$ should arise from the terminal loss peak, and $G''(\omega)$ should show the single Maxwell-mode behaviour $G'' \sim \omega$. (See figure 3.1.)

Within this description, the low-frequency flat $G'(\omega)$ and $G''(\omega)$ of disordered soft solids clearly indicate a broad underlying distribution of time-scales $P(\tau)$, with significant weight at large time-scales. *However*, the tendency of $G''(\omega)$ to curve upward at low frequencies (even to the lowest accessible frequencies) is (apparently) at odds with the requirement that $G'' \propto \omega$ at low frequencies $\omega \ll 1/\tau_{\max}$. The conventional explanation for this puzzle is of course that the experimentally accessible frequency window must actually lie at frequencies $\omega \gg 1/\tau_{\max}$, and that the terminal loss peak *would* eventually be seen, if only the frequency could be tracked low enough.

Although this may often be the case, where a specific search for such slow modes has been carried out, no suitable candidates have emerged (for the example of foams see [BLC95]). An alternative and more generic explanation is that these rearrangement dynamics *age*, such that the majority of modes at any time $t_{\rm w}$ since sample preparation have relaxation time-scale $\tau = O(t_{\rm w})$. The underlying spectrum is now time-dependent: $P = P(\tau, t_{\rm w})$ with $\langle\tau\rangle_P = O(t_{\rm w})$. Here, to get beyond the terminal loss peak one would (in an experiment performed at an epoch $O(t_{\rm w})$) need a measurement frequency $\omega \ll O(1/t_{\rm w})$. *However*, the simple requirement that many cycles must be performed (in order to constitute a realistic oscillatory measurement) automatically restricts one to the higher frequency range $\omega t_{\rm w} \gg 1$, since one obviously cannot commence shearing before the sample was prepared. Within this picture, one can *never* observe the (putative) loss peak: a rising $G''(\omega)$ will always be seen at low frequencies, but (at any fixed frequency) with an amplitude which falls with time as the spectrum ages to progressively larger time-scales. See figure 3.1. Hence, the anomalous loss modulus of these materials is suggestive of underlying ageing behaviour. We now describe the results of some experiments aimed at observing such ageing more explicitly[4].

[4]These experiments were performed after the publication of our predictions for rheological ageing.

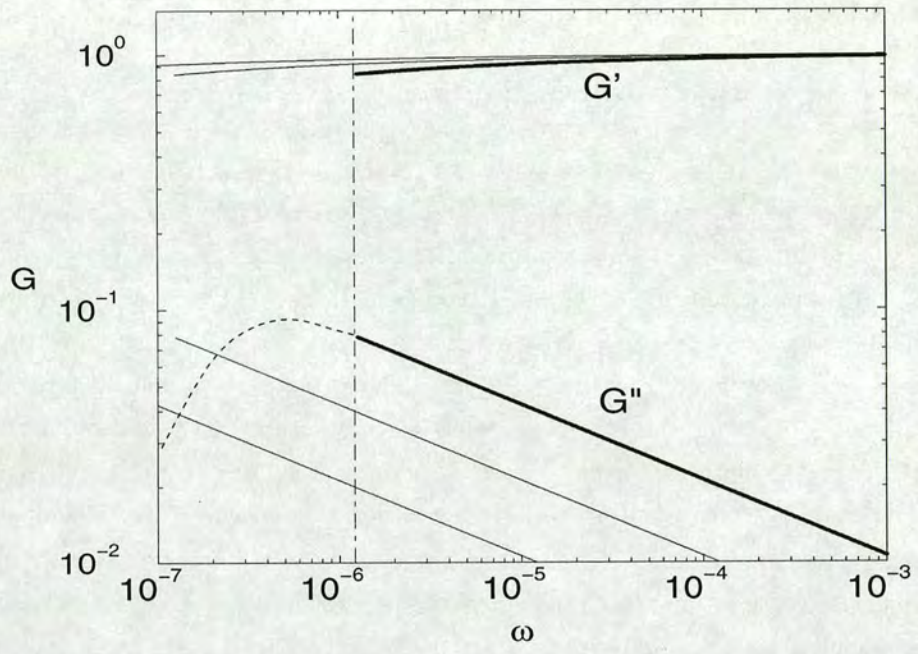

Figure 3.1. Sketch of ageing scenario for dynamic moduli G' (top) and G'' (bottom). Assuming that data shown by the thick solid lines have been measured, the conventional interpretation would be that G'' has a loss peak at low frequencies ω (dashed) outside the experimentally accessible range. But the rise of G'' towards small ω could also be due to *ageing*: if the experiment is repeated at later times, the thin solid lines (calculated from the SGR model at noise temperature $x = 0.7$; see section 5.1.2) might be measured; the putative loss peak would then always be unobservable because no measurement is possible at frequencies below the inverse age of the system.

3.1.3 Ageing stress relaxation in dense colloidal suspensions

Derec *et al.* [DADL00] performed explicit ageing experiments in a dense colloidal suspension for a high concentration $\phi > \phi_c$, at which the system has a yield stress $\sigma_y(\phi)$. In order to obtain reproducible results, before taking any ageing measurements they first always fluidized the material by application of a massive oscillatory shear. After completing this pre-shear step, they then aged the sample for a time t_w, before applying a small step strain, and measuring the stress response as a function of the subsequent time $t - t_w$. Repeating this for progressively larger t_w, they found that the stress data could be collapsed onto a single t_w-independent curve by using an effective time axis

$$t^{1-\mu} - t_w^{1-\mu} \tag{3.4}$$

with an ageing exponent μ between about 0.5 and 0.7. Note that this is the rescaling contained in single term of equation 2.9 with $h(t)$ given by equation 2.10.

3.1.4 Soft micro-gels: ageing and its interruption at large loads

Cloitre *et al.* [CBL] likewise performed explicit ageing experiments, in this case in concentrated ($\phi > \phi_c$) suspensions of soft deformable micro-gels, and now choosing to measure the strain response to a constant imposed stress σ_m. They studied values of σ_m both above and below the yield stress σ_y. In each experiment, to prepare (fluidize) the sample they pre-sheared at a massive steady stress $\sigma_p > \sigma_y$. After completing pre-shear, they waited a time t_w at zero stress before applying a measurement stress σ_m, and observing the strain response as a function of the subsequent time $t - t_w$. Here, they found an interplay between forward creep due to the applied stress σ_m, and reverse creep corresponding to a degree of elastic recovery from recent removal of the larger pre-shear stress. Nonetheless, they obtained strain curves which (for various t_w) could be collapsed by rescaling time according to equation 3.4. Interestingly, the ageing exponent μ was found to vary with the size of the perturbing stress σ_m, ranging from $\mu = 1$ for small σ_m (full ageing), through sub-ageing for $\sigma_m < \sigma < \sigma_y$, to $\mu = 0$ for $\sigma_m \gtrsim \sigma_y$ (restoration of TTI above the yield stress). Hence, in this experiment ageing was interrupted and the system was refluidized by stresses $\sigma \gtrsim \sigma_y$.

3.2 Possible SGR theories

The picture which emerges from the above discussion is that soft glassy materials (SGMs) show *ageing* dynamics in their intrinsic plastic rearrangement processes at small loads. At long times, the materials become effectively stuck in amorphous glassy configurations. They can, however, be re-fluidized by non-linear stress $\sigma > \sigma_y$: they *shear thin.* The interplay between ageing and driving was seen most explicitly by Cloitre *et al.*, who observed an interruption of ageing and a cross over to TTI response by the application of loads $\sigma \gtrsim \sigma_y$.

This phenomenology is in fact rather typical of disordered, glassy systems: as noted above, there is already a well established body of ageing data for such systems (see chapter 1 for references), while the more recent glassy literature contains several instances of re-fluidization by external driving. For example, in recent low-temperature simulations of binary Lennard-Jonesium (a structural glass) [BBK00, YO98], shear was found to interrupt ageing and restore a non-equilibrium steady (TTI) state with a characteristic relaxation time-scale set now by the inverse shear rate, and not the age; elastic

manifolds driven through random media have also been demonstrated to show a loading threshold equivalent to a yield stress [VMC96]. In fact, Kurchan, Cugliandolo *et al.* [Kur98, CKP97] have predicted that effects equivalent to rheological shear-thinning should occur quite generically in driven glassy systems. Intuitively, the physics of this is clear: because the intrinsic relaxation processes are very slow at long times, they are highly susceptible to external driving and therefore respond in a non-linear way to even the slowest of driving rates.

It is therefore natural to look to models of the glass transition to capture the above phenomena. Clearly, to incorporate rheology into any such model one must define suitable strain and stress variables, and some method of coupling the dynamics to the external shear driving. Several promising attempts in this direction have been made [BBK00, HL98] using "mode coupling" theories (of structural glasses) and random bond Ising (spin glass) models. We outline these approaches briefly in section 3.2.2. In section 3.2.3, we outline a more phenomenological Landau-like approach. Finally, in sections sections 3.2.4 and 3.2.5, we outline the approaches to be adopted in this thesis, which are based upon a glassy trap model and a kinetically constrained spin model.

3.2.1 Early approaches: "time, waiting-time superposition"

Before discussing the rheology of foams, emulsions *etc.* , we note that the first attempts to study rheological ageing systematically appear in a monograph by Struik [Str78] in the context of *polymeric* glasses. Using intuitive ideas of a slow relaxation of free volume below the glass point, he argued that a material of age $t_{\rm w}$ should have a characteristic sub-ageing relaxation time-scale of $\tau(t_{\rm w}) = t_{\rm w}^{\mu}\tau_0^{1-\mu}$ where τ_0 is an intrinsic microscopic time and $\mu \lesssim 1$. Although we do not expect the free volume concept to be particularly relevant to the materials studied in this thesis, we shall nonetheless find various phenomenological points of contacts with Struik's work, which we shall indicate where appropriate. Note in particular that the stress relaxation function as measured by Derec *et al.* [DADL00] for dense colloidal suspensions shares this sub-ageing time-scale.

3.2.2 Mode coupling theories and spin glass models

Mode coupling theory (MCT) [GS92] was originally developed to describe the time-evolution of density fluctuations in a TTI liquid: the fluctuations at a given wavelength q, as encoded in the intermediate scattering function[5] $F(q, t - t_{\rm w})$, are described by equations which include non-linear couplings to fluctuations at other wavelengths. At

[5] Where $t_{\rm w}$ is as here an arbitrary time, since we are considering a TTI system.

long times $t - t_w \to \infty$ there are two solutions to these equations [Kob00]. The first, which is the only solution at high temperatures, has $\lim_{t-t_w\to\infty} F(q, t - t_w) = 0$. The second, which only appears at low temperatures $T < T_c$, has $\lim_{t-t_w\to\infty} F(q, t-t_w) > 0$: hence for temperatures $T < T_c$ the system is no longer ergodic. As a result of this singularity, MCT has been widely exploited to describe the glass transition in supercooled liquids (structural glasses)[6]. In fact, an extension of the theory allows ageing effects to emerge: here, an explicit t_w dependence is incorporated, such that we have $F(q, t - t_w, t_w)$. The decay of F as a function of $t - t_w$ becomes slower for larger values of t_w (with non-ergodicity recovered as $\lim_{\Delta t\to\infty} \lim_{t_w\to\infty} F(q, \Delta t, t_w) \neq 0$, where $\Delta t = t - t_w$).

Interestingly, the equations of MCT are, within certain approximations, the same as the equations governing the time-evolution of the Fourier components of spin-spin correlation and response functions in some microscopic mean-field spin glass models[7]. Berthier *et al.* [BBK00] exploited this correspondence to study glassy rheology, by incorporating a non-conservative force into a Langevin description of the well-studied p-spin glass model, as defined by the Hamiltonian

$$H = - \sum_{j_1<\ldots<j_p} J_{j_1\ldots j_p} s_{j_1} \ldots s_{j_p} \tag{3.5}$$

where the couplings J are random Gaussian variables, symmetrical about the permutations of $(j_1 \ldots, j_p)$, with mean zero. Within purely relaxational dynamics (*i.e.* in the limit of zero force) they found a "two stage decay" to the correlation function, and associated a fast and a slow relaxation time-scale to the first and second stages respectively. The slow time-scale, t_s (formally defined as $\int d\Delta t C(\Delta t)$) was found to be finite (although much larger than the fast one) for $T > T_c$, but, under equilibrium conditions, diverged in the limit $T \to T_c$. After a rapid quench to the glass phase $T < T_c$, ageing emerged: t_s grew with the waiting time t_w, and diverged in the long time limit $t_w \to \infty$.

Berthier *et al.* then studied the response of these relaxational dynamics to non-zero driving forces, making the connection with rheology by identifying force with stress σ, the value of t_s at long times after quench with the viscosity η, and the ratio σ/η with the shear rate. (Casting the above "zero-stress" results into this language, the model has finite/infinite zero-shear viscosity for temperatures above/below the glass

[6] at least in the absence of any activation processes, which can be incorporated into the theory by hand, and which can wipe out the glass transition.

[7] In fact, this correspondence suggest some deep link between glassy models with quenched disorder, *e.g.* spin glasses, and those in which the disorder is self induced, *e.g.* structural glasses; we shall not pursue this discussion further in this thesis.

transition.) For any stress $\sigma > 0$, they always found a finite, non-ageing value of t_s, even for $T < T_c$: the stress *interrupted* ageing, and restored a non-equilibrium steady state with a finite shear-thinned viscosity. (In the limit of zero stress at $T < T_c$, this steady state value of t_s was found to diverge, in agreement with the fact it becomes infinite at long times after quench in an unstressed system.) Plotting σ against $\dot{\gamma}$, for $T > T_c$ the authors found a linear, Newtonian regime $\sigma \propto \dot{\gamma}$ at small shear rates (consistent with the fact that t_s is finite at such temperatures), but power law fluid behaviour $\sigma \propto \dot{\gamma}^n$ with $n < 1$ for $T < T_c$.

The authors then gave an intuitive physical picture for these results, by considering the system's dynamical evolution within the free energy landscape of its phase space, as elucidated by a rather complicated previous analysis for the purely relaxational model [CK93]. For temperatures $T > T_c$, the available phase space is dominated by one free energy basin, corresponding to the paramagnetic or "liquid" state. At T_c a threshold level appears, below which the phase space fractures into many disconnected regions. After a quench to $T < T_c$, an undriven system gradually descends towards the threshold level; the dynamics age as more disconnected regions of phase space are encountered. External shear interrupts this ageing process by continuously injecting energy into the system, always dragging it along just above the threshold level. Note that the results described above for $T < T_c$ were obtained by driving a system prepared by means of a rapid quench from a high temperature. They do not show a yield stress because (as argued by the authors) the system never has a chance to reach very deep (sub-threshold) levels, and can always be "unstuck" (dragged up the energy landscape) by even very weak driving forces. However the authors further argued that if the system could somehow be prepared in one of these deep, sub-threshold states, it *would* exhibit a yield stress, since a finite force $\sigma > \sigma_y$ would be needed to "unstick" it.

Another MCT model of glassy rheology, more phenomenological than the one just described, was developed by Hébraud *et al.* [HL98, DAL99]. They considered self-consistent dynamics, within mean field, for an ensemble of coupled elastic elements, each with a local yield threshold σ_c. Under application of external shear, each element affinely follows the applied shear, until it reaches the threshold σ_c. It then yields on a time-scale τ (a free parameter), and redistributes its stress (with a redistribution efficiency set by a free parameter α) to other elements in the system. In MCT parlance, the model considers a single mode (of stress fluctuations) which interacts with itself in a non-linear way, although here the fluctuations are cut off at the yield value σ_c. The model has a "paste-transition" at a critical value of the parameter $\alpha = \alpha_c$. For $\alpha > \alpha_c$ the model has a non-zero rate of yielding, even at zero shear rate: it is a fluid, and shows a linear rheological regime at low shear rates. For $\alpha < \alpha_c$, no rearrangements

occur in an unsheared system, and the model (now a paste) shows a yield stress σ_y. Under external driving, the paste is re-fluidized (shear thinned) and rearrangements recommence.

To summarize, both the MCT models just described exhibit a paste transition, showing a linear Newtonian regime in the liquid phase, and shear-thinning power law fluid or yield stress (Bingham fluid) behaviour for the pasty phase. Note, however, that neither model explicitly addresses rheological ageing (despite the fact that the p-spin model inherently shows ageing in its relaxational dynamics).

3.2.3 A "Landau" approach

A very simple phenomenological approach, adopted by Derec *et al.* [DAL00], assigns the system's intrinsic stress relaxation a single rate, called the "fluidity". (Note that this approach notably simplified with respect to the glassy models which we shall consider, in which stress relaxation is described by a whole spectrum of relaxation time-scales $P(\tau)$.) The model captures a paste-transition by assigning the fluidity its own dynamics within a Landau-like equation, which contains a free parameter r. For a given finite initial ($t_w = 0$) fluidized state, the fluidity can either (for $r > 0$) remain finite at long times $t_w \to \infty$ (liquid behaviour) or (for $r < 0$) tend to zero (*i.e.* show an ageing approach to a "stuck" pasty phase). Competing with the system's intrinsic stress relaxation is a systematic tendency for external driving to increase the stress, and re-fluidize the system. Most importantly, shear can restore a finite fluidity to the model's pasty phase.

In the liquid phase, the authors found a linear Newtonian regime at small strain rates ($\sigma \propto \dot{\gamma}$) with a Maxwellian response to small amplitude oscillatory shear. In the pasty phase, the fluidity decreases in time as $t_w^{-\mu}$ with $0 \leq \mu \leq 1$; the extent of the linear rheological regime was found to decay in time as a power law of this fluidity. Within the linear regime, the stress relaxation modulus was demonstrated to be capable of reproducing the observations of sub-ageing in the experiments of Derec *et al.* [DADL00]. Under steady shear, in the pasty phase, the model was shown to reproduce either power law fluid or Bingham fluid behaviour (equations 2.42 and 2.43), depending of the value of certain free parameters which describe the manner in which stress increases with driving.

Having summarized the various approaches adopted by other authors, we now describe the models which we shall study in detail in the remainder of this thesis.

3.2.4 Phenomenological trap models

We recall that the p-spin MCT model of section 3.2.2 is defined by a fundamental microscopic Hamiltonian (equation 3.5), from which a rather complicated analysis (which we did not describe) reveals a phase space characterized by a disordered, rugged (free) energy landscape [CK93]; ageing emerges in the relaxational dynamics by considering the system's dynamics as a progressive slow evolution towards deeper, more disconnected regions of this landscape. (We reiterate, however, that the intrinsic ageing dynamics of this model have not been interpreted in any rheological way.)

This picture rather obviously suggests a more phenomenological (but much simpler) approach to modelling the glass transition, in which one *directly* assumes a disordered trap-like free energy landscape. An important breakthrough in this area was made by Bouchaud, who realized that an ensemble of uncoupled elements exploring a landscape of traps by thermal activation could capture a true glass transition, at a finite temperature $T = T_g$, *provided the distribution of trap depths has an exponential tail* [Bou92, MB96]. For temperatures $T < T_g$, ageing emerges: the system gets stuck in deeper and deeper traps as time progresses; the model has a time-dependent power-law distribution of trapping (relaxation) times $P(\tau, t_w)$ with $\langle\tau\rangle_P$ an increasing function of t_w. In the simplest case the landscape is assigned no spatial structure, and the time-scale for hopping between any two traps depends only upon the energy of the initial trap[8]: here, the model shows simple full ageing, with a single growing time-scale $\langle\tau\rangle = O(t_w)$. A more recent version [RMB00] locates the traps on a cubic lattice, and furthermore gives the hopping probability between any two traps a dependence upon the depth of the final (as well as the initial) trap; here, multiple scaling regimes occur, with *sub-ageing* time-scales (t_w^μ with $\mu < 1$).

In chapters 4 to 6 below we shall study in detail the rheological predictions of the simplest off-lattice version of the trap model, as extended to rheology by Sollich *et al.* [SLHC97, Sol98], by the incorporation of "intra-trap" strain and stress degrees of freedom which couple to external shear driving. (See section 4.2 for details.) Effectively, this driving pulls elements up the side of their traps, and hence hastens the hopping dynamics, resulting in shear-thinning. In this rheological context it was found necessary to replace the true thermodynamic temperature by an effective noise temperature x which is intended to model interactions between different regions of the sample in a mean field way. For $x < 1$ (the glass phase) the model has a macroscopic yield stress σ_y, in qualitative agreement with the experimental data. Provided this is not exceeded,

[8] Note that several choices are possible (*i.e.* consistent with detailed balance) for this hopping probability, some of which can also depend upon the depth of the final trap.

rheological ageing occurs, with the sample's relaxation time-scale always of order its own age. This is clearly in broad agreement with the observations of ageing described above, although note that we see full ageing ($\langle\tau\rangle = O(t_{\rm w})$) rather than the sub-ageing ($\langle\tau\rangle = O(t_{\rm w}^{\mu})$ with $\mu < 1$) of the experiments by Derec *et al.* (above). The loss modulus curves upwards slightly as frequency is lowered (and falls with age $t_{\rm w}$), explaining the apparent experimental violation of linear response theory. For loads *greater* than the yield stress, ageing is interrupted, and the system is re-fluidized: after a transient, the system approaches a non-equilibrium steady (TTI) state, with a constant strain-rate $\dot{\gamma}$ which is related to the stress by the flow curve $\sigma - \sigma_{\rm y} \propto \dot{\gamma}^{1-x}$; the relaxation time-scale is then set by the inverse shear rate, rather than the age. We also study the approach to this steady state via the imposition of constant strain-rate $\dot{\gamma}$. We show that, before the stress settles to its steady-state value, it "overshoots" by an amount which depends significantly on the age of the system when shearing was commenced. For noise temperatures $x > 1$, ageing does not occur (even for small loads), and there is no yield stress. However, for $1 < x < 2$ we still see non-trivial power law fluid behaviour, and anomalous rheological transients (during the slow approach to equilibrium), which we also describe. For $x > 2$ the model reverts to Newtonian flow behaviour.

3.2.5 Kinetically constrained spin models

The second model to be studied in detail in this thesis is a kinetically constrained spin chain. Unlike the trap model, this has no quenched disorder, but instead directly induces its own glassiness by means of a simple kinetic constraint. In its relaxational dynamics, the model shows a slow glassy coarsening a low temperatures [SE99]. We invoke a means of driving the model in a quasi-rheological way. Note that this model is much more abstract than the phenomenological SGR model: it is not intended as a realistic model of any particular rheological system, but just as an over-simplified description of any glassy system subject to external driving or loading. Nonetheless, we find several points of contact with the phenomenology of the SGR model, and of soft glassy materials. In particular, "shear" driving at a constant rate interrupts the low temperature relaxation process, and restores a steady state with a relaxation time-scale set by the inverse shear rate.

Chapter 4

The trap and SGR models

4.1 Trap model

It is widely accepted that the phase space of any glassy system comprises a rough free energy landscape, with many local minima which can "trap" the system for long times. The system cannot evolve freely, but infrequently "hops" between these metastable minima. For structural glasses, an equivalent interpretation in real space is that mesoscopic elements of material are trapped in "cages" formed by their neighbours: the elements cannot move freely, but occasionally rearrange by hopping between cages.

These intuitive ideas were formalized by Bouchaud into a phenomenological trap model [Bou92, MB96], which considers an ensemble of uncoupled elements hopping around a landscape of free energy traps by thermal activation. The traps are assumed to stem from a common "percolation" level, f_0, (see figure 4.1) and are assigned a prior distribution of depths $\rho(E)$. ($E = f_0 - f$, where f denotes the free energy at the bottom of a trap.) An element stuck in a trap of depth E escapes on an activation time-scale

$$\tau(E) = \tau_0 \exp\left(\frac{E}{T}\right), \tag{4.1}$$

after which it quickly hops into another trap[1], the depth of which is assumed to be drawn at random from the distribution $\rho(E)$, and hence to be uncorrelated with the previous one[2].

Within this assumption, the probability, $P(E,t)$, of finding an element in a trap of

[1]The dynamics between traps are fast – there is negligible probability at any time of finding an element at the level f_0 between two traps.

[2]Because of this lack of correlation is does not make sense to think of a particular spatial distribution of traps.

depth E at time t evolves according to [Bou92, MB96]

$$\frac{\partial}{\partial t}P(E,t) = -\frac{1}{\tau(E)}P(E,t) + Y(t)\rho(E) \tag{4.2}$$

in which the first (second) term on the RHS represents hops out of (into) traps of depth E. $Y(t)$ is the overall average hopping rate, $\langle 1/\tau(E)\rangle_{P(E,t)}$.

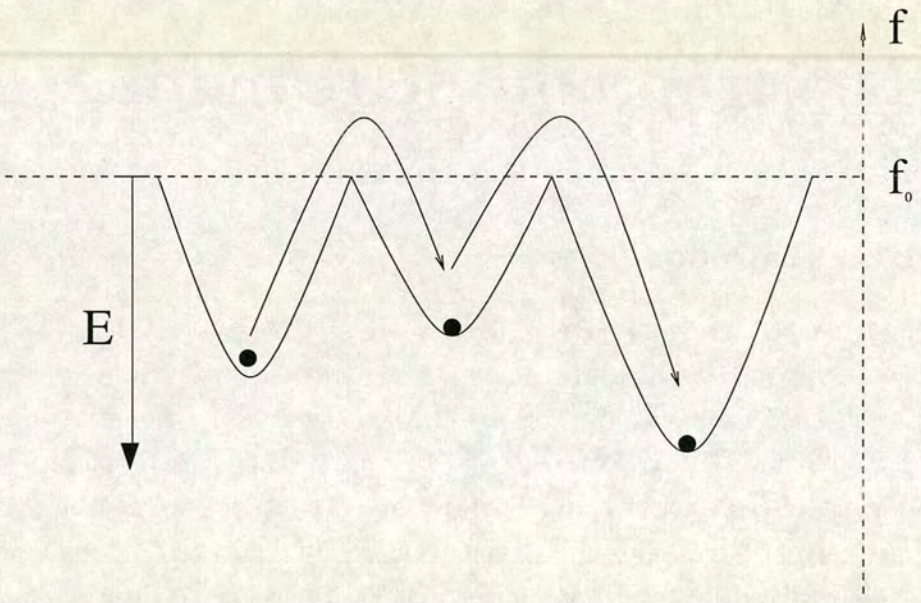

Figure 4.1. Schematic illustration of the dynamics of Bouchaud's trap model.

The remarkable insight of Bouchaud was that, within the following specific choice for the prior distribution [BM97] [3]

$$\rho(E) = \frac{1}{T_g}\exp\left(-\frac{E}{T_g}\right) \tag{4.3}$$

the model exhibits a glass transition at the finite temperature T_g. This can be seen as follows. At a temperature T, the equilibrium state (if it exists) is the Boltzmann distribution

[3] This choice was originally motivated using extreme value statistics in the random energy model of spin glasses.

$$\begin{aligned} P_{\mathrm{EQ}}(E) &\propto \tau(E)\rho(E) \\ &\propto \exp\left(\frac{E}{T}\right)\exp\left(-\frac{E}{T_{\mathrm{g}}}\right). \end{aligned} \tag{4.4}$$

For $T < T_{\mathrm{g}}$, this distribution is unnormalizable, and therefore cannot exist. Equivalently, the lifetime averaged over the prior, *i.e.*

$$\langle\tau\rangle = \int_0^\infty dE\tau(E)\rho(E) \tag{4.5}$$

is infinite. There is therefore no steady state for $T < T_{\mathrm{g}}$. Following a quench into this glass phase the system takes an infinite time to explore phase space – it is "weakly" non-ergodic [Bou92] (see below) – and must therefore age over time. In contrast, for $T > T_{\mathrm{g}}$, the unique equilibrium state $P_{\mathrm{EQ}}(E)$ exists, and must be approached at long times. (There will, however, by transients during the approach to this state.) In what follows, without loss of generality, we re-scale energy such that $T_{\mathrm{g}} = 1$, and time such that $\tau_0 = 1$.

4.1.1 Exact solution

(*Note that the trap model was first solved in [MB96]. Here, we review an alternative solution, offered by [Sol98], which will generalize more easily to the driven trap model (SGR model) in section 4.2. The calculation of the average hopping rate $Y(t)$, with exact prefactors, is the author's own work.*)

We saw above that, for temperatures $T < 1$, the trap model lacks a steady state and must therefore age. We now investigate the dynamics of this ageing process. The time evolution of the trap-depth distribution $P(E,t)$ can be found from equation 4.2 by Laplace transform, and is as follows

$$P(E,t) = P_0(E)\exp\left(-\frac{t}{\tau(E)}\right) + \rho(E)\int_0^t dt' Y(t')\exp\left(-\frac{t-t'}{\tau(E)}\right), \tag{4.6}$$

where $P_0(E)$ is the initial state of the system immediately after preparation at time $t = 0$. (We discuss the preparation procedure in more detail below.) The average hopping rate, $Y(t)$, is found by imposing the normalization $\int_0^\infty dE P(E,t) = 1\ \forall t$ (*i.e.* by conserving probability) to get

$$1 = G_0(t) + \int_0^t dt' Y(t') G_\rho(t-t') \tag{4.7}$$

in which

$$G_\rho(t) = \int_0^\infty dE\rho(E)\exp\left(-\frac{t}{\tau(E)}\right), \tag{4.8}$$

and

$$G_0(t) = \int_0^\infty dEP_0(E)\exp\left(-\frac{t}{\tau(E)}\right). \tag{4.9}$$

Solving equation 4.7 by Laplace transform we get

$$Y(t) = L^{-1}\left\{\frac{L[1-G_0(t)]}{L[G_\rho(t)]}\right\}, \tag{4.10}$$

in which L denotes a Laplace transform with respect to t, and L^{-1} its inversion.

Equations 4.6, 4.8, 4.9 and 4.10 together exactly solve the trap model's dynamics. They can by understood physically by viewing hopping as a "birth and death" process. Each time an element hops it dies and is reborn with an energy selected randomly from the prior distribution $\rho(E)$. The (average) birth rate of elements in traps of depth E is therefore $Y(t')\rho(E)$. The proportion of these which survive without hopping until time t is $\exp[-(t-t')/\tau(E)]$, where $\tau(E) = \exp(E/T)$ is the (mean) lifetime of an element within a trap of depth E. Hence the fraction of elements in traps of depth E, present at time t, which were last reborn at time t' is $Y(t')\rho(E)\exp[-(t-t')/\tau(E)]$. Integrating this over all t', and adding the term $P_0(E)\exp(-t/\tau(E))$ representing the contribution from elements which have survived from time $t = 0$ without hopping at all, we get finally the fraction $P(E,t)$ of elements with energy E. Equivalently, in the integrated version, $G_\rho(t-t')$ is the average of the single-element survival function with respect to all elements born at time t'. $Y(t')G_\rho(t-t')$ is hence the total number of elements, alive at time t, which were last reborn at time t'.

4.1.2 Ageing for $T < 1$ and transients for $T > 1$

We now use this exact solution to describe the trap model's ageing behaviour for $T < 1$, and transient approach to equilibrium for $T > 1$. As a first step, we use equations 4.7 to 4.10 to find the hopping rate $Y(t)$ as a function of the system's age (*i.e.* time t since preparation). We assume an initial condition $P_0(E) = \left(1 - \frac{1}{T_0}\right)\exp\left(\frac{E}{T_0}\right)\rho(E)$, corresponding to a system prepared by means of a rapid quench from equilibrium at an initial temperature T_0. The calculation is performed in appendix 4.3, where the

leading order behaviour in the long time limit ($t \gg 1$) is found to be

$$\begin{aligned} Y(t) &= \frac{T-1}{T} && \text{for } T > 1, \\ Y(t) &= \frac{1}{\ln(t)} && \text{for } T = 1, \\ Y(t) &= \frac{t^{T-1}}{T\Gamma(T)\Gamma(1-T)} && \text{for } T < 1, \end{aligned} \tag{4.11}$$

in which $\Gamma(T)$ is the usual Gamma function. Note that these leading order asymptotes are in fact all independent of the pre-quench temperature[4] T_0 used in the calculation and hence of the choice of initial condition $P_0(E)$. Because of this independence, in much of what follows we can choose a pre-quench temperature $T_0 = \infty$ without loss of generality in the system's behaviour at long-times after quench. We shall hereafter call a quench from an initial temperature $T_0 = \infty$ to a final temperature T a "deep" quench. (See appendix 6.4 for a fuller discussion of this point in a rheological context.)

From the results of equation 4.11, we see that, following a quench to $T > 1$, $Y(t)$ tends to a constant at long times; this suggests that the system reaches (after a transient) a steady state in which most elements have a finite trapping-time. For $T < 1$, in contrast, the hopping rate decays to zero at long times: here, the system must progressively evolve into deeper and deeper traps, such that at very long times it is effectively stuck in infinitely deep traps.

To see this more explicitly, consider the time-evolution of the distribution of time-constants $P(\tau, t)$. Changing variables $E \to \tau$ in equation 4.6, we find

$$P(\tau, t) = P_0(\tau) \exp\left(-\frac{t}{\tau}\right) + \rho(\tau) \int_0^t dt' Y(t') \exp\left(-\frac{t-t'}{\tau}\right). \tag{4.12}$$

At long times $t \gg 1$ the first term on the RHS is negligible compared with the second. Then, approximating the exponential in the integrand of the second term by a sharp cut off $\sim \Theta(\tau - (t - t'))$, we have

$$\begin{aligned} P(\tau, t) &\simeq Y(t)\tau\rho(\tau) \sim Y(t)\tau^{-T} && \text{for } \tau \ll t, \\ P(\tau, t) &\simeq Y(t)t\rho(\tau) \sim Y(t)t\tau^{-(T+1)} && \text{for } \tau \gg t. \end{aligned} \tag{4.13}$$

Using these expressions, together with those of 4.11, we see that for $T < 1$ the limit of $P(\tau, t)$ is zero for any finite τ as $t \to \infty$: the proportion of elements having hopping

[4] They are, however, subject to various sub-dominant corrections (see appendix. 4.3), some of which *are* sensitive to the initial state of the system $P_0(E)$ and hence to the pre-quench temperature.

time of order unity tends to zero as $t \to \infty$. Formally

$$\lim_{t\to\infty} \int_1^b d\tau P(\tau, t) = 0 \tag{4.14}$$

for any constant $b > 1$. The bulk of the distribution's weight is instead at $\tau \simeq t$:

$$\lim_{t\to\infty} \int_{at}^{bt} d\tau P(\tau, t) = O(1) \tag{4.15}$$

for any $0 < a < 1 < b$. This is clearly consistent with the decay of the hopping rate to zero. This ageing evolution of $P(\tau, t)$ is plotted schematically in figure 4.2(b).

In contrast, for a quench temperature above the glass point ($T > 1$), $P(\tau, t)$ shows a transient decay to the final equilibrium state

$$P_{\mathrm{EQ}}(\tau) = \lim_{t\to\infty} P(\tau, t) = (T-1)\tau^{-T} \tag{4.16}$$

as expected. The nature of this transient is shown in Fig. 4.2(a). The final distribution has most of its weight at $\tau = O(1)$.

4.1.3 Weak ergodicity breaking

As noted above, for temperatures $T < 1$ the trap model takes an infinite time to explore phase space: its ergodicity is broken. However, the nature of this ergodicity breaking is somewhat unusual, as we shall now describe. In conventional ("strong") ergodicity breaking, phase space is partitioned into mutually inaccessible "pure states" which are separated by infinite energy barriers: a system rapidly equilibrates within one of these states, and never explores any of the others. (Essentially, the time-scale for hopping between pure states is set to infinity from the outset.) In the trap model, on the other hand, there are a priori (at least for finite times) no infinite barriers between traps. The inter-trap dynamics therefore keep happening on all time-scales, but progressively slow down over time as the system gets into deeper traps. It is this weak ergodicity breaking which is thought to be responsible for ageing in glassy systems [Bou92].

4.2 The SGR model

As described in chapter 3, soft materials as diverse as foams, dense emulsions and pastes all show rheological behaviour suggestive of underlying glassiness and ageing. The trap model just described is a good candidate for modelling this in a unified and simple way, since it reproduces ageing within a very simple set of assumptions, and furthermore

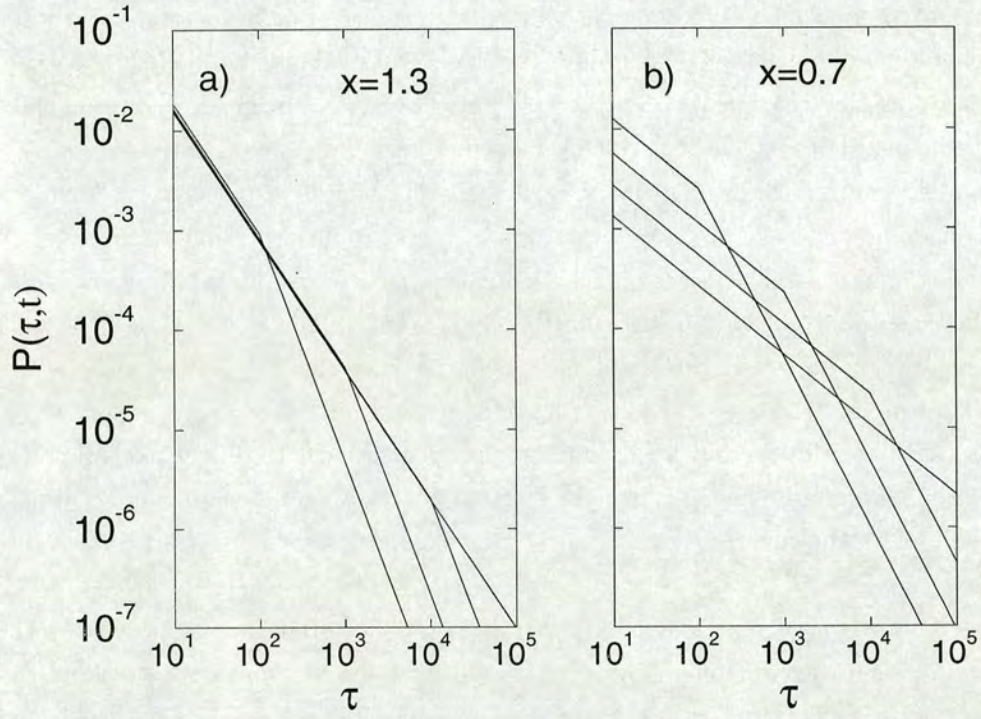

Figure 4.2. Schematic evolution of the relaxation time distribution (a) above the glass transition; (b) below it. The first shows a transient decay onto a steady state, the second shows ageing behaviour. The curves lie in order of increasing t from left to right at the bottom of each figure.

incorporates only those features common to all these "soft glassy materials": namely, (structural) disorder and metastability. This was first recognized by Sollich *et al.*, who incorporated strain and stress degrees of freedom into the model to produce the "soft glassy rheology" (SGR) model [SLHC97, Sol98], which we now describe.

4.2.1 Definition of the model

The SGR model conceptually divides any sample of soft glassy material (SGM) into many mesoscopic elements. By mesoscopic, we mean small enough that any macroscopic sample contains enough elements to allow meaningful averaging over elements, but large enough such that continuum elastic variables can still apply on the elemental scale. To capture the metastability of SGMs, the model assumes these elements to be subject to infrequent local rearrangements, which are the dominant dynamical

processes in the low-frequency regime of interest to us.

In contrast to the dynamics of conventional glassy systems, however, these rearrangements cannot be thermally activated, since they are impeded by energy barriers (denoted E) which (for most SGMs) greatly exceed $k_B T$: in order for an element to rearrange, it must first deform locally which costs energy due to (for the example of a foam) surface tension [WF94]. An obvious alternative origin for rearrangements, in a rheological context, is disturbance caused by external shear. To incorporate this, the model assigns each element its own local strain variable l, measuring deformation away from some local equilibrium with respect to neighbouring elements, and assumes that, under macroscopic straining, each element departs from this equilibrium, acquiring an elastic local stress kl and deformation energy $\frac{1}{2}kl^2$. This elastic straining continues up to the rearrangement threshold $E = \frac{1}{2}kl_{\mathrm{y}}^2$, characterized by a strain l_{y}, beyond which the element "yields", and locally rearranges. Immediately after yield the element is assumed to adopt a new local equilibrium, with respect to different neighbours. Under further macroscopic shear, it deforms from this new equilibrium, and again eventually yields. As the macroscopic strain is increased, therefore, local strains execute a saw tooth motion.

The origin of rearrangements in unsheared materials (or in the linear rheological regime) is less clear, but to allow for these the model assumes that any element can also be "activated" into yielding through noisy non-linear couplings with other elements. These couplings are modelled by means of a "noise temperature", $x \gg T$, although the full physical interpretation of this parameter is as yet unclear.

So far we have discussed "strain-induced" and "noise-induced" yielding in qualitatively different ways. In fact the SGR model captures them both within a unified description: it assumes them *both* to be activated, but with a reduced activation barrier for any elements strained towards its yield threshold. Specifically, an element of yield threshold E and local strain l is assigned a yielding rate [SLHC97, Sol98]

$$\tau^{-1} = \tau_0^{-1} \exp\left[-\frac{\left(E - \frac{1}{2}kl^2\right)}{x}\right]. \tag{4.17}$$

For behaviour between yields, the model makes the simplest assumption that $\dot{l} = \dot{\gamma}$ for each element. In this way, the strain rate is homogeneous throughout the sample. The model does, however, admit inhomogeneities in the local strain l and stress kl, since the time t' at which the local strain was last reset to zero (*i.e.* the time of the last yield event) will in general be different for each element. The main quantity of interest to us for modelling rheological data is of course the macroscopic stress, which

is defined as the average of the local stresses: $\sigma = \langle kl \rangle = \langle k(\gamma(t) - \gamma(t')) \rangle$.

The disorder of SGMs is captured by assuming that each element has a different yield threshold: a freshly yielded element selects its new threshold at random (without regard to the previous one) from a *distribution* $\rho(E)$. This suggests the following interpretation for the SGR model's dynamics, which allows us to make the connection to Bouchaud's trap model. Like the trap model, the SGR model can be thought of as an ensemble of elements exploring a landscape of traps (with a "prior" depth distribution $\rho(E)$) by an activated dynamics (with T replaced by x). The SGR model however also *extends* the trap model's dynamics, by incorporating intra-trap degrees of freedom (local strains) which can be *driven* by external shear. An element in local equilibrium ($l = 0$) is at the bottom of its trap. Macroscopic shear drags it up the side of the trap, thus hastening yielding. This conceptual interpretation is illustrated by figure 4.3.

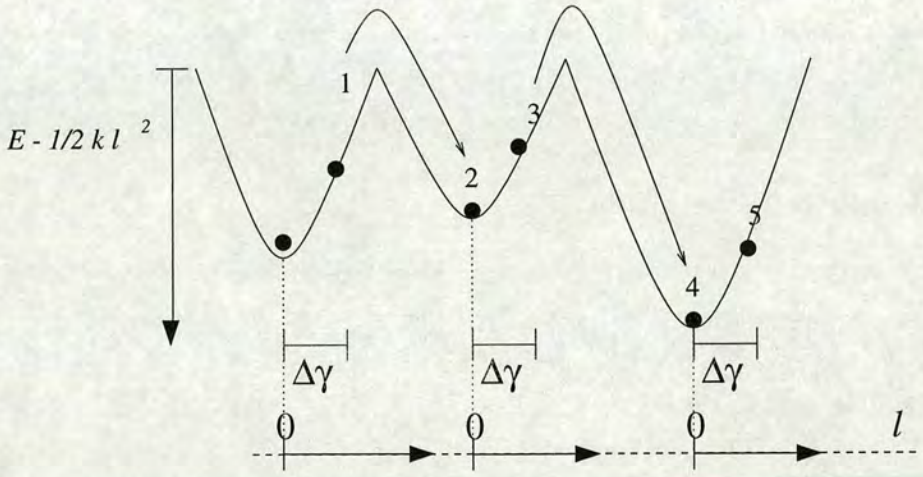

Figure 4.3. Dynamics of the SGR model. A representative particle (1) may hop out of its trap by activated hopping ($1 \to 2$). It enters the new trap in a state of zero local strain ($l = 0$); application of strain $\Delta\gamma$ raises its energy ($2 \to 3$) making a subsequent hop ($3 \to 4$) more likely. Note that the relative horizontal displacement of the quadratic potential wells (traps) is arbitrary; each has its own independent zero for the scale of the local strain l. (Figure taken from [Sol98].)

Following the example of the trap model, the SGR model chooses a prior distribution

$$\rho(E) = \frac{1}{x_g} \exp\left(-\frac{E}{x_g}\right) \tag{4.18}$$

since, when combined with the exponential activation factor 4.17, this captures ageing for $x < x_g$: the steady state $\tau(E)\rho(E)$ becomes unnormalizable at $x = x_g$ (at least in

a regime where all local strains are small). Note, however, that the interpretation of this choice for SGMs is as yet unclear. (In spin glasses it can be justified using extreme value statistics.) The motivation for choosing it is simply that, together with 4.17 (the interpretation of which is equally unclear), it provides a very simple way of capturing a glass transition.

Equation of motion

By analogy to equation 4.2 for the undriven trap model, the dynamics of the SGR model obey

$$\frac{\partial}{\partial t}P(E,l,t) = -\dot{\gamma}\frac{\partial}{\partial l}P - \frac{1}{\tau_0}\exp\left[-\frac{\left(E-\frac{1}{2}kl^2\right)}{x}\right]P + Y(t)\rho(E)\delta(l) \tag{4.19}$$

in which $P(E,l,t)$ is the joint probability for an element to have yield energy E and local strain l at time t. In this equation, (by analogy to equation 4.2) the second (third) term represents hops out (into) of traps. The first term captures the convective increase of local strains due to external driving at rate $\dot{\gamma}$.

4.2.2 Exact solution

We now review the exact solution of the SGR model, as offered by Sollich in [Sol98]. Without loss of generality, we choose energy units in which $x_g = 1$, and time units in which $\tau_0 = 1$. We assume (following [Sol98]) that the material is prepared at time $t = 0$ in a state in which all local stresses kl are zero[5]. The distribution of yield thresholds $P(E,t)$ at a time t after sample preparation is

$$P(E,t) = P_0(E)\exp\left[-\frac{Z(t,0)}{\exp\left(\frac{E}{x}\right)}\right] + \rho(E)\int_0^t dt' Y(t')\exp\left[-\frac{Z(t,t')}{\exp\left(\frac{E}{x}\right)}\right], \tag{4.20}$$

in which $P_0(E)$ is the initial distribution of yield energies, $Y(t)$ is the overall yielding rate at time t, and

$$Z(t,t') = \int_{t'}^{t} dt'' \exp\left(\left[\gamma(t'') - \gamma(t')\right]^2/2x\right). \tag{4.21}$$

[5]Physically, of course, $\langle kl\rangle = 0$ would be a sufficient condition to assume zero macroscopic stress, and is physically more realistic.

Imposing the normalization $\int dEP(E,t) = 1 \; \forall t$ (*i.e.* conserving probability) we find

$$1 = G_0(Z(t,0)) + \int_0^t dt' Y(t') G_\rho(Z(t,t')), \tag{4.22}$$

in which G_ρ and G_0 are defined by equations 4.8 and 4.9 respectively. The macroscopic stress σ at time t is given by

$$\sigma(t) = \gamma(t) G_0(Z(t,0)) + \int_0^t dt' \left[\gamma(t) - \gamma(t')\right] Y(t') G_\rho(Z(t,t')), \tag{4.23}$$

in which strain units have been re-scaled such that $k = 1$. Equations 4.22 and 4.23 (together with 4.8, 4.9 and 4.21) constitute an exact solution for the SGR model. Given any strain (stress) history, one can in principle use them simultaneously to find the hopping rate $Y(t)$ and the required stress (strain) response. Note that the following alternative form of the second constitutive equation (4.23) is sometimes useful:

$$\sigma(t) = \gamma(t) - \int_0^t dt' \gamma(t') Y(t') G_\rho(Z(t,t')). \tag{4.24}$$

This is obtained by substituting equation 4.22 into equation 4.23.

This solution can be understood physically as follows. As in the undriven model, $Y(t')\rho(E)$ is the number of elements "born" at time t' into traps of depth E. A fraction $\exp[-Z(t,t')/\tau(E)]$ of such elements survive until time t without yielding again. Note that in the undriven model this survival function was just $\exp[-(t-t')/\tau(E)]$. In this driven case, the time interval $t - t'$ has been replaced by the effective time $Z(t,t')$, to allow for the fact that strain hastens yielding: in general $Z(t,t') > t - t'$ and the survival function decays more quickly. Averaging the single particle survival function over all particles born at time t', we have an overall survival ("memory") function $G_\rho(Z(t,t'))$. The number of elements present at time t which were last reborn at t' is therefore $Y(t')G_\rho(Z(t,t'))$. Each such element carries a stress $(\gamma(t) - \gamma(t'))$. Integrating $Y(t')G_\rho(Z(t,t'))$ and $(\gamma(t) - \gamma(t')Y(t')G_\rho(Z(t,t'))$ over all t' (and adding terms representing contributions from elements which have not yielded since sample preparation), we therefore get respectively the total number of elements (which is conserved), and the total stress in the sample at time t. Note that in the above solution, the entire effect of strain upon yielding is encoded in the "effective time" interval $Z(t,t')$. In every other respect, equations 4.20 and 4.22 have the same structure as their counterparts for the undriven model.

Linear rheological regime

When all local strains are small, the yield rates are to first order strain-independent. This corresponds to a linear rheological regime, in which external deformation has a negligible effect upon dynamics. We then recover the dynamics of the original trap model. The effective time interval $Z(t,t')$ in equations 4.20 to 4.24 reduces to the actual time-interval $t-t'$; equations 4.20 and 4.22 reduce to their undriven counterparts 4.6 and 4.7 (with T replaced by x); and the model must *age* for $T<1$. (Below, we see that the model can actually sustain ageing even under some non-linear loads, provided these loads do not exceed some threshold σ_y. For large loads ($\sigma > \sigma_y$), or under continuous external shear, elements are prevented from getting stuck in deep traps and ageing is eliminated.)

4.2.3 Sample preparation

As noted above, to solve the consitutive equations 4.22 and 4.23 for the SGR model's rheological behaviour at times $t>0$, one must in principle specify the initial ($t=0$) state, $P_0(E)$. For noise temperatures $x<1$ (which will be the main regime of interest to us), one cannot appeal to equilibrium to fix this, since no equilibrium state exists. Instead, $P_0(E)$ should reflect the way in which the sample was prepared. In what follows we assume for simplicity that the system is prepared at time $t=0$ by means of a rapid quench from $x=\infty$ to the final "working" noise temperature $x=O(1)$.

In practice, of course, such a quench could never be achieved in a laboratory, since x is not tunable from outside the sample. The choice can, however, be motivated by the following speculative arguments [Sol98]. Standard experimental preparation procedure consists of loading the sample into the rheometer, and then (to ensure reproducability in the subsequent behaviour) pre-shearing it. One might argue that the loading stage should introduce a large degree of disorder, and hence to result in a noise temperature $x \gg 1$; indeed the equilibrium state at $x=\infty$ maximises the entropy of the system, and is therefore a reasonable choice in the absence of a more concrete candidate. One might further expect the pre-shear step to order the sample somewhat [WBHA92], causing x to decrease. Indeed, tentative arguments [Sol98] suggest that x should decrease to a final working noise temperature which is close to the glass transition, $x \approx 1$.

Whether or not our deep quench is a good model for this preparation procedure, one can argue that the model's rheological behaviour at long times $t \gg 1$ (which is the regime of interest to us) should in general be rather insenitive to detail of the sample preparation: any system with weak long term memory (of which the SGR model for $x<1$ is an example) will forget perturbations applied at early times (*e.g.* during

preparation) much more rapidly than those applied at late times (*i.e.* during the actual rheological measurement). Indeed, in appendix 6.4 we present the results of a brief study which reveals that the model's rheological behaviour for times $t \gg 1$ is approximately independent of the specific choice of the noise temperature before the quench, x_0. Because of this independence, our choice of $x_0 = \infty$ (deep quench conditions) made in the main text is likely to be a relatively mild assumption.

4.2.4 Rheology under TTI conditions

The rheology of the SGR model under TTI conditions was studied in detail by Sollich [Sol98]. Here we summarize the most important results.

Linear spectra

As noted above, a regime of linear rheological response arises when all local strains l are small. A sufficient condition for this is that the macroscopic strain γ applied to the sample as a whole should be small. For an oscillatory strain, $\gamma = \gamma_0 \exp(i\omega t)$, this is satisfied when $\gamma_0 \ll 1$. At such small amplitudes, the stress response can be encoded in the linear spectra G' and G'' as defined in section 2.2.1. These spectra were calculated by Sollich under equilibrium conditions above the glass point ($x > 1$). The results are as follows

$$\begin{array}{lllll} G'' & \propto \omega & \text{for } 2 < x, & \propto \omega^{x-1} & \text{for } 1 < x < 2. \\ G' & \propto \omega^2 & \text{for } 3 < x, & \propto \omega^{x-1} & \text{for } 1 < x < 3. \end{array} \tag{4.25}$$

(Prefactors are discussed in [Sol98].) Note that these results assume the low frequency limit $\omega \ll 1/\tau_0 = 1$, since experimental time-scales are likely greatly to exceed the attempt time, τ_0.

Hence for $x > 3$, the model behaves (with respect to this oscillatory measurement) as a Maxwell fluid of time-constant $\tau_0 = 1$. At lower noise-temperatures ($1 < x < 3$), $G''(\omega)$ and $G'(\omega)$ show non-trivial power law dependence upon frequency. In particular, as the glass transition $x = 1$ is approached from above, G'' becomes a very flat function of frequency, reflective of the diverging breadth of the underlying spectrum of time-scales.

For $x < 1$ the model ages (at least in this linear regime). The conventional definition of $G'(\omega)$ and $G''(\omega)$ therefore breaks down, and we must use the time dependent counterparts $G'(\omega, t)$ and $G''(\omega, t)$ as introduced in section 2.2.1. These will be calculated in chapter 5.

Flow curves

The flow curve was defined in section 2.2.1 as the steady-state stress response $\sigma = \sigma(\dot{\gamma})$ to shear of constant rate $\dot{\gamma}$. Within the SGR model this is given by (to within prefactors):

$$\begin{array}{lll} \sigma & \propto \dot{\gamma} & \text{for } x > 2, \\ \sigma & \propto \dot{\gamma}^{x-1} & \text{for } 1 < x < 2, \\ \sigma - \sigma_y & \propto \dot{\gamma}^{1-x} & \text{for } x < 1. \end{array} \tag{4.26}$$

(Here the slow driving limit $\dot{\gamma} \ll 1$ is assumed.) Hence for $x > 2$ the model behaves (with respect to this steady shear measurement) as a Newtonian fluid of time-constant $\tau_0 = 1$, with a linear dependence of stress upon strain rate. For $x < 2$, in contrast, there is no regime of linear response (under such steady shear), and the viscosity $\eta = \lim_{\dot{\gamma}\to 0}(\sigma/\dot{\gamma})$ is infinite. For $1 < x < 2$ we see a power law fluid regime. For $x < 1$ the model has a macroscopic yield stress σ_y. For steady loads $\sigma > \sigma_y$ (or for steady shearing at any non-zero rate $\dot{\gamma} > 0$) there exists a steady (TTI) flow regime[6]. This is at first sight rather odd, since for $x < 1$ the model (in its linear regime at least) ages over time. In fact, any applied steady shear of rate $\dot{\gamma} > 0$, or load $\sigma > \sigma_y$, *interrupts* the intrinsic ageing behaviour and restores the driven steady state prescribed by 4.26. (This interruption process is studied more explicitly below, in chapters 5 and 6.) In contrast, for any load $\sigma < \sigma_y$ (still for $x < 1$) we find that the system creeps, with a strain rate which tends to zero at long times (as it must for consistency with 4.26); furthermore, in this regime, the model (like its unloaded counterpart) *ages* over time, such that its characteristic relaxation if always of order the time since quench.

4.2.5 Higher moments

We saw above that the SGR model's ageing behaviour arises from the divergence of the first moment of the distribution $\rho(\tau)$ at the glass transition: the steady-state spectrum of time-constants, $\tau\rho(\tau) \sim \tau^{-x}$, becomes (in the linear regime at least) unnormalizable at $x = 1$. Of course, higher moments of $\rho(\tau)$ become unnormalizable at higher noise temperatures, and formally we can define a whole series of critical x values: as $x = n$ is approached from above, the nth moment of $\rho(\tau)$ diverges. Although this does not lead to ageing in the formal sense defined in section 2.1.1, it does nonetheless lead to anomalous, slow behaviour in any experimental quantity which probes the nth moment of $\rho(\tau)$. In fact, we have already seen two examples of this: the viscosity diverges at

[6]Recall that a flow curve, of which 4.26 is an example, *by definition* refers to a steady-state of constant stress and strain rate.

$x = 2$, reflecting the fact that, under steady shear, the stress response is given by $\sigma \sim \tau P(\tau) \sim \tau^2 \rho(\tau)$. Likewise, the viscoelastic spectra G' and G'' (which probe the second and third moments of $\rho(\tau)$ respectively) show anomalous power law dependence upon frequency for $x < 2$ and $x < 3$ respectively.

This concludes our review of the SGR model, and of its rheology under conditions where TTI apply. In the next two chapters, we describe the novel contribution of this work to the study of the SGR model: a detailed investigation of its rheological behaviour under conditions where TTI does not apply.

4.3 Appendix I: asymptotic analysis for hopping rate $Y(t)$

We now outline our analytical method for solving

$$1 = G_0(t) + \int_0^t dt' Y(t') G_\rho(t - t', T), \tag{4.27}$$

together with

$$G_0(t) = \int_0^\infty dE P_0(E) \exp\left(-\frac{t}{\tau(E)}\right) \tag{4.28}$$

and

$$G_\rho(t, T) = \int_0^\infty dE \rho(E) \exp\left(-\frac{t}{\tau(E)}\right) \tag{4.29}$$

to find the yield rate $Y(t)$ at long times ($t \gg 1$). We assume the system to have been prepared at time $t = 0$ by means of a rapid quench from equilibrium at an initial temperature T_0. This sets the initial state $P_0(E) = \left(1 - \frac{1}{T_0}\right) \exp\left(\frac{E}{T_0}\right) \rho(E)$, and hence $G_0(E) = G_\rho(t, y)$ where $y = T\left(1 - \frac{1}{T_0}\right)$.

As noted in the main text, we use a Laplace transform method. Denoting the conjugate variable to t by λ, we have

$$\frac{1}{\lambda} = \bar{G}_\rho(\lambda, y) + \bar{Y}(\lambda) \bar{G}_\rho(\lambda, T), \tag{4.30}$$

and hence

$$\bar{Y}(\lambda) = \frac{\frac{1}{\lambda} - \bar{G}_\rho(\lambda, y)}{\bar{G}_\rho(\lambda, T)} \tag{4.31}$$

in which

$$\bar{G}_\rho(\lambda, T) = T \int_1^\infty d\tau \frac{\tau^{-T}}{1 + \lambda\tau}. \tag{4.32}$$

The expression for $\bar{Y}(\lambda)$ obtained by substituting equation 4.32 into equation 4.31 is not invertible by any simple method. However a simple expansion which *is* invertible

can be found as follows. Rewriting equation 4.32 we have[7]

$$\bar{G}_\rho(\lambda, T) = T\int_0^\infty d\tau \frac{\tau^{-T}}{1+\lambda\tau} - T\int_0^1 d\tau \frac{\tau^{-T}}{1+\lambda\tau}. \tag{4.33}$$

Rescaling[8] the first integral by putting $s = \lambda t$ we get

$$\bar{G}_\rho(\lambda, T) = T\lambda^{T-1}\int_0^\infty ds \frac{s^{-T}}{1+s} - T\int_0^1 d\tau \frac{\tau^{-T}}{1+\lambda\tau}. \tag{4.34}$$

The first integral on the R.H.S. is just a representation of the beta function [AW95] and therefore

$$\bar{G}_\rho(\lambda, T) = T\Gamma(T)\Gamma(1-T)\lambda^{T-1} - T\int_0^1 d\tau \frac{\tau^{-T}}{1+\lambda\tau}. \tag{4.35}$$

For $|\lambda| < 1$ we expand the second term on the R.H.S. to get

$$\begin{aligned} \bar{G}_\rho(\lambda, T) &= T\Gamma(T)\Gamma(1-T)\lambda^{T-1} - T\int_0^1 d\tau \tau^{-T} \sum_{n=0}^{\infty} (-\lambda\tau)^n \\ &= a(T)\lambda^{T-1} + \sum_{n=0}^{\infty} b_n(T)\lambda^n \end{aligned} \tag{4.36}$$

in which

$$a(T) = T\Gamma(T)\Gamma(1-T), \tag{4.37}$$

and

$$b_n(T) = \frac{T(-1)^{n+1}}{n+1-T}. \tag{4.38}$$

(We note for use elsewhere that the transform 4.36 inverts to give

$$G_\rho(t) = \Gamma(1+T)t^{-T} \tag{4.39}$$

[7]Note that this method can strictly only be used for $T < 1$, since for $T \geq 1$ each term of equation 4.33 is singular. However, our end result equation 4.36 holds for all T by analytic continuation. (At integer T, each term of equation 4.33 has a singular component, but the singularities just cancel one another.)

[8]This simple rescaling argument in principle requires that λ should lie on the positive real axis. By analytic continuation, however, the result of equation 4.34 holds everywhere in the complex λ plane apart from along the negative real axis, where λ^{T-1} has a branch cut.

for $t \gg 1$.) Substituting equations 4.36, 4.37, and 4.38 into equation 4.31, we have

$$\bar{Y}(\lambda) = \frac{\frac{1}{\lambda} - a'\lambda^{y-1} - \sum_{n=0}^{\infty} b'_n \lambda^n}{a\lambda^{T-1} + \sum_{n=0}^{\infty} b_n \lambda^n}, \tag{4.40}$$

where we have adopted the convenient shorthand $a(T) = a$ and $a(y) = a'$, and likewise for the b_n.

For $T > 1$ and $|\lambda| < 1$, expansion of the denominator in this equation gives

$$\begin{aligned} \bar{Y}(\lambda) &= \frac{1}{\lambda}\left(1 - a'\lambda^y - \sum_{n=0}^{\infty} b'_n \lambda^{n+1}\right) \times \\ &\quad \left[\frac{1}{b_0} - \frac{1}{b_0^2}\left(a\lambda^{T-1} + \sum_{n=1}^{\infty} b_n \lambda^n\right) + \frac{1}{b_0^3}\left(a\lambda^{T-1} + \sum_{n=1}^{\infty} b_n \lambda^n\right)^2 + \ldots\right] \\ &= \frac{1}{\lambda}\left[\frac{1}{b_0} - \frac{a}{b_0^2}\lambda^{T-1} - \frac{a'}{b_0}\lambda^y + O\left(\lambda^{2(T-1)}, \lambda^{y+T-1}, \ldots\right)\right], \end{aligned} \tag{4.41}$$

whereas for $T < 1$ and $|\lambda| < 1$ we have

$$\begin{aligned} \bar{Y}(\lambda) &= \frac{1}{\lambda}\left(1 - a'\lambda^y - \sum_{n=0}^{\infty} b'_n \lambda^{n+1}\right) \times \\ &\quad \left[\frac{\lambda^{1-T}}{a} - \left(\frac{\lambda^{1-T}}{a}\right)^2 \sum_{n=0}^{\infty} b_n \lambda^n + \left(\frac{\lambda^{1-T}}{a}\right)^3 \left(\sum_{n=0}^{\infty} b_n \lambda^n\right)^2 + \ldots\right] \\ &= \frac{1}{\lambda}\left[\frac{\lambda^{1-T}}{a} - \frac{b_0 \lambda^{2(1-T)}}{a^2} - \frac{a'}{a}\lambda^{y+1-T} + O\left(\lambda^{3(1-T)}, \lambda^{y+2(1-T)}, \ldots\right)\right] \end{aligned} \tag{4.42}$$

To invert $\bar{Y}(\lambda)$, we must integrate $\bar{Y}(\lambda)\exp(\lambda t)$ round a contour in the complex λ plane which completely encloses all the singularities of $\bar{Y}(\lambda)$. Now the expansions 4.41 and 4.42 are only valid inside the circle for which $|\lambda| < 1$, where they have a branch cut along the negative real axis, corresponding to the trap model's continuous spectrum of time-constants between $\tau_0 = 1$ and ∞. In this region, a term of the form $\lambda^{-(m+1)}$ (with $m < 0$) coincides with the Laplace transform of a function which is $t^{-m}/\Gamma(1+m)$ for $t > 1$. Outside this circle $Y(\lambda)$ must be analytic, since there is no relaxation time-scale in the system greater than one. Hence, up to terms of $O(\exp(-t))$ [9] we can invert

[9] arising from the fact that the Laplace transform of $t^{-m}/\Gamma(1+m)$ also has singularities to the left of the circle $|\lambda| < 1$, which invert to give terms of $O(\exp(-t))$.

equation 4.41 to get

$$Y(t) = \frac{1}{b_0} - \frac{1}{\Gamma(2-T)}\frac{a}{b_0^2}t^{1-T} - \frac{1}{\Gamma(1-y)}\frac{a'}{b_0}t^{-y} + O\left(t^{2(1-T)}, t^{1-T-y}\right), \tag{4.43}$$

the first term of which is the asymptotic expression for $Y(t)$ at $T > 1$, as in equation 4.11.

For $T < 1$, on the other hand, we have

$$Y(t) = \frac{1}{\Gamma(T)}\frac{t^{T-1}}{a} - \frac{1}{\Gamma(1+2(T-1))}\frac{b_0 t^{2(T-1)}}{a^2} - \frac{a'}{a\Gamma(T-y)}t^{T-1-y} + O\left(t^{3(T-1)}, t^{2(T-1)-y}\right) \tag{4.44}$$

the first term of which is the asymptotic expression for $Y(t)$ at $T < 1$, as given in equation 4.11.

To obtain $Y(t)$ *at* the glass point $T = 1$ we rewrite equation 4.42 as

$$\bar{Y}(\lambda) = -\frac{1}{b_0\lambda}\left[\sum_{n=1}^{p}(z(\lambda))^n + O\left(\lambda^y, \lambda, \lambda^{(p+1)(1-T)}...\right)\right] \tag{4.45}$$

in which $z(\lambda) = -b_0\lambda^{1-T}/a$ and p is the largest integer which is less than $(1/(1-T))$. Inversion of the Laplace transform equation 4.45 gives

$$Y(t) = \frac{-1}{b_0}\sum_{n=1}^{p}\frac{[z(t)]^n}{\Gamma(1+n(T-1))} + O\left(t^{-y}, t^{(p+1)(T-1)}, ...\right), \tag{4.46}$$

in which $z(t) = -b_0 t^{T-1}/a$. Expansion of the Gamma function about $T = 1$ gives

$$\begin{aligned} Y(t) &= -\frac{1}{b_0}\left[\sum_{n=1}^{p} z^n(t) - (T-1)\Gamma'(1)\sum_{n=1}^{p} n z^n(t) + O(T-1)^2\sum_{n=1}^{p} n^2 z^n(t)\right] \\ &= -\frac{1}{b_0}\left(\frac{z}{1-z} - (T-1)\Gamma'(1)z\frac{\partial}{\partial z}\left(\frac{z}{1-z}\right) + O\left\{\left[(T-1)z\frac{\partial}{\partial z}\right]^2\left(\frac{z}{1-z}\right)\right\}\right) \\ &= -\frac{1}{b_0}\left(\frac{z}{1-z} - (T-1)\Gamma'(1)\frac{z}{(1-z)^2} + O\left\{\left[(T-1)z\frac{\partial}{\partial z}\right]^2\left(\frac{z}{1-z}\right)\right\}\right) \end{aligned} \tag{4.47}$$

(where there are further corrections of $O\left(t^{-y}, t^{(T-1)(p+1)}\right)$ on each line of the R.H.S.) Setting $\delta = 1 - T$ gives $a = (1-\delta)\Gamma(1+\delta)\Gamma(1-\delta)/\delta$, $b = (1-\delta)/\delta$, $z = t^{-\delta}/(\Gamma(1+\delta)\Gamma(1-\delta)) = 1 - \delta\ln(t) + O(\delta^2\ln^2(t))$ and therefore

$$Y(t) = \frac{\delta}{1-\delta}\left[\frac{1}{\delta\ln(t)} + \frac{\Gamma'(1)}{\delta\ln^2(t)} + O\left(\frac{1}{\delta\ln^3(t)}, \delta^0, ...\right)\right]. \tag{4.48}$$

Taking the limit $\delta \to 0$ (equivalently $T \to 1$) we recover an asymptotic ($t \gg 1$) expression for the yield rate at the glass point

$$\lim_{T\to 1} Y(t) = \frac{1}{\ln(t)} + \frac{\Gamma'(1)}{\ln^2(t)} + O\left(\frac{1}{\ln^3(t)}\right), \tag{4.49}$$

in which the first term on the R.H.S. is the result as given in equation 4.11.

We note that all the long-time asymptotes just extracted are independent of the state of the system at the time of preparation, since none of them depend upon the pre-quench temperature T_0. We now consider briefly the extent to which T_0 (via y) affects sub-leading terms of $Y(t)$. For $T > 1$ the largest y-dependent term in $Y(t)$ is $O(t^{-y})$, which becomes progressively more important as we consider smaller values of the pre-quench temperature T_0. However, provided we restrict ourselves to the regime $T_0 > T$ (*i.e.* to a non-equilibrium situation in which a quench is actually performed[10]) we see that $t^{-y} < t^{1-T}$ and that, even to sub-leading order $Y(t)$ is independent of T_0. (We note furthermore that in the case of the deep quench defined in section 4.2.2, $y = T$ and the term t^{-y} is very small).

For $T < 1$, the largest y-dependent term in $Y(t)$ is $O(t^{T-1-y})$. The relative importance of this term again depends upon the relative values of the pre- and post-quench temperatures. For a high enough pre-quench temperature (specifically, provided $y > 1-T$, *i.e.* $T_0 > T/(2T-1)$, which we note can only be satisfied for $T > 0.5$) the sub-leading term of $Y(t)$ is independent of T_0. For any post-quench temperature $T < 0.5$, the sub-leading term necessarily depends upon T_0 since the above condition for independence can't be satisfied. This is physically intuitively reasonable, because in general we expect a system at a lower temperature to remember its initial condition more strongly.

4.4 Appendix II: numerical calculation of hopping rate $Y(t)$

We shall now outline our numerical method for solving the linearized constitutive equation 4.22 for the yield rate $Y(t)$ at times $t > 0$. Note that nowhere in the thesis do we present our numerical results for this quantity: they are merely used as an input into the stress-strain constitutive equation 4.23 for calculation of the various linear rheological response functions described in chapters 5 and 6.

[10] $T = T_0$ corresponds to equilibrium conditions.

Our basic tactic is to discretize time into a grid $t_0, t_1 ...$ (with $t_0 = 0$), and to calculate Y at each point on this grid. The integral form of 4.22 clearly renders Y at any time t dependent upon its values at all previous times t' where $0 < t' < t$. Our method therefore consists of finding, at any time step t_n an (approximate) expression for Y_n in terms of all previously calculated data points $(t_0 = 0, Y_0), (t_1, Y_1) ... (t_{n-1}, Y_{n-1})$; together with the (known) initial condition $Y_0 = \langle (1/\tau)\rho(\tau) \rangle = x/(1+x)$ this enables us to "march out" along the grid, calculating Y at successively larger time-steps. To find this expression, equation 4.22 is differentiated to give:

$$0 = \frac{dG_0(t_n)}{dt_n} + Y(t_n) + \int_0^{t_n} dt' Y(t') \frac{G_\rho(t_n - t')}{dt_n}. \tag{4.50}$$

Approximating $Y(t')$ for $t_{n-1} < t' \leq t_n$ by linear interpolation between (t_{n-1}, Y_{n-1}) and the as yet unknown point (t_n, Y_n) this gives:

$$\begin{aligned} 0 \;=\; & \frac{dG_0(t_n)}{dt_n} + Y_n + \int_0^{t_{n-1}} dt' Y(t') \frac{G_\rho(t_n - t')}{dt_n} \\ & + Y_n \int_{t_{n-1}}^{t_n} dt' \frac{G_\rho(t_n - t')}{dt_n} - \left(\frac{Y_n - Y_{n-1}}{t_n - t_{n-1}} \right) \int_{t_{n-1}}^{t_n} dt' (t_n - t') \frac{G_\rho(t_n - t')}{dt_n} \end{aligned} \tag{4.51}$$

which can be rearranged for Y_n. $Y(t')$ for t' between 0 and t_{n-1} is then approximated in terms of the previously calculated points $(t_0, Y_0), (t_1, Y_1) ... (t_{n-1}, Y_{n-1})$ using a NAG spline interpolator, and the integrals evaluated using a NAG integrator.

The method described so far is a relatively standard technique [PTVF92] for solving equations of the form of 4.22, which is just a Volterra equation of the second kind. The main subtlety in our case if the choice of grid. Now for times $t \gg 1$ we expect the hopping rate to be a power law, and therefore expect relative discretization errors given a time-step Δt to scale a function of $\Delta t / t_n$. Therefore, once we have chosen an acceptable (constant) value for the discretization error, we are at liberty to increase the time-step Δt linearly in time t_n (*i.e.* to use a geometric time-grid). This allows us to generate data over many decades with relatively little computational effort.

Matching the numerical solution onto the analytical asymptote

The technique just described enables us to get good numerical data for $Y(t)$ for times up to a final time $t_f = O(10^7)$. However, since $Y(t)$ is subsequently to be used as an input into other calculations, it is actually useful to have data for longer times still. Of course, for such long times, $Y(t)$ is very well approximated by its analytical asymptote as given by equation 4.11. In principle, then, once the numerical calculation fails, we could just switch to outputting this asymptote. However, this in fact always gives rise

to a small glitch in $Y(t)$, which causes problems when the data for $Y(t)$ is subsequently used as in input integrand in other calculations. To smooth this glitch, we use the following method.

At any time t, we denote by r the ratio of the "actual" value of $Y(t)$ to the analytical asymptote Y_a of equation 4.11; the quantity $1 - r = \delta$ should clearly tend to zero as $t \to \infty$. Assuming the numerical result to be a very good approximation to the actual value of Y for times $t < t_f$, we use this (together with the formula of equation 4.11) to calculate δ for grid-times in this range. The final *calculated* point in this range, at our final t value, t_f, clearly has a non-zero value for δ. However, the actual (theoretical) final point (corresponding to $t = \infty$, $t' = 0$) is known to have $\delta = 0$. Using this fact, we set up a NAG interpolation of δ vs. the transformed time $t' = 1/(1 + t)$ over the entire range $t' = 0 \to 1$ (corresponding to $t = 0 \to \infty$. For any time $t > t_f$ we used this interpolation to look up the value of δ and then (trivially) to perform the inverse transformation for $Y(t) = Y_a(1 - \delta)$.

Chapter 5

Rheological ageing: imposed strain

So far, we have reviewed the exact constitutive solution of the SGR model, and discussed its mapping, in the linear rheological regime, to that of Bouchaud's trap model. Using this mapping, we have seen that (in the linear regime at least) the SGR model must *age* for $x \leq 1$: its constituent elements evolve towards progressively larger yield thresholds, and the average yield rate correspondingly tends to zero at long times after quench. In contrast, for $x > 1$ the model shows transient approach to an equilibrium state in which the majority of elements have yield thresholds of $O(1)$.

We have also reviewed the SGR model's rheology under TTI conditions, discussing the viscoelastic spectra in equilibrium for $x > 1$, in addition to the flow curves relating strain rate to stress under steady shear. We noted in particular that a steady flow regime can exist (with $\sigma - \sigma_y \sim \dot{\gamma}^{1-x}$) even in the regime $x < 1$, where the *unperturbed* trap model has *no* steady state: hence, ageing must be interrupted by any steady shear of rate $\dot{\gamma} > 0$ or steady load $\sigma > \sigma_y$.

In this chapter, and the following one, we describe our new rheological results for the SGR model. We focus particularly on ageing, *i.e.* on the regime $x < 1$, for experiments in which the stress does not (at least continuously) exceed σ_y. In this rheological context, we expect ageing to manifest itself as a characteristic "hardening" process, in which the material evolves from a liquid-like to a solid-like state over time. We shall also present results for the crossover, via anomalous long transients, to equilibrium behaviour for $x > 1$. (The case $x = 1$ shows its own very weak form of ageing and is, where necessary, treated separately.) We also discuss the interruption of ageing, and corresponding transient approach to a steady flow regime, through the application of stress $\sigma > \sigma_y$ or strain of rate $\dot{\gamma} > 0$.

For simplicity, we consider (for all x values) only the idealized deep quench method of sample preparation described in section 4.2.3 above. This sets the initial distribution of yield energies to be $P_0(E) = \rho(E)$, and hence we have $G_0(Z(t,0)) = G_\rho(Z(t,0))$ in the constitutive equations 4.22 and 4.23. Whether a deep quench is a good approximation to any experimental preparation procedure remains an open question. However, we have shown in appendix 6.4 (at the end of these two chapters of results for this model) that our results are relatively robust to variations in the initial state. Hence our specific choice $P_0(E)$, made largely for convenience, is likely to give a good representation of the model's behaviour.

Finally, we note that the constitutive equations 4.22 and 4.23 are more easily solved to find the stress response to an imposed strain (rather than vice-versa). We therefore focus first on strain-controlled experiments and defer to chapter 6 our study of stress-controlled rheology.

5.1 Linear response

As described in section 4.2.2 above, when local strains are small the dynamics of SGR model are the same as those of the original trap model: this corresponds to a linear rheological regime in which the system's intrinsic dynamics are unperturbed by any external probe. The effective time interval $Z(t,t')$ in equations 4.23 and 4.22 is just the actual time interval $t - t'$, and the hopping rate $Y(t')$ is the strain-independent function of time given in equation 4.11. The stress response to any strain history then follows from equation 4.23, by straightforward integration. In this section, we shall study linear step and oscillatory strains, and linear shear startup.

5.1.1 Step strain

Here, we discuss the SGR model's stress response to a step strain

$$\gamma(t) = \gamma_0 \Theta(t - t_w), \tag{5.1}$$

restricting ourselves to small deformations ($\gamma_0 \ll 1$), for which response is linear[1]. Substituting equation 5.1 into the linearized[2] constitutive equation 4.24 we get[3] the

[1] As we shall describe below, each element deforms by an amount γ_0 upon strain application, and thereafter acquires no further strain. Hence $\gamma_0 \ll 1$ ensures linearity in this experiment.

[2] For which $Z(t,t') = t - t'$.

[3] By construction of the SGR model, the linear step strain response is actually identical to the correlation function defined by Bouchaud for his trap model [Bou92, MB96].

following expression for the stress relaxation modulus (as defined in equation 2.14):

$$G(t-t_{\rm w},t_{\rm w}) = 1 - \int_{t_{\rm w}}^{t} dt' Y(t') G_{\rho}(t-t'). \tag{5.2}$$

In appendix 5.3.1 we extract analytic asymptotes from this expression in the regime $t - t_{\rm w} \gg 1$ and $t_{\rm w} \gg 1$, when experimental time-scales are large compared with the mesoscopic attempt time $\tau_0 = 1$. In this limit, we further identify two distinct regimes, according to whether the observation interval $t - t_{\rm w}$ is small or large compared with the sample age $t_{\rm w}$ at the time of stress application: *i.e.* we have a short time interval regime defined by $t - t_{\rm w} \ll t_{\rm w}$ and long time interval regime $t - t_{\rm w} \gg t_{\rm w}$. Our results are summarized in table 5.1. They can be understood physically as

	$G(t-t_{\rm w},t_{\rm w})$ for $t-t_{\rm w} \ll t_{\rm w}$	$G(t-t_{\rm w},t_{\rm w})$ for $t-t_{\rm w} \gg t_{\rm w}$
$x > 1$	$\Gamma(x)\,(t-t_{\rm w})^{1-x}$	$(x-1)\Gamma(x)\dfrac{t_{\rm w}}{(t-t_{\rm w})^{x}}$
$x = 1$	$1 - \dfrac{\ln(t-t_{\rm w})}{\ln(t_{\rm w})}$	$\dfrac{t_{\rm w}}{t-t_{\rm w}}\dfrac{1}{\ln(t_{\rm w})}$
$x < 1$	$1 - \dfrac{1}{\Gamma(2-x)\Gamma(x)}\left(\dfrac{t-t_{\rm w}}{t_{\rm w}}\right)^{1-x}$	$\dfrac{1}{\Gamma(1+x)\Gamma(1-x)}\left(\dfrac{t_{\rm w}}{t-t_{\rm w}}\right)^{x}$

Table 5.1. Stress response to step strain at short and long times. The limit $t-t_{\rm w} \to \infty$ and $t_{\rm w} \to \infty$ is assumed. $\Gamma(x)$ denotes the usual Gamma function.

follows. Upon application of the step strain, the local strain l of each element exactly follows the macroscopic one[4]. The instantaneous response is therefore elastic: we have $G(0,t_{\rm w}) = 1$. Over subsequent times, $t - t_{\rm w}$, the macroscopic stress is progressively relaxed as elements yield. When any element yields it (by assumption of the model) resets its stress to zero. The stress remaining at any time t is therefore just the fraction of elements which remain unyielded over the interval $t - t_{\rm w}$. Making the approximation that an element of relaxation time τ will yield *at* time $t_{\rm w} + \tau$, this is just the fraction

[4]Recall that $\dot{l} = \dot{\gamma}$ for each element between yields.

$\int_{t-t_w}^{\infty} d\tau P(\tau, t_w)$ which, at time t_w, had time constants greater than $t - t_w$. Using the approximate expressions given in equation 4.13 above, we find

$$\begin{aligned} G(t-t_w, t_w) &\simeq 1 - \int_1^{t-t_w} d\tau P(\tau, t_w) \simeq 1 - x\frac{(t-t_w)^{1-x}-1}{t_w^{1-x}-x} \quad \text{for} \quad t - t_w \ll t_w, \\ G(t-t_w, t_w) &\simeq \int_{t-t_w}^{\infty} d\tau P(\tau, t_w) \simeq \frac{(1-x)t_w(t-t_w)^{-x}}{t_w^{1-x}-x} \quad \text{for} \quad t - t_w \gg t_w. \end{aligned} \tag{5.3}$$

(Hence, in measuring response to a small step strain, we are probing the properties of the system *as they were at the time of strain application.*) In fact, the estimates of equation 5.3 approximate our numerical data (which is presented below) quite well. Even better agreement is obtained by adjusting the prefactors to fit the asymptotic results in table 5.1:

$$\begin{aligned} G(t-t_w, t_w) &\simeq 1 - \frac{\Gamma(x)(t-t_w)^{1-x}-1}{\Gamma^2(x)\Gamma(2-x)t_w^{1-x}-1} \quad \text{for} \quad t - t_w \ll t_w, \\ G(t-t_w, t_w) &\simeq \frac{(x-1)\Gamma(x)t_w(t-t_w)^{-x}}{1-\Gamma(x)\Gamma(x+1)\Gamma(2-x)t_w^{1-x}} \quad \text{for} \quad t - t_w \gg t_w, \end{aligned} \tag{5.4}$$

In the limit $t - t_w \to \infty$ and $t_w \to \infty$, these reproduce (by construction) the results shown in table 5.1 for $x > 1$ and $x < 1$; logarithmic terms at the glass point ($x = 1$) can be recovered by taking the limit $x \to 1$ first. These formulae agree well with our numerical results for $G(t - t_w, t_w)$, at least over the noise temperature range 0 to 2 (see figure 5.1). For fitting experimental data at x values close to 1, they are likely to be more useful than the asymptotic results quoted in table 5.1, since they capture the crossover between the $x = 1$ and $x \neq 1$ behaviour[5].

Ageing for $x \leq 1$; transients for $x > 1$

As already described, following a quench to a noise temperature $x > 1$, the linear SGR model will always eventually equilibrate; in contrast for $x \leq 1$ it perpetually evolves towards ever deeper regions of its energy landscape. Hence we expect our analytical results for $G(t - t_w, t_w)$ (in table 5.1) to violate the equality 2.4 for $x \leq 1$, and to satisfy it for $x > 1$; this is indeed what we find. Equation 2.5 further reveals that the long term memory associated with the ageing behaviour for $x \leq 1$ is *weak*: even in its glass phase, the system has no memory of a perturbation of finite duration which was applied in the distant past.

[5]The expressions quoted in table 5.1 for $x \neq 1$ are only valid after cross over times $(t-t_w)^{|x-1|} \gg 1$ and $t_w^{|x-1|} \gg 1$; for $(t-t_w)^{|x-1|} \lesssim O(1)$ and $t_w^{|x-1|} \lesssim O(1)$, $G(t-t_w, t_w)$ has the forms quoted for $x = 1$.

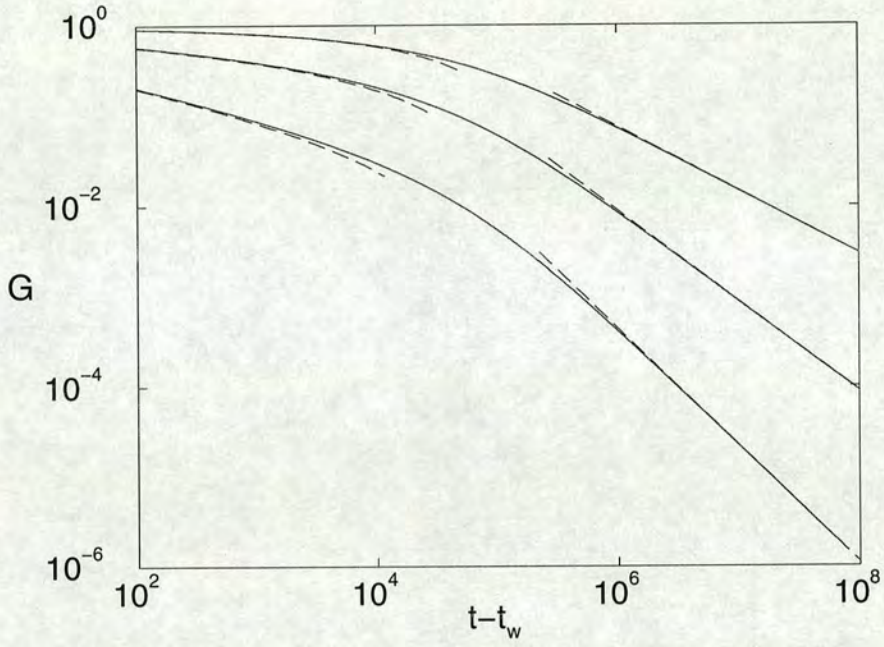

Figure 5.1. Approximate curves for $G(t - t_w, t_w)$ generated using the interpolating formulae 5.4 (dashed lines), compared with numerical data for this quantity (solid lines). Solid curves downwards show numerical data for G vs. $t - t_w$ at noise temperatures $x = 0.7$, $x = 1.0$ and $x = 1.3$ respectively. The waiting time t_w is 10^5.

To see the distinction between ageing and transients more clearly, consider our numerical results for $G(t - t_w, t_w)$, as shown in figure 5.2. Above the glass transition, the stress decay at short time intervals ($t - t_w \ll t_w$) depends only upon the time interval ($t - t_w$) between strain imposition and stress measurement; it does not depend explicitly on the waiting time t_w. This is because the traps which contribute to stress decay at such short times are mainly those with short lifetimes $\tau < t - t_w$; and the population of these traps has already reached equilibrium before the strain is switched on (see figure 4.2(a)). For progressively larger values of t_w, this short-time portion of the decay (which by definition persists to $t - t_w = at_w$ with a a small constant) obviously extends to progressively larger intervals $t - t_w$ and accounts for a correspondingly larger fraction of the total stress decay. Taking the limit $t_w \to \infty$ at constant $t - t_w$ (*i.e.*, letting the system fully equilibrate *before* we apply the strain) we recover a TTI stress relaxation function; the whole of the stress decay decays to zero on time-scales of order the mesoscopic attempt time (one in our units). On the other hand, for any finite waiting time t_w, the stress decay at long times ($t - t_w \gg t_w$) violates TTI, since it

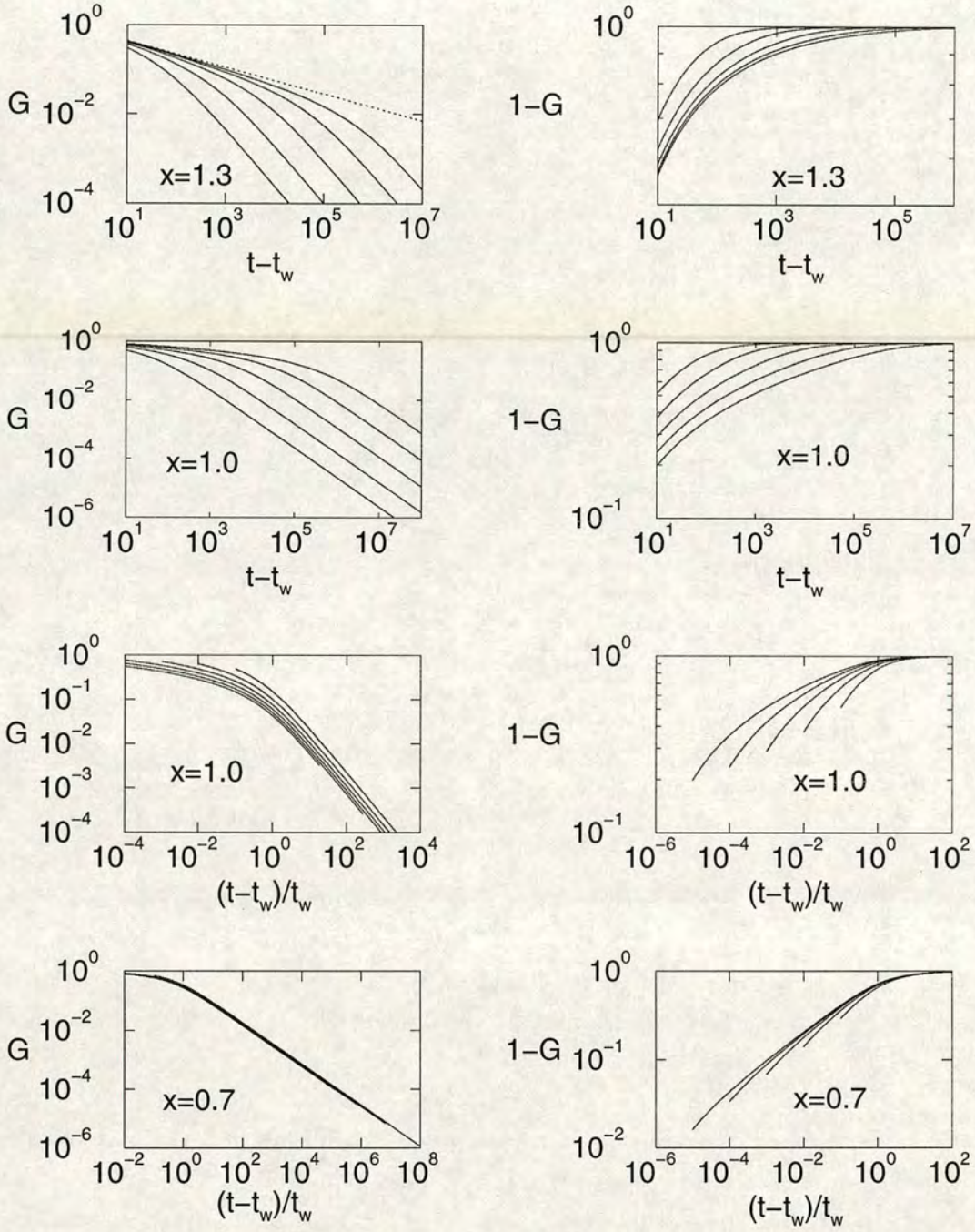

Figure 5.2. Left column: age-dependent stress relaxation modulus $G(t-t_{\rm w}, t_{\rm w})$ against scaled time interval $(t-t_{\rm w})/t_{\rm w}$ (for $x \leq 1$) and time interval $t-t_{\rm w}$ (for $x \geq 1$). Right column: $1-G(t-t_{\rm w}, t_{\rm w})$, plotted similarly. Shown are data for waiting times $t_{\rm w} = 10^2, 10^3 \ldots 10^6$ (left to right for top four graphs, right to left for bottom four graphs). Transients are visible in the top left figure, as follows: The curves coincide at short time intervals $t-t_{\rm w} \ll t_{\rm w}$. At large $t_{\rm w}$, this regime accounts for more and more of the decay of G; the remaining $t_{\rm w}$-dependence is only through an unimportant tail. For $t_{\rm w} \to \infty$, the "short time" regime extends to all finite values of $t-t_{\rm w}$; one recovers the equilibrium response (shown as the dotted line) which decays to zero on a $t_{\rm w}$-independent time-scale. Ageing is visible at bottom left, where the major part of the decay of G occurs on a time-scale of order $t_{\rm w}$ itself, with unimportant corrections to this scaling at early times.

is controlled by decay out of deep traps ($\tau \gg t_w$) which had not already equilibrated before t_w. This is not, however, an ageing effect, since this non-TTI "long-time" tail of $G(t - t_w, t_w)$ accounts for ever smaller fractions of the total decay as t_w becomes large. Equivalently, if we assume that $G(t - t_w, t_w)$ can be measured reliably only as long as it remains greater than some specified "noise" value, the results will become t_w-independent for sufficiently large t_w.

Below the glass point ($x \leq 1$) we see true ageing, rather than the anomalous transients just described: in accordance with our definition of section 2.1.1, a *significant part of the stress relaxation* $G(t - t_w, t_w)$ *now takes place on time-scales that increase with the sample age*, t_w. In fact, in the case of the SGR model, this applies to the *complete* stress relaxation: for $x < 1$, G depends on time only through the ratio $(t - t_w)/t_w$. (Recall that in general, more complicated ageing scenarios are possible: see the discussion of section 2.1.1. For example, one might expect the first part of the stress decay to take place rapidly, on time-scales of $O(1)$, and the final part to decay on time-scales $O(t_w)$.) It is still true that stress decay during the interval $t - t_w$ is dominated by traps for which $\tau < t - t_w$, but no longer true that these traps have reached Boltzmann equilibrium by time t_w: in an ageing system such equilibrium is never attained, even for a subset of shallow traps (see figure 4.2(b)). Instead, the population of such traps gradually falls with age, as the system evolves progressively towards higher yield thresholds. In this case (in contrast for the $x > 1$ behaviour just described) at the end of the short-time regime (*i.e.* for time intervals $t - t_w \approx t_w$), an $O(1)$ fraction of the stress is unrelaxed, even for very long waiting times. Even in an experiment that can only resolve values of G above a given noise threshold, we would detect that the stress relaxation becomes slower and slower as t_w increases. The limit $t_w \to \infty$ (for any fixed finite $t - t_w$) now gives completely arrested, elastic behaviour.

Note that the dependence of G (for $x < 1$) upon the ratio $(t - t_w)/t_w$ means that the SGR model gives us a concrete example of Struik's "time ageing-time superposition" principle (see section 3.2.1), with an ageing exponent $\mu = 1$: the relaxation curves for different t_w can be collapsed onto one another by rescaling the time interval $t - t_w$ by the sample age, as seen in figure 5.2.

5.1.2 Oscillatory strain

Here, we calculate the SGR model's stress response to an oscillatory strain

$$\gamma(t) = \gamma_0 \Re e^{i\omega t} \Theta(t - t_s) \tag{5.5}$$

A sufficient condition for linearity is $\gamma_0 \ll 1$, since γ_0 sets the maximum local strain which can be developed by any element.

Inserting equation 5.5 into the linearized version[6] of the constitutive equation 4.24, we find the following expression for the linear viscoelastic spectrum (as defined in equation 2.34)

$$G^*(\omega, t, t - t_s) = 1 - \int_{t_s}^{t} dt' e^{-i\omega(t-t')} Y(t') G_\rho(t - t'). \tag{5.6}$$

We shall as usual be interested in the regime where experimental time-scales are large compared with mesoscopic attempt time, and hence confine ourselves to the low frequency limit $\omega \ll 1$ at large times $t \gg 1$, $t_s \gg 1$, $t - t_s \gg 1$.

In principle, G^* depends upon the time t_s when the oscillation was started: while in non-ageing systems dependence upon t_s is invariably lost after a transient start-up interval, in ageing systems this simplification is certainly *not* guaranteed (see section 2.2.1). However, for the SGR model we find that dependence upon t_s in fact *is* weak, *even in the ageing (glass) phase, provided* the conditions $\omega(t - t_s) \gg 1$ and $\omega t_s \gg 1$ are satisfied. (See figure 5.3.) The first condition decrees that many cycles of oscillatory strain are performed before the stress is measured (and must automatically be satisfied in any realistic oscillatory measurement); the second ensures that transient contributions from the initial sample preparation stage (the quench at $t = 0$) are negligible. The fact that these criteria are sufficient even in the glass phase is far from obvious, and is given careful discussion in appendix 5.3.2.

Broadly speaking, these criteria for t_s-independence are satisfied in any experiment that would reliably measure a conventional $G^*(\omega)$ spectrum for systems with TTI. Hence we hereafter drop the t_s argument from G^*, and define a simplified spectrum $G^*(\omega, t)$. Although this has lost its transient start-up dependence, it still in general depends on time t as a result of the ageing (or transient) time-dependence of the underlying material properties. Our results for the long-time behaviour ($t \gg 1, \omega \ll 1$,

[6] In which $Z(t, t') = t - t'$.

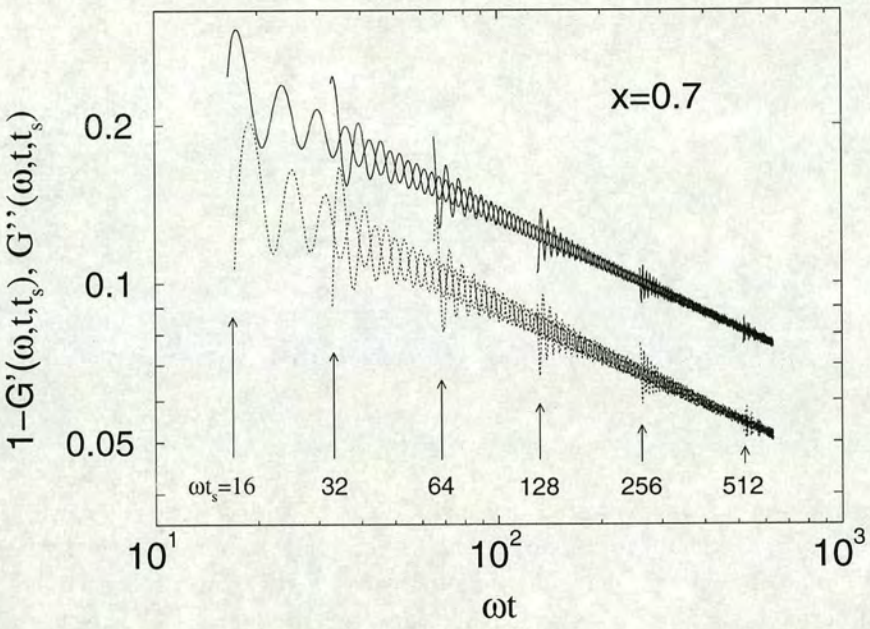

Figure 5.3. Demonstration of t_s-independence $G^*(\omega, t, t_s)$ in the glass phase. Shown are $1 - G'(\omega, t, t_s)$ (solid lines) and $G''(\omega, t, t_s)$ (dotted lines) against ωt. The noise temperature is $x = 0.7$ and the frequency $\omega = 0.01$. Start-time values t_s obey $\omega t_s = 2^4, 2^5, \ldots 2^9$. When $\omega(t - t_s) \gg 1$ (a sufficient number of oscillations after the beginning of each dataset) and $\omega t_s \gg 1$ (datasets beginning further on the right), G^* becomes independent of t_s.

$\omega(t - t_s)$), as calculated in appendix 5.3.2, are as follows:

$$\begin{aligned} G^*(\omega, t) &= \Gamma(x)\Gamma(2-x)(i\omega)^{x-1} \quad \text{for} \quad 1 < x < 2, \\ G^*(\omega, t) &= 1 + \frac{\ln(i\omega)}{\ln(t)} \qquad\qquad\quad \text{for} \quad x = 1, \\ G^*(\omega, t) &= 1 - \frac{1}{\Gamma(x)}(i\omega t)^{x-1} \qquad \text{for} \quad x < 1. \end{aligned} \tag{5.7}$$

For comparison with experimental results, the simple interpolating form

$$G^*(\omega, t) = 1 - \frac{\Gamma(x)\Gamma(2-x)\,(i\omega)^{x-1} - 1}{\Gamma^2(x)\Gamma(2-x)t^{1-x} - 1} \tag{5.8}$$

may be useful: it reproduces the asymptotic behaviour $t \to \infty$, $\omega \to 0$ with $\omega t \gg 1$ for $x \neq 1$, and can also recover the logarithmic terms at the glass transition, provided the

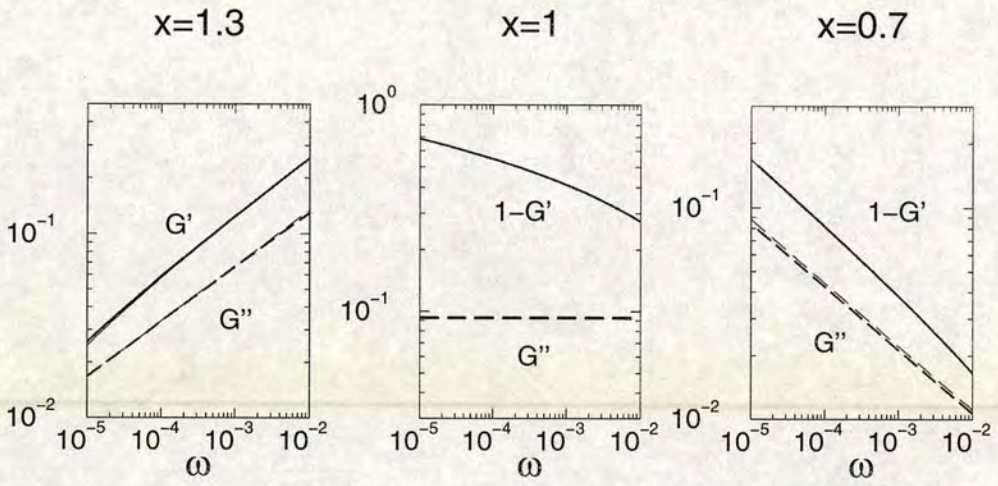

Figure 5.4. Approximate curves for $G'(\omega, t)$ and $G''(\omega, t)$ generated using the simple interpolating formula equation 5.8 (thin lines) compared with the numerical data for these quantities (thick lines), plotted as a function of ω at fixed $t = 10^7$. Noise temperatures x are as shown. Note that the predictions of the interpolating formula are practically indistinguishable from the numerical data over the frequency window shown.

limit $x \to 1$ is taken first. We have checked that it provides a good fit to our numerical data, at least over the noise temperature range 0 to approximately 1.3 (see figure 5.4). In particular, it captures the crossover of our asymptotic results from their $x = 1$ to $x \neq 1$ forms.

By measuring $G^*(\omega, t)$ we are directly probing the properties of the system at the time of measurement[7], t. In light of this, the results of equation 5.7 are relatively easily interpreted. In the ergodic phase ($x > 1$), $G^*(\omega, t)$ will reach a t-independent value within a time of $O(1/\omega)$ after the quench, since any oscillatory measurement can only probe traps with time-constants[8] $\tau \lesssim 1/\omega$, and these traps equilibrate within a time interval $O(1/\omega)$. Furthermore, because we can never in fact access the regime $t < 1/\omega$ (due to the many cycle condition discussed in section 3.1.2), we will actually never see the underlying transient approach to equilibrium in this measurement. The relaxation time in equilibrium is of $O(\tau_0)$ (*i.e.* , $O(1)$ in our units) and the response $G^*(\omega, t)$ depends only upon ω: $G^*(\omega, t) \to G^*(\omega)$. In contrast, below the glass point the characteristic relaxation time at the epoch of measurement is of order t, and the

[7]This will become more apparent after our "masked long term memory" discussion below.
[8]Elements in deeper traps will give entirely elastic response.

response is a function only of the product ωt. Since the losses in an oscillatory measurement arise from traps with lifetimes less than about $1/\omega$ (elements in deeper traps respond elastically), the overall response becomes more elastic as the system ages into traps with $\tau > 1/\omega$, and the population of shallow traps gradually depletes.

Our numerical results for $G^*(\omega, t)$, at various measurement times t, and for various values of x (above and below the glass transition) are shown in figure 5.5. The results for $x \leq 1$ indeed show a characteristic hardening of the glassy material as it ages towards a more elastic state. At a given (fixed) low frequency, the storage modulus G' evolves upwards in time, and the loss modulus G'' downward [SLHC97, Sol98]. Each spectrum terminates at frequencies of order $\omega t \simeq 1$. This is because one cannot measure a true oscillatory response for periods *beyond* the age of the system (due to the many cycle requirement). Therefore, the rise (at a given measurement time) of G'' spectra as frequency is tracked downwards (as in figure 3.1) represents the ultimate rheological behaviour, and provides an explanation of the apparent experiment violation of linear response theory (described in section 3.1.2). Note that this explanation can only be used for[9] $\mu = 1$ in Struik's scheme (section 3.2.1): whenever $\mu < 1$, the characteristic relaxation time-scale $O(t_{\rm w}^{\mu})$ always (eventually) becomes small compared with the waiting time $t_{\rm w}$, and the region to the left of the loss peak can, in principle, be accessed.

It is shown in appendix 5.3.2 that the insensitivity of $G^*(\omega, t, t-t_{\rm s})$ to $t_{\rm s}$ in practical measurements of the viscoelastic spectrum (where many cycles are performed) arises because (even when $x < 1$) the most recently executed strain cycles dominate the stress response at time t: as long as oscillatory strain was started many cycles ago, the system has no memory of when it was switched on. Correspondingly (by linearity) an oscillatory strain started in the distant past and then switched off at $t_{\rm s}$, will leave a stress that decays on a time-scale comparable with the period of the oscillation. This is markedly different from non-oscillatory stresses, where long term memory implies that the response to a step strain, applied for a long time $O(t_{\rm w})$, persists for a similarly long time $O(t_{\rm w})$ after it is removed (see section 2.1.1 above). Thus the fact that the SGR glass "forgets" the $t_{\rm s}$ argument of $G^*(\omega, t, t - t_{\rm s})$, is directly linked to the oscillatory nature of the perturbation. In the language of section 2.1.1, the (weak) long term memory (for $x < 1$) is "masked" by the oscillatory perturbation, such that memory is *apparently* short term.

In section 2.2, we noted that in an equilibrium system, step and oscillatory response functions are automatically related by Fourier transform. We further noted that this

[9] As noted above, the SGR model has $\mu = 1$.

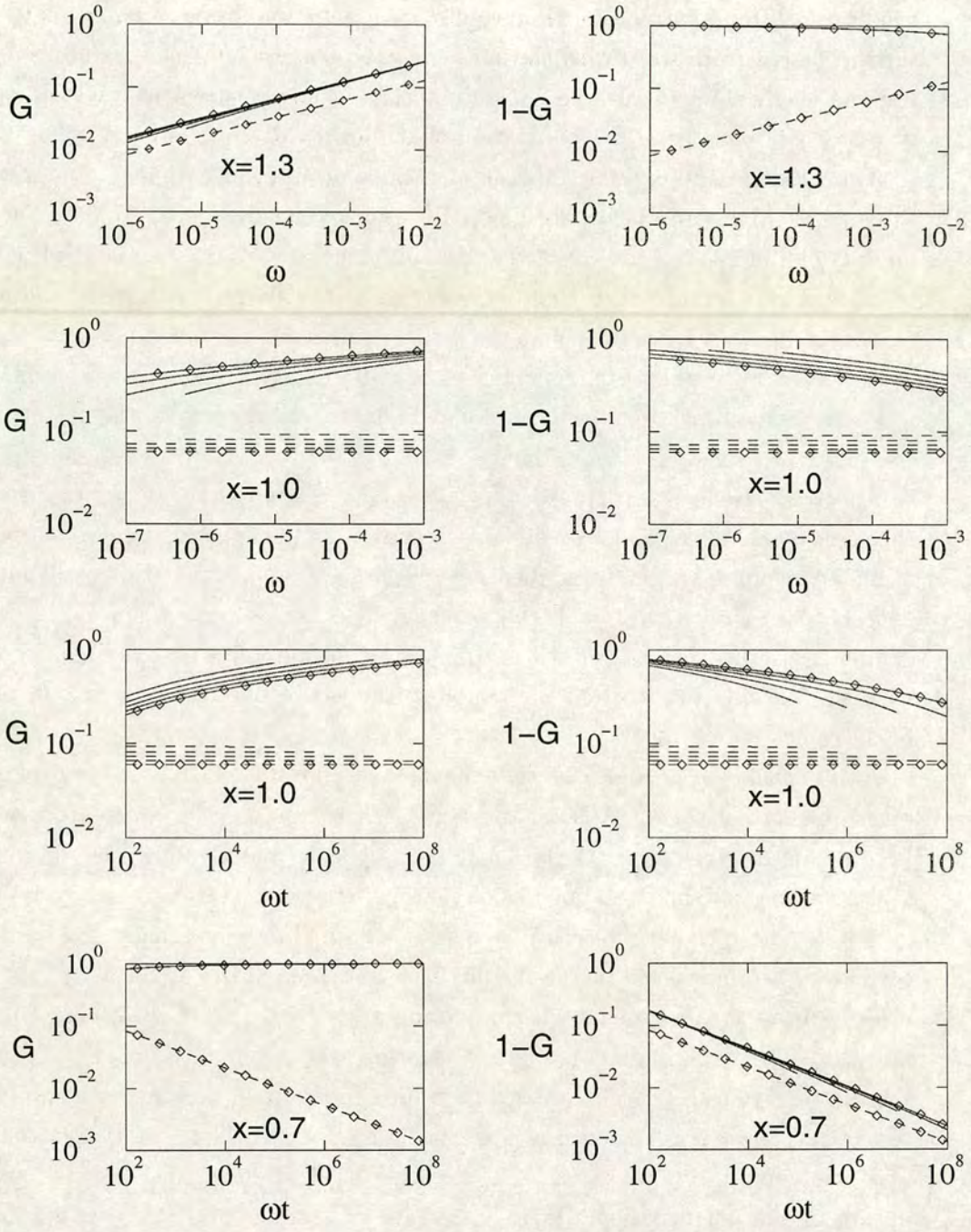

Figure 5.5. Left column: viscoelastic spectra $G'(\omega)$ (solid lines) and $G''(\omega)$ (dashed lines) versus frequency, ω (for $x \geq 1$) or scaled frequency ωt (for $x \leq 1$). Right column: frequency-dependent corrections to Hookean elasticity, $1 - G'$ (solid lines), G'' (dashed lines). Data are shown for systems aged $t = 10^7, 10^8, \ldots 10^{11}$. At any fixed ω the curves lie in order of age; data on the oldest system is marked by the symbols. There is good data collapse both above and below the glass point (with the appropriate scalings); the data for $x = 1$ do not collapse in either representation due to logarithmic terms. If plotted against ω rather than ωt, the data for $x = 0.7$ would resemble figure 3.1.

relation is not guaranteed in an ageing system. However, in appendix 5.3.2, we find that the forgetfulness of G^* to anything but the most recent strain cycles means that, even for $x < 1$, a Fourier relationship between oscillatory and step strain responses does hold ("locally" at any given time t). Physically, this is due to the fact that both the step and the oscillatory response functions $G(t - t_w, t_w)$ and $G^*(\omega, t_w)$ are probing the properties of the system as they are at the waiting time t_w. To good approximation, one has the relation

$$G^*(\omega, t) = i\omega \int_0^\infty dt' e^{-i\omega t'} G(t', t), \tag{5.9}$$

which is just the relation 2.36 conjectured above. Apart from the explicit dependence on the measurement time t, this is the usual (TTI) result, although here the result is nontrivial due to the presence of ageing effects. As discussed in section 2.2.1, we speculate that the relation 5.9 holds not only for the SGR model, but in fact for all systems which have only *weak* long term memory.

5.1.3 Startup of steady shear

We now study the SGR model's response to shear of constant rate $\dot{\gamma}$ commenced at time t_w. In this case, the overall strain always becomes large at long times, and linearity need not be preserved indefinitely. In the spirit of our introductory discussion of section 2.2.1, we proceed first by assuming that linearity *does* hold, and consider the self consistency of this assumption a posteriori. (Note, though, that linearity must at least be preserved as long as $\dot{\gamma}(t - t_w) \ll 1$, since this $\gamma(t)$ sets the maximal local strain of any element.)

Calculation within the assumption of linear response

Within the linear regime, any element's lifetime is independent of strain and obeys $\tau = \exp(E/x)$. As described in section 4.2.2 above, at a time t after a deep quench, the distribution of lifetimes obeys $P(\tau, t) \sim \tau\rho(\tau)$ for $\tau \ll t$ and $P(\tau, t) \sim t\rho(\tau)$ for $\tau \gg t$. Since the local stress associated with a given trap is of order $\dot{\gamma}\tau$ for $\tau \ll t - t_w$, and $\dot{\gamma}(t - t_w)$ for $\tau \gg t - t_w$, we can construct an estimate of the macroscopic stress. For $t - t_w \ll t_w$, we have:

$$\begin{aligned} \sigma(t) &\simeq \frac{\dot{\gamma}\left[\int_1^{t-t_w} d\tau\tau^2\rho(\tau) + (t - t_w)\int_{t-t_w}^{t} d\tau\tau\rho(\tau) + (t - t_w)t\int_t^\infty d\tau\rho(\tau)\right]}{\int_1^t d\tau\tau\rho(\tau) + t\int_t^\infty d\tau\rho(\tau)} \\ &\simeq \frac{\dot{\gamma}\left[x(t - t_w)^{2-x} + (x - 2)(t - t_w)t^{1-x} + x(1 - x)\right]}{(x - 2)\left(t^{1-x} - x\right)}. \end{aligned} \tag{5.10}$$

	$\frac{\sigma(t-t_w,t_w)}{\dot\gamma}$ for $t-t_w \ll t_w$	$\frac{\sigma(t-t_w,t_w)}{\dot\gamma}$ for $t-t_w \gg t_w$
$2<x$	$\frac{x-1}{x-2}$	$\frac{x-1}{x-2}$
$1<x<2$	$\frac{\Gamma(x)}{2-x}(t-t_w)^{2-x}$	$\frac{(x-1)\Gamma(x)}{2-x}(t-t_w)^{2-x}$
$x<1$	$(t-t_w)$	$(1-x)(t-t_w)$

Table 5.2. Stress response to shear strain of constant rate $\dot\gamma$ at short and long times ($t-t_w \gg 1$, $t \gg 1$, $\dot\gamma \ll 1$ assumed). These results apply to the regime $\dot\gamma(t-t_w) \ll 1$, where strain-induced yielding can be neglected, making the response linear. $\Gamma(x)$ denotes the Gamma function.

This gives, for long times and in the linear response regime, $\sigma(t) \sim \dot\gamma(t-t_w)$ for $x<1$ (which is purely elastic behaviour), $\sigma(t) \sim \dot\gamma(t-t_w)^{2-x}$ for $1<x<2$ (an anomalous power law), and $\sigma(x) \sim \dot\gamma$ for $x>2$ (Newtonian flow behaviour). Repeating the same calculation with $t \gg t_w$ gives the same asymptotic scaling in each case. An asymptotic analysis of the constitutive equations (see appendix 5.3.3) confirms these scalings; the prefactors are summarized in table 5.2. Because the results depend only on $t-t_w$, any explicit dependence on t_w (ageing, or anomalously slow transients) must reside in subdominant corrections to these leading asymptotes. Hence, *linear* shear startup is not a good experimental test of such effects (but see section 5.2.2 below). In particular, the underlying ageing behaviour for $x<1$ is masked by the triviality of the elastic response.

Self consistency of linear response assumption

We now consider the time window over which our above calculation, performed within an assumption of linearity, is expected to remain valid. The results for $x<2$ show that, if a linear regime were to be preserved for all times $t-t_w$, the stress would eventually

diverge. This can be understood as follows. Rewriting equation 5.10 as

$$\sigma(t) = \int d\tau s(\tau, t), \tag{5.11}$$

where $s(\tau, t)$ is the typical stress carried by elements of time-constant τ at time t, we see that the dominant contributions to $\sigma(t)$, for $x > 2$, come from traps of lifetime $O(1)$. Hence, stress can be relaxed as quickly as it develops due to the application of shear, and $\sigma(t)$ tends to a finite limit (of order $\dot{\gamma}$) as $t \to \infty$; the viscosity of the system is finite, and linearity will be maintained to arbitrarily long times $t - t_w$, provided $\dot{\gamma} \ll 1$. For $x < 2$, on the other hand, most of the weight in the $s(\tau, t)$ distribution involves lifetimes of order t. As time passes, stress is carried by deeper and deeper traps. Hence stress cannot be relaxed as quickly as it develops due to the shear, and, in the absence of non-linear flow-induced yielding, the mean stress would diverge as $t \to \infty$; we discuss the crossover to non-linear behaviour in section 5.2.2 below. As discussed in section 4.2.5 above, just as the Boltzmann distribution for the relaxation times $P_{eq}(\tau) = P(\tau, \infty) \sim \tau\rho(\tau)$ is non-normalizable for $x \leq 1$ (giving glassiness and ageing), so, in the absence of strain-induced yielding, is the ultimate distribution $s(\tau, \infty) \sim \tau^2\rho(\tau)$ of stresses residing in traps of lifetime τ, whenever $x < 2$. The zero shear viscosity η is therefore infinite for such values of x, as noted previously.

5.2 Nonlinear response

We now turn to the nonlinear behaviour of the SGR model under imposed strain. We shall consider step strain and non-linear shear start-up. We start with the step strain case.

5.2.1 Step strain

The nonlinear step strain response function was defined in equation 2.13. It is found for the SGR model from equation 4.24:

$$G(t - t_w, t_w; \gamma_0) = G_0(Z(t, 0)) + \int_0^{t_w} dt' Y(t') G_\rho(Z(t, t')) \tag{5.12}$$

where, using equation 4.21:

$$Z(t, t') = (t - t_w) \exp\left(\gamma_0^2/2x\right) + (t_w - t'). \tag{5.13}$$

In the linear regime (recall equation 5.2), we have:

$$\begin{aligned} G(t-t_{\rm w}, t_{\rm w}, \gamma_0 \to 0) &\equiv G(t-t_{\rm w}, t_{\rm w}) \\ &= G_0[(t-t_{\rm w}) + (t_{\rm w}-0)] \\ &\quad + \int_0^{t_{\rm w}} dt' Y(t') G_\rho \left[(t-t_{\rm w}) + (t_{\rm w}-t')\right]. \end{aligned} \tag{5.14}$$

Direct comparison of 5.12 and 5.14 reveals that:

$$G(t-t_{\rm w}, t_{\rm w}; \gamma_0) = G\left((t-t_{\rm w}) \exp\left(\gamma_0^2/2x\right), t_{\rm w}\right). \tag{5.15}$$

This result generalizes that of [Sol98] for the non-ageing case ($x > 1$). It can be understood as follows. Within the SGR model, instantaneous response to a step strain at $t_{\rm w}$ is always elastic (that is, $G(0, t_{\rm w}, \gamma_0) = 1$); the fraction of stress remaining at time $t > t_{\rm w}$ is the fraction of elements which have survived from $t_{\rm w}$ to t without yielding (see section 5.1.1 above). The stress decay is therefore determined entirely by the distribution of relaxation times in the system just after the strain is applied at time $t_{\rm w}$. The effect of a finite strain is solely to modify the distribution of barrier heights, and hence to modify this distribution of relaxation times τ; in fact (within the model) nonlinear strain reduces the yield time of every element by an identical factor of $\exp(\gamma_0^2/2x)$ [Sol98]. Thus the relaxation after a nonlinear step strain at $t_{\rm w}$ is found from the linear case by rescaling the time interval $t - t_{\rm w}$ using this same factor. Accordingly, the asymptotic results given for $G(t-t_{\rm w}, t_{\rm w})$ in table 5.1 can be converted to those for the nonlinear regime by replacing the time interval $t - t_{\rm w}$ by a strain-enhanced value $(t-t_{\rm w})\exp(\gamma_0^2/2x)$, wherever it appears there.

5.2.2 Startup of steady shear

In section 5.1.3, we discussed the response of the SGR model to start up of steady shear of rate $\dot{\gamma} \ll 1$ commenced at time $t_{\rm w}$. We assumed there that linearity of response was maintained. Indeed, for $x > 2$ we showed that linearity *is* preserved to arbitrarily long times $t - t_{\rm w} \to \infty$, provided $\dot{\gamma} \ll 1$ (in agreement with the SGR model's prediction [Sol98] of Newtonian fluid behaviour in that regime; see our review of the TTI flow curve results in section 4.2.4). This results from the fact that the main stress contribution is from elements which, were they unstrained, would have lifetime $\tau(E) = \exp(E/x)$ of order unity. So, if the strain rate obeys $\dot{\gamma} \ll 1$, these elements will acquire only negligible stress before they yield spontaneously. Hence their lifetimes are not affected by strain, and the stress response remains linear at all times, including the steady state limit: $\sigma(t \to \infty) \to \eta\dot{\gamma}$. Put simply, stress can be relaxed as quickly as it

develops due to external shear; the zero-shear viscosity is finite.

Hence for the remainder of the discussion we focus on the case $x < 2$, where non-linearities always do appear at long times. In section 5.1.3 we showed that, under shear start-up with $\dot{\gamma} \ll 1$ (for times $t - t_w \ll 1/\dot{\gamma}$, where response must be linear) the dominant stress contributions are from elements with (linear regime) lifetimes of order $t - t_w$. Now linearity can apply only if such elements are unlikely to acquire a non-negligible local strain before they yield spontaneously. But within their natural lifetimes, such elements develop strains of order $\dot{\gamma}(t-t_w)$, which enhances their yield rate by a factor $\exp[(\dot{\gamma}t)^2/2x]$. Hence linearity can hold only so long as $\dot{\gamma}(t-t_w) \ll 1$. Hence the predictions of the linear theory of section 5.1.3 can be maintained to arbitrarily long times only by taking the limit $\dot{\gamma} \to 0$ before one takes the steady state limit of $t - t_w \to \infty$. This means that the width of the linear response regime in steady flow is vanishingly small for $x < 2$, as discussed in section 4.2.4. Equivalently, for any small fixed $\dot{\gamma}$, the linear period ends (to within weak logarithmic terms discussed below) at $t-t_w \simeq \dot{\gamma}^{-1}$; at later times, the main stress-bearing elements will, during their lifetimes, become strongly strained. At a strain rate $\dot{\gamma}$, an element with yield energy E will be strained to the top of its yield barrier in a time $l_y/\dot{\gamma} = E^{1/2}/\dot{\gamma} \simeq (\log \tau)^{1/2}/\dot{\gamma}$ (where l_y is the yield strain of the element). The tendency of the stress distribution $s(\tau, t)$ – *and also, for any* $x < 1$, *the lifetime distribution* $P(\tau, t)$ – to evolve toward deeper and deeper traps is thereby *interrupted*: the lifetime of a deep trap is converted from τ to a much smaller value, of order $(\log \tau)^{1/2}/\dot{\gamma}$ [SLHC97, Sol98]. This truncation of the lifetime distributions means that neither $P(\tau, t)$ nor $s(\tau, t)$ can become dominated by values of τ which diverge at long times. Instead, (for $x < 2$ in the case of $s(\tau, t)$, and for $x < 1$ in the case of $P(\tau, t)$) they are dominated by traps which, were they unstrained, would (to within logarithmic corrections) have lifetime of $O(1/\dot{\gamma})$. Hence (to within logs) we expect that under steady shear

$$\begin{aligned} P(E,t) &\sim \tau(E)\rho(E) \quad \text{for} \quad \tau(E) \ll 1/\dot{\gamma} \\ P(E,t) &\sim \frac{1}{\dot{\gamma}}\rho(E) \qquad \text{for} \quad \tau(E) \gg 1/\dot{\gamma} \end{aligned} \tag{5.16}$$

and likewise

$$\begin{aligned} s(E,t) &\sim \tau(E)^2\rho(E) \quad \text{for} \quad \tau(E) \ll 1/\dot{\gamma} \\ s(E,t) &\sim \frac{1}{\dot{\gamma}^2}\rho(E) \qquad \text{for} \quad \tau(E) \gg 1/\dot{\gamma} \end{aligned} \tag{5.17}$$

where we have reverted to trap depths rather than trap lifetimes, since trap depth is unaffected by local strains. Hence we can say that (for $x < 1$) ageing has been

interrupted by shear: a steady state is restored in which the typical relaxation time-scale is set not now by t_w, but instead by $1/\dot{\gamma}$ (to within logarithmic corrections).

We noted in section 5.1.3 that linear shear startup is not a good test of ageing effects for $x < 1$: any t_w dependence in the stress response reside in corrections to the leading behaviour. Effectively, the underlying ageing behaviour is masked by the triviality of the elastic response. We have further shown (in this section) that at *long* times, ageing is actually absent: it has been interrupted by shear. Note, however, that the stress at

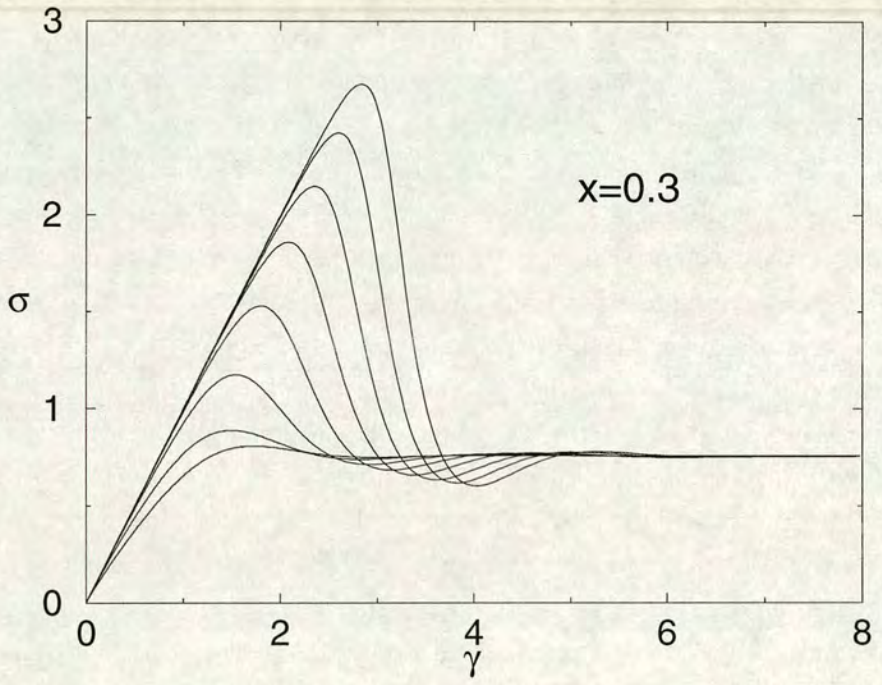

Figure 5.6. Stress response σ, in shear startup, vs. strain γ at noise temperature $x = 0.3$ and strain rate $\dot{\gamma} = 0.001$. Curves from bottom to top correspond to increasing ages $t_w = 10^2, 10^3 \ldots 10^9$ at time of startup.

intermediate times (at the end of the linear regime) can be higher than the steady state value by an amount which depends strongly upon the age of the system when shearing commenced. See figure 5.6. The physics of this age-dependent overshoot is clear: the extent of the linear regime progressively gets larger as t_w is increased, because the system has aged into deeper traps (and because the SGR model assumes that within each trap the relation between stress and strain is linear). Thus the strain at which strong yielding sets in increases (roughly logarithmically) with t_w; the height of the overshoot is correspondingly increased before dropping onto the same, t_w-independent,

steady-shear plateau.

5.3 Appendix: analysis for linear rheological response functions

In this appendix, we outline our analytical calculation of the linear stress relaxation function $G(t-t_w, t_w)$, the linear viscoelastic spectrum $G^*(\omega, t)$, and the stress response to linear shear startup.

5.3.1 Linear stress relaxation function

In the main text, we used the linearized constitutive equation 4.23 to find the following exact expression for the stress relaxation modulus

$$G(t-t_w, t_w) = 1 - \int_{t_w}^{t} dt' Y(t') G_\rho(t-t'). \tag{5.18}$$

Here we extract the asymptotic time-dependences of this expression in the limit $t-t_w \gg 1$, $t_w \gg 1$. We identify two distinct regimes: short times, $t - t_w \ll t_w$ and long times, $t - t_w \gg t_w$.

Short Time regime, $t - t_w \ll t_w$

Here we Taylor expand $Y(t')$ about t to get

$$G(t-t_w, t_w) = 1 - \sum_{m=0}^{\infty} (-1)^m \frac{1}{m!} \left. \frac{Y^m(t')}{dt'^m} \right|_{t'=t} I_m(t-t_w) \tag{5.19}$$

in which

$$I_m(t) = \int_0^t dt' t'^m G_\rho(t'). \tag{5.20}$$

Using the fact that $G_\rho(t)$ and $Y(t)$ are (for $t \gg 1$) both power laws, we find that successive terms in the expansion of 5.19 decrease by a factor $(t-t_w)/t_w$. Hence to leading order we have

$$G(t-t_w, t_w) = 1 - Y(t) I_0(t-t_w). \tag{5.21}$$

To evaluate the integral in this expression, we take its Laplace transform:

$$\bar{I}_0(\lambda) = \frac{1}{\lambda} \bar{G}_\rho(\lambda). \tag{5.22}$$

where λ denotes the conjugate variable to $t - t_w$, and in which (see appendix 4.3)

$$\bar{G}_\rho(\lambda) = x \int_1^\infty d\tau \frac{\tau^{-x}}{1+\lambda\tau} \tag{5.23}$$

Upon inversion, only the singularities of the transform can contribute to $I_0(t - t_w)$. These comprise a pole at the origin (due to the factor $1/\lambda$), and a branch cut along the real axis for $-1 < \lambda < 0$ (due to the factor $\bar{G}_\rho(\lambda)$). Within the circle $|\lambda| < 1$, and hence in the vicinity of these singularities, $\bar{G}_\rho$ can be expanded as follows:

$$\bar{G}_\rho(\lambda) = a\lambda^{x-1} + \sum_{n=0}^{\infty} b_n \lambda^n \tag{5.24}$$

in which

$$a = x\Gamma(x)\Gamma(1-x), \tag{5.25}$$

and

$$b_n = \frac{x(-1)^{n+1}}{n+1-x}. \tag{5.26}$$

(See appendix 4.3.) Inserting equations 5.24 to 5.26 into equation 5.22 and inverting the Laplace transform, we get[10]

$$I_0(t - t_w) = \frac{a(t-t_w)^{1-x}}{\Gamma(2-x)} + b_0 \tag{5.27}$$

Substituting this (together with our results for the yield rate $Y(t)$; see appendix 4.3), into 5.21, we get finally the formulae for $G(t - t_w, t_w)$, as summarized in table 5.1 of the main text.

Long Time Regime

Here we rewrite equation 5.18 as follows

$$\begin{aligned} G(t-t_w, t_w) &= 1 - \int_0^t dt' Y(t') G_\rho(t-t') + \int_0^{t_w} dt' Y(t') G_\rho(t-t') \\ &= G_0(t) + \int_0^{t_w} dt' Y(t') G_\rho(t-t'). \end{aligned} \tag{5.28}$$

[10] We note that our expansion of $\bar{G}_\rho$, which is strictly only valid inside the circle $|\lambda| < 1$, introduces into $\bar{I}$ a spurious additional branch cut along the real axis for $\lambda < -1$. However, upon inversion of the transform this gives only negligible corrections of $O(e^{-t})$.

where we have used the linearized "conservation of probability" constitutive equation (4.22) to obtain the second line from the first. We neglect the term $G_0(t)$, since[11] it is of $O(t^{-x})$, and thus (see below) negligible with respect to the integral. To evaluate the integral, we adopt a method closely analogous that used above for the short time regime. Expanding $G_\rho(t-t')$ about $t'=0$, we get (to leading order)

$$G(t-t_w,t_w) = G_\rho(t)I(t_w) \tag{5.29}$$

in which

$$I(t_w) = \int_0^{t_w} dt' Y(t'). \tag{5.30}$$

Taking the Laplace transform of this integral, with λ the conjugate variable to t_w, we get:

$$\bar{I}(\lambda) = \frac{1}{\lambda}\bar{Y}(\lambda). \tag{5.31}$$

Using our expressions 4.41 and 4.42 for $\bar{Y}(\lambda)$, we find

$$I(t_w) = \frac{t_w}{b_0} \tag{5.32}$$

for $x > 1$ (to leading order) while for $x < 1$,

$$I(t_w) = \frac{t_w^x}{a\Gamma(1+x)}. \tag{5.33}$$

(again to leading order). To obtain $I(t_w)$ *at* the glass point, we substitute expression 4.45 (for $\bar{Y}(\lambda)$ at $x \approx 1$) into 5.31, and invert the transform to get

$$I(t_w) = \frac{-t_w}{b_0}\sum_{n=1}^{p}\frac{[z(t_w)]^n}{\Gamma(2+n(x-1))} + \ldots \tag{5.34}$$

in which $z(t_w) = -b_0 {t_w}^{x-1}/a$ and p is the largest integer which is less than $1/(1-x)$. Taking the limit $x \to 1$ (using an analysis analogous to that of equations 4.46 to 4.48), we get finally

$$I(t_w) = t_w\left\{\frac{1}{\ln(t_w)} + \frac{\Gamma'(2)}{\ln^2(t_w)} + O\left[\frac{1}{\ln^3(t_w)}\right]\right\}. \tag{5.35}$$

Using equations 5.32, 5.33 and 5.35 in conjunction with the asymptotic ($t \gg 1$) expression for $G_\rho(t) = \Gamma(1+x)t^{-x}$ (see equation 4.39), we recover the results quoted for

[11] Assuming the sample to have been prepared by deep quench.

$t - t_w \gg t_w$ in table 5.1 of the main text. [12]

5.3.2 Linear spectra

We saw in the main text that the constitutive equation 4.23 gives the following exact expression for the linear viscoelastic spectrum:

$$G^*(\omega, t, t - t_s) = 1 - \int_{t_s}^{t} dt' e^{-i\omega(t-t')} Y(t') G_\rho(t - t'). \tag{5.38}$$

We now outline our asymptotic analysis of this expression in the "macroscopic time" regime $\omega \ll 1$, $t \gg 1$. We shall find that (in this regime) the following simplifications

$$G^*(\omega, t, t - t_s) \to G^*(\omega, t) \tag{5.39}$$

(negligible switch-on transients) and

$$G^*(\omega, t) = i\omega \int_0^\infty dt' e^{-i\omega t'} G(t', t). \tag{5.40}$$

(local Fourier relation to the step response function) are obtained – *whatever the value of* x – *provided* enough strain cycles are performed to constitute a realistic oscillatory measurement (*i.e.* provided $\omega(t - t_s) \gg 1$). The fact that these simplifications hold even for $x < 1$ is non-trivial, since they are not automatic in non-TTI systems.

As a first step, we note that G^* can be recast into the following (still exact) form

$$G^*(\omega, t, t - t_s) = \int_{t_s}^{t^+} dt' e^{-i\omega(t-t')} \frac{dG(t - t', t')}{dt'} \tag{5.41}$$

in which $G(t - t', t')$ is the linear stress relaxation modulus, as given by equation 5.18 above[13], and hence in which

$$\frac{dG(t - t', t')}{dt'} = \delta(t - t') - Y(t') G_\rho(t - t'). \tag{5.42}$$

---

[12] To obtain I_0 at the glass point, we put $\Delta = 1 - x$ to get

$$I_0(t - t_w) = \frac{1}{\Delta}\left((1 - \Delta)(1 - \Gamma'(1)\Delta)(1 + \Delta \ln(t - t_w)) - (1 - \Delta)\right), \tag{5.36}$$

and take the limit $\Delta \to 0$ to get for $x = 1$:

$$I_0(t - t_w) = \ln(t_w) - \Gamma'(1). \tag{5.37}$$

[13] The delta function in equation 5.42 arises from the causality Theta function which is assumed, but not explicitly written, in equation 5.18.

To simplify the analysis, we consider first the case $t-t_s \ll t_s$, for which the perturbation was switched on in the recent past relative to the sample's age. (We shall consider the opposite limit, $t \gg t_s$, below.) Proceeding, then, initially within the assumption that $t - t_s \ll t_s$, we expand $Y(t')$ in equation 5.38 about t, and retain only the first term[14] to get

$$G^*(\omega, t, t - t_s) = 1 - Y(t) \int_{t_s}^{t} dt' G_\rho(t - t') e^{-i\omega(t-t')}. \tag{5.43}$$

The integral (denoted hereafter by $I(\omega, t - t_s)$) is evaluated on page 83 (by integrating "backwards" over t' from the present time t), where we find

$$I(\omega, t - t_s) = a(i\omega)^{x-1} + b_0 - \frac{1}{i\omega} G_\rho(t - t_s) e^{-i\omega(t-t_s)} \tag{5.44}$$

Notably, this converges to a t_s-independent value within an interval $t - t_s = O(1/\omega)$. Hence for any realistic many-cycle ($(t - t_s) \gg 1/\omega$) measurement, the viscoelastic spectrum depends (to leading order) only upon the sample age, t, and *not* upon the start-up time t_s: the simplification 5.39 is realized, and we have

$$G^*(\omega, t, t - t_s) \to G^*(\omega, t) = 1 - Y(t) \left[a(i\omega)^{x-1} + b_0 \right], \tag{5.45}$$

which amounts to setting $t_s \to -\infty$ in equation 5.43. Notably, this simplification is valid for all noise temperatures, and therefore holds even in the glass phase.

Physically, the above analysis tells us that, once many cycles have been performed, the system forgets that the strain was only switched on a short time ($t - t_s \ll t_s$) ago: equivalently, at any time t the system's memory (to oscillatory straining) only extends a short interval $O(1/\omega) \ll t$ into the past. Now over this interval, the underlying material properties (as encoded in, say, the hopping rate, $Y(t)$, or the relaxation spectrum, $P(\tau, t)$) will not have aged much. (The absolute time argument of equation 5.42 is correspondingly constant: $Y(t') \approx Y(t)$.) Hence, this oscillatory measurement is "local" in time. Given this (and recalling from section 5.1.1 that the stress response to a *step* strain applied at time t depends only upon the instantaneous distribution $P(\tau, t)$) we expect the usual Fourier relation between step and oscillatory response functions to hold locally (at any time t), *even in the glass phase.* Indeed, comparing equation 5.45 with 5.41 and 5.42, we find that we can set $G(t-t', t')$ equal to $G(t-t', t)$ in equation 5.41 (and furthermore set $t_s \to -\infty$) to get

$$G^*(\omega, t) = \int_{-\infty}^{t} dt' e^{-i\omega(t-t')} \frac{dG(t - t', t)}{dt'}. \tag{5.46}$$

[14] this amounts to neglecting small terms of relative size $(t - t_s)/t_s$.

Upon a change of variables $t' \rightarrow t'' = t - t'$, this gives the Fourier relation (5.40), as expected.

In the language of section 2.1.1, then, the model has "short term memory" with respect to this oscillatory measurement: the temporal extent of memory to oscillatory straining is only the constant interval $O(1/\omega)$, and not the diverging interval $O(t)$. The fact that this holds even in the glass phase is at first sight rather surprising since here, with respect to *constant* perturbations, the model has (weak) *long term* memory[15]: for a constant strain applied between t_s and t, the analogous expression to 5.43 is

$$\sigma(t) = \gamma_0 \left[1 - Y(t) \int_{t_s}^{t} dt' G_\rho(t - t') \right] \tag{5.47}$$

in which (because $G_\rho(t) \sim t^{-x}$), the integral has significant contributions from t' near t_s whenever $x \leq 1$[16]. The contrasting rapid convergence of the oscillatory integral (in equation 5.43) is due to the fact that, in this case, the stress at time t due to any previous strain cycle scales with the *change* in $Y(t')G_\rho(t - t')$ over that cycle: hence the non-integrable (for $x \leq 1$) factor $G_\rho(t - t') \sim (t - t')^{-x}$ is (effectively) converted into the integrable factor $(1/\omega) dG_\rho(t - t')/d(t - t')$. (This argument can be formalized via a mathematical theorem known as Jordan's lemma [Cop62].)

So far, we have only considered relatively large switch-on times $t_s = O(t)$. What happens if instead we have a switch-on time t'_s such that $t'_s \ll t$? By blind extension of the preceding analysis, one might expect that the system's memory to cycles executed at times $O(t'_s)$ becomes ever weaker as t'_s is tracked progressively backwards. Although this is almost always true, as t_s approaches zero it *may* break down, for the following reason. As noted above, the dominant contributions to the integral in 5.38 arise from regions in which $Y(t')G_\rho(t-t')$ changes most rapidly. These comprise: *i)* $t-t' \lesssim O(1/\omega)$, where G_ρ varies rapidly; and *ii)* $t' \lesssim O(1/\omega)$, where (for small values of x) $Y(t')$ varies rapidly. (See the schematic figure 5.7.) Region *i)* has already been accounted for in the result 5.45. Region *ii)* is obviously absent for the regime $t - t_s \ll t_s$, but for $t'_s \ll t$ could clearly contribute a term comparable with those already given in 5.45, *if* t'_s is small enough to be of $O(1/\omega)$, and if x is well below the glass point. To see this more rigorously, we note that for an arbitrary start-up time t_s, the result of 5.45 is subject

[15] *i.e.* constant strain perturbation applied for an interval $O(t)$ is remembered for a subsequent time $O(t)$.

[16] In fact, in the absence of the factor $Y(t')$, the integral would not even converge to a finite limit as $t - t_s$ becomes large.

to an extra contribution

$$G_c^*(\omega, t_s, t_s' - t_s) = \int_{t_s}^{t_s'} dt' e^{-i\omega(t-t')} Y(t') G_\rho(t - t') \tag{5.48}$$

(where t_s' is the start time already considered above, and therefore obeys $t - t_s' \ll t_s'$ and $\omega(t - t_s') \gg 1$). On page 85 below, we demonstrate that this correction is small only if $\omega t_s \gg 1$ and $x > 0.5$. [For $x < 0.5$ we need the stronger condition $t - t_s \ll t_s$ to ensure start time independence.] Throughout this thesis we assume that, in any conventional measurement of G^*, $\omega t_s \gg 1$ *will* hold, and that our t_s–independent result of 5.45 still stands. In fact, even if this condition is not satisfied, the rapid variation of $Y(t)$ at short times (which causes this possible extra start-time dependence) is in any case likely to be an artifact of our (probably) unphysical rapid quench at $t = 0$.

We therefore conclude that, in any realistic experiment, G^* is always given by equation 5.45, and furthermore obeys equation 5.40. Substituting the asymptotic expressions for the hopping rate (as calculated in appendix 4.3) into equation 5.45, we get finally the results for $G^*(\omega, t)$ as summarized in equation 5.7.

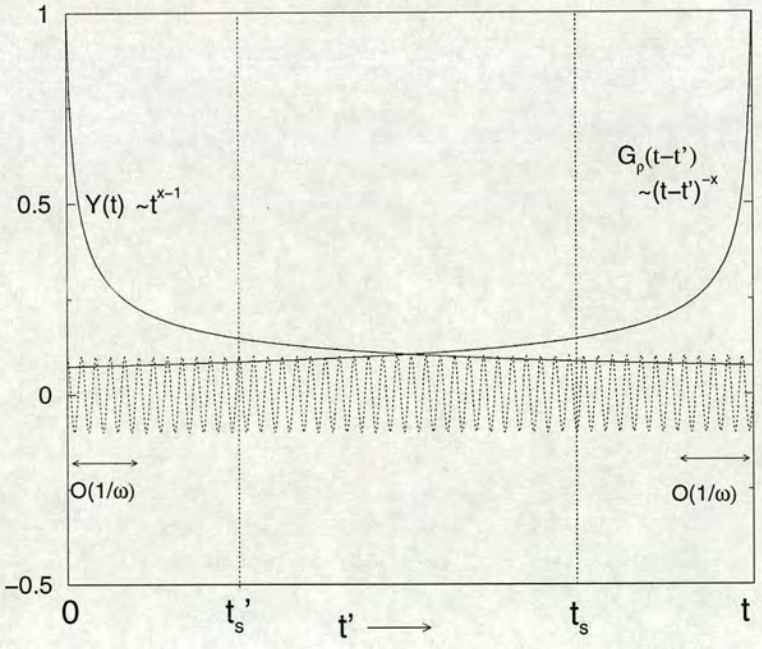

Figure 5.7. Schematic representation of the constituents of the integrand in equation 5.38 for a noise temperature $x < 1$.

Integrals for analysis of linear spectra

Here we evaluate the integral

$$I(\omega, t - t_s) = \int_{t_s}^{t} dt' G_\rho(t - t') e^{-i\omega(t-t')} \tag{5.49}$$

of equations 5.43 and 5.44 of the above discussion, in the regime $\omega \ll 1$, $t - t_s \gg 1$, $t - t_s \gg 1/\omega$. Taking the Laplace transform of this quantity, with λ the conjugate variable to $t - t_s$, we get

$$\bar{I}(\omega, \lambda) = \frac{1}{\lambda} \bar{G}_\rho(\lambda + i\omega) \tag{5.50}$$

in which $\bar{G}_\rho(\lambda + i\omega)$ is the Laplace transform of $G_\rho(t)$ with conjugate variable $\lambda + i\omega$:

$$\bar{G}_\rho(\lambda + i\omega) = x \int_1^\infty d\tau \frac{\tau^{-x}}{1 + (\lambda + i\omega)\tau}. \tag{5.51}$$

Now upon inversion of the transform 5.50, only the singularities of $\bar{I}(\omega, \lambda)$ can contribute to I. These comprise a pole at $\lambda = 0$ (due to the factor $1/\lambda$), and (due to the factor $\bar{G}_\rho(\lambda + i\omega)$) a branch cut along the line $\lambda = -i\omega + \lambda'$ with λ' real, $-1 < \lambda' < 0$. (See figure 5.8.) Now the simplified expansion

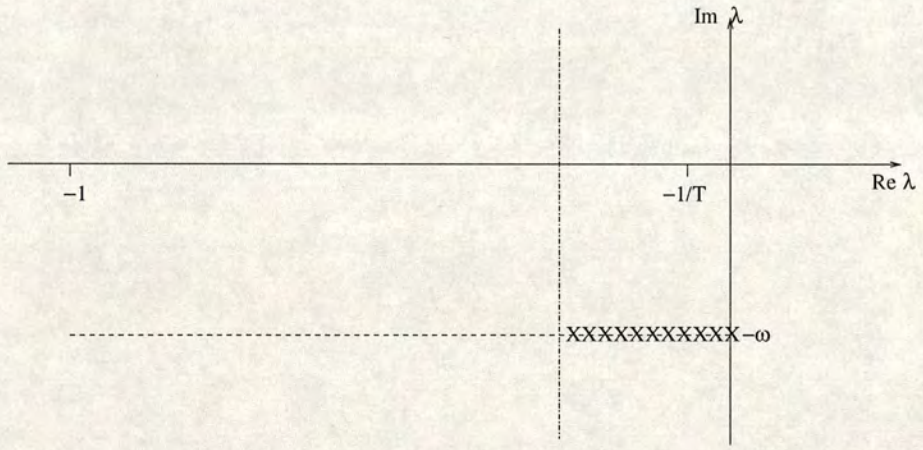

Figure 5.8. Singularities of the Laplace transform $\bar{I}(\omega, \lambda)$. Note the separation of time-scales: $1/T \ll \omega \ll 1$.

$$\bar{G}_\rho(\lambda + i\omega) = a(\lambda + i\omega)^{x-1} + \sum_{n=0}^{\infty} b_n (\lambda + i\omega)^n \tag{5.52}$$

(in which a and b are given by equations 5.25 and 5.26 respectively) is valid within the circle $|\lambda + i\omega| < 1$ (see appendix 4.3) and therefore[17] also in the vicinity of all these singularities. Hence, the following expression

$$\bar{I}(\omega, \lambda) = \frac{1}{\lambda}\left[a(\lambda + i\omega)^{x-1} + \sum_{n=0}^{\infty} b_n(\lambda + i\omega)^n\right]. \tag{5.53}$$

should invert to give $I(\omega, t - t_s)$ to within negligible corrections[18].

To simplify the inversion process, we exploit the separation of time-scales ($\omega \ll 1$, $t - t_s \gg 1$, $\omega(t - t_s) \gg 1$) relevant to this regime to see that any singularity to the left of the line $\Re(\lambda) = -\omega$ will contribute to I only negligible terms $O(e^{-\omega(t-t_s)})$. We therefore need to consider only those singularities which lie to the right of this line. These "relevant" singularities comprise the pole at the origin, and that segment of the branch cut which is marked with X's in Fig 5.8. Near this relevant portion of the branch cut we have $|(\lambda + i\omega)/(i\omega)| < 1$; expanding $\bar{I}(\omega, \lambda)$ in powers of this small quantity we get

$$\bar{I}(\omega, \lambda \simeq -i\omega) = \left[-\frac{1}{i\omega} + O\left(\frac{\lambda + i\omega}{(i\omega)^2}\right)\right]\bar{G}_\rho(\lambda + i\omega). \tag{5.54}$$

Near the pole at the origin, on the other hand, equation 5.22 can be rewritten

$$\bar{I}(\omega, \lambda \simeq 0) = \frac{1}{\lambda}\bar{G}_\rho(i\omega) \tag{5.55}$$

to lowest order in λ.

Hence, upon inversion of the transform the branch cut gives to $I(\omega, t - t_s)$ a contribution[19]

$$-\frac{1}{i\omega}G_\rho(t - t_s)e^{-i\omega(t-t_s)}\left[1 + O\left(\frac{1}{\omega(t - t_s)}\right)\right] \tag{5.56}$$

while the pole at the origin gives a contribution

$$\left[-\frac{d}{d(i\omega)}\right]\bar{G}_\rho(i\omega). \tag{5.57}$$

[17] provided $\omega < 1$, which is satisfied in the regime of interest here.

[18] This expression only coincides with $\bar{I}(\lambda)$ inside the circle $|\lambda + i\omega| < 1$. *Outside* the circle, where $\bar{I}(\lambda)$ must be analytic, the expansion of equation 5.52 has a "spurious" branch cut along $\lambda = -i\omega + \lambda'$ with λ' real, $\lambda' < -1$. However upon inversion this gives only small terms $O(e^{-t})$ which can be neglected.

[19] We have used the fact that $\bar{G}_\rho(\lambda + i\omega)$ is a power law in $\lambda + i\omega$ to obtain the scaling of the sub-leading terms, which we hereafter neglect.

Adding these two contributions, we get finally[20]

$$I(\omega, t-t_s) = a(i\omega)^{x-1} + b_0 - \frac{1}{i\omega} G_\rho(t-t_s) e^{-i\omega(t-t_s)} \tag{5.59}$$

as quoted in equation 5.44 of the main discussion above.

Correction term $G_c^*(\omega, t_s, t_s' - t_s)$

We now obtain an upper bound for the correction term of equation 5.48:

$$G_c^*(\omega, t_s, t_s' - t_s) = \int_{t_s}^{t_s'} dt' e^{-i\omega(t-t')} Y(t') G_\rho(t-t') \tag{5.60}$$

As stated above, this represents a correction to the results quoted for $G^*(\omega, t)$ in equation 5.45, for a start-up time t_s which does not obey $t - t_s \ll t_s$. t_s' is the start-up time considered previously, and *does* obey $t - t_s' \ll t_s'$ (and furthermore $\omega(t - t_s') \gg 1$). We consider only the glass phase, since it is here that memory to the distant past is potentially most pronounced. Splitting up the range of integration, we have

$$G_c^*(\omega, t_s, t_s' - t_s) = \int_{t_s}^{\frac{t}{2}} dt' e^{-i\omega(t-t')} Y(t') G_\rho(t-t') + \int_{\frac{t}{2}}^{t_s'} dt' e^{-i\omega(t-t')} Y(t') G_\rho(t-t'). \tag{5.61}$$

Using the fact that Y and G_ρ are both non-increasing functions of their respective arguments, we obtain the upper bound

$$G_c^*(\omega, t_s, t_s' - t_s) \leq G_\rho\left(\frac{t}{2}\right) \int_{t_s}^{\frac{t}{2}} dt' e^{-i\omega(t-t')} Y(t') + Y\left(\frac{t}{2}\right) \int_{\frac{t}{2}}^{t_s'} dt' e^{-i\omega(t-t')} G_\rho(t-t'). \tag{5.62}$$

By comparison with equation 5.43, we see that the second integral in this expression is $I(\omega, t_s') - I(\omega, t/2)$ (where I is the integral 5.59 above) and hence is just $O[(1/\omega) G_\rho(t_s')]$. The first integral, by direct analogy, is $O[(1/\omega) Y(t_s)]$. Substituting these into 5.62, we find

$$G_c^*(\omega, t_s', t_s - t_s') \;\leq\; O\left[G_\rho\left(\frac{t}{2}\right) \frac{1}{\omega} Y(t_s)\right] + O\left[Y\left(\frac{t}{2}\right) \frac{1}{\omega} G_\rho(t - t_s')\right]$$

[20] To obtain I at the glass point $x = 1$, we put $\Delta = 1 - x$ and use $\Gamma(1-x) = \Gamma(2-x)/(1-x)$ to get (after some algebra)

$$I(\omega, t-t_s) = \frac{1}{\Delta}\left[(1-\Delta)(1+\Delta\Gamma'(1))(1-\Delta\Gamma'(1))(1-\Delta\ln(i\omega)) - 1 + \Delta\right] - \frac{(t-t_s)^{-(1-\Delta)} \exp^{i\omega(t_s-t)}}{i\omega}, \tag{5.58}$$

Taking the limit $\Delta \to 0$ (equivalently $x \to 1$), we get $I(\omega, t - t_s) = -\ln(i\omega)$.

$$\sim \quad (\omega t)^{x-1}\left\{(\omega t)^{1-2x}(\omega t_s)^{x-1} + [\omega(t-t'_s)]^{-x}\right\}. \qquad (5.63)$$

The term outside the brackets is the scaling of the leading correction to elastic behaviour already given in 5.45. The terms inside the brackets are both small provided $\omega t_s \gg 1$ and $x > 0.5$. This correction term is thus negligible with respect to the terms already quoted in equation 5.45, as noted in the main discussion.

5.3.3 Linear shear start-up

We now outline our analytical calculation of the stress response at time t to steady shear of constant rate $\dot{\gamma}$ commenced at time t_w. Using the constitutive equation 4.23, we have the following exact expression for this quantity

$$\sigma(t) = \dot{\gamma}\eta(t - t_w, t_w) \qquad (5.64)$$

where for convenience we have defined an "instantaneous viscosity"

$$\eta(t - t_w, t_w) = (t - t_w) - \int_{t_w}^{t} dt'(t' - t_w)Y(t')G_\rho(t - t') \qquad (5.65)$$

We consider as usual the "macroscopic time" regime $t_w \gg 1$, $t - t_w \gg 1$, $1/\dot{\gamma} \gg 1$, and identity long and short time regimes for which $t - t_w \gg t_w$ and $t - t_w \ll t_w$ respectively.

Short Time Regime

Writing $t' - t_w = t' - t + t - t_w$ in equation 5.64, we get:

$$\begin{aligned}
\eta(t - t_w, t_w) &= (t - t_w)\left[1 - \int_{t_w}^{t} dt' Y(t')G_\rho(t - t')\right] \\
&\quad - \int_{t_w}^{t} dt'(t' - t)Y(t')G_\rho(t - t') \\
&= (t - t_w)G(t - t_w, t_w) - \int_{t_w}^{t} dt'(t' - t)Y(t')G_\rho(t - t') \qquad (5.66)
\end{aligned}$$

where we have used equation 5.18 to get the second line from the first. Expanding $Y(t')$ about $t = t'$, and retaining only the first term in the expansion[21], we get

$$\eta(t - t_w, t_w) = (t - t_w)G(t - t_w, t_w) + Y(t)I(t - t_w) \qquad (5.67)$$

[21] the second term is sub-dominant by a factor $(t - t_w)/t_w$.

in which

$$I(t-t_{\rm w}) = \int_0^{t-t_{\rm w}} dt' t' G_\rho(t') \tag{5.68}$$

Taking the Laplace transform of this integral, we have

$$\bar{I}(\lambda) = \frac{1}{\lambda}\frac{d\bar{G}_\rho(\lambda)}{d\lambda} \tag{5.69}$$

in which λ denotes the conjugate variable to $t-t_{\rm w}$, and in which (inside the circle $|\lambda|<1$)

$$\bar{G}_\rho(\lambda) = a\lambda^{x-1} + \sum_{n=0}^{\infty} b_n \lambda^n; \tag{5.70}$$

here, a and b are given respectively by equations 5.25 and 5.26 above. Substituting this into 5.69 and inverting the transform we get

$$I(t-t_{\rm w}) = -\frac{a(x-1)(t-t_{\rm w})^{2-x}}{\Gamma(3-x)} - b_1 \tag{5.71}$$

to leading and sub-leading orders. Substituting this, together with the yield rate $Y(t)$ (see appendix 4.3 above), and stress relaxation modulus $G(t-t_{\rm w}, t_{\rm w})$ (see earlier in this appendix) into equation 5.67, we recover the results which are summarized in table 5.2.

Long Time Regime

Here we rewrite equation 5.64 as

$$\begin{aligned}\eta(t-t_{\rm w}, t_{\rm w}) &= t - \int_0^t dt' t' Y(t') G_\rho(t-t') - t_{\rm w}\left[1 - \int_0^t dt' Y(t') G_\rho(t-t')\right] \\ &\quad + \int_0^{t_{\rm w}} dt' (t'-t_{\rm w}) Y(t') G_\rho(t-t').\end{aligned} \tag{5.72}$$

This can be immediately simplified by noting (see equation 4.22) that the third term on the R.H.S. is just $-t_{\rm w}G_\rho(t)$, while the modulus of the fourth is bounded from above by $Y(0)t_{\rm w}G_\rho(t-t_{\rm w}) = O[t_{\rm w}G(t-t_{\rm w})]$; these are both small compared with the difference of the first and second and we neglect them. To evaluate the integral of the second term (which we denote by $I(t)$), we take its Laplace transform:

$$\bar{I}(\lambda) = -\frac{d\bar{Y}(\lambda)}{d\lambda}\bar{G}_\rho(\lambda) \tag{5.73}$$

in which λ denotes the conjugate variable to t. Now $\bar{Y}(\lambda) = 1/(\lambda \bar{G}_\rho(\lambda))$ (see equation 4.31[22]) and hence, after some algebra, we find

$$\bar{I}(\lambda) = \frac{1}{\lambda^2} + \frac{1}{\lambda \bar{G}_\rho(\lambda)} \frac{d\bar{G}_\rho(\lambda)}{d\lambda}. \tag{5.74}$$

Substituting the expansion 5.70 into this equation, we get (for $|\lambda| \ll 1$)

$$\bar{I}(\lambda) = \frac{1}{\lambda^2} + \frac{(x-1)a\lambda^{x-2} + b_1 + O(\lambda)}{\lambda\left[a\lambda^{x-1} + b_0 + b_1\lambda + O(\lambda^2)\right]} + \ldots \tag{5.75}$$

Expanding the fraction in this expression for small λ (separately for the noise temperature regimes $2 < x$, $1 < x < 2$ and $x < 1$) and inverting the Laplace transform we get (for $t \gg 1$)

$$\begin{aligned} I(t) &= t + (1-x)/(x-2) && \text{for } 2 < x, \\ I(t) &= t + \frac{(1-x)\Gamma(x)}{2-x} t^{2-x} && \text{for } 1 < x < 2, \\ I(t) &= xt && \text{for } x < 1. \end{aligned} \tag{5.76}$$

Substituting these into 5.72 we get finally the results quoted in table 5.2 of the main text. [23]

[22] in which we have neglected the small term $\bar{G}_\rho(\lambda, y)$ denoting the initial condition.

[23] Note that for consistency with the short time regime results we have expressed the long time results as a function of $t - t_w$ in table 5.2, whereas in this appendix we found then as a function of t. The two forms are clearly the same to within small corrections of $O(t_w/t)$.

Chapter 6

Rheological ageing: imposed stress

We now analyze the SGR model's predictions for various stress-controlled rheological experiments. As noted above, the structure of the constitutive equations (4.22 and 4.23) makes the analysis more difficult for imposed stress than for imposed strain. The following discussion is therefore largely based on our numerical results, with asymptotic analysis of a few limiting cases.

6.1 Linear response

6.1.1 Step stress

We here study the strain response of the SGR model to a step stress imposed at time t_w. The model predicts that upon the application of a step stress there will be an instantaneously elastic response. Elements then progressively yield and reset their local stresses to zero; thus we must apply progressively more strain to maintain the macroscopic stress at a constant value. In this way strain must in general increase with time (although its rate could tend to zero at long times). Therefore, individual elements can potentially acquire large local strains, and linearity need not be preserved to arbitrarily long times. However, to simplify the analysis of this step stress case, we proceed by assuming that first the response *is* linear (*i.e.* we set $Z(t,t')$ equal to $t-t'$ in the constitutive equations *by hand*). Within this assumption, we calculate the corresponding $\gamma(t)$. Finally we consider *a posteriori* up to what time t the linear results remain self-consistently valid.

For a step stress $\sigma(t) = \sigma_0\Theta(t-t_w)$, the linearized constitutive equation 4.23 can

be written

$$1 = J(t - t_w, t_w) - \int_{t_w}^{t} dt' J(t' - t_w, t_w) Y(t') G_\rho(t - t'). \tag{6.1}$$

in which $J(t - t_w, t_w)$ is the creep compliance as defined in section 2.2.2. We computed this quantity numerically (from the above equation), using a method closely analogous to that described in appendix 4.4 for extracting the linear regime's yield rate $Y(t)$ from the linearized constitutive equation 4.22. The results are shown in figures 6.1 and 6.2. In analyzing these results, we focused as usual on the "macrosopic time" regime $t - t_w \gg 1$, $t_w \gg 1$, and identified regimes of short and long time interval between stress application and strain measurement: $t - t_w \ll t_w$ and $t - t_w \gg t_w$ respectively.

From the results for the long time interval regime ($t - t_w \gg t_w$), we were able to extract simple scalings of $J(t - t_w, t_w)$ with time. (For example, we found $J \sim (t - t_w)^{x-1}$ for $1 < x < 2$.) We then used these as ansätze for analytic substitution into the constitutive equation (6.1). In each case this allowed us to confirm the observed functional form, and also to compute exactly the x-dependent prefactors, which were finally cross-checked by comparison with the numerical results. The functional forms for J (in this long time regime) obtained using this method are summarized in table 6.1.

For short time intervals, we were only able to obtain analytical results for the regime $x > 1$, since our tactic here was to assume that the resulting compliance $J(t - t_w, t_w)$ was the same as if we first let $t_w \to \infty$ (in which case the dominant traps are, for $x > 1$, in Boltzmann equilibrium; see figure 4.2a). We then calculated $J(t - t_w, t_w \to \infty)$ analytically from $G(t - t_w, t_w \to \infty)$, using the reciprocal relations between the corresponding Fourier transforms (which are automatic in an equilibrium system; see section 2.2.2 above). The results of this calculation were again checked numerically; good agreement was obtained. They are summarized in table 6.1.

Physical insight into the results of table 6.1 can be gained as follows. At any time during this creep experiment, in order to maintain the stress at a constant level σ_0, we must match the rate at which stress is lost (due to local yielding events) with the rate at which stress increases due to straining. We identify the former as a "stress-weighted hopping rate" $Y_s = \int d\tau \tau^{-1} s(\tau, t)$; hence, we require $Y_s = \dot{\gamma}$. Using the results of table 6.1, we see that for $x > 2$, Y_s remains a constant of order σ_0. For $x < 2$, however, Y_s decays as a power law of $(t - t_w)$: $Y_s \sim (t - t_w)^y$ where $y = x - 2$ for $1 < x < 2$ and $y = -1$ for $x < 1$. Using our concept of the "stress distribution" $s(\tau, t)$ (developed in section 5.1.3 above), these results for Y_s indicate that for $x > 2$, $s(\tau, t)$ must be dominated by traps of time constant $O(1)$ (for all times t), while for $1 < x < 2$ it is dominated by at time t by traps with lifetimes τ of order $t - t_w$ (the time interval

	$J(t-t_w,t_w)$ for $t-t_w \ll t_w$	$J(t-t_w,t_w)$ for $t-t_w \gg t_w$
$x>2$	$\frac{x-2}{x-1}(t-t_w)$	$\frac{x-2}{x-1}(t-t_w)$
$1<x<2$	$\frac{(t-t_w)^{x-1}}{\Gamma^2(x)\Gamma(2-x)}$	$\frac{(t-t_w)^{x-1}}{\Gamma^2(x)\Gamma(2-x)-\Gamma(x)}$
$x=1$	—	$\frac{3}{\pi^2}\ln^2(t-t_w)$
$x<1$	—	$\frac{1}{\psi(1)-\psi(x)}\ln\left(\frac{t-t_w}{t_w}\right)$

Table 6.1. Linear creep compliance in the SGR model at long and short times ($t-t_w \gg 1$, $t_w \gg 1$ assumed). $\Gamma(x)$ denotes the Gamma function, and $\psi(x) = \Gamma'(x)/\Gamma(x)$ the usual psi function. The blank entries for $x < 1$ are explained in the text.

since the stress application). Hence, for $x > 2$ the stress remains in traps of lifetime $\tau = O(1)$ and the creep response is purely viscous, while for $x < 2$, the stress evolves to progressively deeper traps, consistent with the fact that the zero-shear viscosity is infinite in this regime.

For $1 < x < 2$, the scenario given above for the time-dependence of Y_s is closely analogous to that given in section 4.2.2 above for the hopping rate $Y = \int d\tau \tau^{-1} P(\tau, t)$ in systems with $x < 1$. In fact, one can show that, for an *equilibrium* system whose noise temperature is $x > 1$, the evolution of the stress distribution $s(\tau, t)$ following application of a step stress at $t = 0$ is, at long times, equivalent to that of the probability distribution $P(\tau, t)$, in a system deep-quenched to a noise temperature $x - 1$ at $t = 0$. This result is connected with the discussion made in section 4.2.5 above, of the variation with x of the dynamics of successive moments of the lifetime distribution: at noise temperature $x + n$, the dynamics of the nth moment is like that of the zeroth moment at noise temperature x.

As seen in table 6.1, for $x < 1$ the linear compliance $J(t - t_w, t_w)$ is (not unexpectedly) a function of the scaled time interval $(t - t_w)/t_w$. (See figure 6.1.) However,

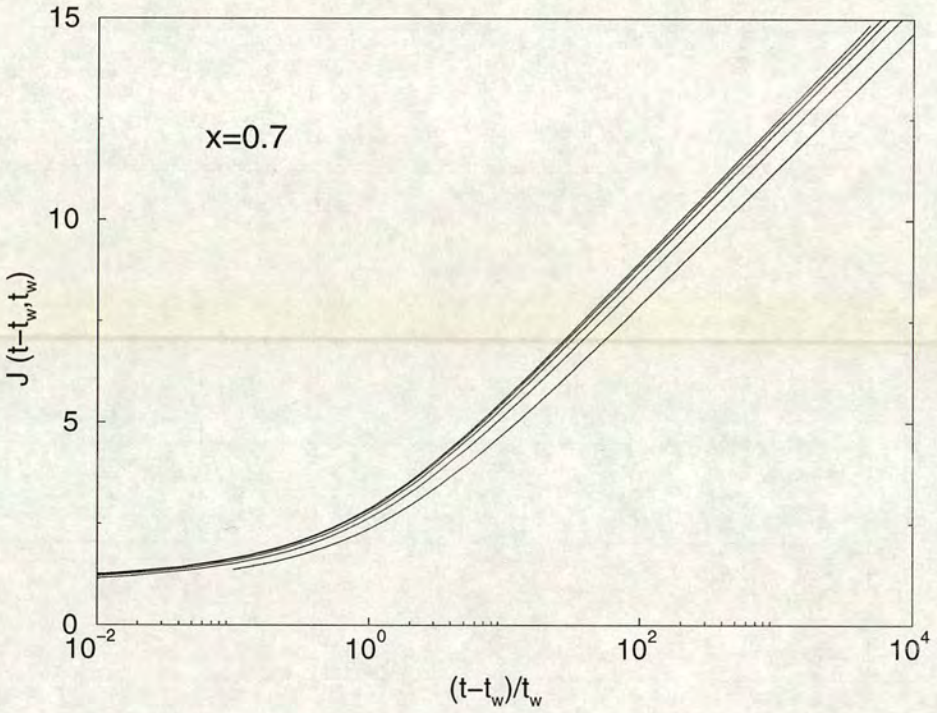

Figure 6.1. Linear creep compliance $J(t - t_w, t_w)$ against scaled time interval $(t - t_w)/t_w$ for noise temperature $x = 0.7$. Curves from bottom to top correspond to increasing times $t_w = 10^2, 10^3 \ldots 10^6$ of stress onset. Note the approach to a limiting scaling form as t_w becomes very large compared with the microscopic time $\tau_0 = 1$.

this ageing of the linear creep compliance shows significant differences from that of the step strain modulus $G(t - t_w, t_w)$ discussed in section 5.1.1 above. In particular, the dependence of $J(t - t_w, t_w)$ on $(t - t_w)/t_w$ for long time intervals $(t - t_w \gg t_w)$ is only logarithmic; $J(t - t_w, t_w) \sim \ln[(t - t_w)/t_w] = \ln(t - t_w) - \ln t_w$ (see table 6.1) which means that the explicit waiting time dependence $(\ln t_w)$ is (in contrast to the step strain behaviour; see table 5.1) formally a "small" correction to the leading behaviour $\ln(t - t_w)$. This relatively slight t_w-dependence is intuitively reasonable: the strain response at time t to step stress is *not* determined purely by the relaxation spectrum at t_w (as was the case for the stress response to step strain, table 5.1), but by the dynamics of the system over the entire interval between t_w and t. This decreases the sensitivity to the time t_w at which the perturbation was switched on. Similar remarks hold above the glass point $(1 < x < 2$, see figure 6.2): in step strain, we found for $t - t_w \gg t_w$ a slow transient behaviour which depended to leading order upon t_w (table 5.1). For step stress, however, the corresponding t_w dependence is demoted to lower order, and

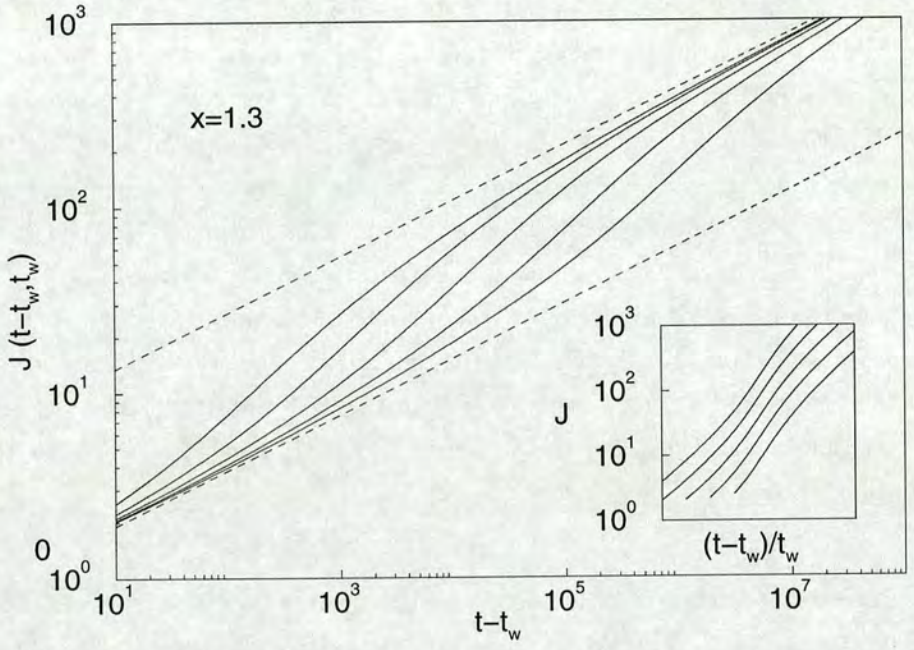

Figure 6.2. Linear creep compliance $J(t-t_{\rm w},t_{\rm w})$ against time interval $t-t_{\rm w}$ for noise temperature $x=1.3$ for $t_{\rm w}=10^3,10^4\ldots10^7$ (solid lines, top to bottom). Lower dashed line: theoretical prediction for the short time regime $t-t_{\rm w}\ll t_{\rm w}$. Upper dashed line: asymptote for long time regime $t-t_{\rm w}\gg t_{\rm w}$. Note that short time and long time behaviours are each independent of $t_{\rm w}$ (as expected for $x>1$), but that the crossover time between them scales with $t_{\rm w}$. Inset: same data plotted against scaled time $(t-t_{\rm w})/t_{\rm w}$; the order of the curves is reversed. The crossover between short and long time behaviour takes place at a value of $(t-t_{\rm w})/t_{\rm w}$ which is roughly the same for all curves, demonstrating the scaling with $t_{\rm w}$.

the late-time response is dominated by TTI terms.

6.1.2 Oscillatory stress

For the SGR model it was noted in section 5.1.2 that *i*) in the oscillatory stress response $G^*(\omega,t,t-t_{\rm s})$, the $t_{\rm s}$ dependence is negligible for low frequencies ($\omega\ll1$) whenever $\omega(t-t_{\rm s})\gg1$ and $\omega t_{\rm s}\gg1$; *ii*) these conditions are satisfied in most conventional ("many cycle") measurements of the viscoelastic spectrum; and *iii*), perhaps surprisingly, these facts are true even in the glass phase, $x\leq1$, of the SGR model. We also noted that, because response to oscillatory strain is dominated by memory of the few most recent cycles (over which the system has barely aged), $G^*(\omega,t)$ is the Fourier transform (with respect to the time interval Δt) of the step strain response function $G(\Delta t,t)$ that would

be measured if a step strain were applied immediately after the oscillatory measurement had been done. (See equation 5.9.)

We have confirmed numerically that similar remarks apply to the oscillatory stress response function $J^*(\omega, t, t - t_s)$, as defined in section 2.2.2. (In light of our analysis for G^*, this is unsurprising. It does however require explicit confirmation since, for example, the transient effects from switching on the perturbation could be different in the two cases.) Memory of the startup time t_s is indeed small in $J^*(\omega, t, t - t_s)$ so long as $\omega(t - t_s) \gg 1, \omega t_s \gg 1$ (and $\omega \ll 1$). Hence we have $J^*(\omega, t, t - t_s) \to J^*(\omega, t)$, and strain response is dominated by the previous few cycles, over which the system has barely ages. $J^*(\omega, t)$ still obviously (in general) depends non-trivially upon time t, due to the underlying ageing time evolution of the material properties.

We have checked numerically (see figure 6.3) that $J^*(\omega, t)$ obeys the reciprocal relation

$$J^*(\omega, t)G^*(\omega, t) = 1, \tag{6.2}$$

which is a non-trivial result for ageing systems. (It is the counterpart of the trivial result $G^*(\omega)J^*(\omega) = 1$ for TTI systems.) We emphasize that this result, like the previous one, has been confirmed here specifically for the SGR model; but it may hold more widely for ageing systems in which the long term memory is *weak* (see section 2.1.1), although to date we have no proof of this conjecture.

6.2 Nonlinear response

6.2.1 Step stress

In section 6.1.1, we studied the SGR model's response to a small step stress [$\sigma(t) = \sigma_0\Theta(t - t_w)$ for which $\sigma_0 \ll 1$] assuming that linearity applied. We found a strain response which increases over time. We further argued that the results obtained within this assumption of linearity must hold at least as long as the (macroscopic) strain remains small, since this sets the upper bound for the local strain of each element.

Although sufficient to ensure linearity, this condition is not always necessary; we require only that the characteristic strain *of those elements which dominate the stress* is small. Referring back to our arguments of section 6.1.1, we recall that for $x > 2$ the dominant elements have lifetimes $O(1)$ and so the response is linear to indefinite times (provided $\sigma_0 \ll 1$, which ensures that $\dot{\gamma}(t) \ll 1$ for all times t). Hence, for such values of x, we have a linear flow regime with a steady strain rate $\dot{\gamma}$ given by $\sigma = \eta\dot{\gamma}$.

In contrast, whenever $x < 2$, the dominant elements have lifetimes of order $t - t_w$; so (as in the case of steady shear; see section 5.2.2) our assumption of linear response

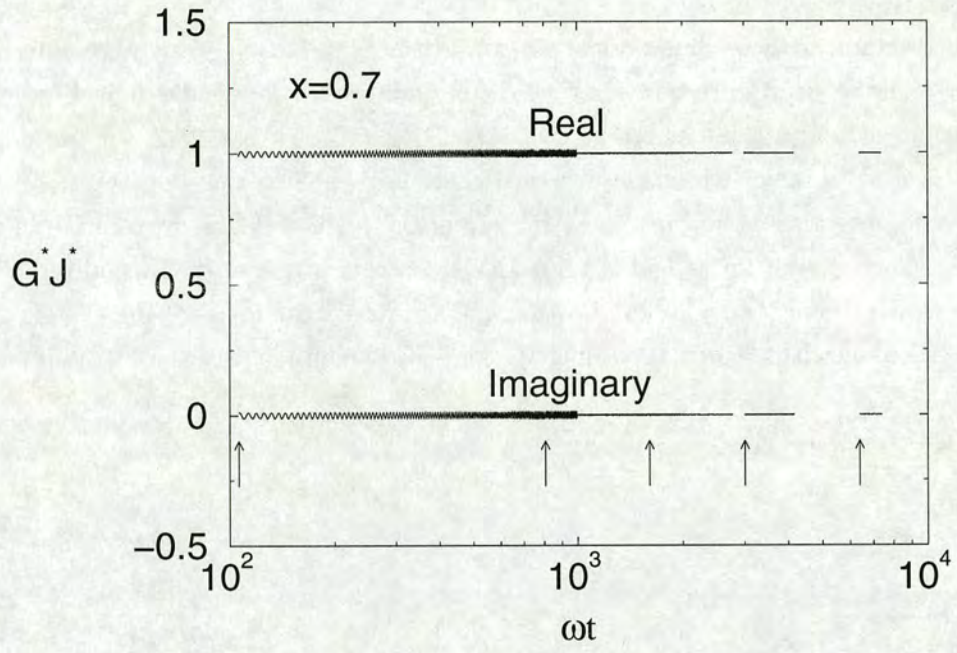

Figure 6.3. Real and imaginary parts of the product $G^*(\omega,t)J^*(\omega,t)$ vs. ωt at noise temperature $x = 0.7$ and frequency $\omega = 0.01$. The usual reciprocity relation between G^* and J^* is seen to hold to within about one percent. Shown are the results of several runs, each over a different time window. A vertical arrow marks the horizontal co-ordinate of the start of each data set. In each run shearing was commenced 20 cycles before the start of data output, to ensure that $\omega(t - t_s) \gg 1$ (necessary for t_s-independence). The oscillatory deviations, visible for the leftmost data set, arise because the other condition for t_s-independence ($\omega t_s \gg 1$) is only just satisfied.

is self consistent only as long as

$$\dot{\gamma}(t)(t - t_w) \ll 1 \tag{6.3}$$

(Here we are obviously making the additional assumption that $\dot{\gamma}$ changes negligibly between t_w and t.) Using the forms for $J(t - t_w, t_w)$ as summarized in table 6.1, we predict that for $1 < x < 2$ the strain response to step stress of size $\sigma_0 \ll 1$ remains linear only for as long as $t - t_w \ll (1/\sigma_0)^{1/(x-1)}$; beyond this time we expect strain-induced yielding to become important. In contrast, for $x < 1$ and $\sigma_0 \ll 1$, we predict (using our linear regime result $J(t - t_w, t_w) \sim \ln[(t - t_w)/t_w]$) that linear response should actually hold for all times. In this case, although it is still true that the dominant elements have lifetimes $O(t - t_w)$, the strain rate $\dot{\gamma} \sim \sigma_0/(t - t_w)$ never becomes large enough to

pull these elements a significant distance up their traps before they yield anyway due to activation.

To confirm these predictions, we solved the non-linear constitutive equations 4.22 and 4.23 by an iterative method which is described in appendix 6.5. For $1 < x < 2$ we indeed found a linear regime with $J(t - t_w, t_w) \sim (t - t_w)^{x-1}$ for times $t - t_w \ll (1/\sigma_0)^{1/(x-1)}$, after which we observed a crossover into a non-linear steady-state flow regime, in which $\gamma(t) \propto \sigma_0^{1/(x-1)} t$ (in agreement with the flow curve 4.26). For $x < 1$, as predicted, the numerical results for step stress of very small amplitude $\sigma_0 \ll \sigma_y$ show no crossover to a steady flow regime at late times. Instead, the system continues to creep logarithmically, according to the linear creep result given in table 6.1.

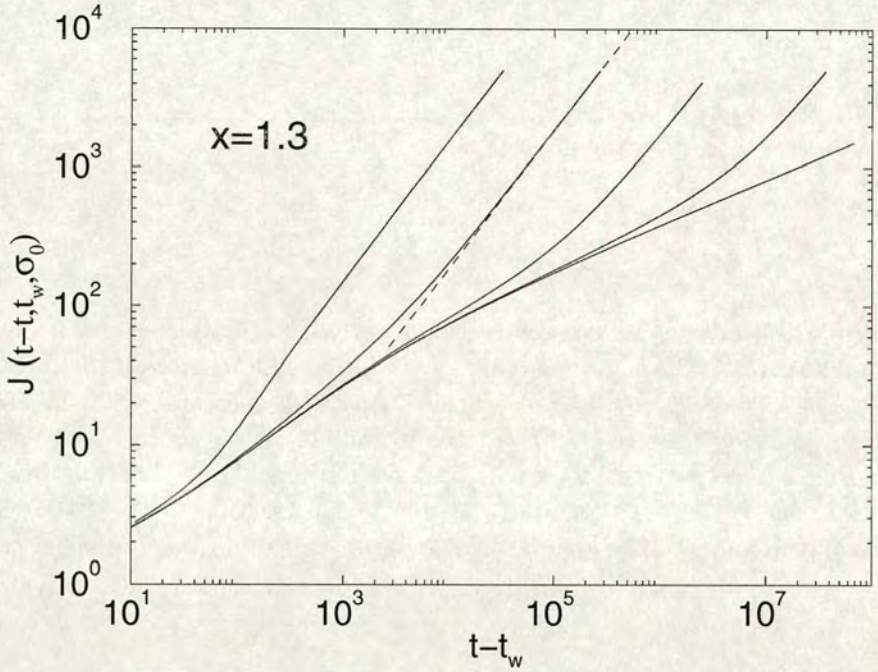

Figure 6.4. Nonlinear creep compliance $J(t - t_w, t_w, \sigma_0)$ as a function of time interval $t - t_w$, for a step stress of size σ_0 applied at time $t_w = 100$. The noise temperature is $x = 1.3$. Solid lines, bottom to top: $\sigma_0 = 10^{-3}, 10^{-2.5}, 10^{-2}, 10^{-1.5}, 10^{-1}$. Over the time intervals shown, the curve for $\sigma_0 = 10^{-3}$ is indistinguishable from the linear compliance (not shown). Dotted line: final flow behaviour predicted from steady state flow curve for $\sigma_0 = 10^{-1.5}$.

To summarize: for a step stress of size $\sigma_0 \ll 1$, we find

i) for $x > 2$: a Newtonian flow regime with $\dot{\gamma} \propto \sigma_0$ persisting for all times,

ii) for $1 < x < 2$: an initially linear strain response [with $\gamma(t) \sim \sigma_0 (t - t_w)^{x-1}$] crossing

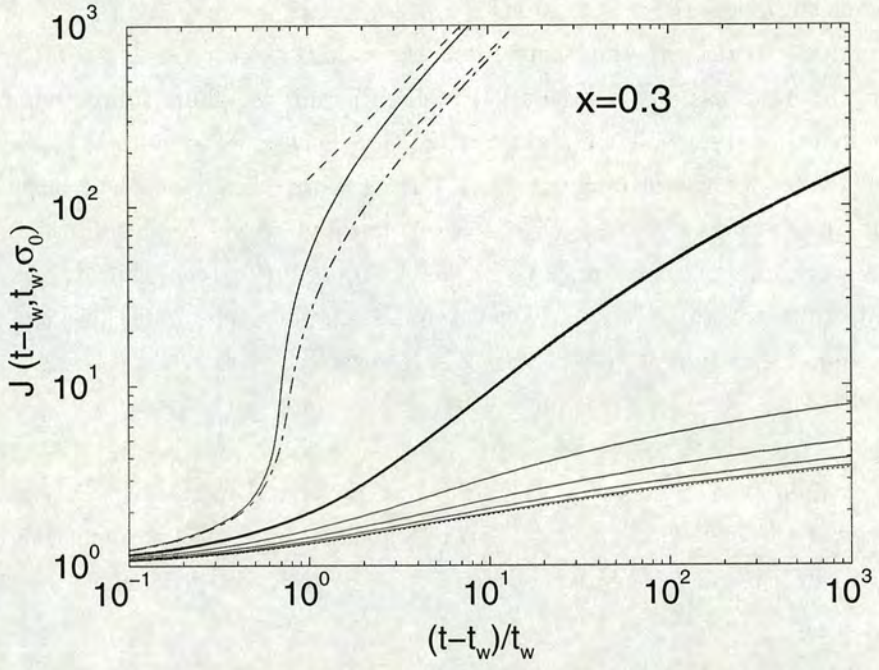

Figure 6.5. Nonlinear creep compliance $J(t - t_w, t_w, \sigma_0)$ as a function of scaled time interval $(t-t_w)/t_w$, for a step stress of size σ_0 applied at time t_w. The noise temperature is $x = 0.3$. Solid curves, bottom to top: $\sigma_0/\sigma_y = 0.2, 0.4, \ldots, 1.2$, all for $t_w = 100$. The case $\sigma_0 = \sigma_y$ is shown in bold; the dotted curve is the linear response result ($\sigma_0 \to 0$). The dot-dashed curve shows the effect of decreasing the waiting time to $t_w = 50$, for $\sigma_0/\sigma_y = 1.2$. Comparison of the curves for the two different waiting times for this stress value shows that before the crossover into flow, the response scales with $(t - t_w)/t_w$; once ergodicity has been restored and the system flows, on the other hand, scaling with $t - t_w$ is recovered. The dashed lines are the predictions for final flow behaviour (for the stress above yield) from the steady state flow curve.

over after a characteristic time $t - t_w \ll (1/\sigma_0)^{1/(x-1)}$ into a steady-state flow regime with $\dot{\gamma} \propto \sigma_0^{1/(x-1)}$,

iii) for $x < 1$: a linear regime with $\gamma(t) \sim \sigma_0 \ln[(t - t_w)/t_w]$ persisting to arbitrarily long times.

For values of $x < 1$, we also used our iterative code to study values of σ_0 which were not small. Recall from section 4.2.4 that the flow curve shows a yield stress $\sigma_y(x)$ for such values of x. We first considered values σ_0 less than the yield stress σ_y. For stresses not too close to the yield stress, we found that the creep was still logarithmic to a good approximation, but now with a nonlinear dependence of its amplitude on stress: $\gamma(t) \approx \sigma_0 A(\sigma_0) J(t - t_w, t_w)$. The prefactor $A(\sigma_0)$ increases rapidly as σ_0 approaches

the yield stress σ_y from below. (See figure 6.6.) Very close to the yield stress, the creep ceases to be logarithmic; $\gamma(t)$ then grows more quickly, but with a strain rate that still decreases to zero at long times. On the basis of these observations, we suspect that for a given stress σ_0 the creep will be logarithmic for short times (where "short times" might mean the whole time window which is accessible numerically), but will gradually deviate from this for longer times. The deviation is expected to be noticeable sooner for stress values closer to yield. We attempted to verify this conjecture numerically, but were unable to access a large enough range of values of $\ln((t-t_w)/t_w)$ to do so. Note that, for any $\sigma_0 < \sigma_y$, the system ages indefinitely, and there is no approach to a regime of steady flow.

Finally, as expected from the flow curve, only for stress amplitudes exceeding the yield stress σ_y did we see an eventual crossover from logarithmic creep to steady flow at long times; in the steady flow regime, we recovered numerically the flow-curve result, $\gamma(t) \propto (\sigma_0 - \sigma_y)^{1/(1-x)}(t-t_w)$. Figure 6.5 shows examples of our numerical results that illustrate the various features of nonlinear creep in the glass phase mentioned above. [1]

6.3 Conclusion

This concludes our analysis of the SGR model's rheological predictions. We have seen that, for noise temperatures in the glass phase $x < 1$, the model has a macroscopic yield stress. Provided this is not exceeded, ageing occurs, with the sample's apparent relaxation time-scale always of order its own age.

In linear response, the stress relaxation modulus and the linear creep compliance are (for $x < 1$) functions of the scaled time $(t - t_w)/t_w$. The model has *weak* long term memory. Despite this, the time-dependent linear viscoelastic spectrum G^* is (at any time) dominated by only the previous few strain cycles, and hence, in any realistic (many cycle) oscillatory measurement, should show no dependence upon the time at which the straining was commenced. Hence we have $G^*(\omega, t, t-t_s) \to G^*(\omega, t)$, which (due to ageing) is a function of the *scaled* frequency ωt. At any fixed time, the loss modulus curves upwards slightly at low frequencies, explaining the apparent experimental violation of linear response theory. The step and oscillatory response functions, $G(t - t_w, t_w)$ and $G^*(\omega, t)$ obey a Fourier relation, which is a non-trivial result in an ageing system. Similarly non-trivial is the fact that $G^*(\omega, t)$ is reciprocal

[1] Note that whereas for most other shear scenarios we chose to present glass phase results for a noise temperature $x = 0.7$, we here chose $x = 0.3$. The yield stress is larger at this value of x, giving us a larger window $0 < \sigma_0 < \sigma_y$ over which we see ageing and creep uninterrupted by a crossover into flow.

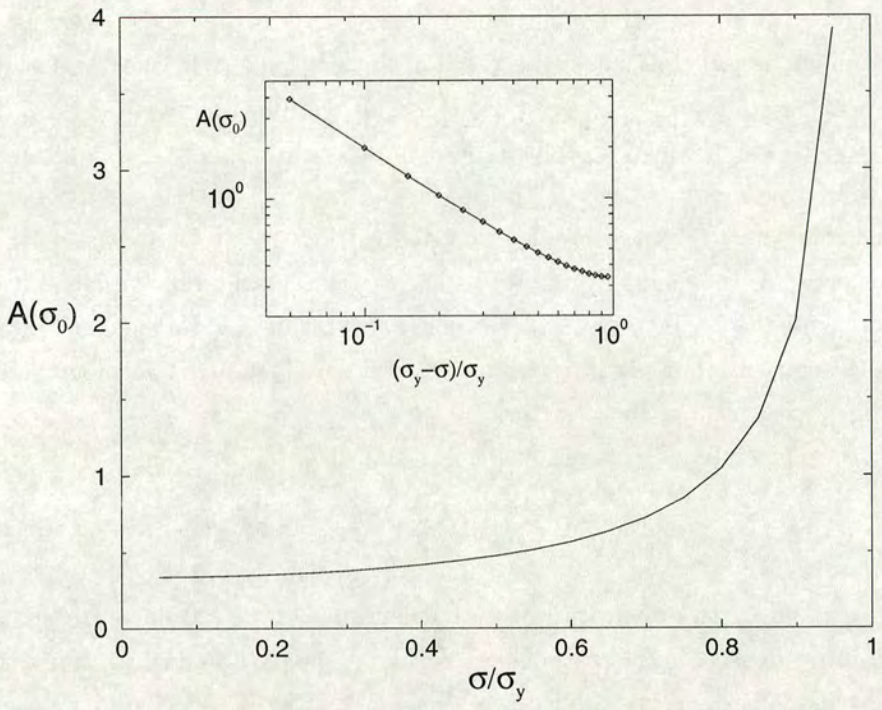

Figure 6.6. Prefactor $A(\sigma_0)$ to the logarithmic creep response to a step stress $\sigma_0 < \sigma_y$ in the glass phase of the SGR model: $\gamma(t) \approx \sigma_0 A(\sigma_0) J(t - t_w, t_w)$, where $J(t - t_w, t_w)$ is the linear regime result.

to its counterpart compliance spectrum $J^*(\omega, t)$.

Interesting ageing behaviour is also seen (for $x < 1$) in the model's non-linear rheology. Under shear startup, we see (after an early linear regime) a stress overshoot which is strongly dependence upon the system's age; the stress then subsequently falls to its ultimate steady-state (non-TTI) value as prescribed by the non-linear flow curve $\sigma - \sigma_y \sim \dot{\gamma}^{1-x}$. Ageing is interrupted by shear at any rate $\dot{\gamma} > 0$. We also studied the approach to this steady state via the imposition of a steady stress greater than the yield stress, $\sigma > \sigma_y$ (*i.e.* through a non-linear creep experiment).

6.4 Appendix I: irrelevance of initial state

To solve the constitutive equations 4.23 and 4.22 for flow behaviour at any time $t > 0$, one must in principle specify the initial state[2], $P_0(E)$. In the glass phase, one cannot appeal to equilibrium to fix this, since no equilibrium state exists. Instead, $P_0(E)$ should reflect the way in which the sample was prepared. Our analysis in the main text of this chapter and the previous one assumes for simplicity the idealized deep quench route to sample preparation defined in section 4.2.2; this fixes $P_0(E) = \rho(E)$. However, for rheological behaviour to be experimentally reproducible, it must be largely independent of the details of sample preparation, and hence of $P_0(E)$. With this motivation in mind, we now demonstrate the SGR model's rheology to be qualitatively robust with respect to variations in $P_0(E)$.

As a first step, we generalize the initial distribution, thus:

$$P_0(E) \propto \rho(E) \exp(E/x_0) \tag{6.4}$$

corresponding to preparation via quench from a *finite* temperature x_0. $P_0(E)$ can then be conveniently varied by means of the single parameter x_0, which must obviously obey $x_0 > 1$, since no equilibrium state exists for $x_0 \leq 1$. To focus the discussion, we shall consider only the linear regime (small local strains $l \ll 1$) for a working (post-quench) temperature in the glass phase ($x < 1$), because it is here that memory to initial state is likely to be most pronounced. As discussed in the main text, linear response is determined entirely by the evolution of the energy distribution $P(E,t)$. We therefore begin by studying the extent to which this distribution is, at large times $t \gg 1$, dependent upon x_0. From equation 4.6, we have

$$P(E,t) = P_0(E) \exp\left(-\frac{t}{\tau(E)}\right) + \rho(E) \int_0^t dt' Y(t') \exp\left(-\frac{t-t'}{\tau(E)}\right) \tag{6.5}$$

For convenience, we change variables from trap-depths (E) to trapping times (τ) (using $\tau(E) = \exp(E/x)$) to get

$$P(\tau,t) = P_0(\tau) \exp\left(-\frac{t}{\tau}\right) + \rho(\tau) \int_0^t dt' Y(t') \exp\left(-\frac{t-t'}{\tau}\right) \tag{6.6}$$

[2]In deriving the constitutive equation, we already imposed (for simplicity) the condition that each element should be locally unstrained at time $t = 0$: $P_0(E,l) = P_0(E)\delta(l)$. In this appendix, we do not attempt to relax this condition, but merely consider variations in $P_0(E)$. Possible effects of "frustration" in the local stresses were argued to be insignificant by Sollich in [Sol98].

in which[3]

$$P_0(\tau) \propto \tau^{-(1+y)} \tag{6.7}$$

with $y = x\left(1 - \frac{1}{x_0}\right)$. Inserting into equation 6.6 our asymptotic ($t \gg 1$) expression $Y(t) \sim t^{x-1}$ for the hopping rate in the glass phase $x < 1$ (see appendix 4.3), and approximating the exponential $\exp(-t/\tau)$ by the hard cut-off $\Theta(\tau - t)$, we obtain for $t \gg 1$ the following approximate distribution

$$\begin{aligned} P(\tau,t) &\sim t^{x-1}\tau^{-x} \quad \text{for} \quad \tau \ll t, \\ P(\tau,t) &\sim t^{x}\tau^{-(1+x)} \quad \text{for} \quad t \ll \tau \ll t^{x_0}, \\ P(\tau,t) &\sim \tau^{-(1+y)} \quad \text{for} \quad \tau \gg t^{x_0}. \end{aligned} \tag{6.8}$$

At any time $t \gg 1$, therefore, the only traps to have a population which depends to leading order upon the pre-quench temperature x_0 are those with trapping time $\tau \gg t^{x_0}$. Hence, in linear rheology, only those response functions which probe this tail of the distribution are expected to show pronounced dependence upon x_0. This is clearly consistent with the fact that the hopping rate, $Y(t)$, is (to leading order) always independent of x_0 (see appendix 4.3), since this quantity is always dominated by traps with $\tau = O(1)$. With the above remarks in mind, we now analyze each rheological response function in turn.

6.4.1 Linear stress relaxation function

In section 5.1.1, we argued that the stress relaxation modulus, $G(t-t_w, t_w)$, is (approximately) equal to the proportion of elements which, at the time t_w of strain switch-on, have time constants greater than $t - t_w$:

$$\begin{aligned} G(t-t_w, t_w) &\approx \int_{t-t_w}^{\infty} d\tau P(\tau, t_w) \\ &= 1 - \int_{1}^{t-t_w} d\tau P(\tau, t_w). \end{aligned} \tag{6.9}$$

Using the approximate distribution 6.8 we see that $G(t-t_w, t_w)$ must be insensitive to x_0 for time intervals $t - t_w \ll t_w^{x_0}$. The long-time tail, $t - t_w \gtrsim t_w^{x_0}$, however, does depend upon x_0. (In fact here $G(t-t_w, t_w)$ loses the scaling $(t - t_w/t_w)$, and returns to TTI

[3] We note that $P_0(\tau)$ is in fact just the prior distribution $\rho(\tau)$ evaluated at the effective noise temperature y.

behaviour, since the x_0-dependent tail of $P(\tau, t_w)$ is independent of age, t_w.) *However,* because this tail accounts only for a small fraction $O(t_w^{-x(x_0-1)})$ of the total decay, it is likely to be insignificant. Indeed, at long waiting times, $t_w = O[(1/\epsilon)^{1/(x(x_0-1))}]$, it will become unresolvable from the noise (assumed to be $O(\epsilon)$) in any realistic experiment. Hence we conclude that the stress relaxation modulus shows at most a small "transient" dependence upon pre-quench temperature. Our numerical results for this quantity are shown in figure 6.7, (for various pre-quench temperatures) and support this conclusion.

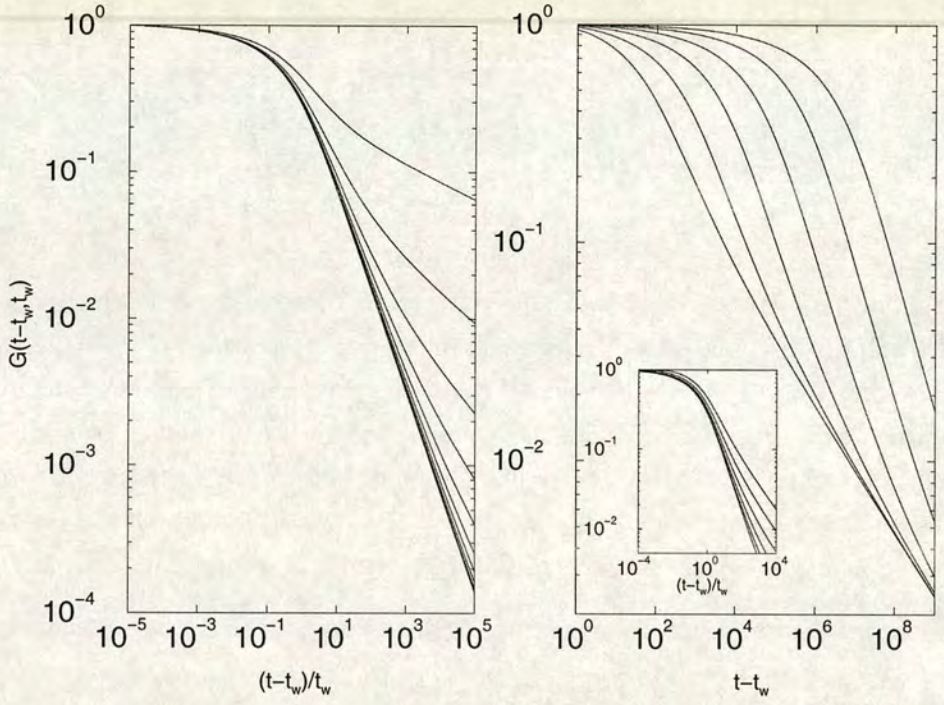

Figure 6.7. Left hand graph: stress relaxation modulus $G(t-t_w, t_w)$ vs. time interval $t-t_w$ following the imposition of a step strain at time $t_w = 10^2$. The noise temperature $x = 0.7$. Curves downwards correspond to a system prepared at time $t = 0$ via rapid quench from initial noise temperatures $x_0 = 1.2, 1.4...3.0$. Right hand graph: $G(t-t_w, t_w)$ vs. $t-t_w$ for a pre-quench noise temperature $x_0 \simeq 1.67$, and various waiting times $t_w = 10^2, 10^3...10^7$ (increasing left to right); the working temperature $x = 0.7$. Note particularly how the x_0-dependent tail shifts to smaller values of $G(t-t_w, t_w)$ as t_w increases. Inset: same data plotted against scaled time $(t-t_w)/t_w$; here t_w increases right to left.

6.4.2 Oscillatory response functions $G^*(\omega,t)$, and $J(\omega,t)$

We remarked in section 5.1.2 of the main text that any oscillatory perturbation can probe only those traps which have time constants $\tau \lesssim 1/\omega$. Coupled with the fact that the x_0-dependence of the distribution $P(\tau,t)$ shifts to ever deeper traps ($\tau \gtrsim O(t_{\rm w}^{x_0})$) as time progresses, this means that, for long enough waiting times ($t_{\rm w} \gtrsim (1/\omega)^{1/x_0}$), $G^*(\omega,t)$ and $J^*(\omega,t)$ must always become independent of x_0. Indeed, in any realistic oscillatory measurement the "many cycle" condition $\omega t_{\rm w} \gg 1$ is itself sufficient to ensure such independence.

6.4.3 Creep compliance

As noted in the main text, the structure of the constitutive equations 4.22 and 4.23 makes analytical progress difficult for imposed strain probes. Therefore we present only numerical results for this case: see figure 6.8. From these results we note that, although the compliance depends upon x_0 more strongly than (say) the stress relaxation modulus (figure 6.7), its behaviour is at least qualitatively independent of x_0. Indeed, for $x_0 \gtrsim 2$ it becomes quantitatively similar to the results given in the main text for $x_0 = \infty$.

6.4.4 Summary

We have demonstrated the linear rheology of the SGR model's glass phase to be relatively robust with respect to variations in the pre-quench temperature x_0, at least for $x_0 \gtrsim 2$. We have also argued that non-linear rheology (or rheology at higher working noise temperatures) is likely to be even less dependent upon initial state. Hence we predict that a material's behaviour at long times after quench should be relatively insensitive to the precise details of the procedure used to prepare the sample. We also conclude that the results shown for the SGR model in the main text (which assume $x_0 = \infty$) should be representative of the model's behaviour even for non-infinite values of x_0.

6.5 Appendix II: numerical calculation of non-linear compliance

We now outline the numerical scheme used to solve the constitutive equations 4.23 and 4.22 to find the strain response to an imposed step stress $\sigma(t) = \sigma_0\Theta(t - t_{\rm w})$. This is in fact rather complicated, because both the strain *and* the hopping rate, which are coupled through the non-linear equations 4.23 and 4.22, have to be calculated as

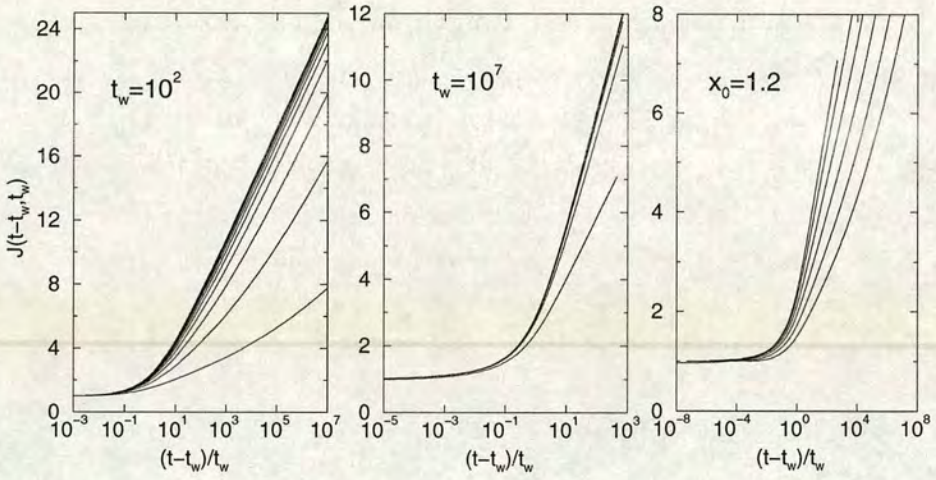

Figure 6.8. Left hand graph: creep compliance vs. scaled time $(t - t_{\rm w})/t_{\rm w}$ following the imposition of a step stress at time $t_{\rm w} = 10^2$. The noise temperature $x = 0.7$. Curves upwards correspond to a system prepared at time $t = 0$ via rapid quench from initial noise temperatures $x_0 = 1.2, 1.4...3.0$. Middle graph: same as LH graph, but now for a waiting times $t_{\rm w} = 10^7$. Right hand graph: creep compliance vs. scaled time $(t - t_{\rm w})/t_{\rm w}$ following the imposition of a step stress at a noise temperature $x = 0.7$ after a quench from a noise temperature 1.2. Curves right to left correspond to increasing waiting time: $t_{\rm w} = 10^2$, $10^3...10^7$.

functions of time. Our basic tactic is to discretize time into a grid $t_0, t_1...t_n$, where $t_0 = t_{\rm w}^+$, and to proceed along the grid calculating the strain γ_n and the hopping rate Y_n for successive values of the index n. The first point on the grid [$\gamma_0 = \gamma(t_{\rm w}^+)$ and $Y_0 = Y(t_{\rm w}^+)$], is obtained by treating the discontinuity at $t_{\rm w}$ "by hand": $\gamma(t_{\rm w}^+) = \sigma_0$ (since the SGR model assumes elasticity of instantaneous response) while $Y(t_{\rm w}^+) = Y(t_{\rm w}^-)\exp(\sigma_0^2/(2x))$ (since at $t_{\rm w}$ each element has its time constant instantaneously reduced by the identical factor $\exp(\sigma_0^2/(2x))$). (The yield rate $Y(t)$ for values of $t < t_{\rm w}$ can be read in from the results of the code described in appendix 4.4 above.)

At any subsequent time-step (t_n for $n \geq 1$) the two non-linear constitutive equations 4.23 and 4.22 are solved simultaneously. The first is essentially of the form:

$$0 \;=\; f[\gamma_n, Y_n, \{\gamma_{n'}\}, \{Y_{n'}\}, t_{\rm w}, \sigma_0, Y(t < t_{\rm w})] \quad \text{for} \quad 0 \leq n' < n \tag{6.10}$$

while the second can be differentiated and rearranged to give

$$Y_n \;=\; g[\gamma_n, \{\gamma_{n'}\}, \{Y_{n'}\}, t_{\rm w}, \sigma_0, Y(t < t_{\rm w})] \quad \text{for} \quad 0 \leq n' < n. \tag{6.11}$$

Since equation 6.10 can't be solved for γ_n, we use an iterative process. At each time-step we start by placing sensible upper and lower bounds[4] on γ_n. Each bound in turn is substituted into equation 6.11 (to find the corresponding value of Y_n) and (with its Y_n) into the function f of the right hand side of equation 6.10. The secant method is then used to update one of the bounds, and the new bound used to calculate a new Y_n and f. This process is repeated until we obtain a small value of f, such that $|f| < 10^{-8}$. The current (bound for) γ_n, and its corresponding Y_n, are then accepted and we proceed to the next time-step.

We now address the issue of choice of the grid $\{t_0, t_1 ...\}$. Given that strain and hopping rate are expected in general to be power laws one might expect a geometric grid to be suitable. However this actually results in numerical instability. We therefore choose an adaptive time-step update algorithm, which ensures that the strain always increases by approximately the same amount in any step.

Note finally that, at each iteration loop of each time-step, we in principle need to evaluate double integrals of the form:

$$I = \int_0^t dt' h(Z(t,t')), \tag{6.12}$$

in which

$$Z(t,t') = \int_{t'}^t dt'' \exp((\gamma(t'') - \gamma(t'))^2/(2x)). \tag{6.13}$$

This is however very costly computationally, so at each loop we first calculate $Z(t,t')$ on a grid of t' values ranging from 0 to t, and set up an interpolation over the calculated points. We are then left with the single integrals of the same form as I, and look up the value of Z whenever the integrand is called.

[4]The lower bound is just γ_{n-1} since γ must increase in time. In general we expect γ to have downward curvature. Hence an upper bound is found (expect at $n = 1$) by linear extrapolation from the previous two points $(t_{n-1}, \gamma_{n-1}), (t_{n-2}, \gamma_{n-2})$. Note however that the secant algorithm is relatively robust to choice of bounds. Even in regimes in which the strain has upwards curvature our choice of upper bound still results in the algorithm converging to a solution. At t_1 we are unable to use our usual method of extrapolate from two previous points to choose an upper bound. We therefore make the somewhat arbitrary choice $1.2\sigma_0$.

Chapter 7

Slow dynamics in branched polymer melts

So far, we have shown that the rheology of soft glassy materials (SGMs) such as foams and dense emulsions can be captured using a trap model of activated dynamics, with large free-energy barriers and a broad, power-law spectrum of activation time-scales. In this chapter, we turn to the rheology of another disordered soft material: the multiply branched polymer melt. Within the "tube model" (see below), such polymers reconfigure by retracting into their tubes, and poking out sideways through the tube "walls". Retraction is entropically impeded by molecular entanglements, and must be activated. The time-scale of relaxation at any molecular branch point thus increases steeply with branch point "seniority" (loosely, the curvilinear distance from the nearest chain end; see below). Therefore, as in the SGMs studied previously, the (equilibrium) relaxation spectrum, $P_{\rm EQ}(\tau)$, for the material as a whole, is very broad. In fact, in what follows we show that, for certain power law branching distributions, $P_{\rm EQ}(\tau)$ can be mapped onto its counterpart in the linear SGR model at a noise temperature just above the glass transition, $x \gtrsim 1$. Hence the linear equilibrium rheology of these polymers should follow directly from the results of previous chapters, without any further calculation. Our main interest, however, will be in the extension of this equilibrium model to melts which have recently been prepared in a *non*-equilibrium state by a rapid (non-linear) pre-shear. Here, after cessation of pre-shear, the linear relaxation spectrum is predicted to show qualitatively the same slow approach to equilibrium as that of the SGR after a quench to $x \gtrsim 1$. Using this similarity, we argue that the melts should, after pre-shear, show very long transients in their linear rheology. Experimentally, of course, such transients could be very difficult to distinguish from the true ageing which occurs in the SGR model at $x \leq 1$.

The chapter is organized as follows. In section 7.1, we introduce the necessary basics of polymer dynamics. In section 7.2, we describe the application of the tube model to branched polymer melts. In section 7.3 we demonstrate the mapping of this model (for certain power-law branching distributions) to the SGR model at $x \gtrsim 1$, and study in detail its predictions for long rheological transients in a melt prepared by a rapid pre-shear.

7.1 Background polymer physics

Polymers are large, chain-like molecules which comprise many[1] small atomic groups (monomers) connected into linear chains by covalent chemical bonds. Branch points can occur in these chains, resulting in various topologies ranging from simple stars (one branch point) to highly complex, multiply branched structures.

7.1.1 Polymer flexibility: the "random walk" chain

In their bending properties, polymers range from totally rigid to highly flexible. A chain's rigidity can be quantified by comparing its curvilinear length, L, with the curvilinear distance, b, over which correlations in segmental orientations decay to zero. A rigid rod has $b \gg L$. In contrast, a highly flexible chain has $b \ll L$, and effectively performs a random walk on the scale b: the distribution of the chain end-to-end vector, $\mathbf{R}$, in this case follows from the standard diffusion result

$$P(\mathbf{R})d^3\mathbf{R} \propto \exp\left(-\frac{3R^2}{2Nb^2}\right) d^3\mathbf{R}, \tag{7.1}$$

where N denotes the number of steps in the walk. $P(\mathbf{R})$ is clearly peaked at $\langle \mathbf{R} \rangle = 0$, and any macrostate in which $\mathbf{R} \neq 0$ (*e.g.* a chain pulled taut by an external force) will experience a Hookean entropic tension

$$T\frac{\partial}{\partial \mathbf{R}} \ln\left[P(\mathbf{R})\right] = -\frac{2k_BT}{Nb^2}\mathbf{R} \tag{7.2}$$

tending to restore $\mathbf{R}$ to zero. The spread of the distribution 7.1 gives the mean-squared end-to-end vector as

$$R^2 = \frac{3}{2}Nb^2. \tag{7.3}$$

In what follows, we consider "melts" (see next section) of such highly flexible molecules.

[1] 10^2 to 10^4 for synthetic polymers. 10^9 to 10^{10} for large biological polymers such as DNA.

7.1.2 Polymer melts: the tube model and reptation

A melt comprises many molecules which can, for long enough chains, be highly entangled with one another. Due to the entanglements, if any molecule attempts to move in a direction perpendicular to its axis, it must drag many other molecules with it and will therefore feel a large resistance. Each molecule is therefore effectively confined to a "tube" formed by the topological constraints of entanglements (figure 7.1). It cannot move laterally, and it instead (provided it is not branched; see below) "reptates" (creeps) along the axis of the tube. The molecular configuration at some time $t = 0$ is gradually refreshed as the free ends reptate out of the original ($t = 0$) tube and adopt new configurations, in new tubes (figure 7.2).[2]

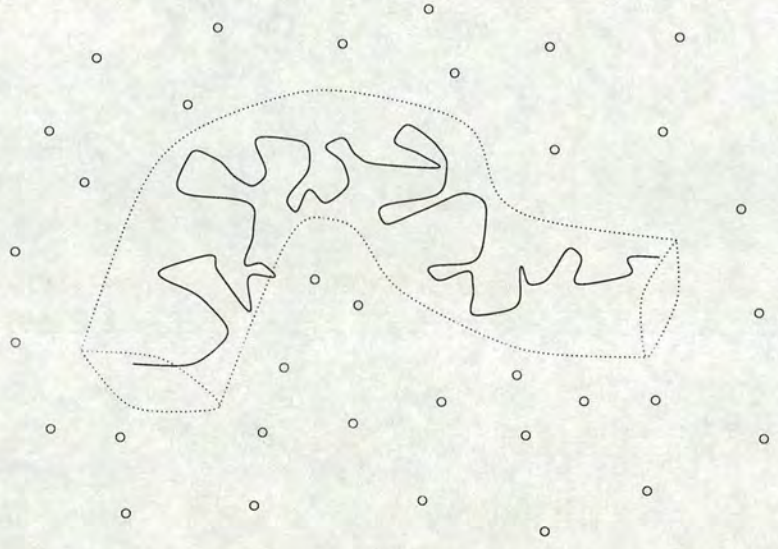

Figure 7.1. Schematic illustration of the tube of topological constraints (intermolecular entanglements) which inhibits lateral molecular motion in melts. For clarity, the majority of molecules have been assumed to have their axes perpendicular to the page, and have therefore been represented as dots.

Primitive path length

The actual configuration of a chain within its tube can be decomposed into two components (see figure 7.3). The first is the "primitive path", which is defined as the shortest path from one end of the chain to the other with the same constrained topology as the

[2]Entanglements only impede *dynamics*. *Static* properties are unaffected, since the system is still ergodic. For example, the end-to-end vector still obeys $R^2 \sim Nb^2$.

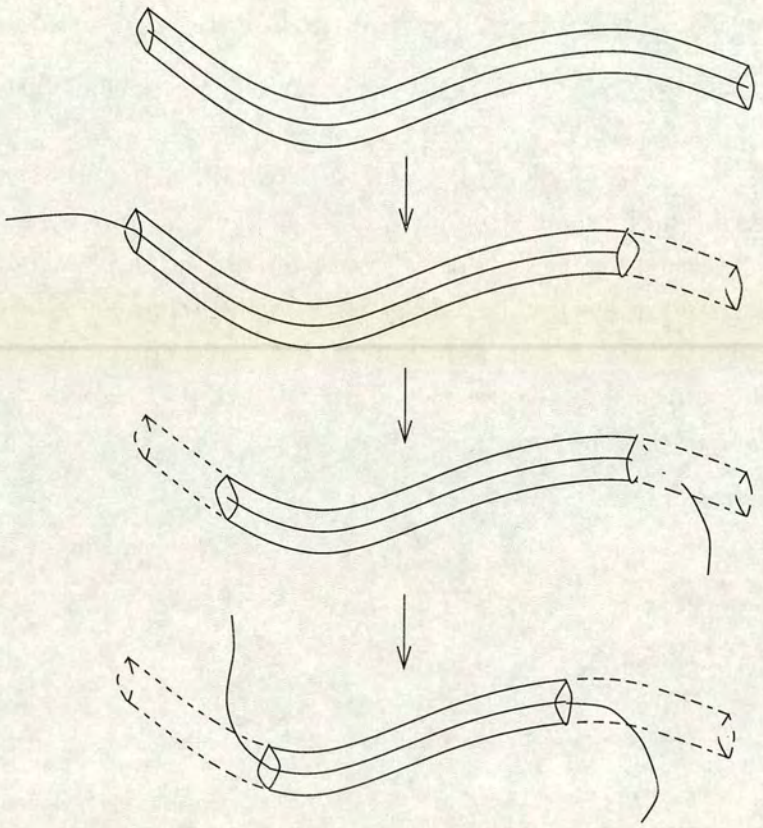

Figure 7.2. Four successive stages in the reptation process via which a linear polymer molecule refreshes its configuration ("escapes its tube").

chain itself. (Loosely, it is the path of the tube itself.) We shall denote its curvilinear length by z. Superposed on this are intra-tube "defects", *i.e.* "wiggles" of the actual chain (which were omitted from figures 7.1 and 7.2).

Tube step length and diameter. Entanglement length

Assuming that the chain performs a random walk between any two entanglements, we have

$$a^2 = \frac{4}{5} N_e b^2 \tag{7.4}$$

in which a and N_e are respectively the typical distance and number of chain segments between entanglements. (The prefactor 4/5 is discussed in [DE86].)

The primitive path itself performs a random walk coarse grained at this length scale

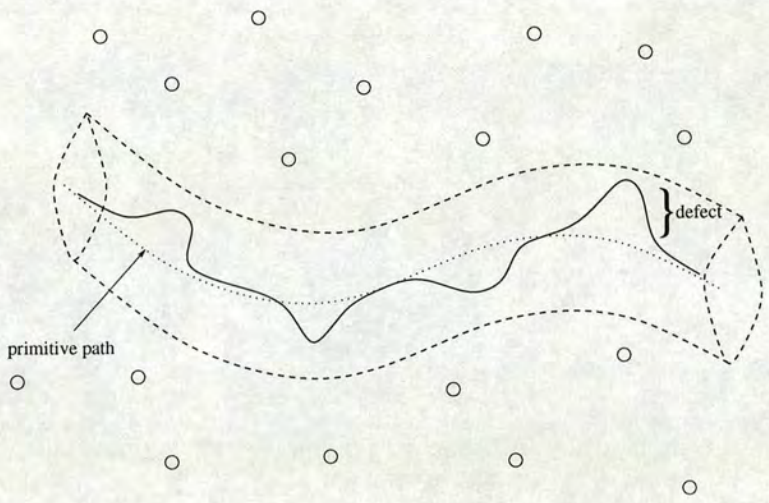

Figure 7.3. Decomposition of molecular configuration into the primitive path, and defects of the actual chain about this primitive path.

a. Its mean-squared end-to-end distance is thus

$$R^2 = \frac{3}{2} z a \tag{7.5}$$

(which must obviously equal the mean-squared end-to-end distance of the chain itself, as given by equation 7.3). In what follows we shall also refer to the tube diameter, a_0, which is of order a.

7.2 Activated retraction in branched topologies

7.2.1 Star molecules

In star polymers, reptation is inhibited by the molecular branch point. Instead, each constituent molecular arm reconfigures by *retracting* into its tube, and then poking out sideways through the tube "walls" (figure 7.4). In any retraction event, all chain segments between the arm's free-end and the deepest point of retraction are relaxed. Retraction is impeded by an outward entropic force (due to entanglements; see below) and must be activated. The time-scale for relaxation thus increases rapidly with segmental curvilinear distance from the arm's free end. This gives rise to a very broad spectrum of relaxation time-scales, which can be seen experimentally, for example, via a plateau in the loss modulus, $G''(\omega)$, over several decades of frequency.

To calculate this relaxation spectrum [MM99], we recognize that retraction up to

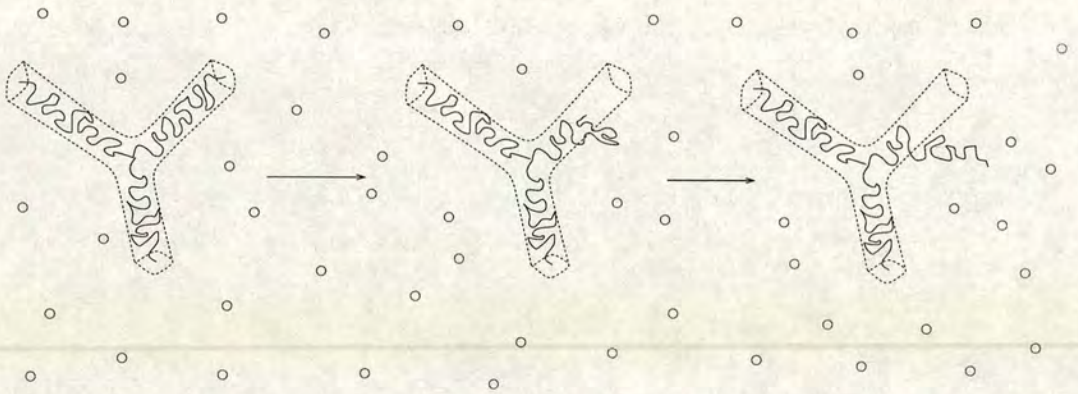

Figure 7.4. Relaxation in branched polymer melts: a molecular arm retracts into its tube, and subsequently escapes by poking out sideways though the tube walls.

a given curvilinear distance, s, from the arm's free end corresponds to a fluctuation in which the primitive path of the arm contracts from its mean length, $\bar{z}$, down to $z = \bar{z} - s$. Hence the time-scale follows as $\tau(s) = \tau_0 P(\bar{z})/P(z = \bar{z} - s)$ where τ_0 is an attempt time[3] and $P(z)$ is the static distribution of primitive path lengths.

$P(z)$ can be calculated by counting the number of microstates consistent with any path length, z. There are two contributions. The first measures the number of states consistent with *one* realization of a primitive path. Considering a random walk in a tube of length z and diameter a_0, this is just

$$\omega(z) = \omega_0 \exp\left(-\frac{3z^2}{2Nb^2} - \alpha_0 \frac{Nb^2}{a_0^2}\right) \tag{7.6}$$

(where α_0 is a numerical factor which depends on the shape of the tube's cross-section). The z dependence of this term is just a random walk distribution, analogous to that given above for the end-to-end vector of a free chain; it results in an entropic tension which tends to contract z to zero. The second contribution, $\Omega(z)$, counts the number of possible primitive paths of length z, and scales as $\exp(z/a)$. This clearly increases with z (since there are more ways of realising a longer path) and therefore provides an *outward* entropic force which balances the "collapsing tension" of $\omega(z)$: it maintains z

[3] τ_0 is actually the "Rouse" time of a typical entanglement length, *i.e.* it is smallest time-scale on which the chain experiences entanglements. See any standard text on polymer dynamics, *e.g.* [DE86].

at a non-zero average, $\bar{z}$, and opposes retraction:

$$P(z) \propto \omega(z)\Omega(z) \propto \exp\left[-\frac{3}{2Nb^2}(z-\bar{z})^2\right] \tag{7.7}$$

in which the mean primitive path length $\bar{z} = Nb^2/a$. Fluctuations in z (and hence in $s = \bar{z} - z$) are thus impeded by an entropic potential

$$U(s) = \frac{3k_BTs^2}{2Nb^2}, \tag{7.8}$$

and the time-scale for relaxation up to a curvilinear distance s is

$$\tau(s) = \tau_0 \exp\left(\frac{3s^2}{2Nb^2}\right). \tag{7.9}$$

For a given arm length (of N segments), the terminal time (on which retraction reaches segments right at the branch point) is given by putting $s = \bar{z} = Nb^2/a$ to get [MM99]

$$\tau(\bar{z}) = \tau_0 \exp\left(\frac{15N}{8N_e}\right) \tag{7.10}$$

in which we have also used $a = \frac{4}{5}N_eb^2$ from equation 7.4. Notably, $\tau(\bar{z})$ is determined entirely by the number of entanglement lengths per arm, N/N_e. In what follows, we denote this ratio by ν.

Dynamic dilution

Although the theory just described is qualitatively appealing, equation 7.10 actually over-estimates the terminal time (as measured via the terminal loss "peak" in the viscoelastic spectrum $G''(\omega)$) by several orders of magnitude. To resolve this puzzle, Ball and McLeish [BM89] argued that the dynamics must actually be "diluted" with respect to those described above: specifically, the tube to which any arm is confined is itself composed of arms of other molecules, the outermost parts (low s) of which reconfigure many times on the time-scale of innermost parts (high s), and cannot act to confine them. Hence, the degree of entanglement experienced by innermost segments is diluted with respect to that used above; the entanglement length relevant for any curvilinear distance s is not N_e but rather $N_e/[1-(s/\bar{z})]$.

As a first step towards incorporating this dilution effect quantitatively, we rewrite

equation 7.9 in a "hierarchical" (but as yet undiluted) form as follows [MM99]

$$\frac{\partial}{\partial s}\tau(s) = \tau(s)\frac{\partial}{\partial s}U(s). \tag{7.11}$$

We can now easily insert the s-dependent N_e to get

$$\frac{d}{ds}\tau(s) = \tau(s)\frac{\partial}{\partial s}U[s; N_e(s)] \tag{7.12}$$

which can be integrated to find $\tau(s)$. The spectrum thus obtained, for a given arm length N, agrees with the frequency range of the plateau in $G''(\omega)$ to within a factor 2.

7.2.2 Highly branched molecules

Highly branched "tree-like" molecules also reconfigure by activated retraction. As for the simple star molecules discussed above, one could in principle calculate the curvilinear extent of chain which relaxes on any given time-scale. However, for this more complicated case we choose to coarse-grain the dynamics, and instead consider the number of levels in the tree which relax. Instead of considering the curvilinear distance of any arm segment from the chain's free end, we now consider the "seniority" s at a given branch point [McL00], which measures the number of branch points between that point, and the dangling end from which retraction is quickest to reach it.[4] It is found (see figure 7.5) by identifying all the "sub-molecules" which stem from the point, and, for each sub-molecule, identifying the number of branch points s_{sub} to the dangling end which is the furthest curvilinear distance away. (s_{sub} sets the time-scale via which retraction would reach our branch point via that particular sub-molecule). The seniority s of the point is then the *minimum* value, over all sub-molecules, of s_{sub}.

To calculate the relaxation time-scale at a given seniority, s (for the moment in an undiluted picture), we work within a hierarchical description analogous to equation 7.11: the attempt time at seniority s is set by the relaxation time-scale at $s-1$, while the incremental barrier (between any two seniorities) is prescribed by equation 7.10 above to be $N/N_e = \nu$, where N is now the number of monomers between any two branch points. We thus have

$$\frac{d\tau(s)}{ds} = \nu\tau(s) \tag{7.13}$$

[4] Hence, whereas in the discussion of simple star molecule the seniority s had dimensions of (curvilinear) length, in this case s is a dimensionless counter.

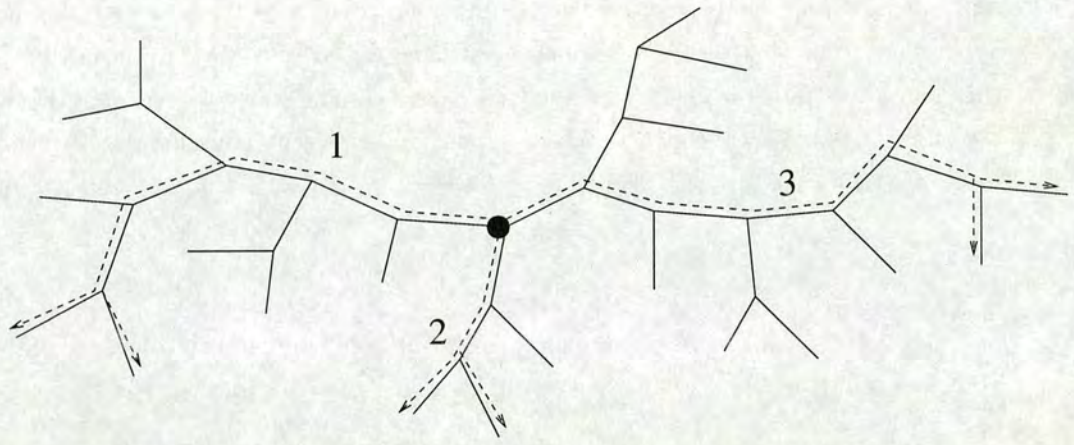

Figure 7.5. Relaxation in highly branched polymer melts: here, retraction reaches the circled point most quickly via path 2. (See main text for explanation.)

and hence

$$\tau(s) = \tau_0 \exp(s\nu). \tag{7.14}$$

To incorporate "dilution dynamics" into this picture, we recognize (as above) that, on the time-scale of relaxation at seniority s, all lower seniorities ($s' < s$) will reconfigure many times. Segments of seniority s therefore see a diluted entanglement concentration $\nu \int_s^\infty ds' \phi(s')$, where $\phi(s)$ is the "branching distribution" (*i.e.* the fraction of molecular branch points with seniority s). We then have [MM99]

$$\frac{d\tau(s)}{ds} = \nu\tau(s) \left(\int_s^\infty ds' \phi(s') \right)^\alpha . \tag{7.15}$$

In this equation, according to the preceding discussion, α should equal 1. Experimentally[5] one actually finds $\alpha \approx 4/3$. The discrepancy is due to the fact that entanglements are not just (as the above discussion implicitly assumed) "binary" events between two chains. Note that, if we were artificially to set $\alpha = 0$ in equation 7.15, we would recover the undiluted equation 7.13: α is therefore called the "dilution exponent".

In what follows we extend [MM99] by choosing a power-law branching distribution, $\phi(s) = (\sigma - 1)s^{-\sigma}$, imposing $\sigma > 1$ to ensure normalizability. Within this choice, 7.15 can be integrated to give

$$\ln \left[\frac{\tau(s)}{\tau_0} \right] = \frac{\nu}{\epsilon}(s^\epsilon - 1) \tag{7.16}$$

[5]The experiments were actually performed on linear melts, although one expects the result to apply also to branched polymers.

in which $\epsilon = 1 + \alpha(1 - \sigma)$. Without loss of generality, we hereafter work in time units chosen such that $\tau_0 = 1$. The behaviour of $\tau(s)$ as s becomes large is markedly dependent upon the sign of ϵ, which is in turn determined by the interplay between the degree of dilution (which is fixed as $\alpha \approx 4/3$ as noted above) and the width of the distribution (as prescribed by σ, which can be varied by chemistry). For $\epsilon \leq 0$ (corresponding to "broad" branching distributions, for which $\sigma \leq 1/\alpha + 1$) we find

$$\lim_{s\to\infty} \tau(s) = \infty, \tag{7.17}$$

and the spectrum of tube escape times, like the spectrum of seniorities, is unbounded above. In contrast, for $\epsilon < 0$ ("narrow" branching distributions with $\sigma > 1/\alpha + 1$), we find

$$\lim_{s\to\infty} \tau(s) = \frac{\nu}{|\epsilon|} = \text{const.} \tag{7.18}$$

Here, the terminal time is finite.

If dilution were to be switched off ($\alpha = 0$), all distributions would, in the above classification scheme, be broad: *i.e.* , the terminal time would be infinite, regardless of the exponent σ in $\phi(s)$. Our (experimentally determined) non-zero value of $\alpha \approx 4/3$, on the other hand creates sufficient dilution such that any (narrow) unbounded seniority spectrum[6] (with $\sigma > 1/\alpha + 1$) is converted into an *bounded* spectrum of tube escape times.

7.3 Rheology of highly branched polymer melts

7.3.1 Equilibrium rheology

So far, we have discussed the equilibrium dynamics of molecular reconfiguration. We now examine how these dynamics are probed by linear rheology. To simplify the analysis, we make the following set of assumptions [DE86]. First: that stress resides entirely in the inter-molecular entanglements. Second: that, upon any sudden small strain increment, each entanglement initially deforms elastically. And third: that each entanglement completely relaxes its stress when it reconfigures.

Within these assumptions, the linear stress relaxation function[7], $G(t-t_w)$, is just the number of entanglements which do not reconfigure over the interval $t_w \to t$. Assuming

[6] We are assuming here the thermodynamic limit in which $\phi(s)$ will be unbounded above. Finite system size would obviously introduce an upper cutoff into $\phi(s)$.

[7] In this equilibrium case, t_w is an arbitrary time variable which could be set to zero. However we retain it in anticipation of the fact that we shall soon discuss a non-equilibrium system in which TTI breaks down.

initially that all entanglements are binary events, this is found as follows. At any time, the population of entanglements formed between segments of seniorities s and s' is $N\phi(s)\phi(s')$. Of these, a fraction $\exp[-(t-t_{\rm w})/\tau(s)]\exp[-(t-t_{\rm w})/\tau(s')]$ remains unrelaxed after a time interval $t-t_{\rm w}$. Integrating over all combinations (s,s'), we find the total number of unrelaxed entanglements to be

$$G(t-t_{\rm w}) = N\int_1^\infty ds\phi(s)\exp\left(-\frac{t-t_{\rm w}}{\tau(s)}\right)\int_s^\infty ds'\phi(s')\exp\left(-\frac{t-t_{\rm w}}{\tau(s')}\right). \qquad (7.19)$$

(The lower limit of the second integral is s, and not 1, to avoid double counting.) To simplify this expression, we exploit the fact that the tube-escape time-scales for different seniorities are well separated, and hence that the relaxation time-scale of any entanglement is just the escape time for the lower of its two constituent seniorities. Hence we have

$$\begin{aligned} G(t-t_{\rm w}) &= N\int_1^\infty ds\phi(s)\exp\left(-\frac{t-t_{\rm w}}{\tau(s)}\right)\int_s^\infty ds'\phi(s') \\ &= \frac{N}{2}\int_1^\infty ds\frac{d}{ds}\left(\int_s^\infty ds'\phi(s')\right)^2\exp\left(-\frac{t-t_{\rm w}}{\tau(s)}\right). \end{aligned} \qquad (7.20)$$

So far, we have assumed that entanglements are purely binary events. To relax this assumption we must (see [MM97]) replace the power 2 in the above equation by $1+\alpha$:

$$G(t-t_{\rm w}) = G_0\int_1^\infty ds\frac{d}{ds}\left(\int_s^\infty ds'\phi(s')\right)^{1+\alpha}\exp\left(-\frac{t-t_{\rm w}}{\tau(s)}\right). \qquad (7.21)$$

Inserting our chosen branching distribution $\phi(s) = (\sigma-1)s^{-\sigma}$, and switching variables s to τ using equation 7.16, we find

$$G(t-t_{\rm w}) = G_0\int_1^\infty d\tau P_{\rm EQ}(\tau)\exp\left(-\frac{t-t_{\rm w}}{\tau(s)}\right) \qquad (7.22)$$

in which

$$P_{\rm EQ}(\tau) = \frac{(1+\alpha)(1-\epsilon)}{\nu\alpha}\frac{1}{\tau}\left(1+\frac{\epsilon}{\nu}\ln\tau\right)^{-\frac{1}{\alpha\epsilon}(1+\alpha-\epsilon)}. \qquad (7.23)$$

This distribution clearly depends for its normalizability upon the bracketed logarithmic term, since the factor $1/\tau$ would by itself be unnormalizable: for $\epsilon < 1$ [corresponding to $(1+\alpha-\epsilon)/\alpha\epsilon > 1$], it is normalizable, while for $\epsilon \geq 1$ it is (as it stands) unnormalizable (although normalizability could be restored by the imposition of a cutoff, $\tau_{\rm max}$).

For $\epsilon = 0$, the exponent $(1+\alpha-\epsilon)/\alpha\epsilon$ diverges, and the logarithmic term in equation 7.23 crosses over to a power law. To see this, we expand 7.23 for small $\frac{\epsilon}{\nu}\ln\tau$

as

$$\begin{aligned} P_{\rm EQ}(\tau) &\sim \frac{1}{\tau}\exp\left[-\frac{\sigma}{\epsilon}\left(\frac{\epsilon}{\nu}\ln\tau - \frac{\epsilon^2}{\nu^2}\ln^2\tau + ...\right)\right] \\ &\sim \tau^{-(1+\delta)}\tau^{\frac{\sigma\epsilon}{\nu^2}\ln\tau} \end{aligned} \tag{7.24}$$

In this equation, $\delta = \frac{1+\alpha}{\nu\alpha}$ where (as noted above) $\alpha \approx 4/3$; the degree of entanglement, $\nu = N/N_{\rm e}$, can be tuned (by appropriate chemical synthesis) to lie anywhere from zero (unentangled) to $O(100)$ (highly entangled). Taking the limit $\epsilon \to 0$ we have:

$$P_{\rm EQ}(\tau) = \delta\tau^{-(1+\delta)}. \tag{7.25}$$

For values of ϵ which are small but negative, the distribution has the form 7.24 when $\frac{|\epsilon|}{\nu}\ln\tau \ll 1$, but has an upper cut-off at $\frac{\epsilon}{\nu}\ln\tau = 1$, which marks the existence of a terminal time

$$\tau_{\rm term} = \exp\left(\frac{\nu}{|\epsilon|}\right). \tag{7.26}$$

Hence, as noted in section 2.1.1 above, for negative values of ϵ, dynamic dilution is sufficient to convert an unbounded spectrum of seniorities into a bounded spectrum of relaxation time-scales.

To summarize: for ϵ anywhere in the range $-\beta < \epsilon < 1$ (where β is small), the relaxation spectrum is effectively of the form $1/\tau$, with logarithmic corrections, a weak power law correction, or a very large cut-off terminal time rendering it normalizable. Hence, we expect to see qualitatively similar sluggish rheological response for all such values of ϵ, reflecting the fact that the underlying relaxation spectrum is extremely broad. We also expect to see similarities with the rheology of the SGR model just above its glass point, since the equilibrium distribution in that model (equation 4.4 with variables changed from E to τ) is very broad for $x \gtrsim 1$, and formally becomes unnormalizable for $x = 1$. Indeed, comparing equation 7.25 to equation 4.16, we see that, for $\epsilon = 0$, $P_{\rm EQ}(\tau)$ is formally identical to its counterpart in the linear SGR model at a noise temperature δ above the glass point. In what follows, we specialise to this case $\epsilon = 0$, since here we can make predictions for the rheology of the polymer model without any formalism beyond that used in previous chapters: for example, the stress relaxation modulus $G(t - t_{\rm w}) = \Gamma(1+\delta)(t - t_{\rm w})^{-\delta}$, while the viscoelastic spectrum is a very weak function of frequency $[G^*(\omega) = \Gamma(1+\delta)\Gamma(1-\delta)(i\omega)^{\delta}]$. We consider only very small values of δ $[O(1/100)]$ corresponding to highly entangled melts with very sluggish dynamics.

7.3.2 Non-equilibrium rheology: recovery after strong shearing

So far, we have considered the rheology of an equilibrium melt. We now consider a melt prepared in a non-equilibrium state by means of pre-shear at a high rate $\dot{\gamma} \gg 1/\tau_0 = 1$. During pre-shear, all elements are assumed to align to the shear direction. The entanglements thus become inactive for shear stress [DE86]. After cessation of pre-shear (at time $t = 0$), each entanglement grows back to rheological significance on its own relaxation time-scale. So after any waiting time t_w we have

$$\begin{aligned} P(\tau, t_w) &= P_{EQ}(\tau)\left[1 - \exp\left(-\frac{t_w}{\tau}\right)\right] \\ &= \delta\tau^{-(1+\delta)}\left[1 - \exp\left(-\frac{t_w}{\tau}\right)\right]. \end{aligned} \tag{7.27}$$

Writing this in the approximate form

$$\begin{aligned} P(\tau, t_w) &\approx \delta\tau^{-(1+\delta)} \quad \text{for} \quad \tau \ll t_w \quad \text{and} \quad t_w \gg 1 \\ &\approx \delta t_w \tau^{-(2+\delta)} \quad \text{for} \quad \tau \gg t_w \quad \text{and} \quad t_w \gg 1, \end{aligned} \tag{7.28}$$

we see that it is, to within a normalization factor $N(t_w)$, the same as the approximate distribution of the SGR model following a deep quench to a noise temperature just above its glass transition ($x = 1 + \delta$):

$$\begin{aligned} P_{SGR}(\tau, t_w) &\approx \tfrac{1}{N(t_w)}\delta\tau^{-(1+\delta)} \quad \text{for} \quad \tau \ll t_w \quad \text{and} \quad t_w \gg 1 \\ &\approx \tfrac{1}{N(t_w)}\delta t_w \tau^{-(2+\delta)} \quad \text{for} \quad \tau \gg t_w \quad \text{and} \quad t_w \gg 1, \end{aligned} \tag{7.29}$$

in which $N(t_w) \approx 1 - (1 + t_w)^{-\delta}$. Hence, we expect the two models to show strong similarities in their non-TTI rheology. (We recall that their *equilibrium* rheology is formally identical: $\lim_{t_w \to \infty} N(t_w) = 1$.) With this in mind, we briefly remind ourselves of the long transients which the SGR model shows during the slow equilibration following a quench to a noise temperature $x = 1 + \delta$.

Recap: long transients in the SGR model

Immediately after a deep quench to $x = 1 + \delta$, the relaxation spectrum of the SGR model is $(1 + \delta)\tau^{-(2+\delta)}$; it has most of its weight at time-scales $\tau = O(1)$. In contrast, the ultimate equilibrium spectrum $[\delta\tau^{-(1+\delta)}]$ has most of its weight spread over the very broad interval $1 < \tau < \exp(1/\delta)$. Hence, during equilibration, the distribution spreads over progressively larger time-scales. To compensate for this, the population of elements with time-scales $\tau = O(1)$ falls as $1/N(t_w) \sim 1/\ln t_w$ (to leading order) from its initial value $O(1)$ to its final value $O(\delta)$. This time evolution is shown schematically

in figure 7.6a. The ergodic time $\tau_{\rm erg} = O(\exp(1/\delta))$: for $t_{\rm w} \gg \tau_{\rm erg}$ the relaxation spectrum is, to good approximation, equal to the equilibrium distribution $\delta\tau^{-(1+\delta)}$; $N(t_{\rm w}) = 1$ to leading order.

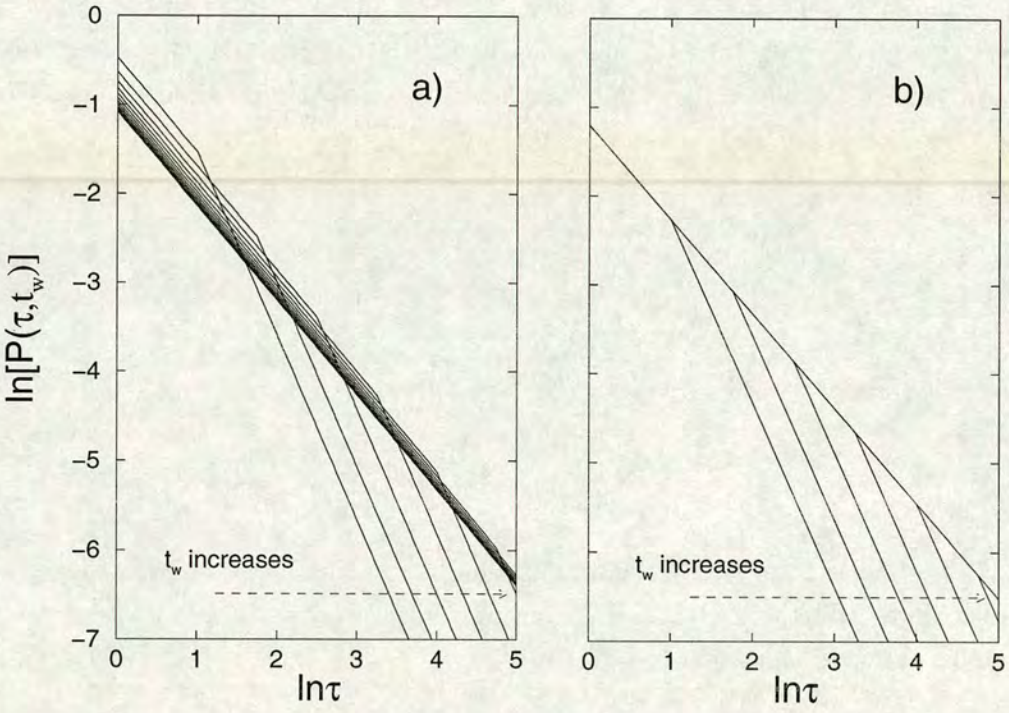

Figure 7.6. Schematic evolution of the relaxation time distribution for a) the SGR model just above its glass transition ($x = 1.0625$) and b) the dynamic dilution model of branched polymer melts at $\epsilon = 0, \delta = 0.0625$. Waiting times between $t_{\rm w} = 10$ and $t_{\rm w} = 10^{10}$ are shown, with a factor $10^{0.75}$ between successive values. (The largest waiting times are not distinguishable from each other in the right hand graph.) The ergodic time at this value of δ is $\tau_{\rm erg} = O(10^8)$. For the SGR model (which has a conserved population of elements), the population of shallow traps depletes over the interval $0 < t_{\rm w} < \tau_{\rm erg}$ as the weight of the distribution shifts to deeper traps. In the dynamic dilution model the population grows over time from, and this depletion of shallow traps does not occur. The final equilibrium distributions are the same for both models.

For waiting times $t_{\rm w} \ll \tau_{\rm erg}$ (when the relaxation spectrum has non-trivial dependence upon $t_{\rm w}$ as just described), we see non-TTI linear rheology. To leading order, the response functions $G(t - t_{\rm w}, t_{\rm w})$, $J(t - t_{\rm w}, t_{\rm w})$ and $G^*(\omega, t)$ have respectively the forms given for $x = 1$ (equivalent to $\delta = 0$) in tables 5.1 and 6.1, and equation 5.7. For example, $G(t - t_{\rm w}, t_{\rm w})$, in its long-time regime, $t - t_{\rm w} \gg t_{\rm w}$, (which accounts for

a fraction $O(1/\ln t_w) = O(1)$ of the total stress decay) scales as $(t - t_w)/t_w$ to within corrections[8] $O(\ln t_w)$. The short time ($t - t_w \ll t_w$) behaviour of $G(t - t_w, t_w)$ is also t_w dependent, although less so: it can actually be scaled either as $(t - t_w)/t_w$ *or* $t - t_w$, in both cases to within corrections $O(\ln t_w)$. The loss modulus, $G^*(\omega, t)$, likewise (at any fixed frequency) falls logarithmically with t. Physically, this reflects the logarithmic depletion of traps with $\tau \lesssim (1/\omega) \ll t$ ([9]) as the spectrum shifts to slower modes. Furthermore, because most modes are elastic on the time-scales of order the inverse measurement frequency, the loss modulus does not show its usual decay towards zero as frequency is tracked downwards.

For the small values of δ [$O(1/100)$] considered here, the ergodic time $\tau_{erg} = O[\exp(1/\delta)]$ is huge, and therefore unlikely to be reached in any realistic experiment: for all practical purposes, TTI will appear to have permanently broken down. Experimentally, this behaviour is likely to be very difficult to distinguish from the true ageing which occurs for noise temperatures $x < 1$. Theoretically, however, this transient approach to equilibrium can be distinguished from formal ageing (as described in section 2.1.1) by the fact that the tail of $P(\tau, t_w)$ which depends upon t_w accounts for a smaller and smaller fraction of the total spectrum as t_w becomes large.[10] Hence, if waiting times comparable with the ergodic time *could* be accessed, the spectrum would then be time-independent in all but an unimportant tail ($\tau \gg t_w$). The early ($t - t_w \ll t_w$) part of the decay of $G(t - t_w, t_w)$ (which would account for all but a negligible fraction of the total decay) would be independent of t_w. Likewise $G^*(\omega)$ would be time independent to leading order. TTI would be effectively restored[11].

Long rheological transients in hierarchically branched polymers

As noted above, the tube model of highly branched polymer melts, for certain "critical" power law branching distributions ($\epsilon = 0$) and high levels of entanglement (δ small) shows exactly the same equilibrium rheology as the SGR model at a small noise temperature above its glass point, $x = 1 + \delta$. Furthermore, after rapid pre-shear, it shows approximately the same slow relaxation to equilibrium as the SGR model shows after a quench to $x = 1 + \delta$. Hence we expect to see long transients in these melts, similar to those just described for the SGR model. The results of this section will

[8] Recall the discussion on "marginal" $(t - t_w)/t_w$ scalings for $x = 1$ of section 5.1.

[9] which are the only traps to be probed by the loss modulus.

[10] For ageing systems, this tail always accounts for $O(1)$ of the total weight, even in the limit $t_w \to \infty$.

[11] Formally, of course, TTI could only be *completely* recovered in the true limit $t_w \to \infty$, since, even for waiting times $t_w \gg \tau_{erg}$, the final (small) fraction $t_w^{-\delta}$ of the stress decay following a step strain still depends upon t_w.

show that this is indeed the case. Before presenting the results, however, we note that the relaxation spectrum of the polymer model differs from that of the SGR model in one important respect. (See figure 7.6b.) In the SGR model, the total population of elements is conserved over time. Hence, immediately after quench [when the spectrum has width $O(1)$], traps with time constants $\tau = O(1)$ have a non-negligible ($O(1)$) population. As the system slowly evolves (over the interval $0 < t_w < \tau_{erg}$) towards the final very broad equilibrium distribution, these shallow traps gradually deplete to their final population $O(\delta)$. In the polymer model, however, there are no elements at time $t_w = 0$; here, elements merely grow back to rheological significance on their own relaxation time-scale. In this case, the population of elements with $\tau = O(1)$ starts at zero, and attains its equilibrium value $O(\delta)$ within a time-scale $O(1)$.

With these remarks in mind, we now present our results for the linear rheology of the polymer model at $\epsilon = 0$, for small values of δ. We consider strain-controlled and stress-controlled experiments separately, and start with the strain-controlled case.

A: Strain controlled rheology.

The stress relaxation modulus is given exactly by

$$\begin{aligned} G(t-t_w, t_w) &= \int_1^\infty d\tau P(\tau, t_w) \exp\left(-\frac{t-t_w}{\tau}\right) \\ &= \delta \int_1^\infty d\tau \tau^{-(1+\delta)} \left[1 - \exp\left(-\frac{t_w}{\tau}\right)\right] \exp\left(-\frac{t-t_w}{\tau}\right) \end{aligned} \quad (7.30)$$

in which we have used equation 7.27 to obtain the second line from the first. In appendix 7.5 we use this equation to calculate analytically the asymptotic behaviour of $G(t-t_w, t_w)$ in the limit $t_w \gg 1$, $t - t_w \gg 1$, identifying as usual a short time regime $t - t_w \ll t_w$, and a long time regime $t - t_w \gg t_w$. The results are shown in table 7.1. In the same appendix, we also calculate an exact expression for the linear viscoelastic spectrum $G^*(\omega, t, t-t_s)$, and use it to extract asymptotic expressions for this quantity in the limit $t \gg 1$, $1/\omega \gg 1$, $\omega(t - t_s) \gg 1$. We find:

$$\begin{aligned} G^*(\omega, t) &= \Gamma(1+\delta)\left[\ln(t) + \ln(i\omega)\right] \quad \text{for} \quad \omega \gg 1/t_w \quad \text{and} \quad t_w \ll \tau_{erg}, \\ &= \Gamma(1+\delta)\Gamma(1-\delta)(i\omega)^\delta \quad \text{for} \quad \omega \gg 1/t_w \quad \text{and} \quad t_w \gg \tau_{erg} \end{aligned} \quad (7.31)$$

which we note is (as in the SGR model) independent of start time t_s.

Our numerical results for these quantities are shown in figures 7.7 and 7.8. As

	$G(t-t_w,t_w)$ for $t-t_w \ll t_w$	$G(t-t_w,t_w)$ for $t-t_w \gg t_w$
$t_w \ll \tau_{erg}$	$\Gamma(1+\delta)\,[\ln(t_w) - \ln(t-t_w)] + O(\delta^2)$	$\delta\Gamma(1+\delta)\dfrac{t_w}{t-t_w}$
$t_w \gg \tau_{erg}$	$\Gamma(1+\delta)\,(t-t_w)^{-\delta}$	$\delta\Gamma(1+\delta)\dfrac{t_w}{(t-t_w)^{1+\delta}}$

Table 7.1. Stress response to step strain at short and long time intervals ($t-t_w \ll t_w$ and $t-t_w \gg t_w$) for waiting times much less than and much greater than the ergodic time ($1 \ll t_w \ll \tau_{erg}$ and $t_w \gg \tau_{erg}$). $\Gamma(x)$ denotes the usual Gamma function.

predicted, they are qualitatively similar to the corresponding results for the linear SGR model at (or just above) its glass transition (see section 5.1). For example, (for $t_w \ll \tau_{erg}$) the stress relaxation modulus shows strong dependence upon t_w. The viscoelastic spectra are very weak power laws of frequency, reflective of the breadth of the underlying relaxation spectrum. The loss modulus does not show the usual Maxwellian decay to zero as frequency is tracked downwards, since the greatest contribution to this quantity comes from modes which are elastic on the time-scale of the inverse frequency.

The most notable rheological difference between the two models is as follows. In the SGR model, the loss modulus slowly falls over time (for $t_w \ll \tau_{erg}$) from an initial value $O(1)$ to a final value $O(\delta)$. In contrast, in the polymer model it is constant, and always $O(\delta)$. This is a direct consequence of the fact that, in the SGR model, the population of the relevant traps (those with $\tau \ll 1/\omega$) starts at $O(1)$ and gradually depletes (over times $0 < t_w < \tau_{erg}$) to its final value $O(\delta)$. In the polymer model, however, shallow traps equilibrate to their final population $O(\delta)$ in time-scales $O(1)$ (*i.e.* far sooner than any realistic measurement of the loss modulus can be performed). The other main difference is that, in the SGR model the amplitude of the stress relaxation modulus $[G(0,t_w)]$ is always equal to one; in contrast, in the polymer model it starts at zero, is $O(\delta)$ for $1 \ll t_w \ll \tau_{erg}$, and only becomes $O(1)$ for $t_w \gg \tau_{erg}$. This difference is also a direct consequence of the fact that there is a constant population of elements in the SGR model, while in the polymer model the population gradually grows over time.[12]

[12]For long waiting times $t_w \gg \tau_{erg}$ (which, as noted above, are likely to be inaccessible experimentally

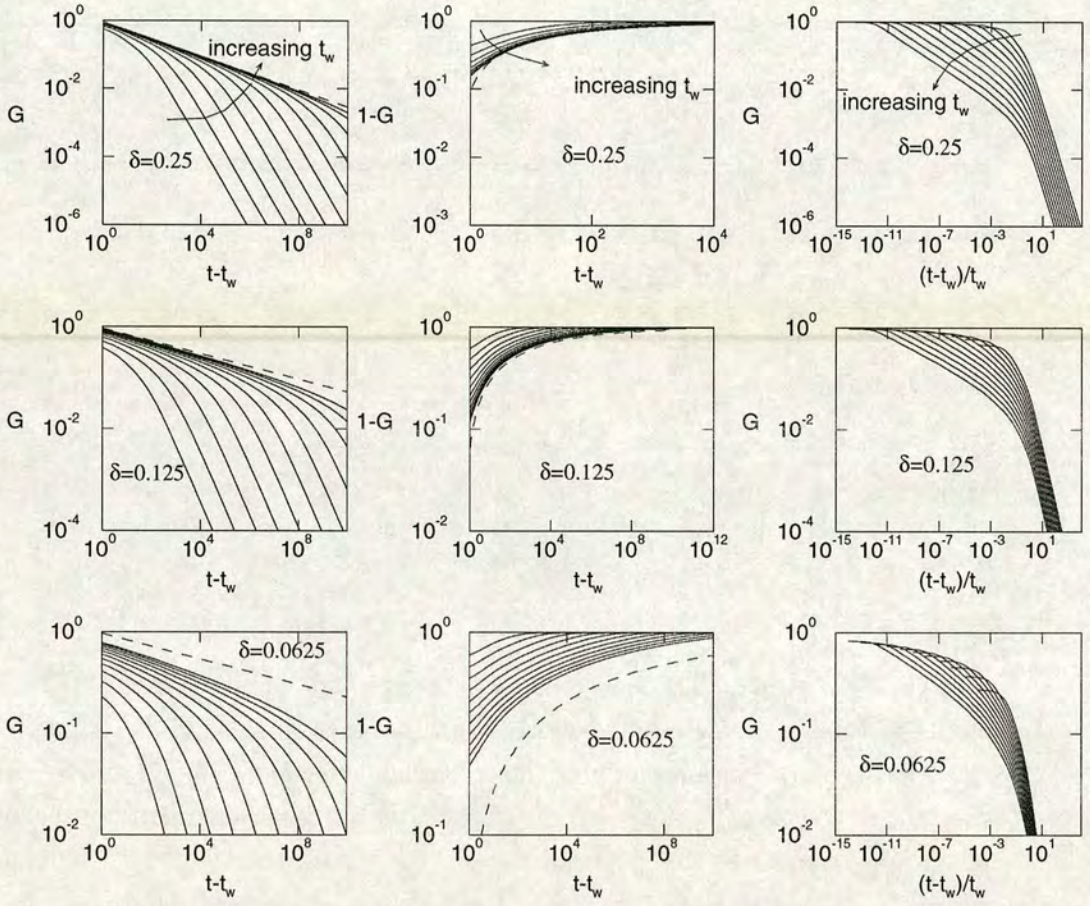

Figure 7.7. Left column: age-dependent stress relaxation modulus $G(t-t_w, t_w)$ against time interval $t-t_w$. Middle column: $1-G(t-t_w, t_w)$, plotted similarly. Right column: $G(t-t_w, t_w)$ against scaled time $(t-t_w)/t_w$. Shown are data for waiting times $t_w = 10^2$, $10^3 ... 10^{12}$. The equilibrium prediction has been marked in each relevant graph as a dashed line.

Clearly, if we were, in the polymer model, to re-scale $G(t-t_w, t_w)$ or $G^*(\omega, t_w)$ by $G(0, t_w)$ or $G'(\omega \to \infty, t_w)$ (both of which equal the normalization factor $\int d\tau P(\tau, t_w)$), we would probe the normalized distribution $P(\tau, t_w)/\int d\tau P(\tau, t_w)$, and see exactly the same behaviour as in the SGR model.

---

for small values of δ), the majority of rheological elements in the polymer model have been re-activated: $N(t_w) \approx 1$, and the rheology of the two models obviously coincides (to good approximation), becoming formally identical in the limit $t_w \to \infty$.

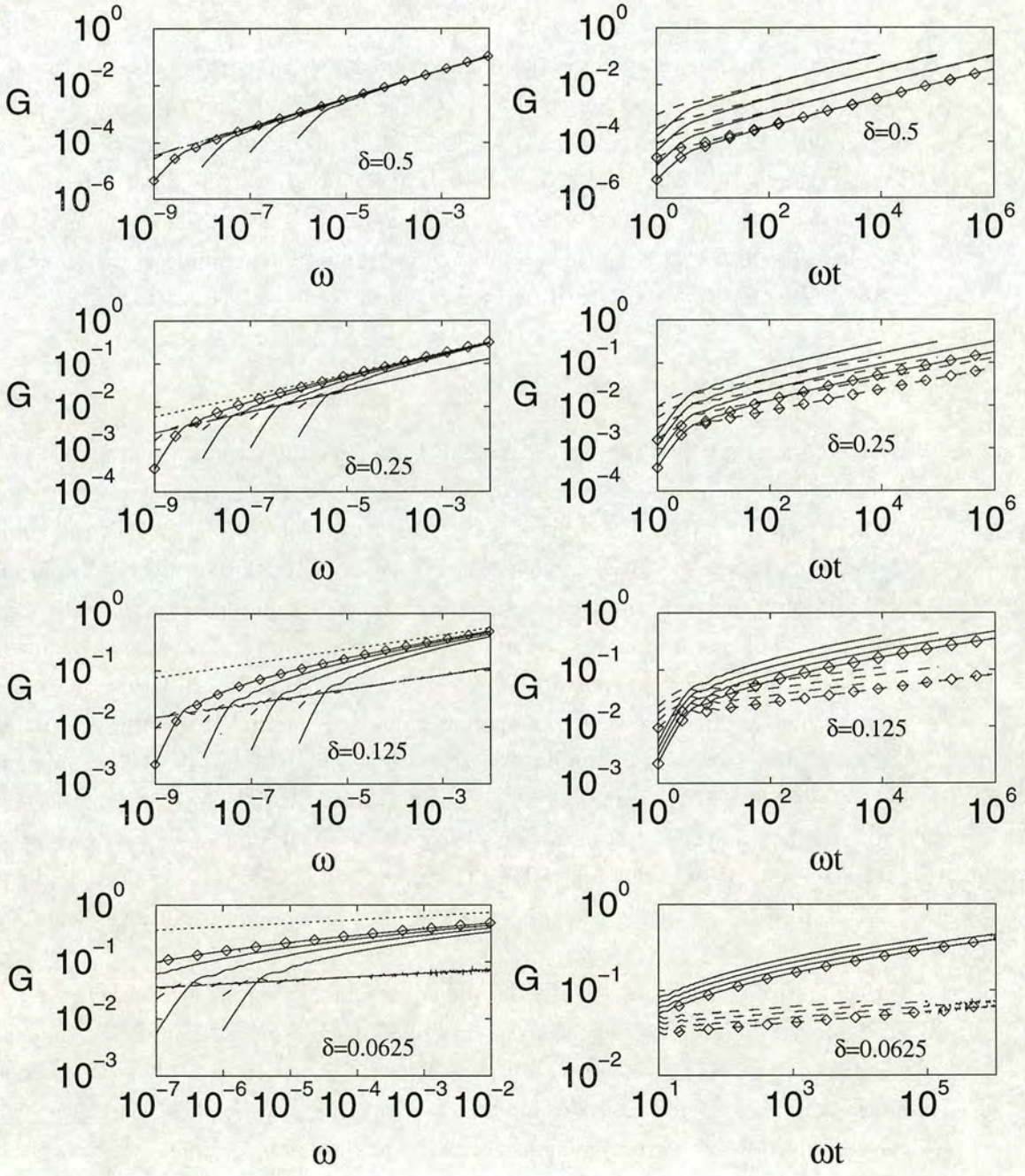

Figure 7.8. Viscoelastic spectra $G'(\omega, t)$ (solid lines), $G''(\omega, t)$ (dashed lines) vs. ω (LH column) and ωt (RH column). Shown are data for waiting times $t = 10^6,\ 10^7,\ 10^8,\ 10^9$. The equilibrium predictions have been marked as dotted lines for G', and dot-dashed lines (which are almost undiscernible) for G''.

A: Stress controlled rheology.

As in the SGR model, analysis of imposed-stress experiments is much more difficult than that for imposed-strain experiments: indeed, we have been unable to calculate analytical expressions for the creep compliance $J(t - t_w, t_w)$ in the interesting regime for which $t_w \ll \tau_{erg}$. Our numerical results for the this quantity are shown in figure 7.9. Unsurprisingly, like the strain-controlled response functions, for small values of δ they show non-trivial dependence upon t_w even for long times after pre-shear. For $t_w \gg \tau_{erg}$, of course (once $N(t_w) \approx 1$) the compliance for the polymer model is the same as that of the SGR model: see table 6.1, with x replaced by $1 + \delta$.

7.4 Conclusion

We have seen that the tube model of highly entangled, hierarchically branched polymer melts leads to a picture of activated dynamics taking place against large free energy barriers, with a broad spectrum of relaxation time-scales. Recognising the similarity to the dynamics of the SGR model, we have shown that, for certain critical branching distributions, the tube model can (in equilibrium) be mapped exactly onto the SGR model at a noise temperature just above its glass transition. We have also shown that the mapping can be (approximately) extended to non-equilibrium situations: following preparation by rapid pre-shear, the polymer model is predicted to show approximately the same slow approach to equilibrium as the SGR model following a deep quench. We have exploited this mapping to make rheological predictions for these melts, without any formalism beyond that used in previous chapters. In particular, we have predicted that the melts should show very long transients (which experimentally could be very difficult to distinguish from true ageing) as they slowly equilibrate following a rapid pre-shear.

We note finally that, despite the phenomenological similarities, there are several fundamental differences between the tube model and the SGR model. For example, the disordered energy landscape of the SGR model is not motivated by any underlying molecular theory, but taken as a fundamental postulate; we have no way of prescribing the distribution of energy barriers from outside the system. Hence we cannot control the distribution of time-scales, or the distance of the system from its glass transition. In contrast, the hierarchy of entropic barriers in the polymer model emerges naturally from the application of the physically justifiable tube model to highly branched molecules, in which the random branching distribution can be thought of as a kind of quenched

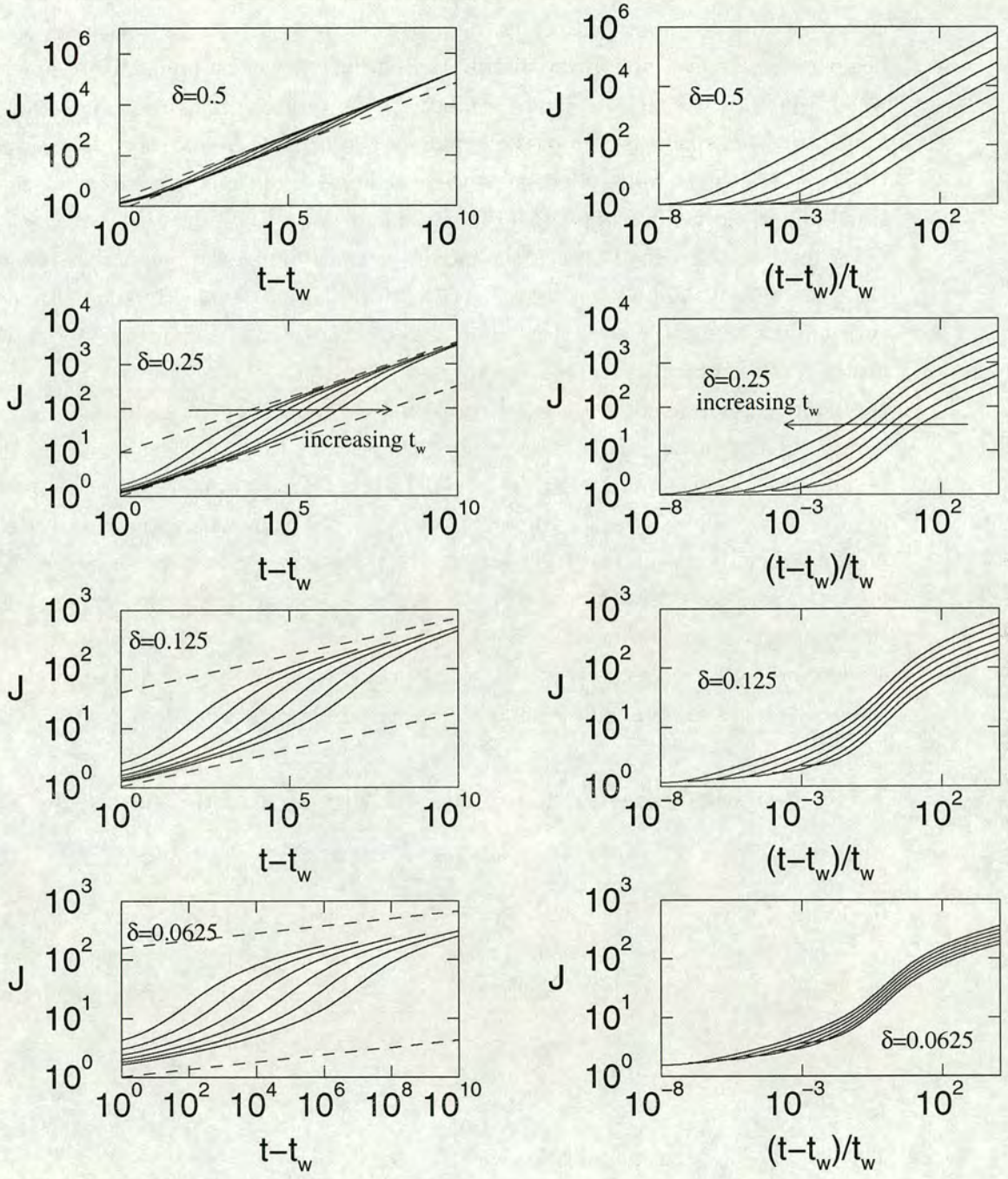

Figure 7.9. Linear creep compliance against time interval $t - t_w$ and scaled time interval $(t-t_w)/t_w$ for $t_w = 10^2, , 10^3 ... 10^7$ (solid lines). Lower dashed line: theoretical prediction for the early time $(t - t_w) \ll t_w$ creep in the limit $t_w \gg \tau_{erg}$. Upper dashed line: theoretical prediction for $(t - t_w) \gg t_w$ in the limit $t_w \gg \tau_{erg}$. Note that these predictions for the long and short time behaviours are each independent of t_w, but that the crossover time between then scales as t_w.

disorder. Here, the distribution of entropic barriers can be tuned by appropriate chemical synthesis: for broad branching distributions ($\epsilon \geq 0$), the model shows solid-like behaviour, whereas for narrow distributions ($\epsilon < 0$), we see liquid like behaviour in which (due to the effects of dynamic dilution) the terminal relaxation time-scale is infinite. In the critical case $\epsilon = 0$, the dynamics can be further controlled by appropriate tuning of the degree of entanglement (ν), becoming more sluggish (closer to the glass transition in the SGR mapping) for larger values of ν.

A further difference between the models is that, unlike the one-body SGR model, the dynamics of the polymer model are (a priori at least) explicitly coupled: the tube surrounding any molecule is itself composed of other molecules, and is therefore manifestly a dynamic entity which gets diluted over time. (Note, however, the effects of this coupling can be completely accounted for at the level of calculating the relaxation spectrum. Hence there is no paradox in the fact that the coupled polymer model can be mapped onto the uncoupled SGR model.) Finally: both models are athermal, but in profoundly different senses. In a realistic foam, the energy barrier are orders of magnitude larger than k_BT and this necessitates the use in the SGR model of an effective noise temperature, the origin of which to date has no convincing physical explanation. In the polymer model, on the other hand, the barriers are purely entropic and there is therefore no energy scale to which we can compare k_BT: any (true thermodynamic) temperature, however small, is sufficient to initiate the dynamics.

7.5 Appendix: calculation of rheological response functions

In this appendix, we outline our calculation of the linear rheological response functions $G(t-t_{\rm w},t_{\rm w})$, $G^*(\omega,t)$, and $J(t-t_{\rm w},t_{\rm w})$, for a melt prepared by a rapid non-linear pre-shear. We confine ourselves to the case $\epsilon = 0$ when the polymer model can be mapped to the SGR model.

7.5.1 Linear stress relaxation modulus

The stress relaxation modulus is given by

$$\begin{aligned} G(t-t_{\rm w},t_{\rm w}) &= \int_1^\infty d\tau P(\tau,t_{\rm w}) \exp\left(-\frac{t-t_{\rm w}}{\tau}\right) \\ &= G_0 \int_1^\infty d\tau P_{\rm EQ}(\tau) \left[1-\exp\left(-\frac{t_{\rm w}}{\tau}\right)\right] \exp\left(-\frac{t-t_{\rm w}}{\tau}\right) \\ &= G(t-t_{\rm w}) - G(t) \end{aligned} \tag{7.32}$$

in which we have used equation 7.27 to obtain the second line from the first, and in which $G(t)$ is the equilibrium stress relaxation modulus

$$G(t) = \delta \int_1^\infty d\tau \tau^{-(1+\delta)} \exp\left(-\frac{t}{\tau}\right). \tag{7.33}$$

After a change of variables to $s = t/\tau$, we see that this is just $t^{-\delta}$ times an incomplete Gamma function. For $t \gg 1$ the incomplete Gamma function becomes "complete" [to within a negligible correction $O(e^{-t})$], and we have

$$G(t) = \Gamma(1+\delta)t^{-\delta}. \tag{7.34}$$

Hence for $t - t_w \gg 1$ and $t_w \gg 1$, we have

$$G(t - t_w, t_w) = \Gamma(1+\delta)\left[(t-t_w)^{-\delta} - t^{-\delta}\right] \tag{7.35}$$

as quoted in table 7.1 of the main text (where, to highlight the analogy with the results of table 5.1 for the SGR model, we have separately the limits of this expressions for $t - t_w \ll t_w$ and $t - t_w \gg t_w$).

7.5.2 Constitutive equation

Given the stress relaxation function, $G(t - t_w, t_w)$, the stress response at an arbitrary strain history can be found using the principle of linear superposition via the constitutive equation:

$$\sigma(t) = \int_0^t dt' \dot{\gamma}(t') G(t - t', t'). \tag{7.36}$$

Integrating this by parts once we get

$$\sigma(t) = \gamma(t)(1 - G(t)) - \frac{\delta}{1+\delta} \int_0^t dt' \gamma(t') G_\rho(t - t') \tag{7.37}$$

in which we have use the notation

$$\begin{aligned} G_\rho(t - t_w) &= -\frac{1+\delta}{\delta} \frac{\partial}{\partial t_w} G(t - t_w) \\ &= \int_1^\infty d\tau \rho(\tau) \exp\left(-\frac{t - t_w}{\tau}\right) \end{aligned} \tag{7.38}$$

where $\rho(\tau) = [(1+\delta)/\delta][P_{EQ}(\tau)/\tau] = (1+\delta)\tau^{-(2+\delta)}$.

7.5.3 Oscillatory strain

Using the constitutive equation just derived (equation 7.37), we find the stress response at time t to an oscillatory strain commenced at time t_s as follows

$$\begin{aligned} G^*(\omega, t, t-t_s) &= (1-G(t)) - \frac{\delta}{1+\delta}\int_{t_s}^{t} dt' e^{-i\omega(t-t')} G_\rho(t-t') \\ &= (1-G(t)) - \frac{\delta}{1+\delta}\int_{0}^{t-t_s} dt' e^{-i\omega t'} G_\rho(t'). \end{aligned} \tag{7.39}$$

For $\omega(t-t_s) \gg 1$ the t_s-dependence becomes small and we find analytically

$$\begin{aligned} G^*(\omega, t) &= -\Gamma(1+\delta)t^{-\delta} - \delta\Gamma(1+\delta)\Gamma(-\delta)(i\omega)^{\delta} \\ &= \Gamma(1+\delta)t^{-\delta}\left[1 + \delta\Gamma(-\delta)(i\omega t)^{\delta}\right]. \end{aligned} \tag{7.40}$$

7.5.4 Creep compliance

As noted in the main text, we have been unable to calculate this quantity analytically. For the purposes of numerical calculation, we note that for $\sigma(t) = \sigma_0\Theta(t-t_w)$, the constitutive equation 7.37 is a Volterra equation of the second kind, which can be solved using the standard technique described in section 4.4.

Chapter 8

Ageing FDT in the trap model

The fluctuation-dissipation theorem (FDT) is the cornerstone of linear response theory in systems which are close to equilibrium. Its essential physical content [Rei80] is to place on an equal footing two types of infinitesimal departure from equilibrium which are at first sight very different from each other: small, externally induced deviations on the one hand; and fluctuations which occur spontaneously as a system explores its phase space on the other. FDT therefore tells us that linear response functions (which characterize perturbed deviations) contain the same information as correlation functions (which characterize intrinsic fluctuations). It also provides one way (which can be shown to be consistent with the several others) of defining equilibrium thermodynamic temperature.

Central to the theorem's derivation is the assumption of (close to) equilibrium conditions. In non-equilibrium systems, the equilibrium relationship between correlator and response breaks down (in general) and FDT does not apply. Despite this, it has recently emerged that non-equilibrium systems of the type considered in this thesis – those with slow dynamics – can display a non-trivial (although modified) relationship between correlator and response, which can be encoded in a non-equilibrium FDT [CK99, Cug99]. This can be used to define a non-equilibrium "effective" temperature, which has been demonstrated to display many of the properties one intuitively associates with a normal thermodynamic temperature [CKP97].

Non-equilibrium systems with slow dynamics include aged (or coarsened) systems which are relaxing infinitely slowly, and glassy systems which are driven at an infinitesimal rate. They all share the quasi-equilibrium feature of producing entropy (for the combined system plus universe) at a vanishingly small rate. However they are still far from equilibrium, as can be seen from the non-trivial dependence of their correlation and response functions upon absolute time t_{w} (for ageing systems) or driving rate $\dot{\gamma}$

(for driven systems).

In the literature, non-equilibrium FDT has already been studied in (for example) the coarsening constrained kinetic Ising model [CRRS00], the coarsening Glauber-Ising chain with ferromagnetic interactions [GL00], the Backgammon Model [GL99], MD simulations of a sheared fluid [BB00], finite dimensional spin glasses [MPRTRL98], long-range spin glasses [CK93], and glassy glycerol [GI99]. Here we consider FDT in another such "small entropy production" (SEP) system: the ageing regime of Bouchaud's trap model [Bou92].

The chapter is organized as follows. We start in section 8.1 with a reminder of the usual equilibrium FDT. In section 8.2 we outline the framework within which ageing FDT has been discussed in the existing literature, and generalize it slightly (in anticipation of our own work on the trap model) to allow the treatment of correlators with a time-dependent amplitude. In section 8.3 we use this framework to study FDT in the ageing regime of the trap model. We invoke an observable m, such that each particle has a value of m chosen randomly from an "intra-trap" distribution $\sigma(m|E)$. We derive an exact analytical expression for the correlator describing fluctuations in m. We then define the way in which the system's dynamics are perturbed by a small field h (conjugate to m), and derive an exact expression for the response of m to h. Our expressions for correlator and response depend only upon the first two cumulants of the distribution $\sigma(m|E)$. We compute them numerically, and study the FDT relation between them, for various functional dependences of the these cumulants upon E. In section 8.3.4 we discuss the relevance of the FDT relations to non-equilibrium temperatures. We conclude in section 8.4.

8.1 Equilibrium FDT

Before discussing FDT in non-equilibrium systems, we pause to remind the reader of the more familiar equilibrium version of the theorem. Consider, then, an equilibrium system in which some observable m has an average value $\langle m \rangle$. Deviations from this average can occur in two ways:

1. By external perturbation. Consider, for example, switching on a small field h such that the Hamiltonian H transforms thus: $H \to H - hm$. After some characteristic relaxation time, m settles to a new, perturbed average $\langle m \rangle + \delta m$. Subsequent switch-off of the field at some time t_{w} will result in m relaxing back to its unperturbed equilibrium value. The corresponding decay of δm to zero is encoded in the step-switch-off response function $\chi_{-}(t - t_{\mathrm{w}})$.

2. Even in the absence of such a perturbation, m will spontaneously fluctuate about $\langle m \rangle$ due to the intrinsic motion of the system within its phase space[1]. The average way in which a fluctuation, $\delta m(t_{\rm w}) = m(t_{\rm w}) - \langle m \rangle$, present at some (arbitrary) time $t_{\rm w}$, decays away over the subsequent time $t - t_{\rm w}$ is described by the correlation function

$$C(t - t_{\rm w}) = \langle (m(t) - \langle m \rangle)\,(m(t_{\rm w}) - \langle m \rangle) \rangle\,, \tag{8.1}$$

(where $\langle\ \rangle$ denotes ensemble average).

Note that, in this time-translationally-invariant (TTI) case, $t_{\rm w}$ is an arbitrary time label which could be set to zero. However we retain $t_{\rm w}$ in anticipation of the non TTI case.

The essential content of FDT is to place on an equal footing the induced and spontaneous deviations just described: provided a perturbation is small enough that the deviation it induces stays within the spontaneous fluctuations of a thermodynamically large sample of material, the decay of the induced deviation will be indistinguishable from that of a spontaneous fluctuation. C and χ_- therefore share the same time dependence and can be shown to obey

$$\chi_-(t - t_{\rm w}) = \frac{1}{T} C(t - t_{\rm w}), \tag{8.2}$$

in which T is the thermodynamic temperature. (We use energy units for which $k_B = 1$.) This is FDT. A formal proof of it can be found in many standard texts. (See for example [Rei80].)

Appealing to linearity, we note that FDT can alternatively be written in terms of the response χ_+ to a field which is switched *on* at time $t_{\rm w}$

$$\chi_+(t - t_{\rm w}) = \chi_-(0) - \chi_-(t - t_{\rm w}) = \frac{1}{T}\left[C(0) - C(t - t_{\rm w})\right] \tag{8.3}$$

(where $C(0)$ is the amplitude of the correlator), or in terms of the response to a "blip" (delta function) perturbation at time $t_{\rm w}$

$$\frac{\delta \langle m(t) \rangle}{\delta h(t_{\rm w})} = R(t - t_{\rm w}) = -\frac{\partial}{\partial t_{\rm w}} \chi_+(t - t_{\rm w}) = \frac{1}{T} \frac{\partial}{\partial t_{\rm w}} C(t - t_{\rm w}). \tag{8.4}$$

In what follows, we choose for definiteness to work in terms of the switch-on function, χ_+, which we relabel χ for ease of notation.

[1] unless m is a constant of the motion.

Graphically one represents equilibrium FDT by parametrically plotting χ against C: the plot is a straight line of slope $-1/T$ and intercept $C(0)$. For a system displaying transient approach to equilibrium, one commonly constructs several plots of χ against C, each for a different value of $t_{\rm w}$, with $t - t_{\rm w}$ as the hidden parameter in each case. The plot approaches the equilibrium limit $\chi(C) = C(0) - C/T$ as $t_{\rm w}$ becomes large.

We noted above that the factor T in the FDT equations is thermodynamic temperature. FDT can in fact be used as a way of *defining* temperature: it is the magnitude of the inverse slope of the FDT plot. This definition can be shown to be consistent with the more familiar ones encountered in standard thermodynamics texts. For convenience in what follows, we actually choose to re-scale the field $h \to h/T$ such that the factor T, when multiplied across the above FDT equations, becomes absorbed in the definition of the response function. We then have (in terms of the "switch-on" response function, to which we have now specialized):

$$\chi(t - t_{\rm w}) = C(0) - C(t - t_{\rm w}) \tag{8.5}$$

and the inverse slope of the FDT plot must be multiplied by $-T$ to correspond to temperature.

Having reminded the reader of equilibrium FDT, we now discuss its violation in non-equilibrium systems, and outline the framework within which modified FDTs are discussed in the sub-class of non-equilibrium systems which produce entropy at a vanishingly small rate.

8.2 Non-equilibrium FDT

FDT does not in general apply to systems which are far from equilibrium. Violation of the (differential) FDT is characterized by the "FDT violation factor" $X(t - t_{\rm w}, t_{\rm w})$ [CDK97] which is defined by

$$R(t - t_{\rm w}, t_{\rm w}) = -\frac{\partial}{\partial t_{\rm w}}\chi(t - t_{\rm w}, t_{\rm w}) = X(t - t_{\rm w}, t_{\rm w})\frac{\partial}{\partial t_{\rm w}}C(t - t_{\rm w}, t_{\rm w}). \tag{8.6}$$

The new $t_{\rm w}$-dependence in C and R allows for the generic absence of TTI in a non-equilibrium system[2]. Unlike FDT (equation 8.4), equation 8.6 does not imply any special relationship between correlator and response, since $X(t - t_{\rm w}, t_{\rm w})$ is (in general) an arbitrary function of the two independent variables $t - t_{\rm w}$ and $t_{\rm w}$: there is (in general) no special structure to an FDT plot, and there need not exist a limiting curve

[2] For a system in a non-equilibrium *steady state*, TTI is restored and we again lose the $t_{\rm w}$ dependence.

$\chi = \chi(C)$ as $t_w \to \infty$.

The remarkable feature of many SEP systems, however, is that, in the limit $t_w \to \infty$, $X(t - t_w, t_w)$ depends upon $t - t_w$ and t_w only through the value of C. It is furthermore independent of the particular choice of observable-field pair. (See [CK99].) The (violated) differential FDT equation then becomes (for all observables m),

$$R(t - t_w, t_w) = -\frac{\partial}{\partial t_w}\chi(t - t_w, t_w) = X(C)\frac{\partial}{\partial t_w}C(t - t_w, t_w), \tag{8.7}$$

and we recover a limiting FDT plot $\chi(C)$ of gradient

$$\frac{d\chi}{dC} = -X(C). \tag{8.8}$$

For models in which dynamics take place over several well separated epochs (see section 2.1.1), $X(C)$ has in many cases been shown to be a constant within each epoch. Consider, for example, a system with "fast" ($t - t_w = O(1)$) dynamics (over which C decays from its initial value to some constant[3] q_{EA}), and ageing ($t - t_w = O(t_w)$) dynamics (over which C decays from q_{EA} to zero). In many such systems, $X(C) = 1$ in the fast epoch (and trivial equilibrium FDT is recovered), while $X(C) = X_{\text{age}} < 1$ in the ageing epoch (equilibrium FDT is violated). The FDT plot then has two straight lines spliced together at $C = q_{EA}$: see the schematic figure 8.1.

8.2.1 Effective non-equilibrium temperatures

We recall from section 8.1 that FDT can be used to define temperature in an equilibrium system: it is the magnitude of the inverse slope of the FDT plot. By analogy, the non-equilibrium plots just described have recently been used to define a non-equilibrium effective temperature

$$T_{\text{eff}}(C) = -\frac{T}{\chi'(C)} = \frac{T}{X(C)}. \tag{8.9}$$

Within each epoch, T_{eff} can be shown [CKP97] to display many of the properties which one intuitively associates with normal thermodynamic temperature. For example, for an epoch defined by (say) $t - t_w = f(t_w)$, T_{eff} is the temperature which a thermometer of reaction time $O(f(t_w))$ would read when coupled to the system, while being isolated from the heat bath which surrounds the system. Hence, a thermometer with an ageing reaction time $O(t_w)$ would register the "ageing" temperature T/X_{age} when coupled to the "2-epoch" system described above. It can also be shown that

[3] In the spin glass literature, q_{EA} is called the Edwards-Anderson order parameter.

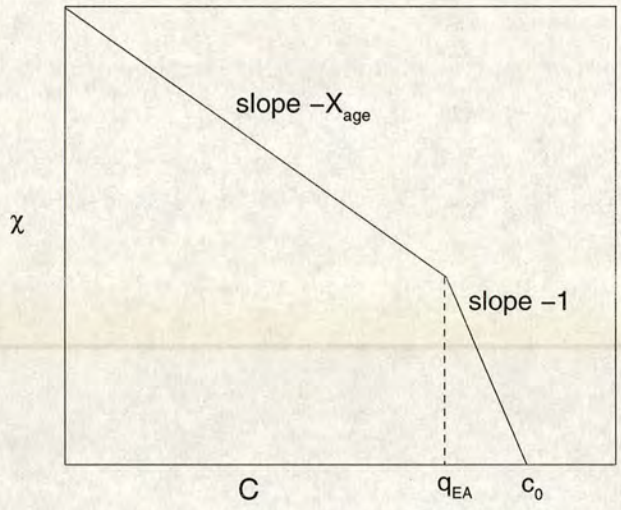

Figure 8.1. Schematic FDT plot for an ageing system with both fast (time-scale $O(1)$) and ageing (time-scale $O(t_w)$) dynamical processes.

(within each epoch) two sub-ensembles coupled together will thermalize to the same value of $T_{\rm eff}$, provided the coupling is strong enough. Finally, in some systems, the ageing temperature, $T/X_{\rm age}$, can be shown to decouple from the bath temperature T at low temperatures, and remain finite in the limit $T \to 0$. It could therefore be relevant to systems such as foams (see section 4.2) in which a huge noise "temperature" is needed for the activation of any dynamical rearrangements, due to the presence of huge energy barriers.

8.2.2 Normalization

In order to apply the framework just described for non-equilibrium FDTs to the ageing regime of the trap model, we need to refine it slightly. The reason for this is as follows. Within the existing convention, the abscissa of the FDT plot ranges from the initial ($t - t_w = 0$) value of the correlator ($C(0, t_w) = C_0$) down to zero. A limiting FDT plot can therefore only exist, within the present framework, if this initial value is independent of the waiting time t_w, *i.e.* , if C depends upon t_w only through the shape of its decay, and not through its amplitude. Although this is indeed the case for many models, it need not hold in general in a non-equilibrium system. In fact, many of the correlators to be calculated by us in the trap model (section 8.3.3) have a time-*dependent* amplitude. In anticipation of this, we choose to work in terms of the

normalized functions

$$\tilde{C}(t-t_{\rm w},t_{\rm w})=\frac{C(t-t_{\rm w},t_{\rm w})}{C(0,t_{\rm w})} \tag{8.10}$$

and

$$\tilde{\chi}(t-t_{\rm w},t_{\rm w})=\frac{\chi(t-t_{\rm w},t_{\rm w})}{C(0,t_{\rm w})}. \tag{8.11}$$

The existence of a limiting *normalized* FDT plot $\tilde{\chi}(\tilde{C})$ then implies a modified non-equilibrium FDT relation of the form

$$-\frac{\partial}{\partial t_{\rm w}}\tilde{\chi}(t-t_{\rm w},t_{\rm w})=X(\tilde{C})\frac{\partial}{\partial t_{\rm w}}\tilde{C}(t-t_{\rm w},t_{\rm w}) \tag{8.12}$$

and the possible identification of $T/X(\tilde{C})=-T/\tilde{\chi}'(\tilde{C})$ as a non-equilibrium temperature.

Finally, we note for completeness that the concepts of this section can be applied to steadily driven SEP systems, provided we identify the inverse driving rate $1/\dot{\gamma}$ with the waiting time $t_{\rm w}$ of the ageing case; the ageing limit, $t_{\rm w}\to\infty$, then becomes the weakly driven limit, $\dot{\gamma}\to 0$. We shall in fact consider a driven FDT in the context of the constrained spin chain in chapter 9.

8.3 FDT in the ageing regime of the trap model

Having outlined the general framework within which non-equilibrium FDT is to be discussed, we now use it to study FDT in the ageing regime of Bouchaud's trap model. We recall that the dynamics of this model are defined by

$$\frac{\partial}{\partial t}P(E,t)=-\frac{1}{\tau(E)}P(E,t)+Y(t)\rho(E). \tag{8.13}$$

(See section 4.1.) Here we extend the model slightly, incorporating an observable m such that a particle in a trap of depth E has a value of m chosen at random from an intra-trap distribution[4] $\sigma(m|E)$. The conjugate field to m is denoted by h. For small h, the jump times are assumed to be perturbed as follows

$$\tau(E)\to\tau(E,mh)=\tau(E)\exp(mh). \tag{8.14}$$

[4]There is a possible source of confusion here. In glassy dynamics, one generally assumes intra-trap distributions to be subject to rapid thermalization. In this case, however, our distribution $\sigma(m|E)$ is merely one from which a particle hopping into a trap of depth E selects its value of m. There is no subsequent rapid thermalization over m.

(There is no factor $1/T$ in the exponent here because we have already rescaled the field $h \to h/T$; see above.) Note that this is just one of several possible choices, all of which ensure detailed balance for the perturbed model. Our reason for adopting the specific choice of equation 8.14 is that, in the spirit of the unperturbed model, it is the choice which ensures that the jump rate between any two states depends only upon the initial state, and not upon the final one. The equation of motion for the perturbed model is as follows

$$\frac{\partial}{\partial t}P(E,m,t,h) = -\frac{1}{\tau(E,mh)}P(E,m,t,h) + Y(t,h)\rho(E)\sigma(m|E). \tag{8.15}$$

At zero field, we obviously recover the original unperturbed dynamics, and have

$$\frac{\partial}{\partial t}P(E,m,t) = -\frac{1}{\tau(E)}P(E,m,t) + Y(t)\rho(E)\sigma(m|E), \tag{8.16}$$

with $P(E,m,t) = P(E,t)\sigma(m|E)$ as expected.

In what follows, we study the FDT relation between the correlator which describes zero-field fluctuations in m, and the response of m to h in the model's ageing regime. For convenience we generically call m "magnetization", although its actual physical identity clearly depends upon the form of its distribution $\sigma(m|E)$: for example, $\sigma(m|E) = \delta(E-m)$ corresponds to $m = E$ (energy depth), in which case the conjugate field is a (negative) temperature change $h = -\delta T/T$ (which – see above – is further scaled by T to get our usual normalized FDT plot). (Sign conventions are discussed more fully below.) In the first instance, however, we make no assumption about the shape of $\sigma(m|E)$, and compute completely general (and exact) expressions for the correlator and response. We find that they depend only on the first two cumulants of $\sigma(m|E)$. We then study various specific forms for the distribution, considering several plausible functional dependences of the two relevant cumulants upon E. For example, we consider the energy-temperature FDT just described (for which the intra-trap distribution has zero variance and mean $\bar{m}(E) = E$). We also reproduce the results of [BD95], which considered a Gaussian $\sigma(m)$ with zero mean, and constant variance (independent of E). For each distribution, we compute the correlator and response numerically (from our analytical expressions), and study the FDT relation between them. In most cases we find a limiting FDT plot $\tilde{\chi}(\tilde{C})$ as $t_{\rm w} \to \infty$, and discuss the relevance of the plot to non-equilibrium temperatures.

8.3.1 Correlation function

The correlation function describing zero-field fluctuations in the observable m is defined by

$$C(t-t_{\rm w},t_{\rm w}) = \int dm \int dm_{\rm w}(m-\langle m\rangle)(m_{\rm w}-\langle m\rangle_{\rm w})P(m_{\rm w},t_{\rm w};m,t) \qquad (8.17)$$

in which $\langle\rangle$ denotes global ensemble average, and $P(m_{\rm w},t_{\rm w};m,t)$ is the joint probability that any particle has magnetization $m_{\rm w}$ at time $t_{\rm w}$, and subsequently m at the later time t. In principle this distribution is rather difficult to calculate, since the dynamics of the model (in zero-field at least) are defined in terms of energies and not magnetizations. To tackle this problem, we rewrite the correlator as

$$\begin{aligned} C(t-t_{\rm w},t_{\rm w}) &= \int dm \int dm_{\rm w} \int dE \int dE_{\rm w}(m-\langle m\rangle)(m_{\rm w}-\langle m\rangle_{\rm w}) \\ &\quad \times P(E_{\rm w},m_{\rm w},t_{\rm w};E,m,t) \end{aligned} \qquad (8.18)$$

in which $P(E_{\rm w},m_{\rm w},t_{\rm w};E,m,t)$ is the probability that any particle has magnetization $m_{\rm w}$ and energy $E_{\rm w}$ at time $t_{\rm w}$ and magnetization m and energy E at time t. We also recognize that the magnetization of any particle can be decomposed into two components. The first, which we denote $\bar{m}(E)$, is the mean of that particle's intra-trap distribution $\sigma(m|E)$, and depends only upon the trap depth E. The second is the deviation Δm of the particle's actual value of m from this "trap-mean". We therefore have

$$m = \bar{m}(E) + \Delta m. \qquad (8.19)$$

Substituting this into 8.18 we get

$$\begin{aligned} C(t-t_{\rm w},t_{\rm w}) &= \int d\Delta m \int d\Delta m_{\rm w} \int dE \int dE_{\rm w}\,(\Delta m + \bar{m}(E) - \langle m\rangle) \\ &\quad \times (\Delta m_{\rm w} + \bar{m}(E_{\rm w}) - \langle m\rangle_{\rm w}) \\ &\quad \times P(E_{\rm w},\Delta m_{\rm w},t_{\rm w};E,\Delta m,t). \end{aligned} \qquad (8.20)$$

The replacement of $\int dm$ by $\int d\Delta m$ and of $P(E_{\rm w},m_{\rm w},t_{\rm w};E,m,t)$ by $P(E_{\rm w},\Delta m_{\rm w},t_{\rm w};E,\Delta m,t)$ between equations 8.18 and 8.20 is trivial since the only part of a particle's magnetization not uniquely prescribed by the energy is that portion which deviates from the trap mean. Partially multiplying out the brackets in 8.20, and denoting an average over the distribution $P(E_{\rm w},\Delta m_{\rm w},t_{\rm w};E,\Delta m,t)$ by $\langle\rangle_P$, we get

$$C(t-t_{\rm w},t_{\rm w}) = \langle(\bar{m}(E)-\langle m\rangle)(\bar{m}(E_{\rm w})-\langle m\rangle_{\rm w})\rangle_P$$

$$
\begin{aligned}
&+\langle \Delta m \Delta m_{\rm w} \rangle_P \\
&+\langle (\bar{m}(E_{\rm w}) - \langle m \rangle_{\rm w}) \Delta m \rangle_P \\
&+\langle (\bar{m}(E) - \langle m \rangle) \Delta m_{\rm w} \rangle_P \, . \qquad (8.21)
\end{aligned}
$$

In this equation, the first term on the RHS is the contribution to the correlator arising from deviations of trap means from the global mean. It is blind to any deviations of particle magnetizations from their trap means, and hence to any spread in the intra-trap distribution $\sigma(m|E)$. It would be the only contribution to the correlator for a system in which $\sigma(m|E)$ had zero variance (but non-zero mean) for all E, *i.e.* in which a particle hopping into a trap of depth E had its value of m deterministically prescribed as $\bar{m}(E)$. The second term on the RHS measures correlations in deviations of particle magnetizations away from their trap means. It is blind to the values of the trap means, and would be the full correlator for a system in which the distribution $\sigma(m|E)$ had zero mean (but non-zero variance) for every value of E. The third and fourth terms measure *cross* correlations between deviations of particle magnetizations from their trap means on the one hand, and deviations of trap means from the global mean on the other. Imposing the mild restriction that $\sigma(m|E)$ is symmetric about its mean, however, we find that each of these cross terms is zero, and we are left with

$$
C(t - t_{\rm w}, t_{\rm w}) = C_1(t - t_{\rm w}, t_{\rm w}) + C_2(t - t_{\rm w}, t_{\rm w}) \qquad (8.22)
$$

in which (writing out $\langle \rangle_P$ fully)

$$
\begin{aligned}
C_1(t - t_{\rm w}, t_{\rm w}) \;=\; & \int d\Delta m \int d\Delta m_{\rm w} \int dE \int dE_{\rm w} (\bar{m}(E) - \langle m \rangle)(\bar{m}(E_{\rm w}) - \langle m \rangle_{\rm w}) \\
& \times P(E_{\rm w}, \Delta m_{\rm w}, t_{\rm w}; E, \Delta m, t) \qquad (8.23)
\end{aligned}
$$

and

$$
\begin{aligned}
C_2(t - t_{\rm w}, t_{\rm w}) \;=\; & \int d\Delta m \int d\Delta m_{\rm w} \int dE \int dE_{\rm w} \Delta m \Delta m_{\rm w} \\
& \times P(E_{\rm w}, \Delta m_{\rm w}, t_{\rm w}; E, \Delta m, t). \qquad (8.24)
\end{aligned}
$$

We now use trap model's equation of motion, 8.16, to derive exact expressions for these two component correlators in turn. We consider as usual a system prepared at a temperature[5] T at time $t = 0$ by means of the deep quench defined in section 4.1.

[5]Note that when we discussed the trap model in the context of soft glassy rheology (chapters 4 to 6), the hopping events were assumed to be macroscopically activated, and we denoted the corresponding

We start with C_1. Integrating out the deviations Δm of particle magnetizations from trap means (these are redundant variables in this portion of the correlator) we have

$$C_1(t-t_w,t_w) = \int dE \int dE_w(\bar{m}(E)-\langle m\rangle)(\bar{m}(E_w)-\langle m\rangle_w)P(E_w,t_w;E,t). \quad (8.25)$$

Writing out the global averages in full we get

$$\begin{aligned} C_1(t-t_w,t_w) &= \int dE \int dE_w \bar{m}(E)\bar{m}(E_w)P(E_w,t_w;E,t) \\ &\quad - \int dE \bar{m}(E)P(E,t) \int dE_w \bar{m}(E_w)P(E_w,t_w). \end{aligned} \quad (8.26)$$

In this equation, $P(E,t)$ is the distribution of energies at time t, and is given by the solution of the trap model's dynamics as described in section 4.1.1:

$$P(E,t) = \rho(E)\exp\left(-\frac{t}{\tau(E)}\right) + \rho(E)\int_0^t dt' Y(t')\exp\left(-\frac{t-t'}{\tau(E)}\right). \quad (8.27)$$

$P(E_w,t_w;E,t)$ is the joint probability that any particle has energy E_w at time t_w and subsequently energy E at the later time t. We decompose this into

$$P(E_w,t_w;E,t) = P(E_w,t_w)P(E,t|E_w,t_w), \quad (8.28)$$

in which the conditional distribution $P(E,t|E_w,t_w)$ is given by

$$\begin{aligned} P(E,t|E_w,t_w) &= \delta(E-E_w)\exp\left(-\frac{t-t_w}{\tau(E_w)}\right) \\ &\quad + \int_{t_w}^t dt' \frac{1}{\tau(E_w)}\exp\left(-\frac{t'-t_w}{\tau(E_w)}\right) P(E,t-t'). \end{aligned} \quad (8.29)$$

This expression can be physically motivated in the following way. Consider the sub-ensemble consisting of those particles which have energy E_w at time t_w. The first term in equation 8.29 represents the proportion of this sub-ensemble which does not hop during the interval $t_w \to t$. The product of the first two factors inside the integral gives the fraction which hops at time t'. This fraction is essentially quenched at time t', since it hops into the prior distribution $\rho(E)$. It then ages into the distribution $P(E,t-t')$ (the third factor inside the integral) over the subsequent time $t-t'$. Integrating over all t', we find the energy distribution at time t for all particles which have hopped since

macroscopic temperature by x. In this context we assume the dynamics to be thermally activated, and hence use the more usual notation T.

time t_w. Combining 8.26, 8.28, and 8.29 we get

$$C_1(t-t_w,t_w) = f_2(t-t_w,t_w) + \int_{t_w}^{t} dt' f_1(t-t') f_3(t'-t_w,t_w) - f_1(t) f_1(t_w) \quad (8.30)$$

in which

$$f_1(t) = \int dE \bar{m}(E) P(E,t), \quad (8.31)$$

$$f_2(t-t_w,t_w) = \int dE (\bar{m}(E))^2 P(E,t_w) \exp\left(-\frac{t-t_w}{\tau(E)}\right), \quad (8.32)$$

and

$$f_3(t-t_w,t_w) = \int dE \bar{m}(E) P(E,t_w) \frac{1}{\tau(E)} \exp\left(-\frac{t-t_w}{\tau(E)}\right). \quad (8.33)$$

Substituting 8.27 into these equations we find finally

$$f_1(t) = G_{\rho\bar{m}}(t) + \int_0^t dt' Y(t') G_{\rho\bar{m}}(t-t'), \quad (8.34)$$

$$f_2(t-t_w,t_w) = G_{\rho\bar{m}^2}(t) + \int_0^{t_w} dt' Y(t') G_{\rho\bar{m}^2}(t-t'), \quad (8.35)$$

and

$$f_3(t-t_w,t_w) = G_{\frac{\rho\bar{m}}{\tau}}(t) + \int_0^{t_w} dt' Y(t') G_{\frac{\rho\bar{m}}{\tau}}(t-t'). \quad (8.36)$$

We have used the notation

$$G_{\rho\bar{m}}(t) = \int dE \rho(E) \bar{m}(E) \exp\left(-\frac{t}{\tau(E)}\right) \quad (8.37)$$

(and similarly for $G_{\rho\bar{m}^2}$ and $G_{\frac{\rho\bar{m}}{\tau}}$), and for convenience we have suppressed the E dependence in the subscript. Equation 8.30, together with 8.34 to 8.37, constitutes an exact solution for the correlation function C_1.

We now turn to C_2, as given by equation 8.24. In this equation, $P(E_w, \Delta m_w, t_w; E, \Delta m, t)$ is the probability that a particle has energy E_w and "deviatoric" magnetization Δm_w at time t_w, and subsequently energy E and deviatoric magnetization m at the later time t. ("Deviatoric" here refers to the deviation of a particle's magnetization from its own trap mean.) We decompose this distribution thus:

$$P(E_w, \Delta m_w, t_w; E, \Delta m, t) = P(E, \Delta m, t | E_w, \Delta m_w, t_w) P(E_w, \Delta m_w, t_w). \quad (8.38)$$

The second factor on the RHS of this equation can further be decomposed by

$$P(E_{\rm w}, \Delta m_{\rm w}, t_{\rm w}) = \sigma'(\Delta m_{\rm w}|E_{\rm w})P(E_{\rm w}, t_{\rm w}) \tag{8.39}$$

in which the distribution $\sigma'(\Delta m_{\rm w}|E_{\rm w})$ is equal to $\sigma(\bar{m}(E_{\rm w}) + \Delta m_{\rm w}|E_{\rm w})$, and is the original intra-trap distribution $\sigma(m_{\rm w}, E_{\rm w})$, shifted to have its mean at zero. The conditional distribution $P(E, \Delta m, t|E_{\rm w}, \Delta m_{\rm w}, t_{\rm w})$ can be written as follows

$$\begin{aligned} P(E, \Delta m, t|E_{\rm w}, \Delta m_{\rm w}, t_{\rm w}) &= \delta(E - E_{\rm w})\delta(\Delta m - \Delta m_{\rm w}) \exp\left(-\frac{t - t_{\rm w}}{\tau(E_{\rm w})}\right) \\ &\quad + \int_{t_{\rm w}}^{t} dt' \frac{1}{\tau(E_{\rm w})} \exp\left(-\frac{t' - t_{\rm w}}{\tau(E_{\rm w})}\right) P(E, t - t'). \end{aligned} \tag{8.40}$$

This can be motivated using the same arguments as those given above for $P(E, t|E_{\rm w}, t_{\rm w})$: the first term on the RHS describes those particles which do not hop over the interval $t - t_{\rm w}$, whereas the second refers to those that do. Due to the symmetry of the distribution $\sigma'(m|E)$, particles which do hop make no contribution to the correlation function. The second term in 8.40 is therefore redundant, and we are left with

$$\begin{aligned} C_2(t - t_{\rm w}, t_{\rm w}) &= \int d\Delta m \int d\Delta m_{\rm w} \int dE \int dE_{\rm w} \Delta m \Delta m_{\rm w} \sigma'(\Delta m_{\rm w}|E_{\rm w}) \\ &\qquad \times P(E_{\rm w}, t_{\rm w})\delta(E - E_{\rm w})\delta(\Delta m - \Delta m_{\rm w}) \exp\left(-\frac{t - t_{\rm w}}{\tau(E_{\rm w})}\right) \\ &= \int d\Delta m \int dE (\Delta m)^2 \sigma'(\Delta m|E) \\ &\qquad \times P(E, t) \exp\left(-\frac{t - t_{\rm w}}{\tau(E_{\rm w})}\right) \\ &= \int dE (\Delta m)^2(E) P(E, t_{\rm w}) \exp\left(-\frac{t - t_{\rm w}}{\tau(E)}\right) \end{aligned} \tag{8.41}$$

where $(\Delta m)^2(E)$ is the variance of the distribution $\sigma(m|E)$. Together with 8.27 for the energy distribution at time $t_{\rm w}$, 8.41 gives finally

$$C_2(t - t_{\rm w}, t_{\rm w}) = G_{\rho(\Delta m)^2}(t) + \int_0^{t_{\rm w}} dt' Y(t') G_{\rho(\Delta m)^2}(t - t') \tag{8.42}$$

which constitutes an exact solution for the correlator C_2.

To summarize: we have seen that the correlation function describing fluctuations in the observable m can be decomposed into two components: C_1, which depends only on the mean of the intra-trap distribution $\sigma(m|E)$; and C_2, which depends only on the

variance.

8.3.2 Response function

To find the response of the observable m to a small step field h applied at time t_w, we would in principle need to solve the full, perturbed equation of motion 8.15. Specifically, we would evolve the system from time 0 to t_w using the unperturbed equation 8.13, and from t_w to t using the perturbed equation 8.15. We would then calculate the average magnetization with respect to the resulting state at time t, and subtract from it the average magnetization found by evolving the system using the unperturbed equation 8.13 over the entire interval 0 to t. Alternatively, we could calculate the response at time t to a delta function perturbation at time t'_w (by using the perturbed equation 8.15 only over a small interval about t'_w). Linearity would then enable us to find the required step response by integrating this blip response over t'_w from t_w to t.

However, we do not need to perform this calculation explicitly, since it has already been done by Sasaki and Nemoto [SN99] for a broad class of Markov processes in which the perturbation to the jump rate between any two states depends only upon the initial state and not upon the final one. They showed that, for such processes, the response function is related to the correlator by the following equation

$$-R(t-t_w,t_w)=\frac{\partial}{\partial t_w}\chi(t-t_w,t_w)=\frac{\partial}{\partial t}C(t-t_w,t_w) \tag{8.43}$$

which is valid whenever the global mean $\langle m\rangle = 0$. Because the trap model is an example of such a process, we can use equation 8.43, at least in the zero-mean case $\bar{m}(E)=\langle\sigma(m|E)\rangle=0$, to calculate the response function directly from the expressions derived above for the correlator. We do not need to consider the specific dynamics of the trap model any further. The generalization of equation 8.43 to the case $\langle m\rangle \neq 0$ (which will clearly arise when $\bar{m}(E)=\langle\sigma(m|E)\rangle\neq 0$) is as follows [Sol]

$$-R(t-t_w,t_w)=\frac{\partial}{\partial t_w}\chi(t-t_w,t_w)=\frac{\partial}{\partial t}C(t-t_w,t_w)+\frac{\partial}{\partial t}\langle m(t)\rangle\langle m(t_w)\rangle\,. \tag{8.44}$$

Substituting our exact expressions for the correlator into this equation, we find that the integral of $d\chi/dt_w$ over t_w (with the boundary condition $\chi(0,t_w)=0\;\forall\, t_w$) can be done analytically to give an exact, although lengthy, expression for χ. We shall not write it down here, but merely note that (unsurprisingly) we find a decomposition $\chi=\chi_1+\chi_2$ in which χ_n (for $n=1,2$) is the response corresponding to the correlator C_n, and depends only upon the nth cumulant of the intra-trap distribution $\sigma(m|E)$.

We note finally that, for the special case of a TTI system in which $\frac{\partial}{\partial t}C=-\frac{\partial}{\partial t_w}C$

and $\frac{\partial}{\partial t}\langle m(t)\rangle = 0$, 8.44 reduces to the usual equilibrium FDT relation. In a non-equilibrium system, however, it is not of the form of an FDT equation (such as 8.6) since in FDT one relates the blip response to the differential of C with respect to its *earlier* time argument, $t_{\rm w}$. 8.44 instead contains the differential of C with respect to its *later* time argument, t. (It also contains the extra term $\frac{\partial}{\partial t}\langle m(t)\rangle\langle m(t_{\rm w})\rangle$.)

8.3.3 FDT plots

So far we have calculated exact analytical expressions for the correlator, C, and response function, χ, in terms of the first two cumulants of the intra-trap distribution $\sigma(m|E)$. We now use these expressions to study FDT for various functional dependences of the two cumulants upon trap depth. For simplicity, we treat the case of distribution $\sigma(m|E)$ which has zero mean, but non-zero variance (for which $C = C_2$) separately from the case of a distribution which has non-zero mean, but zero variance (for which $C = C_1$). In all cases, we present results only for the ageing regime, *i.e.* for bath temperatures $T < 1$, since for $T > 1$ the system rapidly equilibrates, and equilibrium FDT (equation 8.2) is recovered. (We have checked numerically that this is indeed the case.)

FDT for an intra-trap distribution with zero mean, non-zero variance

We start, then, by considering FDT for an intra-trap distribution which has zero mean, for which the correlator is given by C_2 (equation 8.42). We shall study both exponential and power law dependence of the variance $(\Delta m)^2(E)$ upon trap depth E. We start with the exponential case, setting $(\Delta m)^2(E) = \exp(2En/T)$, where n is defined by this relation, and will be used below as a parameter via which $(\Delta m)^2(E)$ can be varied. Substituting this into equation 8.42 we have the following exact expression:

$$C_2(t-t_{\rm w},t_{\rm w}) = G_{\rho\exp(2En/T)}(t) + \int_0^{t_{\rm w}} dt' Y(t') G_{\rho\exp(2En/T)}(t-t'). \qquad (8.45)$$

For the purposes of numerical study, we found an exact expression for the corresponding response function by substituting this into equation 8.43 and integrating over $t_{\rm w}$ to get:

$$\begin{aligned}\chi_2(t-t_{\rm w},t_{\rm w}) \;=\; -\Big[&(t-t_{\rm w})\frac{\partial}{\partial t}G_{\rho\exp(2En/T)}(t)\\ &+\int_0^t dt'(t-t')Y(t')\frac{\partial}{\partial t}G_{\rho\exp(2En/T)}(t-t')\\ &-\int_0^{t_{\rm w}} dt'(t_{\rm w}-t')Y(t')\frac{\partial}{\partial t}G_{\rho\exp(2En/T)}(t-t')\Big]. \qquad (8.46)\end{aligned}$$

We then computed C_2 and χ_2 numerically using these expressions for various values of n at $T = 0.3$. Finally, we constructed FDT plots of the results, always normalizing both correlator and response by the time-dependent initial value of the correlator, as discussed above. (We confined ourselves to the range $n < T/2$, because for larger n we found an unphysical correlation function with infinite initial ($t - t_w = 0$) value immediately after quench ($t_w = 0$); see below for an explanation of this point.) The FDT plots are shown in figure 8.2. They suggest that, for each value of n studied, a limiting curve $\tilde{\chi}(\tilde{C})$ is approached at large values of t_w. For $n = -0.9$ and $n = -0.6$ this curve is of trivial equilibrium form with slope -1. For the larger values of n (-0.1 and 0.1) it has non-trivial shape, clearly demonstrating that equilibrium FDT is violated.

We now describe an analytical study which proves that such limiting curves do indeed exist, and which furthermore derives formulae for the (n-dependent) shape of them. Our method is as follows. In appendix 8.5, we extract from equation 8.45 the dependence of C_2 upon $t - t_w$ and t_w in the limit $t - t_w \to \infty$, $t_w \to \infty$, $(t - t_w)/t_w = \text{const}$. We then substitute the results into equation 8.43 to find corresponding expressions for the response function χ. (See appendix 8.5.) Finally, we normalize both response and correlator by the initial value of the correlator, and express normalized response in terms of normalized correlator. The results, which are summarized in table 8.1, reveal that there are two distinct regimes of n: $(T-1)/2 < n < T/2$, and $n < (T-1)/2$. We now briefly discuss each regime in turn.

For $(T-1)/2 < n < T/2$ we find that $\tilde{C}$ and $\tilde{\chi}_2$ both decay on an ageing time-scale t_w: they share the same scaling variable, $(t - t_w)/t_w$, and hence a limiting curve $\tilde{\chi}_2(\tilde{C}_2)$ must exist. For time intervals which are short compared with the decay time (*i.e.* for $t - t_w \ll t_w$ and $\tilde{C}_2 \approx 1$) we find this curve to be of the form $\tilde{\chi}_2 = 1 - \tilde{C}_2$ (to leading order in $1 - \tilde{C}_2$), whereas at long times ($t - t_w \gg t_w$ and $\tilde{C}_2 \approx 0$) we find $\tilde{\chi}_2 \sim \tilde{C}_2^{\frac{2n}{2n-T}}$. (See appendix 8.5 for details.) These predictions have been marked as dashed lines in figures 8.2a,c and support the numerical results. The short time prediction, $\tilde{\chi}_2 = 1 - \tilde{C}_2$, can be motivated very simply by inspection of equation 8.43. Changes in $\chi_2(t - t_w, t_w)$ due to variations in t_w on the LHS of this equation can be separated into two components: one due to the explicit variation of this absolute time t_w, and the other due to variations in the time interval $t - t_w$. For $t - t_w \ll t_w$, the latter component dominates. We can therefore set $\frac{\partial}{\partial t_w} \approx -\frac{\partial}{\partial t}$ to get $\frac{\partial}{\partial t}\chi_2(t - t_w, t_w) = -\frac{\partial}{\partial t}C_2(t - t_w, t_w)$ and, upon integration, $\tilde{\chi}_2 = 1 - \tilde{C}_2$. The physical content of this result is that the hopping rate $Y(t_w) \sim t_w^{T-1}$ is roughly constant over the short time interval $t - t_w \ll t_w$, and the properties are therefore "locally" (in time) TTI.

For $n < (T-1)/2$, we find that $\tilde{C}_2$ and $\tilde{\chi}_2$ both decay on the fast time-scale $O(1)$. Over this time-scale (and hence over the whole correlator range $C_2 = 1 \to 0$), we

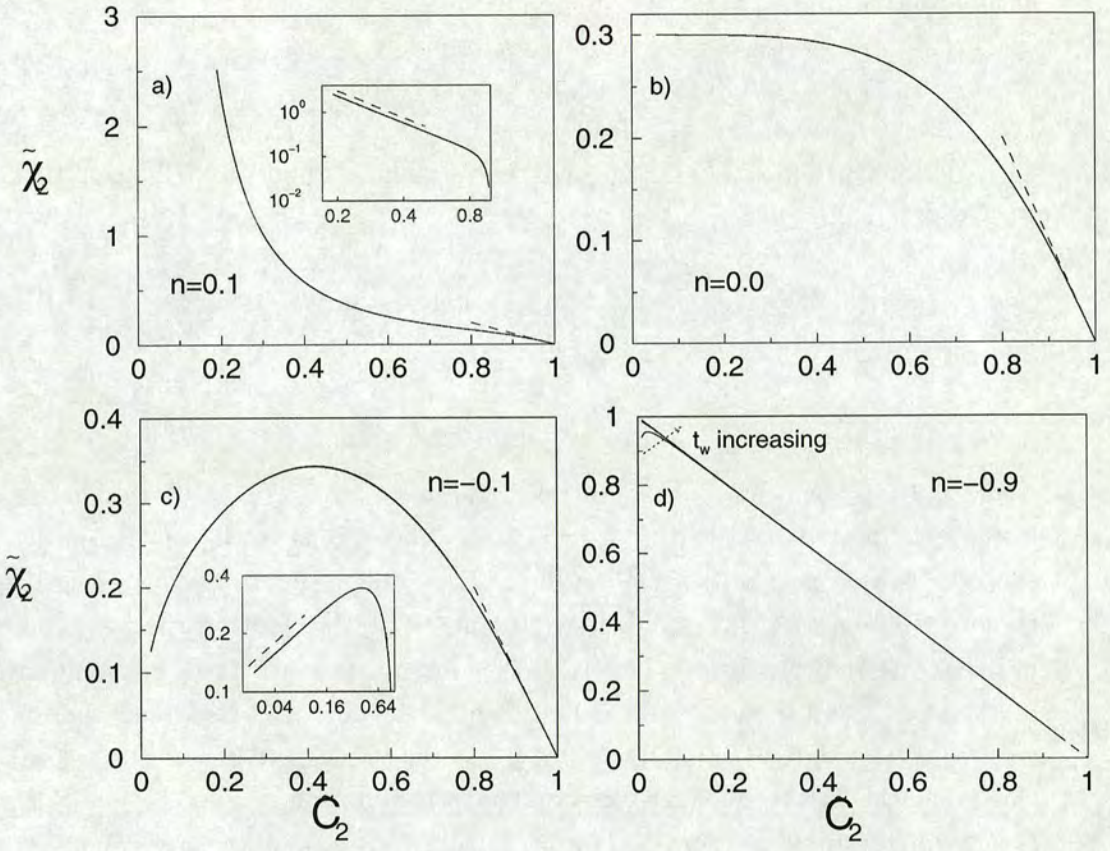

Figure 8.2. FDT plots of normalized response function versus normalized correlator for an intra-trap distribution $\sigma(m|E)$ which has variance $\exp(2nE/T)$ (but zero mean) for $n = 0.1, 0.0, -0.1, -0.9$. The temperature T is 0.3. At each value of n we have shown data for waiting times $t_w = 10^6$, 10^7, 10^8 and 10^9. At $n = 0.1, 0.0$ and -0.1 the curves for different waiting times are indistinguishable. This is also the case for $n = -0.9$, apart from a small region $C_2 \approx 0$. For each value of n, $\tilde{\chi}_2 = 1 - \tilde{C}_2$ (which is the analytically predicted asymptote for the limit $t_w \to \infty$ and $\tilde{C}_2 \to 1$) has been marked as a dashed line. The inset for each of the graphs in the left hand column shows the same data as on its corresponding main plot, but now on log-log axes. On these insets the power law $\tilde{\chi}_2 \sim \tilde{C}_2^{\frac{2n}{2n-T}}$ (which is the analytically predicted asymptote for $t_w \to \infty$, $\tilde{C}_2 \to 0$ for $n > (T-1)/2$) has been marked as a dashed line.

can set $\frac{\partial}{\partial t_w} \approx -\frac{\partial}{\partial t}$ in equation 8.43 using the "local TTI" argument given above. We therefore find that $\tilde{\chi}_2 = 1 - \tilde{C}_2$ over the whole range of the FDT plot: the plot is of trivial equilibrium form. This agrees with the numerical results of figure 8.2d.

The physical distinction between the two regimes of n can be made more transparent

by considering the following expression for the initial value of the correlator $C(0, t_w)$ at any waiting time t_w:

$$C(0, t_w) = \int dE P(E_w, t_w) \exp\left(\frac{2nE_w}{T}\right). \tag{8.47}$$

The energy-distribution $P(E_w, t_w)$ in this equation is approximately (equation 4.13, with variables changed $\tau \to E$)

$$\begin{aligned} P(E, t_w) &\propto t_w^{T-1} \exp\left(\frac{E}{T}\right) \rho(E) \quad \text{for} \quad E \ll \ln(t_w), \\ &\propto t_w^{T} \exp(-E) \qquad\quad \text{for} \quad E \gg \ln(t_w). \end{aligned} \tag{8.48}$$

where $\rho(E) = \exp(-E)$ is the prior distribution of trap depths, and $\exp(E/t)\rho(E)$ is the equilibrated part of the distribution. Now for $n = (T-1)/2$ the decay of this equilibrated part of the distribution is exactly balanced by the divergence $\frac{2nE}{T}$ of the contribution to $C(0, t_w)$ of a trap of depth E. Hence, substituting equation 8.48 into 8.47, we find that for $n < (T-1)/2$, the integral in equation 8.47 converges over an interval $O(1)$, and the correlator is therefore only sensitive to the population of traps with $\tau = O(1)$: it decays on a time-scale $O(1)$ over which the hopping rate t_w^{T-1} doesn't change much. We therefore see locally TTI behaviour, and an FDT plot which is of trivial equilibrium form. For $n > (T-1)/2$, on the other hand, the integral of 8.47 picks up significant weight over the entire interval $\tau = 0 \to t_w$. The correlator is sensitive to the deep traps with $\tau = O(t_w)$, and we therefore expect to see strongly non-equilibrium behaviour in the FDT plot. We can also see from equations 8.47 and 8.48 that the initial value of the correlator for $n > T/2$ would be infinite even at zero waiting time $t_w = 0$, since here the decay of the prior is dominated by the divergence of $\frac{2nE}{T}$; this is the reason for confining ourselves to $n < T/2$.

Now we turn to power law dependence of the variance upon energy: $(\Delta m)^2(E) = E^{2p}$, still assuming zero mean. Analytically, it is easy to calculate the correlator and response in this case, since they follow as a limit of the results given above for the exponential dependence $(\Delta m)^2(E) = \exp(2nE/T)$. Specifically, we use the fact that a power law E^{2p} can be recovered from an exponential $\exp(2nE/T)$ by use of the operator $\lim_{n\to 0}(\frac{\partial}{\partial n})^{2p}$. Together with the fact that correlator and response are both linear in the variance, this means that we can calculate C_2 and χ_2 for this case simply

	$C_2(t-t_w,t_w)$		$\chi_2(t-t_w,t_w)$		$\tilde{\chi}_2(\tilde{C}_2)$	
	$t-t_w \ll t_w$	$t-t_w \gg t_w$	$t-t_w \ll t_w$	$t-t_w \gg t_w$	$\tilde{C}_2 \approx 1$	$\tilde{C}_2 \approx 0$
$\frac{T-1}{2} < n < \frac{T}{2}$	$t_w^{2n}\left[1-\left(\frac{t-t_w}{t_w}\right)^{1-T+2n}\right]$	$t_w^{2n}\left(\frac{t-t_w}{t_w}\right)^{2n-T}$	$t_w^{2n}\left(\frac{t-t_w}{t_w}\right)^{1-T}$	t^{2n}	$\tilde{\chi}_2 = 1-\tilde{C}_2$	$\tilde{C}_2^{\frac{2n}{2n-T}}$
$n < \frac{T-1}{2}$	$t_w^{T-1}(1+t-t_w)^{1-T+2n}$	--	$t_w^{T-1}\left[1-(1+t-t_w)^{1-T+2n}\right]$	--	$\tilde{\chi}_2 = 1-\tilde{C}_2$	--

Table 8.1. Correlation function (first column), response function (second column) and FDT curve (third column) at short ($t-t_w \ll t_w$) and long ($t-t_w \gg t_w$) times ($t_w \gg 1$ assumed) for an intra-trap distribution $\sigma(m|E)$ which has zero mean, and variance $(\Delta m)^2 = \exp(2En/T)$. The entries for the long time regime have been left blank for $(T-1)/2$ since here the correlator decays on a time-scale $O(1)$, and times $t-t_w \gg t_w$ are not seen on the FDT plot in the limit $t_w \to \infty$.

by operating with $\lim_{n\to 0}(\frac{\partial}{\partial n})^{2p}$ on our above results. Doing this we find[6]

$$\begin{aligned} C_2(t-t_w,t_w) &= \lim_{n\to 0}\left\{\left(\frac{\partial}{\partial n}\right)^{2p}\left[t_w^{2n}\tilde{C}_2(t/t_w,n)\right]\right\} \\ &\propto \log^{2p}(t_w)\tilde{C}_2(t/t_w,0) + O(\log^{2p-1}(t_w)\tilde{C}_2'(t/t_w,0)) \end{aligned} \quad (8.49)$$

and likewise

$$\begin{aligned} \chi_2(t-t_w,t_w) &= \lim_{n\to 0}\left\{\left(\frac{\partial}{\partial n}\right)^{2p}\left[t_w^{2n}\tilde{\chi}_2(t/t_w,n)\right]\right\} \\ &\propto \log^{2p}(t_w)\tilde{\chi}_2(t/t_w,0) + O(\log^{2p-1}(t_w)\tilde{\chi}_2'(t/t_w,0)), \end{aligned} \quad (8.50)$$

where the prime denotes differentiation with respect to n. In the limit $t_w \to \infty$, the first term on the RHS dominates in each of these expressions. The scaling functions in

[6] where we have now explicitly included the n dependence in the argument lists of $\tilde{C}_2$ and $\tilde{\chi}_2$.

these terms are just those for $(\Delta m)^2(E) = \exp(2nE/T)$ with $n = 0$. The FDT plot (in which both C_2 and χ_2 are normalized by the initial value $\log^{2p}(t_w)$) should therefore be the same as that of figure 8.2b for $n = 0$.[7]

Numerically, we calculated C_2 and χ_2 by switching $\exp(2En/T)$ for E^{2p} in equations 8.45 and 8.46, and evaluating the integrals afresh. The results for $p = 1$ are shown in figure 8.3. The predicted asymptote (the $n = 0$ curve of 8.2b) has been marked as a dashed line for reference: the inset suggests that the results converge to it roughly logarithmically as $t_w \to \infty$.

This concludes our study of FDT for an intra-trap distribution which has zero mean, but non-zero variance. We have studied both exponential and power law dependence of the variance upon energy, and shown in each case that a limiting FDT curve $\tilde{\chi}_2(\tilde{C}_2)$ is approached as $t_w \to \infty$.

FDT for an intra-trap distribution with zero variance, non-zero mean.

We now discuss FDT for a system in which a particle hopping into a trap of depth E has its value of m deterministically prescribed as $\bar{m}(E)$. In this case the variance of the intra-trap distribution is zero, and the correlator is given by C_1. We shall consider both exponential and power law dependence of $\bar{m}(E)$ upon energy. We start with the exponential case, setting $\bar{m}(E) = \exp(nE/T)$. Substituting this into equation 8.30, and equations 8.34 to 8.37, for C_1 we have

$$C_1(t - t_w, t_w) = f_2(t - t_w, t_w) + \int_{t_w}^{t} dt' f_1(t - t') f_3(t' - t_w, t_w) - f_1(t) f_1(t_w) \quad (8.51)$$

in which

$$f_1(t) = G_{\rho(E)\exp(nE/T)}(t) + \int_0^t dt' Y(t') G_{\rho(E)\exp(nE/T)}(t - t'), \quad (8.52)$$

$$f_2(t - t_w, t_w) = G_{\rho(E)\exp(2nE/T)}(t) + \int_0^{t_w} dt' Y(t') G_{\rho(E)\exp(2nE/T)}(t - t'), \quad (8.53)$$

and

$$f_3(t - t_w, t_w) = G_{\frac{\rho(E)\exp(nE/T)}{\tau(E)}}(t) + \int_0^{t_w} dt' Y(t') G_{\frac{\rho(E)\exp(nE/T)}{\tau(E)}}(t - t'). \quad (8.54)$$

[7]Note that, although it is somewhat unconventional to define a derivative $(\frac{\partial}{\partial n})^{2p}$ with p anything other than a positive integer, these results can be extended to all real p, including negative and fractional values, by taking the Laplace transform of the derivative, and appealing to analytical continuation in Laplace space.

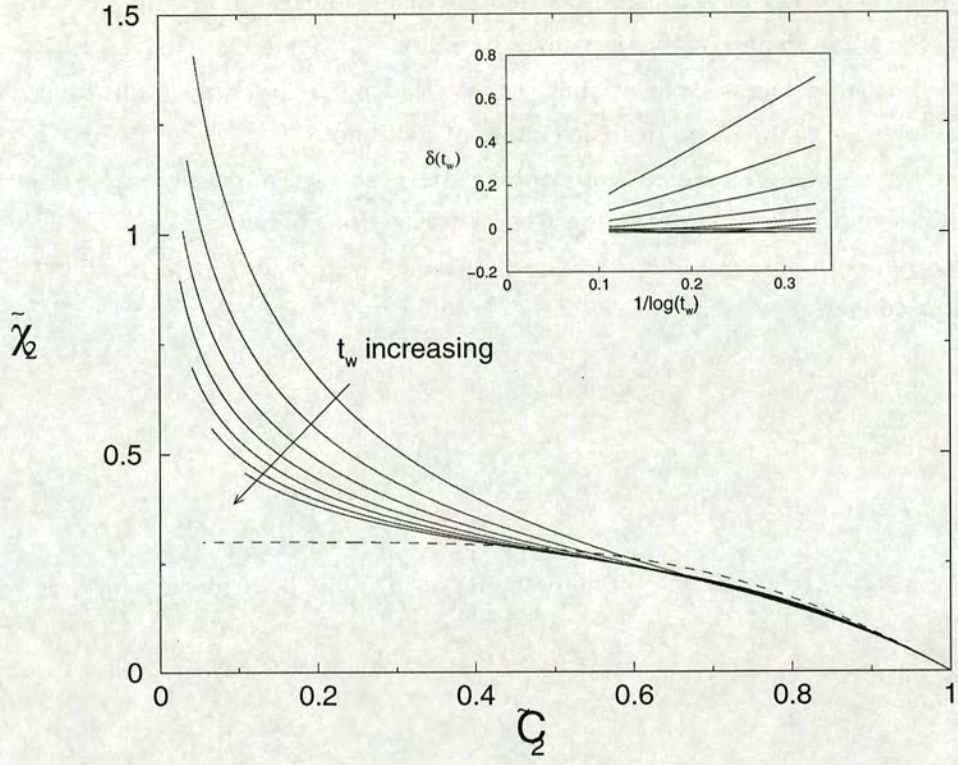

Figure 8.3. FDT plots of normalized response function versus normalized correlator for an intra-trap distribution with variance E^2 (but zero mean). The temperature T is 0.3 and the waiting times are $t_w = 10^3$, 10^4, ...10^9. The dashed curve is numerical data for the limiting curve $\tilde{\chi}_2(\tilde{C}_2)$ for an intra-trap distribution of constant variance and zero mean: this is the predicted asymptote in the limit $t_w \to \infty$ for all $\tilde{C}_2$. (Its slope is -1 at the extreme right of the plot.) The inset shows the way in which the data tends to this asymptote, and has been constructed as follows. For values of $\tilde{C}_2 = 0.1, 0.2 ... 0.9$ we have defined $\delta(t_w)$ to be the (t_w dependent) difference between $\tilde{\chi}_2$ of the data, and $\tilde{\chi}_2$ of the asymptotic dashed curve. For each value of $\tilde{C}_2$, this deviation has been plotted versus $1/\log(t_w)$. Curves upward at fixed $1/\log(t_w)$ correspond to decreasing values of the correlator.

An exact expression for the corresponding response function χ_1 was found by substituting these equations into

$$\frac{\partial}{\partial t_w}\chi_1(t - t_w, t_w) = \frac{\partial}{\partial t}C_1(t - t_w, t_w) + \frac{\partial}{\partial t}f_1(t)f_1(t_w), \tag{8.55}$$

and integrating over t_w. (8.55 is just equation 8.44 transcribed into the notation of this section: $f_1(t) = \langle m(t) \rangle$.)

We then computed C_1 and χ_1 numerically (using these exact expressions) for various values of n at $T = 0.3$. (As for the case of C_2 above, we confine ourselves to values of $n < T/2$.) The results are shown in figure 8.4. They demonstrate that equilibrium FDT is (in general) violated, but suggest that a limiting non-equilibrium FDT plot is approached as $t_w \to \infty$ (for each value of n studied).

We now summarize an analytical study (described in detail in appendix 8.5) which shows that a limiting curve must indeed exist for all values of $n < T/2$. Using equations 8.51 to 8.54, we find the following scaling forms[8] for C_1 in the limit $t_w \to \infty$ with $C = const.$:

$$\begin{aligned} C_1(t - t_w, t_w) &\sim t_w^{2n} \tilde{C}_1(t/t_w) \qquad \text{for} \quad n > \frac{T-1}{2} \\ &\sim t_w^{T-1} \tilde{C}_1(t - t_w) \quad \text{for} \quad n < \frac{T-1}{2} \quad \text{and} \quad t - t_w \ll t_w. \end{aligned} \tag{8.56}$$

We also use equation 8.52 to find the following time dependences for f_1

$$\begin{aligned} f_1(t_w) &\sim t_w^n \qquad \text{for} \quad n > T - 1 \\ &\sim t_w^{T-1} \quad \text{for} \quad n < T - 1. \end{aligned} \tag{8.57}$$

We then substitute these results into equation 8.55 to find the following scaling forms for the response function χ_1:

$$\begin{aligned} \chi_1(t - t_w, t_w) &\sim t_w^{2n} \tilde{\chi}_1(t/t_w) \qquad\qquad \text{for} \quad n > \frac{T-1}{2} \\ &\sim t_w^{T-1} \left[1 - \tilde{C}_1(t - t_w)\right] \quad \text{for} \quad n < \frac{T-1}{2} \quad \text{and} \quad t - t_w \ll t_w. \end{aligned} \tag{8.58}$$

Comparing the results of equations 8.56 and 8.58 we find that, in each regime of n, the normalized functions $\tilde{C}_1$ and $\tilde{\chi}_1$ share the same scaling variable. Hence a limiting FDT plot must exist in each regime.

As in the case of $\tilde{\chi}_2(\tilde{C}_2)$ above, we again identify two distinct regimes of n. For $n < (T-1)/2$, the correlator decays on a fast time-scale $O(1)$. The FDT plot is of trivial equilibrium form with slope -1: $\tilde{\chi}_1 = 1 - \tilde{C}_1$. Physically, this is due to the approximate

[8] We do not need to study C_1 for $n < (T-1)/2$ in the long time regime $t - t_w \gg t_w$, because it here decays on a time-scale of $O(1)$. In the limit $t_w \to \infty$, therefore, the $t - t_w \gg t_w$ regime is not visible on an FDT plot.

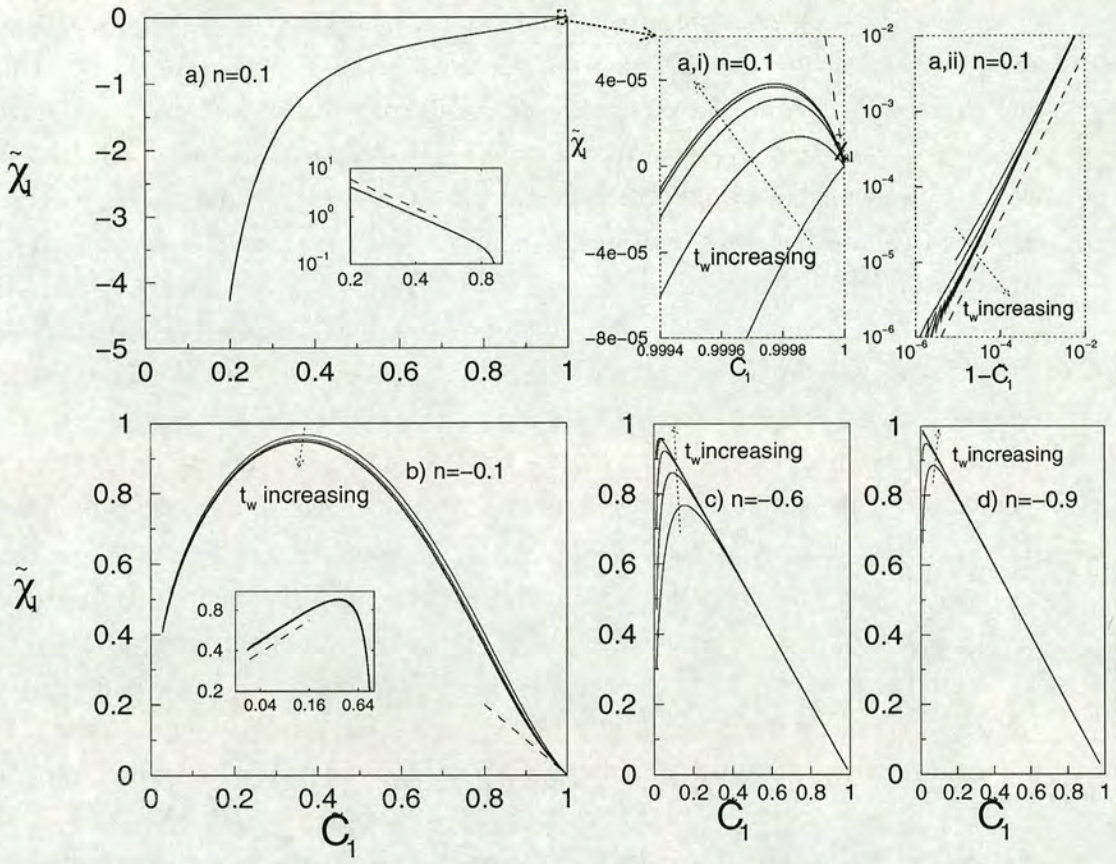

Figure 8.4. FDT plots of normalized response function versus normalized correlator for an intra-trap distribution which has mean $\exp(nE/T)$ (but zero variance), for $n = 0.1, -0.1, -0.9$. The temperature T is 0.3 and the waiting times are $t_w = 10^3, 10^4, 10^5, 10^6$. The curves for different t_w are indistinguishable for $n = 0.1$. The inset on each of the left two graphs shows the same data as on its corresponding main graph, but now on a log-log plot. On these insets the dashed line is the power law $\tilde{\chi}_1 \sim \tilde{C}_1^{\frac{2n}{2n-T}}$, and is the predicted analytical asymptote in the limit $t_w \to \infty$ $\tilde{C}_1 \to 0$. On the bottom left graph, the dashed line $\tilde{\chi}_1 = 1 - \tilde{C}_1$ is the analytically predicted asymptote as $t_w \to \infty$ for $\tilde{C}_1 \to 1$. $\tilde{\chi}_1 = 1 - \tilde{C}_1$ is also the predicted asymptote (as $t_w \to \infty$ and $\tilde{C}_1 \to 1$) for the data the top left graph. However here this asymptote is only approached for such small values of $1 - \tilde{C}_1$ that it is impossible to discern. Therefore in the two graphs in the top right quadrant we have shown a zoom of the region $\tilde{C}_1 \approx 1$. Of these two graphs, the left one is the raw data together with the predicted asymptote $1 - \tilde{C}_1$. The right one is the $\tilde{\chi}_1$ minus the leading asymptotic term $1 - \tilde{C}_1$, plotted versus $1 - \tilde{C}_1$: the dashed line here is the power $(1 - \tilde{C}_1)^{\frac{1}{1-T+2n}}$ and is the analytical prediction for the sub-leading term of $\tilde{\chi}_1$ as $t_w \to \infty$ and $\tilde{C}_1 \to 1$.

constancy of the hopping rate $Y(t)$ over the short time interval $t - t_w \ll t_w$, as described above for $\tilde{\chi}_2(\tilde{C}_2)$. See appendix 8.5 for details of the calculation.

For $n > (T-1)/2$ the correlator decays on the ageing time-scale $O(t_w)$, and we see a non-trivial shape to the plot, showing that equilibrium FDT is strongly violated. To find expressions for the shape of this plot, we of course need to know expressions for the shapes of C_1 and χ_1. Due to the rather complicated structure of equation 8.51, we have been unable to find the shape of C_1 analytically. Numerically, however, is appears to share the same dependence upon t_w and $t - t_w$ as C_2. Substituting this into equation 8.55 (together with the scalings of f_1 given in equation 8.57) we find an expression for the corresponding response χ_1. We then express the normalized response $\tilde{\chi}_1$ in terms of $\tilde{C}_1$ in the normal way. (See appendix 8.5 for details.) The results are summarized in table 8.2. We again identify a short time and a long time regime. In the short time regime ($t - t_w \ll t_w$, $\tilde{C}_1 \approx 1$) we find $\tilde{\chi}_1 = 1 - \tilde{C}_1$ to leading order. (Again, this can be motivated by a local TTI argument.) For the long time regime ($t - t_w \gg t_w$, $\tilde{C}_1 \approx 0$) we find $\tilde{\chi}_1 \sim \tilde{C}_1^{\frac{2n}{2n-T}}$. These predictions have been marked as dashed lines in figure 8.4 and are in good agreement with the numerical results.

We now turn to consider power law dependence of mean upon energy: $m = E^p$, still with zero variance. We focus particularly upon the case $p = 1$, and, before presenting any results, pause briefly to consider the physical interpretation of this regime. Here, the magnetization m is just trap depth E. This is a *negative* energy, since trap depth is measured downwards in energy space. But because the correlator is invariant under changes in the sign of m, it can be taken to measure fluctuations in either trap depth or energy. For convenience we use the latter interpretation. The corresponding response function can be found by evolving the system under a perturbing field h which modifies the unperturbed Hamiltonian ($H = -E$) in the following way: $\frac{H}{T} \to \frac{H}{T} - \frac{h}{T}m$. Hence $\frac{H-hm}{T} = -\frac{E}{T+\delta T} = -\frac{E}{T} + \frac{\delta T E}{T^2}$, which corresponds to $h = -\delta T/T$ (which is subject to a further rescaling by $1/T$ to get our normalized FDT plot as discussed above). Hence the response function is the response of the trap-depth to a negative step temperature. Equivalently, (reversing the sign of both h and m), it is the energy response to a positive step temperature.

We now present our results for this "energy-temperature" FDT. We computed C_1 and χ_1 numerically by switching $\exp(nE/T)$ for E^p with $p = 1$ in equations 8.52 to 8.55 and evaluating the integrals afresh. The results for C_1 and χ_1 are plotted against $t - t_w$, for various temperatures T and waiting times t_w, in figure 8.5. We obtained an independent check of these results via direct Monte Carlo (MC) simulation of the model. The MC results also shown in figure 8.5 and are seen to agree well with the numerical solutions of the exact equations.

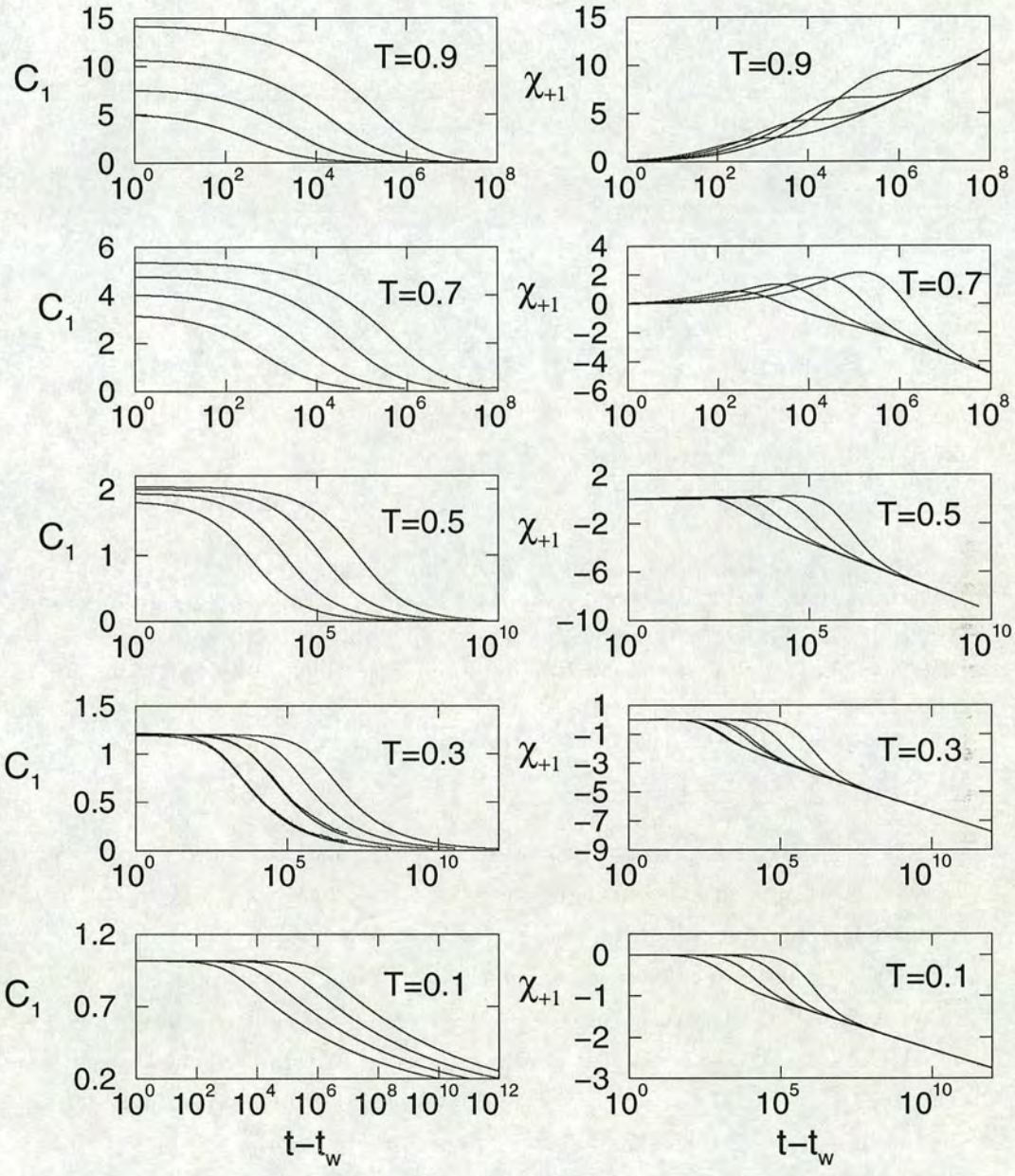

Figure 8.5. Correlator (left graphs) and response (right graphs) for an intra-trap distribution which has zero variance, and mean $\bar{m}(E) = -E$. The conjugate field h is a positive temperature shift. Data is shown for temperatures $T = 0.1$, 0.3, 0.5, 0.7 and 0.9. At each temperature data is given for waiting times $t_w = 10^6$, 10^7, 10^8 and 10^9. At a fixed value of $t - t_w$, curves upwards are for increasing t_w.

	$C_1(t-t_w,t_w)$		$\chi_1(t-t_w,t_w)$		$\tilde{\chi}_1(\tilde{C}_1)$	
	$t-t_w \ll t_w$	$t-t_w \gg t_w$	$t-t_w \ll t_w$	$t-t_w \gg t_w$	$\tilde{C}_1 \approx 1$	$\tilde{C}_1 \approx 0$
$\frac{T-1}{2} < n < \frac{T}{2}$	$t_w^{2n}\left[1-\left(\frac{t-t_w}{t_w}\right)^{1-T+2n}\right]$	$t_w^{2n}\left(\frac{t-t_w}{t_w}\right)^{2n-T}$	$t_w^{2n}\left(\frac{t-t_w}{t_w}\right)^{1-T}$	t^{2n}	$\tilde{\chi}_1 = 1-\tilde{C}_1$	$\tilde{C}_1^{\frac{2n}{2n-T}}$
$n < \frac{T-1}{2}$	$t_w^{T-1}(1+t-t_w)^{1-T+2n}$	--	$t_w^{T-1}\left[1-(1+t-t_w)^{1-T+2n}\right]$	--	$1-\tilde{C}_1$	--

Table 8.2. Correlation function (first column), response function (second column) χ_1 and normalized FDT curve (third column) at short ($t-t_w \ll t_w$) and long ($t-t_w \gg t_w$) times ($t_w \gg 1$ assumed) for an intra-trap distribution with zero variance, and mean $\bar{m}(E) = \exp(En/T)$. The long time regime entries have been left blank for $(T-1)/2$ since, for this regime of n, the correlator decays on a time-scale $O(1)$, and times $t-t_w \gg t_w$ are not seen on the FDT plot in the limit $t_w \to \infty$.

At $T = 0.3$, we constructed a normalized FDT plot from these results in the usual way. The results are shown in figure 8.6. They suggest that in this case we do *not* approach a limiting plot $\tilde{\chi}(\tilde{C})$ as $t_w \to \infty$. We now give an analytical argument supporting this observation, showing that correlator and response scale in different ways as $t_w \to \infty$. To do this, we consider the time dependences of C_1 and χ_1 in turn.

We start with the correlator, and compute its initial ($t - t_w = 0$) value $C_1(0, t_w)$ in the limit $t_w \to \infty$. This is clearly just the variance of the distribution $P(E, t_w)$ which, in the limit $t_w \to \infty$, has the following approximate form

$$\begin{aligned} P(E,t_w) &\sim \exp\left(E\left(\tfrac{1}{T}-1\right)\right) && \text{for } E \ll T\log(t_w) \\ &\sim t_w \exp(-E) && \text{for } E \gg T\log(t_w). \end{aligned} \tag{8.59}$$

(This is equation 4.13, with the variable τ transformed to E by $\tau(E) = \exp(E/T)$.) This is just two exponentials (spliced together at $T\log(t_w)$) and has a variance which is independent of time. Likewise, therefore, the initial value of the correlator $C(0, t_w)$

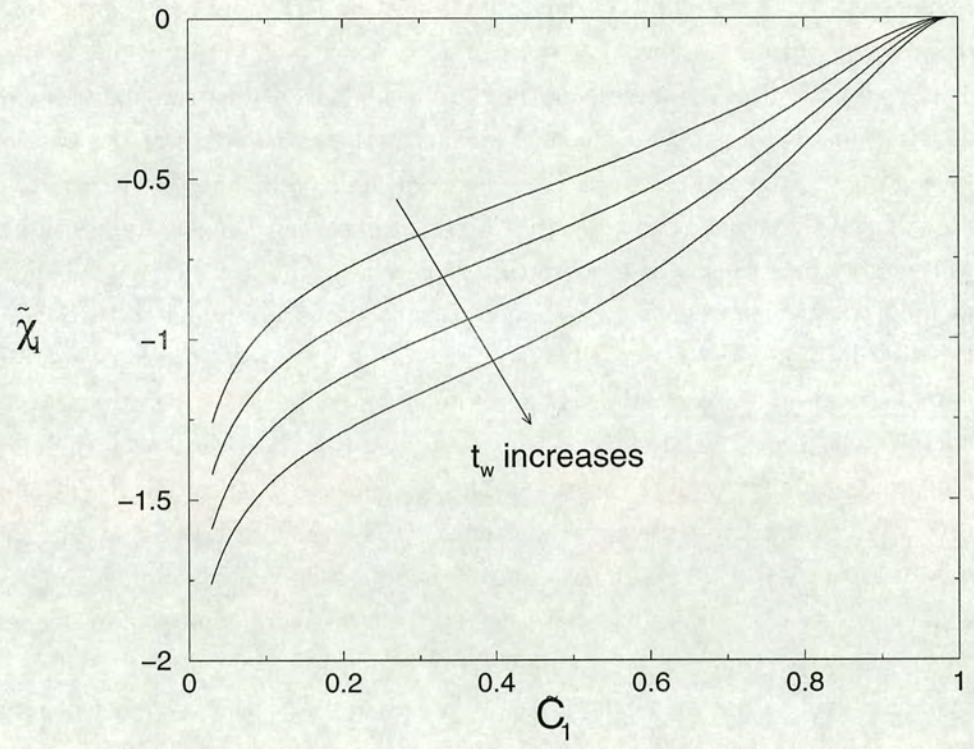

Figure 8.6. FDT plots of normalized response function versus normalized correlator for an intra-trap distribution which has mean E. The temperature T is 0.3. The waiting times are $t_w = 10^3$, 10^4, 10^5 and 10^6.

is time independent, and remains of $O(1)$ as $t_w \to \infty$. Furthermore, because the correlator is a monotonically decreasing function of $t - t_w$, it can never exceed this $O(1)$ initial value for any value of the scaled variable $(t - t_w)/t_w$.

The response function, on the other hand, diverges logarithmically with t_w at fixed value of t/t_w in the limit $t - t_w \to \infty$, $t_w \to \infty$, $(t - t_w)/t_w = \text{const}$. This can be seen from 8.55. In this equation $f_1(t) \sim \log(t_w)$ as $t_w \to \infty$, and hence dominates the $(O(1))$ correlator. To leading order, then, 8.55 becomes

$$\frac{\partial}{\partial t_w}\chi_1(t - t_w, t_w) = \frac{\partial}{\partial t} f_1(t) f_1(t_w) \sim \log(t_w)/t. \tag{8.60}$$

Integrating over t'_w from t to t_w (using the boundary condition $\chi_1(0, t_w) = 0 \, \forall t_w$) we find that

$$\chi_1(t - t_w, t_w) \sim \frac{t_w \log(t_w) - t \log(t)}{t}. \tag{8.61}$$

Hence the energy response diverges logarithmically as $t_w \to \infty$ while the correlator remains of $O(1)$, and no limiting energy-temperature FDT plot can exist. This argument can be generalized to show that there is no limiting plot for any value of p.

Finally, we discuss the signs of the response functions just calculated for the various distributions with non-zero mean. We start with the response of the system's energy to a positive step temperature. We see from figure 8.6 that this is negative. This is at first sight somewhat surprising: the usual experience in an equilibrium system is that energy increases with temperature. The reason for this unexpected sign change is as follows. After a quench to a temperature T, the trap model tries to equilibrate to the distribution $P(E) \sim \exp[E(1/T - 1)]$. This is weighted to smaller energies (deeper traps) for lower temperatures. Therefore, for any bath temperatures at which this equilibrium can be attained (*i.e.* above the glass point), we expect the energy to be higher at a higher temperature, and the response to be positive in the normal way. (We have checked numerically that this is indeed the case.) Below the glass point, however, this "static" effect is swamped by the following dynamical one. Following a quench into the glass phase, the system progressively evolves into deeper traps of lower energy. Comparing two temperatures which are both inside the glass phase, the dynamics will be faster at the higher temperature and the system will more rapidly get to deeper traps. At a fixed time, therefore, a system at a higher temperature will have less energy (will be in deeper traps) than one at a smaller temperature. This is the origin the negative energy response to a positive step temperature.

This argument can be generalized to explain the sign of the response functions in figure 8.4 for a distribution in which the mean depends exponentially upon energy: $\bar{m}(E) = \exp(En/T)$. We recall that under a small field, h, the system's Hamiltonian is defined to perturb thus: $H \to H - hm$. Hence all the energies are reduced slightly (assuming hm to be positive), or, equivalently, all the traps are made slightly deeper: the dynamics are therefore slower than in zero field conditions. Hence the perturbed system stays in shallower traps for longer. This means that, if the mean $\bar{m}(E)$ is an increasing function of trap depth, we at any time see a smaller global average m in a perturbed system: the response is negative. If, on the other hand, the mean decreases with trap depth, the response will be positive. This argument is consistent with the results of figure 8.4 which predict a positive response for $n < 0$ and negative response for $n > 0$.

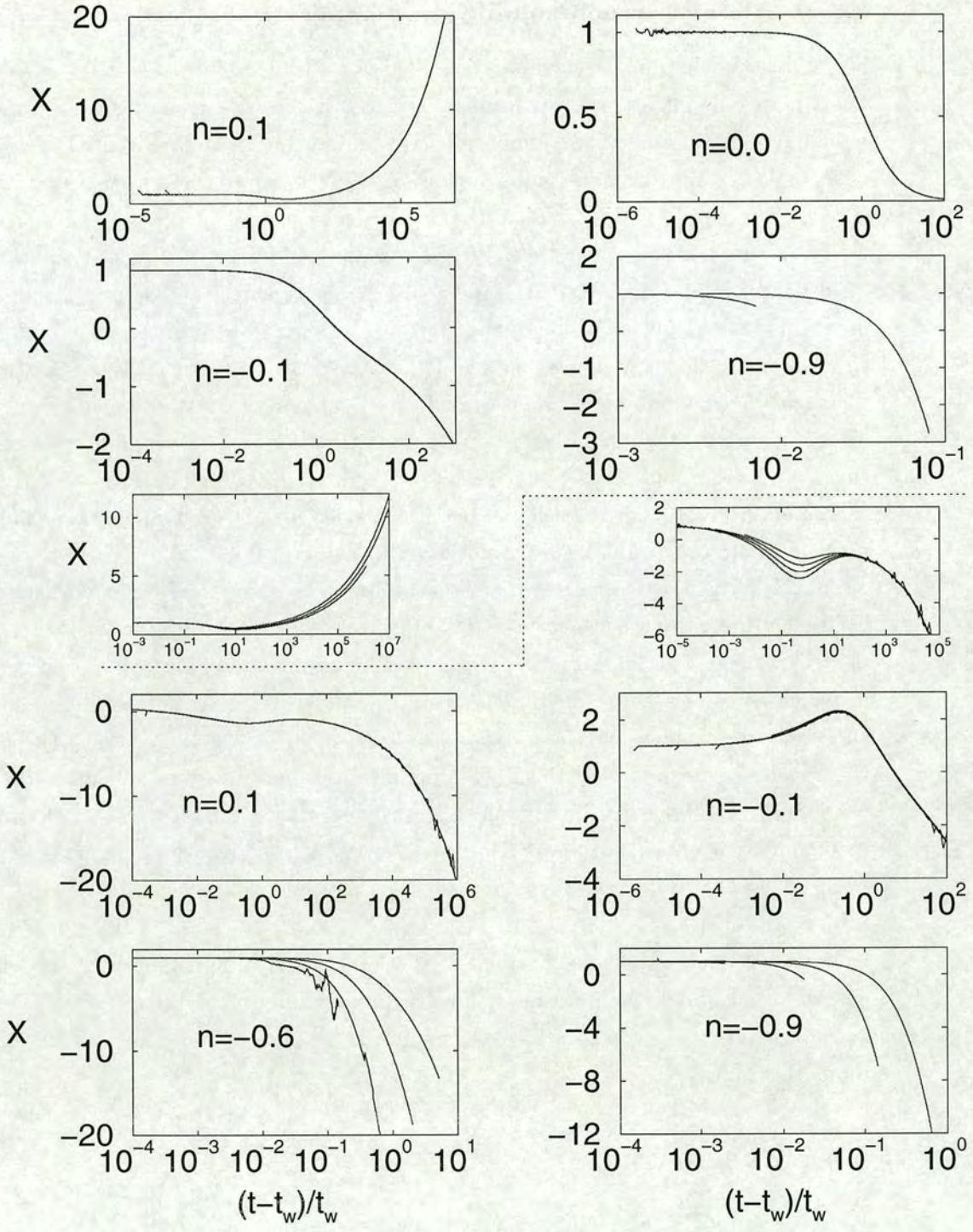

Figure 8.7. Gradient of the FDT plots vs. scaled time variable $(t - t_w)/t_w$. Graphs above the dotted line are calculated from the results of figures 8.2 and 8.3, for intra-trap distributions with non-zero variance, but zero mean. Those below the dotted line (calculated using the results of figures 8.4 and 8.6) are for distributions with non-zero mean, but zero variance. The small graph in each case is for logarithmic dependence of the relevant cumulant upon trap depth.

8.3.4 Absence of non-equilibrium temperature

So far in this chapter we have studied FDT for various observable-field (m, h) pairs (*i.e.* for various intra-trap distributions $\sigma(m|E)$) within the ageing regime of the trap model. We have found that equilibrium FDT is (in general) violated but that, for most observables, a limiting non-equilibrium FDT curve is approached as $t_{\rm w} \to \infty$ at fixed C. The case $(m, h) = (E, \Delta T)$ is a notable exception.

In section 8.2 we noted that, for many non-equilibrium SEP systems, FDT can be used to define an effective temperature $T_{\rm eff}$. Specifically, $T_{\rm eff}$ is defined as the magnitude of the inverse slope of the limiting FDT curve. As discussed in section 8.2, this has been shown to display many of the properties one intuitively associates with a normal thermodynamic temperature. In particular, it is constant within each epoch of the system's dynamics, and is the temperature which a thermometer of reaction time $O(f(t_{\rm w}))$ would read when coupled to the system (while being isolated from the surrounding heat bath). It is furthermore the same for all observables m, as indeed it must be to accord to the intuitive notion of a temperature.

In this section, we comment briefly on the extent to which the FDT curves calculated by us for the trap model can be used to define a non-equilibrium temperature in the model's ageing regime. We recall that in this regime, there exists just one "epoch", in which dynamics occur on time-scales $O(t_{\rm w})$. Hence we see immediately that any effective temperature could not satisfy the usual requirement of constancy throughout the epoch, due to fact that the FDT plots are in general not straight lines. However, one might still hope to identify an effective temperature which, although it varies throughout the epoch, is the same for all observables at a given scaled time $(t - t_{\rm w})/t_{\rm w}$. In an attempt to find such a temperature, we plotted the gradients of the FDT plots against this variable. The results are shown in figure 8.7 and clearly show that at any value of scaled time the gradient of the FDT plot is different for each observable. Therefore, although the existing of limiting non-equilibrium FDT plots is interesting and non-trivial, we conclude that they cannot be used to define a meaningful effective temperature.

8.4 Conclusion

We have studied FDT in the ageing regime of Bouchaud's trap model. We have considered several choices of observable-field pair, each of which is defined by a particular intra-trap distribution $\sigma(m|E)$. For each choice, we have computed the correlation and response function, and have used these to construct an FDT plot. For most choices of

distribution, we find that a limiting FDT curves exists as $t_w \to \infty$. Energy-temperature FDT is a notable exception. We have discussed the possible use of the limiting curves to define a non-equilibrium temperature. We concluded that we any effective temperature defined using the curves is not likely to be a useful quantity, since it will be strongly dependent upon both observable and time.

8.5 Appendix: analysis for correlation and response functions

8.5.1 Correlation functions

In this appendix we calculate analytically the dependence of the correlator $C_2(t-t_w, t_w)$ upon $t - t_w$ and t_w (in the usual limit $t_w \to \infty$) for an intra-trap distribution $\sigma(m|E)$ which has variance $(\Delta m)^2(E) = \exp(2En/T)$, and zero mean. We also calculate the time-scale of decay (again in the limit $t_w \to \infty$) for the correlator $C_1(t - t_w, t_w)$ of a distribution which has zero variance, and mean $\bar{m}(E) = \exp(En/T)$. (We have been unable analytically to derive the explicit time-dependences of C_1, due to the rather complicated structure of its exact expression 8.30.)

We start by rewriting equations 8.30 and 8.42 for C_1 and C_2 as [9]:

$$C_1(t - t_w, t_w) = I(t - t_w, t_w, 2n) + \int_{t_w}^{t} dt' I(0, t - t', n) I(t' - t_w, t_w, n - 1) - I(0, t, n) I(0, t_w, n) \quad (8.62)$$

and

$$C_2(t - t_w, t_w) = I(t - t_w, t_w, 2n) \quad (8.63)$$

in which the integral I is defined by

$$I(t - t_w, t_w, p) = \int_0^t dt' Y(t') G_{\rho(E)\exp(\frac{Ep}{T})}(t - t'). \quad (8.64)$$

Our strategy will be to calculate the dependence of this integral upon $t - t_w$ and t_w in the limit $t_w \to \infty$, and the substitute the results into equations 8.62 and 8.63 to find the required time dependence of C_2, and the time-scale upon which C_1 decays. (Of course in the case of C_2 this merely amounts to making the substitution $p = 2n$.)

[9] In each of equations 8.62 and 8.63, we have neglected a small term which represents memory to initial condition.

We start, then, by extracting the dependence of I upon $t - t_w$ and t_w in the limit $t_w \to \infty$. As a first step, we examine the time dependence of each of the constituent factors of its integrand. We recall from appendix 4.3 that the hopping rate $Y(t)$ has the form

$$Y(t) \sim (1+t)^{T-1}. \tag{8.65}$$

The time dependence of the memory function to get

$$G_{\rho(E)\exp(\frac{Ep}{T})}(t) = \int dE\rho(E)\exp(Ep/T)\exp\left(-\frac{t}{\exp\left(\frac{E}{T}\right)}\right) \tag{8.66}$$

is found by changing variables to $s = t/\exp(E/T)$

$$G_{\rho(E)\exp(\frac{Ep}{T})}(t) = Tt^{p-T}\int_0^t dss^{T-p-1}\exp(-s). \tag{8.67}$$

which tells us that

$$\begin{array}{rcll} G_{\rho(E)\exp(\frac{Ep}{T})}(t) & \sim & t^{p-T} & \text{for} \quad t \gg 1 \\ & \to \text{const} & \text{for} & t \to 0. \end{array} \tag{8.68}$$

The interpolating form

$$G_{\rho(E)\exp(\frac{Ep}{T})}(t) \sim (1+t)^{p-T} \tag{8.69}$$

correctly reproduces both these asymptotes.

Substituting 8.69 and 8.65 into 8.64 we get

$$I(t-t_w, t_w, p) = \int_0^t dt'(1+t')^{T-1}(t-t'+1)^{p-T}. \tag{8.70}$$

We can now proceed to extract the required dependences of this integral on $t - t_w$ and t_w. As usual we identify a short time regime $t - t_w \ll t_w$ and a long time regime $t - t_w \gg t_w$. For long times ($t - t_w \gg t_w$) we expand the second factor in the integrand about $t' = t_w$. This gives

$$I(t-t_w, t_w, p) \sim t_w^T(t-t_w)^{p-T}. \tag{8.71}$$

For short times ($t - t_w \ll t_w$) we treat the case $p < T - 1$ separately from $p \geq T - 1$. For $p < T - 1$ the integral of $(t - t' + 1)^{p-T}$ over t' ("backwards" from t_w) converges in a region of $O(1)$. Over this region, $t'^{T-1} \approx t_w^{T-1}$ and we get

$$I(t-t_w, t_w, p) \sim t_w^{T-1}(1+t-t_w)^{1-T+p}. \tag{8.72}$$

For $p \geq T-1$, $(t-t'+1)^{p-T}$ has a non-integrable tail and we rewrite 8.70 as

$$I(t-t_{\rm w}, t_{\rm w}, p) \sim \int_0^t dt' t'^{T-1}(t-t'+1)^{p-T} - \int_{t_{\rm w}}^t dt' t'^{T-1}(t-t'+1)^{p-T}. \qquad (8.73)$$

Changing variables to $t' \to t/t'$ we find that the first integral scales as $t^{2n} \approx t_{\rm w}^{2n}$. In the second integral we expand t'^{T-1} about $t' = t_{\rm w}$, and retain only the leading term. (The second is smaller by a factor $(t-t_{\rm w})/t_{\rm w}$.) Putting all this together, we find

$$I(t-t_{\rm w}, t_{\rm w}, p) \sim t_{\rm w}^{2n}\left[1-\left(\frac{t-t_{\rm w}}{t_{\rm w}}\right)^{1-T}\right]. \qquad (8.74)$$

Hence we have now found the dependences of the integral I upon $t-t_{\rm w}$ and $t_{\rm w}$ in the limit $t_{\rm w} \to \infty$. We summarize them in table 8.3. Specialising to $p = 2n$ we find the time dependences for C_2 as summarized in table 8.1 of the main text.

	$I(t-t_{\rm w}, t_{\rm w}, p)$ for $t-t_{\rm w} \ll t_{\rm w}$	$I(t-t_{\rm w}, t_{\rm w}, p)$ for $t-t_{\rm w} \gg t_{\rm w}$
$T-1 < p < T$	$t_{\rm w}^p\left[1-\left(\frac{t-t_{\rm w}}{t_{\rm w}}\right)^{1-T+p}\right]$	$t_{\rm w}^p\left(\frac{t-t_{\rm w}}{t_{\rm w}}\right)^{p-T}$
$p < T-1$	$t_{\rm w}^{T-1}(1+t-t_{\rm w})^{1-T+p}$	$t_{\rm w}^T(t-t_{\rm w})^{p-T}$

Table 8.3. Scaling of the integral $I(t, t_{\rm w}, p)$ in the limit $t_{\rm w} \gg 1$.

As noted above, we have been unable *analytically* to find such explicit time-dependences for the correlator C_1. We have, however, been able to extract the time-scale upon which it decays. This was achieved by substituting the results of table 8.3 into equation 8.62

to get[10]:

$$\begin{aligned} C_1(t-t_{\rm w},t_{\rm w}) &\sim t_{\rm w}^{2n}\tilde{C}_1(t/t_{\rm w}) \qquad \text{for} \quad n > \frac{T-1}{2} \\ C_1(t-t_{\rm w},t_{\rm w}) &\sim t_{\rm w}^{T-1}\tilde{C}_1(t-t_{\rm w}) \quad \text{for} \quad n < \frac{T-1}{2} \quad \text{and} \quad t-t_{\rm w} \ll t_{\rm w}. \end{aligned} \tag{8.75}$$

Hence for $n < (T-1)/2$ the correlator decays on a time-scale $O(1)$. For $n > (T-1)/2$ the decay time is $O(t_{\rm w})$. For this n regime, our *numerical* results reveal that C_1 in fact has the same dependences upon $t - t_{\rm w}$ and $t_{\rm w}$ as C_2 (in both the long and short time regimes)[11]. In this case, we can set $p = 2n$ in the results of table 8.3 to see the time-dependence of C_1.

8.5.2 Response functions and FDT plots

Response function χ_1 and FDT plot $\tilde{\chi}_1(\tilde{C}_1)$.

In this appendix we calculate time-dependence of the response function χ_1, and the shape of the corresponding FDT plot $\tilde{\chi}_1(\tilde{C}_1)$ for an intra-trap distribution $\sigma(m|E)$ which has mean $\bar{m}(E) = \exp(En/T)$, and zero variance. As usual we identify two regimes of n, $n > (T-1)/2$ and $n < (T-1)/2$), and consider each regime separately.

We start with $n > (T-1)/2$. For this range of n, we showed analytically in appendix 8.5.1 that the correlator C_1 scales as $t_{\rm w}^{2n}\bar{C}_1(t/t_{\rm w}, n)$ in the limit $t - t_{\rm w} \to \infty$, $t_{\rm w} \to \infty$, $(t-t_{\rm w})/t_{\rm w} = \text{const}$. We further showed that $f_1(t) = \langle m(t)\rangle \sim t^n$ in the limit $t \to \infty$. Substituting these into 8.55 we find $\chi_1 \sim t_{\rm w}^{2n}\bar{\chi}_1(t/t_{\rm w}, n)$. The normalized functions $\tilde{C}_1$ and $\tilde{\chi}_1$ therefore share the scaling variable $t/t_{\rm w}$ and a limiting FDT plot must *exist* for all values of n. This result is based upon purely analytical arguments.

To find the *shape* of the plot, we must find the actual *time-dependence* (and not just the scaling form) of χ_1. To do this we substitute the *numerically* obtained time-dependences of C_1 (table 8.2) into

$$\frac{\partial}{\partial t_{\rm w}}\chi(t-t_{\rm w},t_{\rm w}) = \frac{\partial}{\partial t}C(t-t_{\rm w},t_{\rm w}) + \frac{\partial}{\partial t}f_1(t)f_1(t_{\rm w}) \tag{8.76}$$

(which is just equation 8.44 transcribed into the notation of this appendix: $\bar{m}(t) = f_1(t)$.) We do this now, separately for the short time regime ($t - t_{\rm w} \ll t_{\rm w}$) and the long

[10] Note that we do not need to study C_1 for $n < T-1$ in the long time regime $t - t_{\rm w} \gg t_{\rm w}$, because it falls to a small fraction of its initial value on a time-scale of $O(1)$. In the limit $t_{\rm w} \to \infty$, therefore, the $t - t_{\rm w} \gg t_{\rm w}$ regime is never visible on an FDT plot.

[11] The prefactors are different.

time regime ($t - t_w \gg t_w$).

At short times ($t - t_w \ll t_w$ *i.e.* $C_1 \approx 1$) 8.76 can be simplified as follows. Consider the derivative on the LHS of the equation. Changes in $\chi_1(t - t_w, t_w)$ due to variations in t_w can be separated into two components: one due to the explicit variation of this absolute time t_w, and the other due to variations in the time interval $t - t_w$. For $t - t_w \ll t_w$, the main contribution comes from the latter variation in relative time: contributions due to variations in absolute time are smaller by a factor $t - t_w/t_w$. We can therefore set $\frac{\partial}{\partial t_w} \approx -\frac{\partial}{\partial t}$ to get

$$\frac{\partial}{\partial t_w}\chi_1(t - t_w, t_w) = -\frac{\partial}{\partial t_w}C_1(t - t_w, t_w) + \frac{\partial}{\partial t}f_1(t)f_1(t_w). \tag{8.77}$$

Substituting $f_1(t) \sim t^n$ (appendix 8.5.1) into this equation, integrating over t'_w from t to $t - t_w$, and using the boundary condition $\chi_1 = 0$ when $C_1 = C(0, t_w)$ we find

$$\chi_1 = 1 - \tilde{C}_1 + (t - t_w)t_w^{2n-1}. \tag{8.78}$$

Using the scaling form for C_1 as given in table 8.2 to express the second term on the RHS in terms of $1 - \tilde{C}_1$ we find finally that

$$\tilde{\chi}_1 = 1 - \tilde{C}_1 + (1 - \tilde{C}_1)^{\frac{1}{1-T+2n}}. \tag{8.79}$$

At long times ($t - t_w \gg t_w$ *i.e.* $C_1 \approx 0$) we have $C_1 \sim t_w^T(t - t_w)^{n2-T}$ (see table 8.2) and $f_1 \sim t^n$. Upon inserting these into 8.44, we find that the second term on the RHS ($f_1(t_w)\frac{\partial}{\partial t}f_1(t)$) dominates. Therefore

$$\frac{\partial}{\partial t_w}\chi_1(t - t_w, t_w) \sim t_w^n t^{n-1} \tag{8.80}$$

to leading order. Integrating over t'_w from $t_w = 0$ to t_w, we get

$$\chi_1(t - t_w, t_w) - \chi_1(t, 0) \sim t_w^{n+1}t^{n-1}. \tag{8.81}$$

Numerically, we find that the boundary condition $\chi_1(t, 0)$ scales as t^{2n}, which is much larger than the term on the RHS. Hence to leading order we have $\chi_1(t - t_w, t_w) \sim t^{2n}$ and thus $\tilde{\chi}_1(t - t_w, t_w) \sim (t/t_w)^{2n}$. Comparing this to the normalized correlator $\tilde{C}_1 \sim (t/t_w)^{2n-T}$ we find finally that $\tilde{\chi}_1 \sim \tilde{C}_1^{\frac{2n}{2n-T}}$. This concludes our analysis for the regime $n > (T - 1)/2$.

We now consider $n < (T - 1)/2$ For such values of n, we show in appendix 8.5.1 that the correlator scales as $t_w^{T-1}f(\Delta t)$ and that $f_1(t) \sim t^{T-1}$. The second term on the

RHS of 8.55 is therefore small compared with the first, and hence

$$\frac{\partial}{\partial t_{\rm w}}\chi_1(t-t_{\rm w},t_{\rm w}) = \frac{\partial}{\partial t}C_1(t-t_{\rm w},t_{\rm w}) \tag{8.82}$$

to leading order. Because the correlator decays on a time-scale of $O(1)$, we can set $\frac{\partial}{\partial t_{\rm w}} \approx -\frac{\partial}{\partial t}$ (as above) to find

$$\tilde{\chi}_1 = 1 - \tilde{C}_1. \tag{8.83}$$

Response function χ_2 and FDT plot $\tilde{\chi}_2(\tilde{C}_2)$.

Here we calculate the dependence of the response function χ_2 upon $t-t_{\rm w}$ and $t_{\rm w}$, for an intra-trap distribution which has zero mean and variance $(\Delta m)^2(E) = \exp(2En/T)$. We do this by substituting the corresponding time-dependence of C_2 (as found in appendix 8.5.1) into

$$\frac{\partial}{\partial t_{\rm w}}\chi_2(t-t_{\rm w},t_{\rm w}) = \frac{\partial}{\partial t}C_2(t-t_{\rm w},t_{\rm w}), \tag{8.84}$$

and integrating over $t_{\rm w}$. We then express the normalized response $\tilde{\chi}_2$ in terms of $\tilde{C}_2$ (as found above) to predict the shape of the FDT curve $\tilde{\chi}_2(\tilde{C}_2)$. As usual we identify two regimes of n, $n > (T-1)/2$ and $n < (T-1)/2$, and consider each regime separately.

We start with $n > (T-1)/2$, where we have $C_2 = t_{\rm w}^{2n}\bar{C}_2(t/t_{\rm w}, n)$ (appendix 8.5.1). Substituting this into equation 8.84 we find immediately that $\chi_2 = t_{\rm w}^{2n}\bar{\chi}_2(t/t_{\rm w}, n)$. Hence the normalized functions $\tilde{C}_2$ and $\tilde{\chi}_2$ share the same scaling variable $t/t_{\rm w}$: a limiting FDT plot must *exist* for all values of n. To predict the *shape* of this plot we need to know the actual time-dependence of χ_2 (and not just its scaling variable). We find this now, separately for the short time regime and the long time regime.

At long times, $t - t_{\rm w} \gg t_{\rm w}$ (*i.e.* for $\tilde{C}_2 \approx 0$) we have $C_2 \sim t_{\rm w}^{2n}(t - t_{\rm w}/t_{\rm w})^{2n-T}$ (appendix 8.5.1). Inserting this into 8.84 we get

$$\frac{\partial}{\partial t_{\rm w}}\chi_2(t-t_{\rm w},t_{\rm w}) \sim -\frac{t_{\rm w}^{2n}}{t-t_{\rm w}}\left(\frac{t-t_{\rm w}}{t_{\rm w}}\right)^{2n-T}. \tag{8.85}$$

Integration on $t_{\rm w}$ gives

$$\chi_2(t-t_{\rm w},t_{\rm w}) \sim \chi_2(t,0) - (t-t_{\rm w})^{2n-T-1}t_{\rm w}^{T+1}. \tag{8.86}$$

The "boundary" value $\chi_2(t,0)$ scales as t^{2n} and hence, to leading order, the response is dominated by this boundary value: $\chi_2(t-t_{\rm w},t_{\rm w}) \sim t^{2n}$. Normalizing χ_2 and C_2 by $C(0,t_{\rm w})$ we find finally that $\tilde{\chi}_2 \sim \tilde{C}_2^{\frac{2n}{2n-T}}$.

For short times $t - t_{\rm w} \ll t_{\rm w}$, variations in absolute time $t_{\rm w}$ are negligible compared with those in relative time $t - t_{\rm w}$. Hence we can set the derivative $\frac{\partial}{\partial t_{\rm w}}$ in the LHS of 8.84 equal to $\frac{\partial}{\partial t}$ to get $\frac{\partial}{\partial t}\chi_2 \approx -\frac{\partial}{\partial t}C_2$. Integrating over t, using the boundary condition $\chi_2 = 0$ when $C = C(0, t_{\rm w})$, and normalizing by $C(0, t_{\rm w})$, we find finally that $\tilde{\chi}_2 = 1 - \tilde{C}_2$.

For values of $n < (T-1)/2$, the correlator decays on a time-scale $O(1)$. (See appendix 8.5.1.) Over this short time interval, we can set $\frac{\partial}{\partial t} = -\frac{\partial}{\partial t_{\rm w}}$ in equation 8.84 (as above) to that find $\tilde{C}_2 = 1 - \tilde{\chi}_1$.

Chapter 9

A driven spin chain

So far in this thesis we have studied glassy dynamics in the context of Bouchaud's trap model. In this chapter we continue to study glassy dynamics, but now in the context of a kinetically constrained spin chain. This model, which was originally introduced by Jäckle and Eisinger [JE91], comprises a chain of uncoupled Ising spins which reside in a uniform field, and whose dynamics are rendered non-trivial by a simple kinetic constraint: at any time, any given spin can flip only if its left neighbour is up. At low temperatures, this constraint results in large energy barriers which impede the system's dynamical evolution. Following a quench to a low temperature, the spin chain (like the trap model in its glass phase) encounters progressively larger barriers as it explores phase space. This results in a glassy relaxation process in which the dynamics become progressively more sluggish over time. We start this chapter in section 9.1 by reviewing the publication [SE99], which solved this relaxation exactly in the zero temperature limit.

We then proceed to the novel contribution of this work (section 9.2), which consists of incorporating non-Hamiltonian driving into this (hitherto purely relaxational) model, and analyzing the resulting driven dynamics. In an abstract sense, this driving parallels the rheological driving incorporated into the trap model to produce the SGR model. To highlight this analogy, we identify (abstract) strain and stress variables in the spin chain. (Unlike the SGR model, however, the driven chain is not intended as a direct model of a rheological system, but rather as a schematic model of a driven glassy system.) We outline possible (abstract) dynamical analogues of various imposed-strain and imposed-stress rheological experiments. We then focus on just one such experiment: strain of constant rate $\dot{\gamma}$. We present simulation results which demonstrate that such driving interrupts the slow low-temperature relaxation of the chain, resulting in a non-equilibrium steady state in which the average relaxation time-scale is strain-rate

dependent. We describe an "independent interval" theory aimed at describing this steady state, and demonstrate that it gives excellent agreement with the simulation results. We then discuss the analogy of this driven steady state to that of the SGR model at $x < 1$.

Finally, we discuss the possible existence of a non-trivial, out-of-equilibrium fluctuation dissipation theorem (FDT) in the weakly driven limit ($\dot{\gamma} \to 0$) of the chain's steady state. This work should be compared with that of chapter 8, in which we studied FDT in the ageing limit $t_{\rm w} \to \infty$ of the trap model. Both $\dot{\gamma} \to 0$ (as considered for the spin chain) and $t_{\rm w} \to \infty$ (as considered for the trap model) correspond to a limit in which the rate of entropy production is vanishingly small, but in which the system is still very far from equilibrium (as can be seen, for example, from the non-trivial dependence of the correlation and response functions upon $t_{\rm w}$ or $\dot{\gamma}$). It is in this limit that one generally seeks such non-trivial out-of-equilibrium FDT relations.

Before describing the spin chain in detail, we note that the topics to be considered for this model parallel many of those studied for the trap model in previous chapters; in what follows we shall find several striking similarities in the phenomenology of the two models. However, we note from the outset the following fundamental conceptual difference between the models. The glassiness of the trap model arises directly from the rugged, disordered structure of its phase space. And because this disorder is one of the model's basic postulates, the trap model is said to contain quenched disorder. The spin chain, however, lacks any such quenched disorder: its Hamiltonian is that of a collection of Ising spins in a uniform field, and its static distribution is just the Boltzmann one for this trivial Hamiltonian. The non-trivial nature of the spin chain's dynamics is instead the result of a *kinetic* constraint (see section 9.1). The spin chain is therefore more obviously relevant to systems such as structural glasses which themselves lack any underlying quenched disorder, and in which any glassiness is dynamically self-induced. We note finally that the trap model is a one-body model since it describes an ensemble of independent particles hopping in a spatially unstructured landscape of traps. In contrast, the spin chain's kinetic constraint is of course a spatial interaction.

9.1 The undriven kinetically constrained spin chain

In this section we define the undriven constrained spin chain and briefly review its dynamics, focusing particularly upon the anomalous "coarsening" relaxation which follows a deep quench to a low temperature. The reader is referred to [SE99] for further details.

The model consists of a chain of L Ising spins $s_i \in 0, 1$ $(1 < i \leq L)$ in a uniform

field of unit magnitude, which is oriented such that $E(0) = E(1) - 1$ (where $E(0)$ ($E(1)$) is the energy of a down (up) spin). Periodic boundary conditions apply: the left neighbour of s_1 is s_L. The dynamics are subject to the following constraint: at any time, only those spins whose left neighbour is up are allowed to flip. For these "mobile" spins, the rate of down-flips is 1 while the rate of up-flips is $\epsilon = \exp(-1/T)$. As we shall describe below, the constraint renders the dynamics very sluggish at low temperatures: it leads to large energy barriers which impede the system's evolution, and the ergodic time, $\tau_{\rm erg}$, diverges as $\exp(a/T^2)$ ($a = $ const.) in the limit $T \to 0$. In contrast, the chain's underlying *equilibrium* distribution is unaffected by the constraint: detailed balance is obeyed and the static distribution is the trivial one prescribed by the Hamiltonian $H = \sum_{i=1}^{L} s_i$.

We now review the low temperature dynamics in some detail, focusing particularly upon the relaxation of a chain prepared by means of a deep quench from a high initial temperature $T_i = \infty$. At any time during the relaxation, we shall describe the system's state using the concept of "domains". As shown by the vertical lines in

$$...1|\cdot\cdot1|\cdot\cdot\cdot\cdot\cdot\cdot\cdot\cdot1|\cdot1|\cdot\cdot\cdot\cdot1|\cdot\cdot\cdot1|1|1|\cdot1...$$

a domain is defined as an up-spin, and all the down-spins separating it from the next up-spin to the left. The 0 spins have been represented by "·" for clarity.

Consider, then, a system which has just been quenched from $T = \infty$ to a low temperature $T \ll 1$. Immediately after the quench, the concentration of up-spins, c, is $O(1)$. Similarly, the average domain length $\bar{d} = O(1)$. The system then relaxes towards the equilibrium state of the new low temperature, in which $c = O(\epsilon)$ (small) and $\bar{d} = O(1/\epsilon)$ (large). In the absence of the kinetic constraint, this relaxation would of course merely consist of a fast down-flip of a fraction $1 - \epsilon = O(1)$ of up-spins and would take place on a time-scale $O(1)$. The constraint drastically modifies the dynamics of this process in the following way.

Consider, at some time after quench, a domain of length d together with its left-bounding up-spin. For the purposes of the present argument, we assume that the left-bounding is "clamped"[1], and consider how the right-bounding spin relaxes – that is, how the domain is destroyed by coalescence with its right neighbour. (For reasons discussed below we confine ourselves to the low temperature limit $\epsilon \to 0$, and to domains of finite length $d = O(1) \ll 1/\epsilon$, corresponding to lengths of chain which in equilibrium have vanishingly few up spins.) Because of the constraint, before the relaxation can occur a facilitating up-spin has first to be generated immediately to the left of the

[1]This merely amounts to assuming that the right spin relaxes before the left one.

right-bounding up-spin; and (again because of the constraint) this can only happen by propagation of the up state rightwards through the domain, from the left-most of the original up-spins. There is thus an energy barrier impeding the relaxation, and the associated time-scale is dramatically increased from the non-constrained $O(1)$ value, being now a function of $1/\epsilon$. The time-scale must clearly also increase with d because, for a larger gap of down-spins, more up-spins need to be generated and the energy barrier is correspondingly larger. In fact, the maximal number of spins which need to be up at any one time (and hence the energy barrier to be surmounted) scales as n for $2^{n-1} < d \leq 2^n$ (*i.e.* logarithmically in domain length) [SE99, SE]. This leads to a relaxation time-scale of ϵ^{-n}, which clearly increases with increasing "domain index" n. Hence the equilibration process consists of "stages" (labelled by integer indices n), each of which involves the relaxation of longer domains than those of the previous stage, and takes a correspondingly longer time: the nth stage has time-scale ϵ^{-n} and results in domains of index n being destroyed by coalescence with their right neighbours.

In the limit $\epsilon \to 0$, the time-scales for successive stages become infinitely separated (by a factor $1/\epsilon$).[2] Here, viewed on a movie played in log time, $t_{\text{movie}} = \nu \sim T \ln t$, the nth stage collapses to the point $\nu = n$. The average domain size $\bar{d}$ thus exhibits step-wise increases (each corresponding to one stage) at successive integer values of ν. Furthermore, because the rate of the movie slows by the divergent factor $1/\epsilon$ between successive stages, the intra-domain (barrier-surmounting) flip processes which occur during the nth stage (resulting in the transient creation of shorter "sub-domains" with index $n' < n$) are infinitely quick on the movie time-scale $\nu = n$ and will not be resolved by the viewer. In this way, the down-flips of domain walls at any stage is irreversible to leading order: any transient up-flips in subsequent stages is a small effect. Simulation data for $\bar{d}$ is plotted in figure 9.1 (taken directly from [SE99]) and supports the above predictions.

This coarsening description remains valid only as long as the average domain length is much less than the average equilibrium domain length, $1/\epsilon$. The reason for this is as follows. The coarsening process, at any time, entails lengths of chain comparable with the current average domain length becoming completely emptied of up-spins during the next stage. However, for chain lengths of $O(1/\epsilon)$, there is an $O(1)$ probability of encountering at least one up-spin even at infinite times (*i.e.* in equilibrium). The coarsening description therefore breaks down once $\bar{d} \sim 1/\epsilon$. Nonetheless, by extrapolating the coarsening regime into the equilibrium regime (where it is no longer strictly valid for

[2] Strictly, one should only actually speak of stages in this limit, since for finite ϵ the time-scales of successive "quasi-stages" overlap.

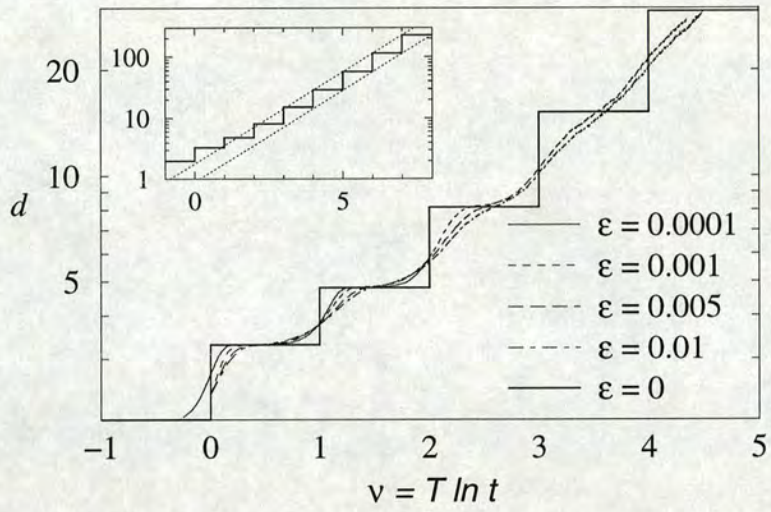

Figure 9.1. Evolution of the average domain length $\bar{d}$ after a quench from $T_i = \infty$ at $t = 0$, plotted on a log scale vs. $\nu = T \ln t$. Simulation results for four values of $\epsilon = \exp(1/T)$ are shown, obtained from a single run for a spin chain of length $L = 2^{15}$. Bold line: theoretical prediction for $T \to 0$. Inset: theory for larger ν and $\nu \to \infty$ asymptotes. (Figure taken from [SE99].)

the reason just described) one can extract an equilibration time $t_{\rm eq} = \exp(1/T^2 \ln 2)$. Credence is lent to the validity of this time by the fact that it is provably also the time-scale for relaxation of correlations in equilibrium [SE99].

Within the coarsening regime ($\bar{d} \ll 1/\epsilon$), the full domain length distribution $P(d)$ has been solved exactly [SE99], using an independent interval approximation [BDG94] which assumes that no correlations can build up in the length of adjacent domains provided that none are present in the initial state. The weight of the distribution obviously shifts to larger d at each stage of the dynamics, as the chain coarsens. A scaling limit is approached for large stage number n: the rescaled distribution $\tilde{P}_n(x) = 2^{n-1} P_n(d)$ converges to the limit $\tilde{P}(x)$ which is given by

$$\tilde{P}(x) = \sum_{m=1}^{\infty} \frac{(-1)^{m-1}}{m!} \int_1^{\infty} \prod_{r=1}^{m} \frac{dx_r}{x_r} \delta\left(\sum_{s=1}^{m} x_s - x \right). \tag{9.1}$$

Simulation results for $P(d)$, taken directly from [SE99], are shown in figure 9.2. They converge convincingly towards this theoretical asymptote.

We have seen, then, that the spin chain relaxes towards its low temperature equilibrium state by means of an anomalous coarsening process which, in the limit $\epsilon \to 0$,

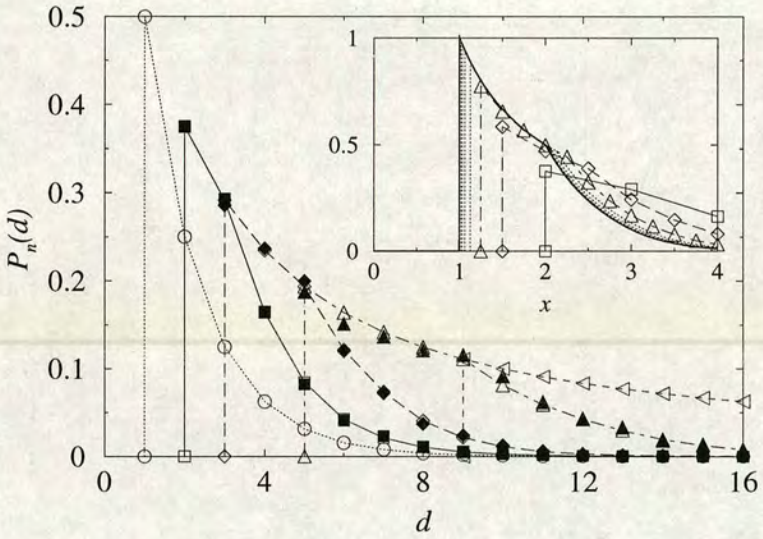

Figure 9.2. Domain length distributions $P_n(d)$ at the end of stage $n-1$ of the low T coarsening dynamics, for an initial temperature $T_i = \infty$. Open symbols and lines: theoretical results for $n = 0$ (circles; initial condition), 1 (squares), 2 (diamonds), 3 (triangles). Full symbols: simulation results for a chain of length $L = 2^{15}$ and $\epsilon = 10^{-4}$ ($n = 1, 2$) and $\epsilon = 10^{-3}$ ($n = 3$). Inset: scaled predictions $2^{n-1}P_n(d = 2^{n-1}x)$ vs. x for $n = 1, ..., 8$. Bold line: predicted scaling function. (Figure taken from [SE99].)

consists of well separated stages. The average domain length increases as the chain coarsens; the energy barriers impeding further relaxation become corresponding larger, and the dynamics correspondingly slower. We note at this point the analogy to ageing dynamics of the trap model. After a quench into its glass phase, this model explores progressively more rugged regions of its postulated landscape of traps, encounters larger energy barriers, and likewise suffers a slowing of its dynamics. However, at long times there is a fundamental difference in the phenomenology of the two models: the ergodic time of the trap model formally diverges at the finite temperature T_g and after a quench to $T < T_g$ aging persists indefinitely. In contrast, the spin chain equilibrates after the finite – but, at low temperatures, very long – time $\exp(1/T^2 \ln 2)$: the strict time-scale divergence only occurs at zero temperature.

9.2 Incorporating driving

9.2.1 Definition of the driving rules

The spin chain described above has purely relaxational dynamics. In this section we incorporate non-Hamiltonian driving into it and examine the dynamics of the resulting driven model. As a preliminary step we extend state space such that each spin can assume the values $s_i \in -1, 0, 1$. We define the Hamiltonian $H = \sum_{i=1}^{L} |s_i|$. As in the original model, the dynamics are constrained: at any time, only those spins for which the left neighbour has $|s_i| \neq 0$ are allowed to flip. For these mobile spins, the rate of flips $1 \to 0$ and $-1 \to 0$ is 1, and the rate of flips $0 \to 1$ and $0 \to -1$ is ϵ. The high energy states 1 and -1 here collectively assume the role of the single state 1 of the original model, and the uniform field has effectively been replaced by a potential well for each spin, with a minimum at the ground state 0. So far, of course, the model can be exactly mapped onto the original one by a trivial relabelling of -1 as 1 and a rescaling of ϵ by a factor 2. Its dynamics are still purely relaxational. The point of including the extra -1 state is to allow a sensible definition of a quantity analogous to rheological stress: we define $\sigma = \frac{1}{L}\sum_{i=1}^{L} s_i$. The -1 state allows the system to be *macroscopically* devoid of stress, whilst still having internal local stresses (some positive, some negative) and a non-zero rate of internal dynamical rearrangements.

We now incorporate driving into this three state version, discussing a possible dynamical analogue of the standard rheological experiment which consists of applying shear of constant rate $\dot{\gamma}$. To mimic this shear, we impose a flip rate of $\dot{\gamma}$ for $s : -1 \to 0$ and $\dot{\gamma}$ for $s : 0 \to 1$. This is *additional* to the constrained rates defined above and *free of the kinetic constraint.* This stochastic straining clearly tends to increase the global stress, as required. We note, however, that it contrasts with the deterministic driving of the SGR model in the following way. In the spin chain, the increase of spin ("elemental") stress with strain occurs in a jump-wise manner (by the finite amount 1 in each transition) and probabilistically (*i.e.* at random times). In the SGR model, on the other hand, elemental stresses increase deterministically by the infinitesimal amount $\dot{\gamma}dt$ in each time increment dt. We further note that our stochastic rules only make sense for $\dot{\gamma} \geq 0$. For negative $\dot{\gamma}$ we would envisage redefining the rates as equal to $|\dot{\gamma}|$ for the transition $1 \to 0$ and $|\dot{\gamma}|$ for $0 \to -1$. Our driven chain is in this sense singular at $\dot{\gamma} = 0$.

In what follows, we shall examine this steadily driven chain in detail. First, however, we define possible dynamical analogues of two other standard rheological tests: step strain and step stress, although we shall not analyze the dynamics of these scenarios in any detail. We start with step strain. Here we promote, at the time t_w of strain

application, a fraction γ_0 of -1 spins (chosen randomly) from $-1 \to 0$ and of 0 spins (again chosen at random) from $0 \to 1$. We do this *without regard to any kinetic constraint.* For all other times we let the system relax under its undriven constrained dynamics. Note that the step at t_w is just the "impulsive limit" of the above steady shear case: $\dot{\gamma} dt = \gamma_0$, with $dt \to 0$ and $\dot{\gamma} \to \infty$.

To achieve a step stress, we apply the same dynamics as above for step strain up until the time t_w^+. (We can merely rename γ_0 by σ_0 because the "spring constant" is equal to 1.) For $t > t_w$ we implement the "constant" strain-rate dynamics defined above, but with $\dot{\gamma}$ continuously adjusted to ensure that σ_0 remains (on average) a constant.

9.2.2 Steady shear in the driven spin chain

We now analyze the dynamics of the steadily driven chain in some detail. We start by presenting the results of a simulation which demonstrated that steady shearing interrupts the low temperature relaxation process described in section 9.1, and restores a steady state in which the relaxation time-scale is prescribed by $1/\dot{\gamma}$. We then describe an "independent interval approximation" aimed at describing this steady state, and demonstrate that it gives excellent agreement with the simulation data. We conclude by comparing the steady state of the spin chain to that of the SGR model.

Simulation results

We simulated the spin chain under conditions of constant strain rate for various values of ϵ using the method described in appendix 9.4. For each run we initialized the chain either in equilibrium at the temperature of interest ($T = -\log \epsilon$), or by quenching to $T = -\log \epsilon$ from $T = \infty$. For the quenched case, we then let the system relax according to the undriven rules ($\dot{\gamma} = 0$) until time t_w, at which time we set $\dot{\gamma}$ to the non-zero value of interest. Equilibrium initialization formally corresponds to a quenched chain subsequently allowed to relax until $t_w = \infty$, and in this case we applied the non-zero $\dot{\gamma}$ from the start of the simulation. In each run we monitored stress, σ, as a function of time. In all cases we found that, after a transient startup period, the system eventually reached a time-independent steady state which depended only upon $\dot{\gamma}$ and ϵ, and not upon details of the initial condition or (for the quenched case) startup time t_w. For the remainder of the chapter we shall be interested only in this ultimate steady state, and not in the start-up process. We are therefore free in the simulations to confine ourselves to just one initial condition. We chose for convenience the equilibrium one.

Figure 9.3 shows simulation results for the steady state stress σ as a function of

strain rate $\dot{\gamma}$ for various small values of ϵ. In rheological parlance, this is the flow curve. For reasons which will become clear below, the shear rate axis has been rescaled logarithmically by $\dot{\gamma} \to -\nu = -\ln \dot{\gamma} / \ln \epsilon$. The flow-curve appears to approach a step-like function as temperature is tracked towards zero, consisting of plateaux separated by jump-wise discontinuities at integer values of[3] ν.

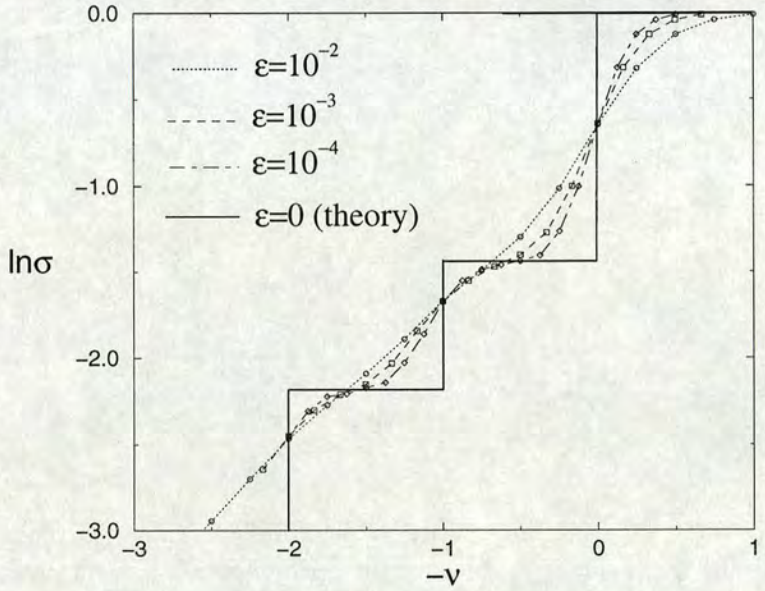

Figure 9.3. Steady state flow curves plotted on a log scale vs. $-\nu = -\ln \dot{\gamma} / \ln \epsilon$. Simulation results for three values of $\epsilon = \exp(1/T)$ are shown, obtained from a single run for a spin chain of length $L = 2^{16}$. Bold line: theoretical prediction for $T \to 0$.

We recall that stress is defined as the difference between the fractional populations of 1 spins (n_1) and of -1 spins (n_{-1}). For all the steady states considered, we found by simulation that n_{-1} is negligibly small (see figure 9.4). We therefore assume the chain to consist of only 0 and 1 spins. The stress is then effectively equal to the fractional population of 1 spins: $\sigma \approx n_1$. Using the domain description of section 9.1, we have then $\sigma = 1/\bar{d}$ where $\bar{d}$ is the average domain length[4]. Simulation data for the full

[3] A note on sign conventions: $\dot{\gamma} = \epsilon^{\nu}$, as prescribed by the above rescaling, means that $\dot{\gamma} \to 0$ as $\nu \to \infty$. To get $\dot{\gamma}$ to decrease with decreasing abscissa, we need to set the abscissa to *minus* ν. We have chosen this convention to allow a close analogy with the coarsening model in which coarsening times are $t \sim \epsilon^{-\nu}$.

[4] In general, of course, in this three state version we should refine our definition of domains to account for the presence of -1 spins. However, because the population of such spins is negligible for all steady states considered here, we can unambiguously retain the definition of domains as provided

domains length distribution $P(d)$ on the developing plateaux of the flow curves are shown in figure 9.5.

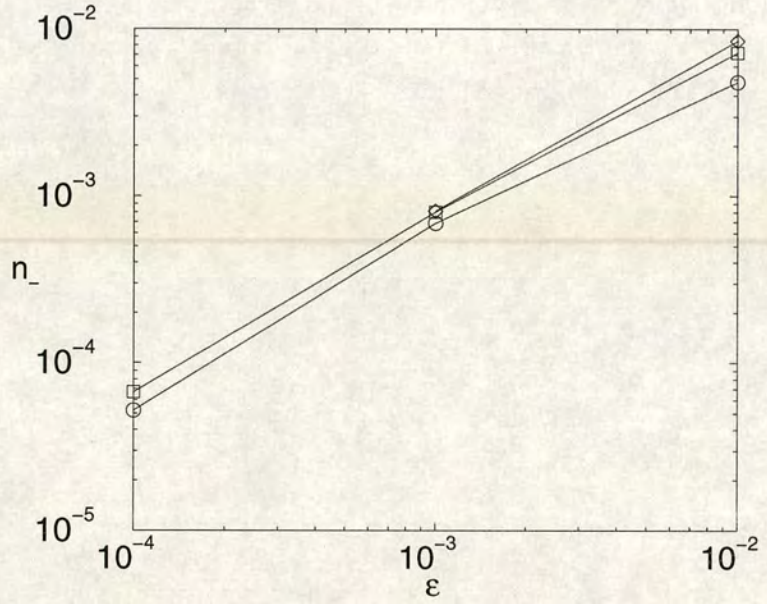

Figure 9.4. Fractional population of -1 spins vs. ϵ in the driven steady state on the first (circles), second (squares) and third (diamonds) plateau of the flow curves.

Theory

We now present a theory aimed at calculating the steady state distribution $P(d)$ and (via this) the stress $\sigma = 1/\bar{d}$. We shall assume "a priori" that the population of -1 spins is negligible in the steady states of interest. We have already presented simulation data which supports this assumption, and in fact the following theory will enable us to justify it "a posteriori". Our other basic assumption is that no correlations exist between the lengths of adjacent domains. This independent interval method was used in [SE99] for the coarsening process described in section 9.1, and in that case is provably exact. We have not been able to prove its strict validity for this driven case. However, our simulation results show that the relevant correlation function

$$C = \frac{1}{n \langle d \rangle^2} \sum_{j=0}^{n} (d_j - \langle d \rangle)(d_{j+1} - \langle d \rangle) \tag{9.2}$$

in section 9.1.

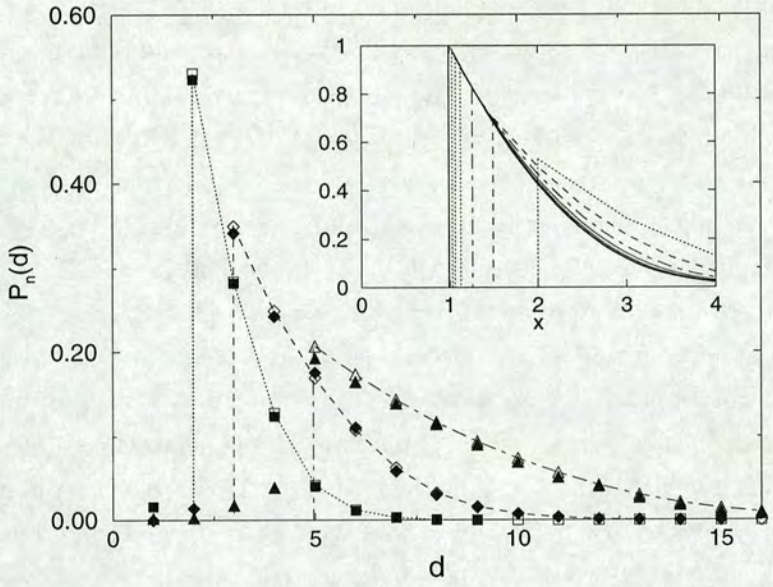

Figure 9.5. Domain length distributions $P_n(d)$ on the plateau $\nu = n + 1/2$ of the flow-curves. Open symbols and lines: theoretical results for $n = 1$ (squares), 2 (diamonds), 3 (triangles). Full symbols: simulation results for a chain of length $L = 2^{16}$ and $\epsilon = 10^{-4}$ ($n = 1, 2$) and $\epsilon = 10^{-3}$ ($n = 3$). Inset: scaled predictions $2^{n-1}P_n(d = 2^{n-1}x)$ vs. x for $n = 1, ..., 16$.

is not greater that than 10^{-3} in any of the steady states considered. (In equation 9.2, d_j is the length of jth domain from the left hand end of the chain, and n is the total number of domains.) The independent interval assumption therefore is likely to be a good one. Note that our observation of a non-zero correlation function could still be consistent with the independent interval approximation being exact in the limit $\epsilon \to 0$ at fixed ν. Indeed, we have observed that, as ϵ is tracked downwards, the numerical value of the correlation function gets smaller.

Before giving quantitative details, we pause to identify the two processes which dominate the chain's dynamics, and which must balance each other in the steady state. Firstly, domains tend to coalesce with each other via the coarsening processes of section 9.1: this tends to increase the typical domain length. Secondly, domains tend to divide into smaller sub-domains as their internal ($s = 0$) spins are promoted to the 1 state by driving[5].

[5]Driving can also lead to the transition $-1 \to 0$, but this is neglected due to the small concentration of -1 spins in the steady state, as described above.

We now make this more quantitative. We choose a flow rate $\dot{\gamma} = \epsilon^{\nu}$, and consider these two balancing processes in the limit $\epsilon \to 0$ for fixed ν. For the finite domain lengths to which we shall restrict ourselves, driven domain intersection occurs on a time-scale $O(1/\dot{\gamma}) = O(\epsilon^{-\nu})$. For a non-integer value of ν, say $m < \nu < m+1$, this time-scale sits between the time-scales[6] ϵ^{-m} and $\epsilon^{-(m+1)}$ for the adjacent coarsening stages m and $m+1$ (recall section 9.1), and separates from them in the limit $\epsilon \to 0$. We therefore take $1/\dot{\gamma}$ as our basic clock, and re-scale time thus: $t \to \dot{\gamma}t$. On this driving time-scale, domains labelled by $n \leq m$ (*i.e.* of length $d \leq 2^m = d_c$) relax infinitely quickly. We therefore expect a vanishingly small population of these "short" domains in the steady state: as soon as one is created (via a driven up-flip of a spin within an existing domain of length $d > 2^m$ a distance $d \leq 2^m$ from a domain boundary) it will immediately coarsen away. Hence we already have $\lim_{\epsilon \to 0} P(d) = 0$ for $d \leq 2^m$. Domains labelled by $n > m$ (*i.e.* of length $d > 2^m$), on the other hand, coarsen infinitely slowly. The only dynamical processes which can affect these "long" domains (on the driving time-scale) are those initiated by driven up-flip of an intra-domain 0 spin. We next identify four sub-classes of such a process, according to the subsequent fate of the sub-domains created by the initial up-flip.

- **A.** If the original long domain was longer than $2d_c+1$, and if the up-flip occurred at a distance of at least d_c+1 from both ends, the two sub-domains will both be long, and in this case will not subsequently relax by coalescence. The original long domain has therefore been destroyed, and two shorter domains (which are still both long in the sense that they have $d > d_c$) have been created. For example:

(For definiteness all the diagrams in this section assume an arbitrary cutoff value $d_c = 4$.)

Considering the chain as a whole, such processes lead to the destruction of domains of length $d > 2d_c + 1$ at a rate

$$(d - 2d_c - 1)P(d) \tag{9.3}$$

[6] Any coalescence process actually entails intra-domain spin-flip events, but we shall use only the coarse grained description in which we attach the time-scale ϵ^{-n} to the entire coalescence process.

and to the creation of domains of length $d > d_c$ at a rate

$$2 \sum_{d'=d+d_c+1}^{\infty} P(d'). \tag{9.4}$$

Formula 9.3 can be understood in the following way. The rate at which domains of length d are destroyed by the process just described is proportional to the population of such domains, and to the number of ways in which each domain can be thus destroyed. The latter factor is equal to the number of "0" sites within such a domain, for which up-flip to the 1 state will result in the creation of two long sub-domains: the sites within $2d_c$ of each domain end cannot be counted here, since in this case one of the sub-domains would be short. Formula 9.4 can be motivated by similar arguments.

- **B.** If the up-flip occurred within a distance d_c of the right-hand end of the original domain, but at a distance greater than d_c from the left hand end, the left sub-domain will not subsequently relax on the driving time-scale. The right sub-domain, on the other hand, will relax immediately by coalescence with its right neighbour:

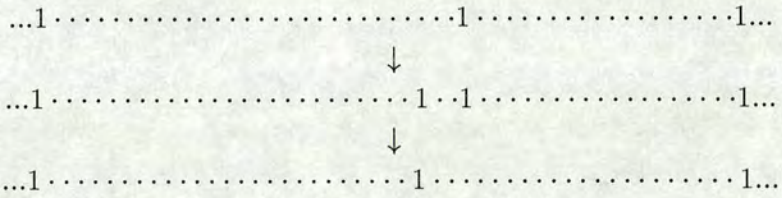

Hence in this process, the two original long domains have been "destroyed", while two new long domains have been created. Considering the chain as a whole, and by arguments similar to those given in bullet point "A" (above), processes such as this lead to the creation of domains of length d at a rate

$$\sum_{d'=d+1}^{d+d_c} P(d') + \sum_{d'=1}^{d_c} \left[\sum_{d''=d_c+d'+1}^{\infty} P(d'') \right] P(d-d') \tag{9.5}$$

and to the destruction of domains of length d at a rate

$$\begin{aligned} &\Theta(d-2d_c)d_c P(d) + \Theta(2d_c-d-1)(d-d_c-1)P(d) \\ &+P(d)\left(\sum_{d'=d_c+1}^{2d_c} (d'-d_c-1)P(d') + d_c \sum_{d'=2d_c+1}^{\infty} P(d') \right) \end{aligned} \tag{9.6}$$

where the discrete Theta function is defined by

$$\begin{aligned} \Theta(n-m) &= 1 \quad \text{for } n > m \\ &= 0 \quad \text{for } n \leq m. \end{aligned} \tag{9.7}$$

- **C.** If the up-flip occurred within a distance d_c of the *left*-hand end of the original domain, but at a distance greater than $d_c + 1$ from the right hand end we see a process such as

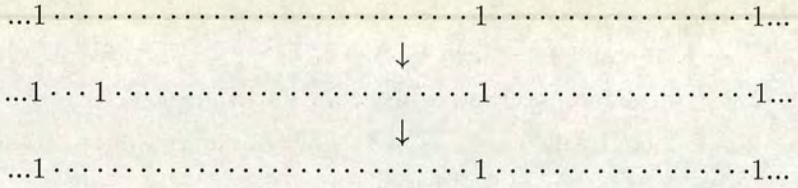

which does not need to be considered further since it results in no net change in the length distribution of long domains.

- **D.** If the original domain was of length $d \leq 2d_c$, both the sub-domains could be of length $d \leq d_c$. In this case there are two possible outcomes, which by symmetry each occur with a probability one half. First, the freshly flipped up-spin could relax before the right-bounding spin of the original domain and (as in the bullet point "C" above) we would see no net change. Alternatively, we could see a process such as

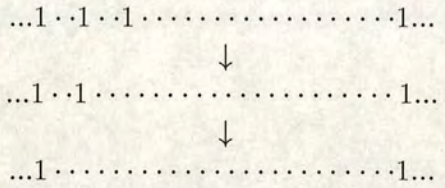

in which the net result is destruction of the two original long domains (via "aided coalescence") and creation of one new "super-domain". For the chain as a whole, processes such as these lead to destruction of domains of length d at a rate

$$P(d)\frac{1}{2}\left(2d_c - d + 1\right) + \frac{1}{2}P(d)\sum_{d'=d_c+1}^{2d_c} P(d')\left(2d_c - d' + 1\right) \tag{9.8}$$

and creation at a rate

$$\frac{1}{2}\sum_{d'=d_c+1}^{2d_c}\left(2d_c - d' + 1\right)P(d')P(d-d'). \tag{9.9}$$

Results of theory

Having identified (through "A" to "D" above) the three processes which act on the population of long domains, we now combine them to find (for $d > d_c$):

$$\begin{aligned}\frac{\partial}{\partial t}P(d) &= -g(d)P(d) - P(d)\left[\sum_{d'=d_c+1}^{2d_c}\left(\frac{d'-1}{2}\right)P(d') + d_c\sum_{d'=2d_c+1}^{\infty}P(d')\right] \\ &+2\sum_{d'=d+1}^{\infty}P(d') - \sum_{d'=d+1}^{d+d_c}P(d') + \sum_{d'=1}^{d_c}\sum_{d''=d_c+d'+1}^{\infty}P(d'')P(d-d') \\ &+\sum_{d'=d_c+1}^{2d_c}\left(\frac{2d_c-d'+1}{2}\right)P(d')P(d-d'), \qquad (9.10)\end{aligned}$$

in which $g(d) = d - d_c - 1$ for $d > 2d_c + 1$ and $g(d) = (d-1)/2$ for $d \leq 2d_c + 1$.[7] In the steady state we set $\frac{\partial}{\partial t}P(d) = 0$ and solve 9.10 numerically using an iterative procedure which is described in appendix 9.5. The solutions (for various d_c, or equivalently, recalling that $d_c = 2^m$, for various m where $m < \nu < m+1$) are marked as dashed lines in figure 9.5, and give excellent agreement with the simulation results. As ν is tracked upwards, and the driving time-scale $\epsilon^{-\nu}$ crosses successive coarsening time-scales ϵ^{-n} $(n = 1, 2, 3...)$, the distribution shifts discontinuously to larger values of d. As $d_c \to \infty$, (corresponding to $\nu \to -\infty$) the theoretical distribution $P(d)$ approaches a scaling limit $P(d) = d_c P(d/d_c)$ (see figure 9.3). We predicted above that for short domains ($d \leq d_c$), $P(d) = 0$ in the limit $\epsilon \to 0$. For the finite values of ϵ accessed in the simulations, $P(d \leq d_c)$ is small, but non-zero. It is smaller for smaller values of ϵ[8]. Finally, we calculated the stress, $\sigma = 1/\bar{d}$ using our theoretical distribution $P(d)$. Not unexpectedly, σ exhibits discontinuous jumps at integer values of ν. It is marked as a dot-dashed line in figure 9.5 and again agrees well with the simulation data.

Using the above theoretical arguments, we now justify our earlier assumption that the population of -1 spins is negligible for all the steady states considered. Consider a chain with an $O(1)$ population of 1 spins, and a complementary (but still $O(1)$) population of 0 spins. The 1 spins will be separated by long intervals ($d > d_c$) for reasons described above. Over times which are not large in comparison with the driving time-scale, $1/\dot{\gamma}$, the only mechanism in which -1 spins can be created involves propagation of the facilitating state (-1 or 1), via constrained thermal activation, to within a distance

[7] We have checked that equation 9.10 yields a distribution $P(d)$ which is correctly normalized.

[8] Note that, although these short domains mediate many of the processes described above, they exist only for an infinitesimal time in the limit $\epsilon \to 0$, and there are infinitesimally few of them present at any one time.

$d < d_c$ to the right of one of the existing facilitating spins. Denoting by $\tau_c(d)$ the time-scale on which domains of length d coarsen, the time-scale upon which a -1 spin is created at a distance d from an existing facilitator is $\tau_c(d)/\epsilon$. (The factor ϵ is needed because here the outermost spin is being promoted in energy from 0 to the -1 state, whereas during coarsening the outermost spin is relaxed downwards in energy.) Once created, such a spin will be relaxed back to the 0 state on a time-scale $\tau_c(d)$. Hence in the steady state, the population of -1 states must be $O(\epsilon)$, which does not exceed 10^{-2} in any of our simulations. This argument is supported by the results of figure 9.4.

Discussion

We recall from section 5.2.2 that shear of constant rate $\dot{\gamma}$ interrupts the ageing process of the SGR model, and restores the system to an effective age $1/\dot{\gamma}$. We now consider the extent to which this effect has an analogy in the spin chain. We recall that, for the spin chain, the flow-curve consists of plateaux which are separated by jump-wise discontinuities at integer values of $\nu = \ln\dot{\gamma}/\ln\epsilon$. For a non-integer value of ν, say $m < \nu < m+1$, the driving time-scale $\epsilon^{-\nu}$ sits between the time-scales ϵ^{-m} and $\epsilon^{-(m+1)}$ for the two adjacent coarsening stages m and $m+1$. On this driving time-scale, domains of length $d \leq 2^m$ coarsen away infinitely quickly, and there are infinitesimally few of them in existence at any one time. Domains of length $d > 2^m$, however, coarsen infinitely slowly. This situation is strikingly analogous to that of a relaxational coarsening process viewed on a movie played at a rate ϵ^{ν}: following the quench, domains of length $d \leq 2^m$ coarsen away infinitely quickly, leaving domains of length $d > 2^m$ which never subsequently coarsen. Of course, viewed on a logarithmic time-scale which slows with the dynamics of the undriven chain, the system would continue to coarsen in this relaxational case. In the driven steady state, on the other hand, the chain is permanently arrested in a state comparable with that of the mth stage of coarsening: the typical domain length is prevented from ever exceeding $O(d_c)$, by the tendency of driving to shorten domains. We can therefore say that driving of rate $\dot{\gamma}$, such that $\epsilon^{m+1}\dot{\gamma} < \epsilon^m$, *interrupts* the coarsening process of the undriven model at the mth stage.

At very low shear rates, however, this analogy between the two models breaks down. The reason for this is as follows. We recall from section 9.1 that the coarsening description in the relaxational spin chain is valid only until the typical domain length is $O(1/\epsilon)$, corresponding to a time since quench of order the ergodic time $\tau_{\rm erg}$. Likewise, the above driven steady state description is only valid for the same range of domain lengths, corresponding to flow rates $\dot{\gamma} \gg 1/\tau_{\rm erg}$. Smaller flow rates perturb the chain at

a rate smaller that its own relaxation time, and hence we expect a linear flow regime in which $\sigma \propto \dot{\gamma}$. The spin chain therefore lacks a yield stress[9]. In contrast, the SGR model has a strict glass transition at the finite temperature $x = 1$. Below this temperature the ergodic time is infinite and, however slowly we shear the model, we always strongly perturb its dynamics. Formally, we can take the limit $\dot{\gamma} \to 0$ (from above) and still find a steady state in which the characteristic relaxation time-scale is $O(1/\dot{\gamma})$. Associated with this is the existence of a yield stress in the SGR model: non-zero macroscopic stress can exist even at zero flow rate, since the average relaxation time-scale is infinite.

9.2.3 FDT in weakly driven limit

Finally, we briefly consider violations of the equilibrium FDT for the low temperature, weakly driven limit in the steady state of the driven spin chain. Specifically, we are interested in the limit $\epsilon \to 0$ (where $\epsilon = \exp(-1/T)$) and $\dot{\gamma} \to 0$ at fixed ν (where $\nu = \ln \dot{\gamma} / \ln \epsilon$), *followed by* the limit of large ν: this places us at large plateau number on the flow curve (far to the left in a plot such as 9.3), but ensures that we are still in the non-trivial regime where the inverse flow rate is much smaller than the ergodic time. As noted in chapter 8, the slow driving limit of a driven glassy system can be considered analogous to limit $t_{\rm w} \to \infty$ of an ageing system; in both limits, the rate of entropy production is very small.

In this model, we have considered only energy-temperature FDT (although it would clearly be of interest to look at other observables, as in the study of chapter 8 for the trap model). In this case, the correlation function $C(t - t_{\rm w}, 1/\dot{\gamma})$ measures fluctuations about the steady state value of energy. Our simulation results indicate that this function scales approximately as $\exp[-a\dot{\gamma}(t_{\rm w})]$ in the limit $\epsilon \to 0$ at fixed plateau number ν, with $a \approx 2$ for $\nu = 1$ and $a \approx 3.3$ for $\nu = 2$. (Due to the limitations of our simulation, we have been unable to access larger values of ν.)

The conjugate response function would clearly be the time-dependent energy response to a small step temperature made in the steady state. Clearly, this temperature step (as encoded in a step $\delta\epsilon$ in ϵ) must be small on the scale of T, so we must modify the limit given above to be $\delta\epsilon \to 0$, $\epsilon \to 0$ with $\delta\epsilon/\epsilon \to 0$, concurrently with $\dot{\gamma} \to 0$ at fixed ν (as usual following by $\nu \to \infty$). We in fact argue that this response function will be rather ill behaved, due to the (zero temperature) step-wise dependence of energy[10]

[9] Note that the *double* limit $\dot{\gamma} \to 0$, $\epsilon \to 0$ with $\ln \dot{\gamma} / \ln \epsilon$ fixed – *i.e.* $\epsilon \to 0$ on a fixed plateau of the flow curve – does result in a non-zero stress at zero shear rate. This is not a meaningful yield stress, however, because to achieve it we have to take the *thermodynamic* parameter ϵ to zero in parallel with the flow rate.

[10] Recall that the energy, to within small corrections $O(\epsilon)$ assumes the same value as stress, due to

upon ν. To see this, consider first a small, non-zero value of ϵ, with an associated much smaller change $\delta\epsilon$ (switched on at some arbitrary time t_w). For non-integer values of ν (*i.e.* on the developing plateaux of the flow curve) the ultimate value of the response function (as $t - t_w \to \infty$) should be rather small, due to the weak dependence of energy upon ϵ for such values of ν. For integer values of ν, the long-time value of the response should be rather large, due to the rapid variation of energy with ϵ. Hence, in the limit $\epsilon \to 0$, the (ultimate value of the) response function should become infinite for temperature changes encompassing a step of the flow curve, but should be zero for temperature changes on the plateau of the flow curve. We conclude, therefore, that we cannot find a sensible energy-temperature FDT relation in this regime of the spin chain.

9.3 Conclusion

In this chapter, we studied glassy dynamics in a kinetically constrained spin chain. After reviewing the low temperature coarsening process of the undriven chain, we incorporated quasi-rheological, non-Hamiltonian driving into it. We defined dynamical analogues of several common rheological experiments, and studied in detail the case of shear of constant rate. We found that shear of rate $\dot{\gamma}$, such that $\epsilon^{m+1} < \dot{\gamma} < \epsilon^m$ and $\dot{\gamma} \gg 1/\tau_{\rm erg}$, will interrupt the low temperature relaxation process of the undriven chain at the m stage of coarsening. We noted the similarity of this phenomenology to that of the steadily driven SGR model at $x < 1$. We also noted, however, that the similarity between the two models breaks down at very low shear rates: in the SGR model, where the ergodic time is infinite for $x < 1$, we find a yield stress in the limit of weak shear. In the spin chain, where the ergodic time is long but finite (for any non-zero temperature), we predict (for $\dot{\gamma} \ll 1/\tau_{\rm erg}$) a linear rheological regime in which $\sigma \propto \dot{\gamma}$.

9.4 Appendix I: simulation algorithm for the driven spin chain

Following [SE99], we simulated the driven spin chain using a Waiting Time Monte Carlo (WTMC) method [BKL75] combined with an efficient binary search algorithm [NB99]. Details of the simulation are as follows. We represented the state of the chain (at any time) by an array of spin states $s[i]$ $(1 < i < L)$ together with a corresponding

the small population of minus spins.

array of flip rates $r[i]$. The flip rate of the ith spin, $r[i]$, is the sum of an undriven constrained component, and a driven unconstrained component. After initializing the system (at $t = 0$), the time of the first spin-flip event, Δt, was chosen from the distribution $P(\Delta t) \propto \exp(-\Delta t \sum_{i=1}^{L} r[i])$ in which (using the well known rule for combining exponential rates [BD95]) the relevant rate is the sum of all the flip-rates in the chain. The particular spin to be flipped in that event was then selected by recognising that the ith spin should flip with a probability $P_{\text{flip}}[i] = r[i]/\sum_{i=1}^{L} r[i]$, and by performing a search of the chain weighted according to this "flip-distribution". In order to allow an efficient search, we maintained (at any time) a binary tree of rates (see figure 9.6). The top level, $r_0[1]$, of this tree was a single number, equal to the sum of all flip-rates in the chain $\sum_{i=1}^{L} r[i]$. The second level was an array $r_1[i]$ with $i = 1, 2$. $r_i[1]$ and $r_i[2]$ were respectively the sum of all rates in the left and right hand sides of the chain: r_1 therefore bisected the original chain. The third layer, $r_2[i]$ for $1 < i \leq 4$, bisected each of the halves represented by the components of r_1, and hence overall cut the chain into quarters. We continued with this bisection process, at each step doubling the number of entries in the array, until we reached the original rate array r, which in this notation should be denoted r_l where $l = \log_2 L$. ($L + 1$ is the number of levels in the tree.) The spin search consisted of working progressively downwards through this tree: at each node, a branch was chosen with a probability equal to the total rate under that branch, normalized by the total rate under both branches. Once the spin had been chosen, we flipped it by updating $s[i]$: any spin initially in state $s = 1$ or $s = -1$ was flipped into the state $s = 0$, whereas a spin in state 0 was flipped $0 \to 1$ with probability $p = (\epsilon + \dot{\gamma})/(2\epsilon + \dot{\gamma})$ and $0 \to -1$ with probability $1 - p$. We also updated the entries $r[i]$ and $r[i + 1]$ of the rate array, and propagated these changes upward through the tree of rates. We finally incremented the simulation's "clock" by $t \to t + \Delta t$. This flip process was repeated (always selecting the time-interval Δt before the next flip from spin from $P(\Delta t) \propto \exp(-\Delta t \sum_{i=1}^{L} r[i])$) until the chain had reached (on average) a time-independent steady state.

We chose this method because of the particular suitability of WTMC techniques to simulating the dynamics of systems such as the spin chain which evolve very slowly. A "real-time" method, such as *conventional* Monte-Carlo, would have inefficiently involved many trial flips, the vast majority of which would have been rejected. WTMC, on the other hand, effectively re-scales time such that the simulation time-scale is set by the number of flip-processes which actually occur. This allowed us to access very long times – $O(10^{10})$ – with relatively little computational effort. The binary search allowed us, at each update, to search the chain in a time which scaled only logarithmically with system size. We were therefore able to access very large systems sizes: $L = O(2^{16})$.

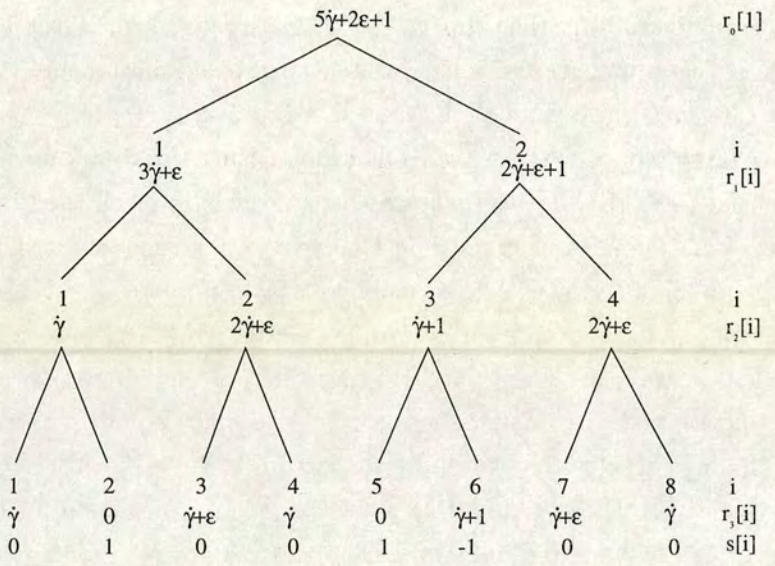

Figure 9.6. Schematic representation of the "binary tree" used for the waiting time Monte Carlo (WTMC) simulation method of the spin chain for strain of constant rate.

9.5 Appendix II: numerical extraction of domain length distribution

In section 9.2.2 we showed that[11] the distribution of domain lengths $P(d)$ in the steady state of the driven spin chain must satisfy

$$\begin{aligned} 0 \;=\; & -g(d)P(d) - P(d)\left[\sum_{d'=d_c+1}^{2d_c}\left(\frac{d'-1}{2}\right)P(d') + d_c\sum_{d'=2d_c+1}^{\infty}P(d')\right] \\ & +2\sum_{d'=d+1}^{\infty}P(d') - \sum_{d'=d+1}^{d+d_c}P(d') \\ & +\sum_{d'=1}^{d_c}\sum_{d''=d_c+d'+1}^{\infty}P(d'')P(d-d') \\ & +\sum_{d'=d_c+1}^{2d_c}\left(\frac{2d_c-d'+1}{2}\right)P(d')P(d-d'). \end{aligned} \tag{9.11}$$

[11] within an independent interval approximation.

for $d > d_c$ at low temperatures, $\epsilon \to 0$. Under the same conditions, $P(d) = 0$ for $d \leq d_c$. In this appendix we outline the numerical method used to solve equation 9.11 for $P(d > d_c)$.

As a first step we rewrite the first term on the second line to get

$$\begin{aligned} 0 \;=\; & -g(d)P(d) - P(d)\left[\sum_{d'=d_c+1}^{2d_c}\left(\frac{d'-1}{2}\right)P(d') + d_c\sum_{d'=2d_c+1}^{\infty}P(d')\right] \\ & +2 - 2\sum_{d'=d_c+1}^{d-1}P(d') - 2P(d) - \sum_{d'=d+1}^{d+d_c}P(d') \\ & +\sum_{d'=1}^{d_c}\sum_{d''=d_c+d'+1}^{\infty}P(d'')P(d-d') \\ & +\sum_{d'=d_c+1}^{2d_c}\left(\frac{2d_c-d'+1}{2}\right)P(d')P(d-d'), \end{aligned} \tag{9.12}$$

which we recast as

$$\begin{aligned} [g(d)+2+f_1(d)]P(d) \;=\; & 2 - 2\sum_{d'=d_c+1}^{d-1}P(d') - f_2(d) + \sum_{d'=1}^{d_c}f_3(d')P(d-d') \\ & +\sum_{d'=d_c+1}^{2d_c}\frac{2d_c-d'+1}{2}P(d')P(d-d'). \end{aligned} \tag{9.13}$$

In the absence of the terms f_1, f_2 and f_3, this equation would be of the form

$$P(d) = P[P(d' < d)] \tag{9.14}$$

and would be simply solved by "marching out" over successive $d = 1, 2, 3, 4...$, at each step calculating $P(d)$ from the known previous values $P(d' < d)$. (To find $P(d_c + 1)$ we would use the initial condition $P(d_c) = 0$.)

However equation 9.13 is complicated by the fact that f_1, f_2 and f_3 depend upon the value of $P(d)$ over the whole range of d, not just over $d' < d$. Hence equation 9.14 is actually of the form

$$P(d) = f[P(d' < d), f_1[P(d)], f_2[P(d)], f_3[P(d)]]. \tag{9.15}$$

In principle this cannot be solved by the simple marching out method just described. To tackle this problem, we refined our method of solution in the following way. We guessed sensible values of f_1, f_2 and f_3, and substituted these into 9.15. We then used the usual "marching out over d" method to calculate a corresponding function $P_1(d)$.

This is clearly only an approximation to $P(d)$, since we have input only approximations to f_1, f_2 and f_3. We then used $P_1(d)$ to find refined guesses for f_1, f_2 and f_3, substituted these into equation 9.15, and again used the marching out method to find a refined function $P_2(d)$. We repeated this many times, at any iteration index $n > 0$ using

$$P_n(d) = f[P_n(d' < d), f_1[P_{n-1}(d)], f_2[P_{n-1}(d)], f_3[P_{n-1}(d)]]. \tag{9.16}$$

We found a convergence $P_n(d) \to P_\infty(d)$ as n became large. We assume this to be the required solution $P(d)$ to equation 9.11. It agrees well with the simulation data.

Chapter 10

Conclusions and outlook

10.1 Summary and discussion of main results

In this thesis, we studied glassy dynamics within two simple statistical models: a trap model, and a kinetically constrained spin chain. We focused particularly on the response of the models to external driving and loading ("strain" and "stress") such that our results could be applied to the rheology of soft glassy materials (foams, dense emulsions, *etc.*) which typically show pronounced non-linearity in their stress response to slow steady shear, and ageing ("hardening" over time) at small loads. We also applied concepts of slow dynamics to the rheology of highly branched polymers. Beyond this rheological motivation, we used our two models to study more general concepts of glassy dynamics, considering in particular violations of the equilibrium FDT in the models' non-equilibrium regimes.

After a brief introductory discussion, we started in section 2.1 by summarizing the basic phenomenology of glassy, ageing systems. We formally defined ageing to be the property that "a significant part of a system's relaxation (following a small step perturbation) takes place on time-scales which grow with age"; an equivalent statement is that ageing systems show "long term memory". We discussed the distinction between "strong" and "weak" long term memory (SLTM and WLTM), noting that an ageing system with WLTM is not affected by perturbations of finite duration which were applied in the distant past.

We then (in section 2.2) reviewed the basic principles of rheology (both linear and non-linear), extending the existing time translationally invariant (TTI) formalism to include ageing samples in which TTI is lost. In particular, we generalized each response function to include an absolute (age-dependent) time variable. We also discussed the likely status (in ageing systems) of:

i) the independence of oscillatory response functions to the time at which the oscillation started,
ii) Fourier relations between step and oscillatory response functions, and
iii) reciprocity between imposed-stress and imposed-strain oscillatory response functions.
We argued that, although such simplifying relations are automatic in TTI systems, they are not guaranteed in ageing systems. However, we suggested that, for many rheological applications, the main interest is in systems with *weak* LTM, and conjectured that "weakness" of memory is in fact sufficient to ensure that these simplifying relations still hold, despite the presence of ageing:
i) the age-dependent linear viscoelastic modulus is (after many strain cycles) start-time independent $[G^*(\omega, t, t - t_s) \rightarrow G^*(\omega, t)]$,
ii) $G^*(\omega, t)$ then obeys the usual Fourier relation with the (ageing) linear step strain response function, in addition to
iii) the usual reciprocal relation $[G^*(\omega, t)J^*(\omega, t) = 1]$ with the ageing compliance.
Pending a general proof of these conjectures, however, all such relationships between age-dependent rheological quantities require explicit verification for each experimental system, or theoretical model.

In chapter 3, we summarized the experimental evidence for glassy dynamics and ageing in the rheology of a broad class of disordered soft materials, such as foams and dense emulsions. In particular, we discussed the existence of a yield stress in the limit of zero shear, and the anomalous upward curvature of the loss modulus at low frequencies (suggestive of underlying ageing), in addition to more explicit observations of ageing in both the stress relaxation modulus of dense colloidal suspensions, and the creep compliance of dense micro-gel suspensions. Interestingly, in the micro-gel creep experiments, ageing was found to be eliminated for loads greater than the yield stress. In section 3.2, we placed our approach to modelling this data into context by reviewing approaches adopted elsewhere in the literature.

We then introduced (in chapter 4) the first of our two glassy models: Bouchaud's trap model. We reviewed its exact solution, and discussed the presence of a true glass transition at a finite temperature T_g. In the glass phase ($T \leq T_g$), ergodicity is "weakly" broken: ageing occurs via a progressive evolution of the system towards ever deeper traps. We studied this ageing from the point of view of the average hopping rate, $Y(t)$, which tends to zero at long times for $T \leq 1$, but which remains finite for $T > 1$.

In section 4.2, we discussed the application of this trap model to rheology, via the incorporation of intra-trap rheological degrees of freedom, the coupling of these degrees

of freedom to external shear, and the identification of inter-trap hops with local yielding events. We also discussed the necessity, in this rheological context, of replacing the true thermodynamic temperature T with an effective noise temperature $x \gg T$ which is intended to model, in a mean field way, interactions between different regions of the sample. We reviewed the exact constitutive solution of this "soft glassy rheology" (SGR) model, via two coupled non-linear integral equations. We also discussed its mapping (in the undeformed limit) to the original trap model, and exploited this mapping to motivate the existence (within linear rheology at least) of a glass phase in which rheological ageing should occur: the gradual evolution of the constituent elastic elements towards ever higher yield thresholds (deeper traps) causes a progression toward more elastic and less plastic behaviour.

We then used our generalized, non-TTI rheological framework to make a detailed, quantitative study (in chapters 5 and 6) of the SGR model's rheological predictions, focusing particularly upon glass phase behaviour ($x < 1$), but also discussing the crossover, via "long transients", to equilibrium response for $x > 1$. In the glass phase, the model has a macroscopic yield stress σ_y. Provided this is not exceeded, ageing occurs, with the sample's apparent relaxation time-scale always of order its own age. (In this rheological context, we interpreted our formal definition of ageing to be the property that a significant part of the stress relaxation, following a small step strain, takes place on time-scales which grow with the age of the system at the time of strain application.)

In the limit of linear rheology, the stress relaxation modulus and the creep compliance both depend (for $x < 1$) upon the scaled time interval $(t - t_w)/t_w$. The model shows *weak* LTM. The viscoelastic spectrum – which is a function of the scaled frequency ωt – obeys the simplifying relations *i*) to *iii*) above, in agreement with our conjectures for oscillatory measurements in systems with WLTM. For $x > 1$, the model lacks true ageing, but for x close to one shows long rheological transients (which can be distinguished from true ageing by the formal criterion given above) during the very slow approach to equilibrium. In equilibrium (for $x \gtrsim 1$), the loss modulus is a very weak power law of frequency, reflecting the divergent width of the underlying relaxation spectrum as $x \to 1$. At high noise temperatures ($x > 3$), the viscoelastic spectra revert to simple Maxwellian behaviour, with a characteristic time-scale of order the mesoscopic attempt time for yielding events.

Significant ageing was also found (for $x < 1$) in the nonlinear rheology of the SGR model. For example, the nonlinear step-strain relaxation shows the same ageing behaviour as the linear one, except that all relaxation rates are enhanced by an identical strain-dependent factor. In startup of steady shear (see figure 5.6), ageing is "masked"

at short time intervals (when stress response is purely elastic), absent at long times (in the steady flow regime), but strongly apparent at intermediate times, when the stress shows an overshoot that is highly dependent on sample age: for an older sample, the elastic elements have higher yield thresholds, and the linear elastic regime therefore extends further before the imposed strain finally causes yielding. At long times, the stress falls to its ultimate steady (time-independent) value, as prescribed by the flow curve $\sigma_{ss}(\dot{\gamma}) - \sigma_y \sim \dot{\gamma}^{1-x}$: hence, steady shear (of any non-zero rate $\dot{\gamma} > 0$) *interrupts* ageing, and restores a steady state in which the characteristic relaxation time-scale is set by the inverse shear rate, and not the system's age.

The non-linear creep compliance shows interesting dependence on both the stress level and the age of the sample. For small stresses ($\sigma < \sigma_y$), we found logarithmic creep (for all $x < 1$) crossing over, as the yield stress is approached, to a more rapid creep that still appears to have zero strain rate in the long time limit (see figure 6.5). For stresses $\sigma > \sigma_y$, we found (as expected) that ageing was interrupted, and that the system approached the steady flow regime with $\sigma - \sigma_y \sim \dot{\gamma}^{1-x}$ (as discussed in the previous paragraph for the long-time limit of shear startup). From this steady limit (attained either via shear start-up or non-linear compliance probes), we conclude that ageing can be interrupted *either* by the imposition of steady shear at any non-zero rate ($\dot{\gamma} > 0$), *or* by any finite stress exceeding the yield stress ($\sigma > \sigma_y$).

For $1 < x < 2$ the model shows power law fluid behaviour: the flow curve is $\sigma(\dot{\gamma}) \sim \dot{\gamma}^{x-1}$. There is no yield stress, but the zero-shear viscosity is nonetheless infinite. After the imposition of a small (but non-zero) step stress, σ_0 such that $0 < \sigma_0 \ll 1$, the creep is initially linear in stress, with a rate which appears to tend to zero at long times (in agreement with the fact that the zero-shear viscosity is infinite). See figure 6.4. However, after a crossover time (which diverges in the limit $\sigma_0 \to 0$), the system approaches a steady flow regime with a strain rate given by the inverted flow curve relation $\dot{\gamma} \sim \sigma_0^{1/(x-1)}$.

Having completed this detailed study of the SGR model's rheological predictions, we then used the concepts of slow dynamics and non-TTI rheology developed in chapters 1 to 6 to study (in chapter 7) the rheology of highly branched polymer melts, in which the "branching distribution" can be considered a type of quenched glassy disorder. We showed that the tube model, in its application to such melts, leads naturally to a picture of activated dynamics taking place against large free energy barriers, with a broad spectrum of relaxation time-scales. Recognising the phenomenological similarity to the dynamics of the linear SGR model, we showed that, for certain power-law branching distributions, the tube model can (in equilibrium) be mapped exactly onto the linear SGR model at a noise temperature which exceeds the glass transition noise

temperature, by a small amount δ; the parameter δ can be tuned by the degree of molecular entanglement. We then discussed the extension of this equilibrium model to melts prepared in a non-equilibrium state by means of rapid pre-shear, demonstrating it to show (approximately) the same slow relaxation towards equilibrium as the linear SGR model following a deep quench to a noise temperature $x = 1 + \delta$. Using this correspondence, we predicted the presence of long rheological transients in these melts, following pre-shear. We noted that these transients could be very difficult experimentally to distinguish from "true" ageing.

To conclude our work on trap models, we studied (in chapter 8) the possible use of the fluctuation-dissipation theorem (FDT) for defining a non-equilibrium temperature in the ageing regime of the linear SGR model. We considered several different observable–field pairs, in most cases (energy-temperature being a notable exception) finding a non-trivial limiting FDT plot as the waiting time became large. However, we found the shape of the plot to be strongly dependent upon the choice of observable and thus concluded that FDT could not be used to define a sensible (observable-independent) non-equilibrium temperature for this model.

Finally, we studied (in chapter 9) a kinetically constrained spin chain. Unlike the trap model (which contains quenched disorder) the spin chain directly induces its own glassiness by means of a simple kinetic constraint: at low temperatures, the constraint leads to large energy barriers which impede the system's dynamical evolution; the ergodic time diverges according to an exponential-inverse-temperature-squared law, $\tau_{\rm erg} \sim \exp(1/T^2)$. (Hence, unlike the trap model, the spin chain lacks a true glass transition: even at very low temperatures, $\tau_{\rm erg}$ is finite, albeit very large.) After a quench to a low temperature, the chain shows (for waiting times $t_{\rm w} \ll \tau_{\rm erg}$) an anomalous coarsening relaxation process, which proceeds via well separated stages. After reviewing this coarsening process, we incorporated driving into the model, to mimic rheological shear. We presented simulation results which reveal that steady driving interrupts coarsening, and restores a steady state in which the characteristic relaxation time-scale is set by the inverse shear rate. We described an independent-interval theory aimed at describing this steady state, and demonstrated it to give excellent agreement to both the "domain length" distribution, and the "flow curve" of the simulation results. We found the flow curve to approach a step-wise function of driving rate in the limit of zero temperature, consistent with the divergent separation of the model's intrinsic relaxation time-scales in that limit. We discussed the phenomenological similarity of the driven spin chain to the steadily sheared SGR model (for $x < 1$) but noted that (in contrast to the SGR model) the spin chain lacks a true yield stress, since its ergodic time is always finite.

Finally, we considered the possibility of finding a sensible non-equilibrium fluctuation-dissipation relation in the weakly driven limit of the chain's steady state. However, we concluded that – at least for energy-temperature FDT – no sensible response function exists, due to the step-wise dependence of energy upon the scaling variable $T \ln \dot{\gamma}$.

10.2 Outlook and suggestions for further work

In this final section, we address some of the outstanding puzzles of the work described above, and outline a few possibilities for further work.

10.2.1 Theoretical framework of non-TTI rheology

In chapter 2, we set up a generalized theoretical framework for the analysis of rheological ageing. We then applied this framework to soft solids which (we believe) age through glassy rearrangements of local elements. The formalism itself is actually broader than this particular application, and should apply to the rheology of any ageing system. For example, we hope it will be useful for studying soft materials such as polydomain defect textures in ordered mesophases of copolymers which might instead age through coarsening domain growth (or a mixture of domain growth and glassy rearrangement of domains).

Although the framework is quite comprehensive in its present form, an obvious open question is the status in ageing systems of the simplifying relations listed *i*) to *iii*) on page 193 above. We have conjectured that these relations may hold in general for the sub-class of ageing systems with *weak* LTM, and that they are likely to break down in systems with *strong* LTM. However, to date we have no proof. It would therefore be interesting to study the relations within a model which contains only the most basic, general ingredients of weak or strong LTM.

10.2.2 Recent ageing rheological data in soft glassy materials

In sections 3.1.3 and 3.1.4, we described recent experimental studies of rheological ageing in dense colloidal suspensions, and in dense micro-gel suspensions. Although the predictions of the SGR model (chapters 5 and 6) are broadly consistent with the results of these studies – both show an ageing relaxation time-scale at small loads, with a return to TTI behaviour at high loads – there are several notable discrepancies. In particular, the SGR model (for $x < 1$) predicts full ageing – *i.e.* data collapse with the scaled time $t^{1-\mu} - t_{\rm w}^{1-\mu}$ with $\mu = 1$ – for any stress $\sigma < \sigma_{\rm y}$, with a return to TTI response ($\mu = 0$) at $\sigma > \sigma_{\rm y}$. The microgel experiments, on the other hand, reveal

a smooth progression of the ageing exponent from $\mu = 1$ for $\sigma \to 0$, through sub-ageing for $0 < \sigma < \sigma_y$, finally recovering TTI response for $\sigma > \sigma_y$. In even starker contrast, the step-strain response of the dense colloidal suspensions showed sub-ageing with $0.5 \lesssim \mu \lesssim 0.7$ even at very low amplitude.

To model such rheological sub-ageing within an approach similar to that adopted above, one might modify the recent lattice sub-ageing trap model (see section 3.2.4) in the way that the basic trap model was modified to produce the SGR model. Clearly, however, any lattice model will be much less amenable to simple analysis than the mean-field SGR model.

Even within our existing analysis, detailed comparison with the micro-gel creep experiments is difficult, due to the nature of the experimental preparation procedure: the system was first fluidized by a large stress, before being aged under zero stress, and finally subjected to the measurement stress. The subsequent strain response comprised an interplay between forward creep due to the measurement stress, and a degree of elastic recovery due to recent removal of the preparatory stress. We have not to date considered this particular rheological scenario within the SGR model, and it would clearly be interesting to do so.

10.2.3 Effective noise temperature. Energy landscape

As described in section 4.2.1, the SGR model captures glassy rearrangements of local material elements within a picture of activated dynamics: the rate at which any element yields is given by

$$\tau^{-1} = \tau_0^{-1} \exp\left[-\frac{\left(E - \frac{1}{2}kl^2\right)}{x}\right] \tag{10.1}$$

in which x has the dimensions of temperature. As already noted, the typical yield energies in any realistic SGM are much larger than thermal energies, and we cannot look to thermal activation to initiate rearrangements. Instead, x is an effective noise temperature ($\gg T$) which is intended to model, in a mean field way, non-linear couplings between elements: the exponential factor in equation 10.1 is the probability with which any element is assumed to yield due to "kicks" which in turn arose from other yielding events, elsewhere in the sample. There is thus no separate energy scale for x; it must be of order the typical yield energy E.

Whether it is fully self-consistent to have a noise temperature $x \gg T$ remains an open question. Indeed, it is difficult to justify a picture of self sustaining dynamics in the face of huge energy barriers, in a material which is not externally driven. Of course, in a rheological context one could look to external shear to maintain the dynamics, although

this clearly cannot explain any lossy component (in the frequency range relevant to such glassy rearrangements) in *linear* rheology (in which by definition the material's intrinsic dynamics are unperturbed by shear).

A possible resolution would be to assume that any non-linear pre-shear procedure leaves the material in a highly frustrated state, with large local elemental stresses (which average to zero in a globally unstressed sample). The energy released in one yielding event might then be sufficient to trigger a self-sustaining avalanche of subsequent yields, persisting over a large time window. Over time, (in an unsheared material) one would expect a gradual ageing progression towards a state of lower frustration, and correspondingly slower dynamics. To model this very simply, one could simulate a cellular automaton in which each site is identified as a local material element, with its own local strain variable which is driven convectively by shear (in the spirit of "self-organized-critical" models [BTW87]) and also coupled diffusively to the rate of energy release in other nearby elements. After an initial interval of driving, one might then hope to recover a subsequent slow decay of activity over time. However, any attempts in this direction of which the author is aware have unfortunately given rapid (exponential) decay of activity after pre-shear [HC]. Note that, beyond any motivation connected with interpreting the noise temperature, one might use lattice SGR models to address the various bundling and banding effects [Pin00] which can arise in sheared complex fluids, and for which the spatially unstructured SGR model obviously cannot account.

Closely connected with this "thermal" activation factor is our choice for the exponential density of states, $\rho(E)$. As noted above, this can be justified in spin glasses by use of extreme value statistics, but its origin in soft glasses is less clear: it was merely used as an ingredient which (in conjunction with the activation factor) could capture a glass transition in the simplest possible way. As a first step towards justifying it, one might consider the motion of an element in a 1−D random potential formed by other elements, which changes over time with a decorrelation rate proportional to $Y(t)$. Both $Y(t)$ and the potential would have to be determined self-consistently, but one might hope that extreme value statistics would in this case generate an exponential density of states.

10.2.4 Other glassy rheology models

As noted in section 3.2 above, in order to capture rheological ageing one can in principle incorporate strain, stress and driving into any suitable model of the glass transition. An obvious alternative to the trap model and spin chain considered in this thesis would be the mode coupling theory (MCT) described in section 3.2.2. Indeed (as

noted in section 3.2.2), a MC model driven into a steady "flow regime" has already been considered in detail by Berthier *et al.* [BBK00]. However, no attempt was made to interpret the intrinsic ageing dynamics of the undriven model within a rheological context. It might therefore be interesting to do so.

10.2.5 Non-equilibrium fluctuation-dissipation theorems

As noted above, the two glassy models studied in this thesis are simple enough to allow (beyond glassy rheology) a study of more general concepts of glassy dynamics. Indeed, in chapter 8, we studied in detail non-equilibrium FDT in the ageing regime of the trap model. We found, perhaps surprisingly, that the FDT ratio was strongly both upon scaled time $(t - t_{\rm w})/t_{\rm w}$ *and* on the choice of the observable-field pair. (Recall that in glassy systems, the FDT ratio is in general constant throughout each regime of the dynamics, and observable independent.) It would therefore clearly be of interest to investigate observable dependence of FDT ratios in other models. For example, one might extend the recent work of Godréche and Luck [GL00] to consider higher order correlation functions in the Glauber Ising chain.

In chapter 9, we considered briefly non-equilibrium FDT in the weakly driven limit of the steadily driven spin chain. We concluded that, for the observable-field pair of energy-temperature at least, one cannot find a meaningful FDT in this case. It would clearly, however, be of interest to consider other observables in the same regime.

We noted in chapter 8 that non-equilibrium FDT temperatures, where they exist, are often found to remain finite in the limit $T \to 0$: $T_{\rm FDT} \gg T$. We have furthermore studied in detail the dynamics of foams, in which, due to the presence of large energy barriers, an effective noise temperature $x \gg T$ is needed to initiate the dynamics. It is therefore tempting to conjecture that there could be some underlying link between these two temperatures.

Finally, a striking experimental phenomenon of glassy systems, unexplored in this thesis, is that of "rejuvenation" by temperature cycling. We do not describe this in detail here, but refer the reader to [Bou00] for a detailed discussion. We merely note that it would be interesting to study, within both the trap model and the spin chain, the effects of temperature steps upon ageing and coarsening.

10.2.6 And finally...

I hope that this work has contributed to the fields of soft rheology and of glassy dynamics. More importantly, I hope it has helped to establish a link between them.

Bibliography

[AW95] G B Arfken and H J Weber. *Mathematical methods for physicists.* Academic Press, London, 1995.

[BB00] J-L Barrat and L Berthier. Fluctuation-dissipation relation in a sheared fluid. 2000. cond-mat/0003346.

[BBK00] L Berthier, J L Barrat, and J Kurchan. A two-time-scale, two-temperature scenario for nonlinear rheology. *Phys. Rev. E*, 61(5):5464–5472, 2000.

[BCKM98] J P Bouchaud, L F Cugliandolo, J Kurchan, and M Mézard. Out of equilibrium dynamics in spin-glasses and other glassy systems. In A P Young, editor, *Spin glasses and random fields*, Singapore, 1998. World Scientific.

[BD95] J P Bouchaud and D S Dean. Aging on Parisi's tree. *J. Phys. (France) I*, 5(3):265–286, 1995.

[BDG94] A J Bray, B Derrida, and C Godreche. Nontrivial algebraic decay in a soluble model of coarsening. *Europhys. Lett.*, 27(3):175–180, 1994.

[BHW89] H A Barnes, J F Hutton, and K Walters. *An introduction to rheology.* Elsevier, Amsterdam, 1989.

[BKL75] A B Bortz, M H Kalos, and J L Lebowitz. *J. Comput. Phys.*, 17:10, 1975.

[BLC95] D M A Buzza, C Y D Lu, and M E Cates. Linear shear rheology of incompressible foams. *J. Phys. (France) II*, 5(1):37–52, 1995.

[BM89] R C Ball and T C B Mcleish. Dynamic dilution and the viscosity of star polymer melts. *Macromolecules*, 22(4):1911–1913, 1989.

[BM97] J P Bouchaud and M Mézard. Universality classes for extreme-value statistics. *J. Phys. A*, 30(23):7997–8015, 1997.

[Bou92] J P Bouchaud. Weak ergodicity breaking and aging in disordered-systems. *J. Phys. (France) I*, 2(9):1705–1713, 1992.

[Bou00] J-P Bouchaud. Aging in glassy systems. In M E Cates and M R Evans, editors, *Soft and fragile matter: non-equilibrium dynamics, metastability and flow*, Edinburgh and Bristol, 2000. SUSSP publications and Institute of Physics publishing.

[BTW87] P Bak, C Tang, and K Wiesenfeld. Self-organized criticality – an explanation of 1/f noise. *Phys. Rev. Lett.*, 59(4):381–384, 1987.

[CAZ94] L B Chen, B J Ackerson, and C F Zukoski. Rheological consequences of microstructural transitions in colloidal crystals. *J. Rheol.*, 38(2):193–216, 1994.

[CBL] M Cloitre, R Borrega, and L Leibler. Rheological ageing and rejuvenation in microgel pastes. *preprint submitted to Phys. Rev. Lett.*

[CDK97] L F Cugliandolo, D S Dean, and J Kurchan. Fluctuation-dissipation theorems and entropy production in relaxational systems. *Phys. Rev. Lett.*, 79(12):2168–2171, 1997.

[CK93] L F Cugliandolo and J Kurchan. Analytical solution of the off-equilibrium dynamics of a long- range spin-glass model. *Phys. Rev. Lett.*, 71(1):173–176, 1993.

[CK94] L F Cugliandolo and J Kurchan. On the out-of-equilibrium relaxation of the Sherrington-Kirkpatrick model. *J. Phys. A*, 27(17):5749–5772, 1994.

[CK95] L F Cugliandolo and J Kurchan. Weak ergodicity breaking in mean-field spin-glass models. *Phil. Mag. B*, 71(4):501–514, 1995.

[CK99] L F Cugliandolo and J Kurchan. Thermal properties of slow dynamics. 1999. cond-mat/9812229 (unpublished).

[CKP97] L F Cugliandolo, J Kurchan, and L Peliti. Energy flow, partial equilibration, and effective temperatures in systems with slow dynamics. *Phys. Rev. E*, 55(4):3898–3914, 1997.

[Cop62] E T Copson. *An introduction to the theory of functions of a complex variable.* Oxford University Press, New York, 1962.

[CRRS00] A Crisanti, F Ritort, A Rocco, and M Sellitto. Inherent structures and non-equilibrium dynamics of 1d constrained kinetic ising models: a comparison study. 2000. cond-mat/0006045.

[Cug99] L F Cugliandolo. Effective temperatures out of equilibrium. 1999. cond-mat/9903250.

[DADL00] C Derec, A Ajdari, G Ducouret, and F Lequeux. Rheological characterization of aging in a concentrated colloidal suspension. *Compte Rendus d'Acad. des Sciences (Paris).* Accepted for publication, 2000.

[DAL99] C Derec, A Ajdari, and F Lequeux. Mechanics near a jamming transition: a minimalist model. *Faraday Discuss.*, (112):195–207, 1999.

[DAL00] C Derec, A Ajdari, and F Lequeux. Rheology and aging: a simple approach. 2000. Submitted for publication.

[DE86] M Doi and S F Edwards. *The Theory of Polymer Dynamics.* Clarendon Press, Oxford, 1986.

[Dic92] E Dickinson. *An introduction to food colloids.* Oxford University Press, Oxford, 1992.

[GI99] T S Grigera and N E Israeloff. Observation of fluctuation-dissipation-theorem violations in a structural glass. *Phys. Rev. Lett.*, 83(24):5038–5041, 1999.

[GL98] T Giamarchi and P LeDoussal. In A P Young, editor, *Spin glasses and random fields*, Singapore, 1998. World Scientific.

[GL99] C Godreche and J M Luck. Correlation and response in the backgammon model: the ehrenfest legacy. *J. Phys. A-Math. Gen.*, 32(33):6033–6054, 1999.

[GL00] C Godreche and J M Luck. Response of non-equilibrium systems at criticality: exact results for the glauber-ising chain. *J. Phys. A-Math. Gen.*, 33(6):1151–1170, 2000.

[GS92] W Gotze and L Sjogren. Relaxation processes in supercooled liquids. *Reports on Progress in Physics*, 55(3):241–376, 1992.

[HC] D A Head and M E Cates (unpublished).

[HL98] P Hébraud and F Lequeux. Mode-coupling theory for the pasty rheology of soft glassy materials. *Phys. Rev. Lett.*, 81(14):2934–2937, 1998.

[HLMP97] P Hebraud, F Lequeux, J P Munch, and D J Pine. Yielding and rearrangements in disordered emulsions. *Phys. Rev. Lett.*, 78(24):4657–4660, 1997.

[Hol93] S D Holdsworth. Rheological models used for the prediction of the flow properties of food products. *Trans. Inst. Chem. Eng.*, 71(C):139–179, 1993.

[HR93] H. Hoffmann and A. Rauscher. Aggregating systems with a yield stress value. *Coll. Polymer Sci.*, 271(4):390–395, 1993.

[JE91] J Jäckle and S Eisinger. A hierarchically constrained kinetic Ising-model. *Zeitschr. Phys. B*, 84(1):115–124, 1991.

[Kob00] W Kob. Supercooled liquids and glasses. In M E Cates and M R Evans, editors, *Soft and fragile matter: non-equilibrium dynamics, metastability and flow*, Edinburgh and Bristol, 2000. SUSSP publications and Institute of Physics publishing.

[KPG88] R J Ketz, R K Prudhomme, and W W Graessley. Rheology of concentrated microgel solutions. *Rheol. Acta*, 27(5):531–539, 1988.

[KSA88] S A Khan, C A Schnepper, and R C Armstrong. Foam rheology. 3: Measurement of shear-flow properties. *J. Rheol.*, 32(1):69–92, 1988.

[Kur98] J Kurchan. Rheology, and how to stop aging. 1998. Preprint cond-mat/9812347. To be published in proceedings of *Jamming and Rheology: constrained dynamics on microscopic and macroscopic scales* (workshop at ITP, Santa Barbara, 1997).

[MB96] C Monthus and J P Bouchaud. Models of traps and glass phenomenology. *J. Phys. A*, 29(14):3847–3869, 1996.

[MBW95] T G Mason, J Bibette, and D A Weitz. Elasticity of compressed emulsions. *Phys. Rev. Lett.*, 75(10):2051–2054, 1995.

[MBW96] T G Mason, J Bibette, and D A Weitz. Yielding and flow of monodisperse emulsions. *J. Coll. Interf. Sci.*, 179(2):439–448, 1996.

[McL00] T C B McLeish. Rheology of linear and branched polymers. In M E Cates and M R Evans, editors, *Soft and fragile matter: non-equilibrium dynamics, metastability and flow*, Edinburgh and Bristol, 2000. SUSSP publications and Institute of Physics publishing.

[MM97] S T Milner and T C B Mcleish. Parameter-free theory for stress relaxation in star polymer melts. *Macromolecules*, 30(7):2159–2166, 1997.

[MM99] T C B Mcleish and S T Milner. Entangled dynamics and melt flow of branched polymers. *Advan Polym Sci*, 143:195–256, 1999.

[MMSZ94] M R Mackley, R T J Marshall, J B A F Smeulders, and F D Zhao. The rheological characterization of polymeric and colloidal fluids. *Chem. Engin. Sci.*, 49(16):2551–2565, 1994.

[MPRTRL98] E Marinari, G Parisi, F Ricci-Tersenghi, and J J Ruiz-Lorenzo. Violation of the fluctuation-dissipation theorem in finite- dimensional spin glasses. *J. Phys. A-Math. Gen.*, 31(11):2611–2620, 1998.

[MW95] T G Mason and D A Weitz. Linear viscoelasticity of colloidal hard-sphere suspensions near the glass-transition. *Phys. Rev. Lett.*, 75(14):2770–2773, 1995.

[NB99] M E J Newman and G T Barkema. *Monte Carlo methods in statistical physics*. Oxford University Press, New York, 1999.

[NS98] P Nordblad and P Svedlindh. Experiments on spin glasses. In A P Young, editor, *Spin glasses and random fields*, Singapore, 1998. World Scientific.

[Pin00] D Pine. Light scattering and rheology of complex fluids far from equilibrium. In M E Cates and M R Evans, editors, *Soft and fragile matter: non-equilibrium dynamics, metastability and flow*, Edinburgh and Bristol, 2000. SUSSP publications and Institute of Physics publishing.

[PRV+96] P Panizza, D Roux, V Vuillaume, C Y D Lu, and M E Cates. Viscoelasticity of the onion phase. *Langmuir*, 12(2):248–252, 1996.

[PTVF92] W H Press, S A Teukolsky, W T Vetterling, and B P Flannery. *Numerical Recipes in C (2nd ed.)*. Cambridge University Press, Cambridge, 1992.

[Rei80] L E Reichl. *A modern course in statistical physics.* University of Texas Press, Austin, 1980.

[RMB00] B Rinn, P Maass, and J-P Bouchaud. Multiple scaling regimes in simple aging models. *Phys. Rev. Lett.*, 84(23):5403–5406, 2000.

[SE] P Sollich and M R Evans (unpublished).

[SE99] P Sollich and M R Evans. Glassy time-scale divergence and anomalous coarsening in a kinetically constrained spin chain. *Phys. Rev. Lett.*, 83(16):3238–3241, 1999.

[SLHC97] P Sollich, F Lequeux, P Hébraud, and M E Cates. Rheology of soft glassy materials. *Phys. Rev. Lett.*, 78:2020–2023, 1997.

[SN99] M Sasaki and K Nemoto. Aging phenomena of magnetization in a hierarchical diffusion model. *J. Phys. Soc. Jpn.*, 68(4):1148–1161, 1999.

[Sol] P Sollich (unpublished).

[Sol98] P Sollich. Rheological constitutive equation for a model of soft glassy materials. *Phys. Rev. E*, 58:738–759, 1998.

[Str78] L C E Struik. *Physical aging in amorphous polymers and other materials.* Elsevier, Houston, 1978.

[VMC96] V M Vinokur, M C Marchetti, and L W Chen. Glassy motion of elastic manifolds. *Phys. Rev. Lett.*, 77(9):1845–1848, 1996.

[VMMWM98] W Van Megen, T C Mortensen, S R Williams, and J Muller. Measurement of the self-intermediate scattering function of suspensions of hard spherical particles near the glass transition. *Phys. Rev. E*, 58(5):6073–6085, 1998.

[WBHA92] D Weaire, F Bolton, T Herdtle, and H Aref. The effect of strain upon the topology of a soap froth. *Phil. Mag. Lett.*, 66(6):293–299, 1992.

[WDC85] D A Weitz, W D Dozier, and P M Chaikin. Periodic structures in driven colloidal crystals. *J Phys-Paris*, 46(C3):257–268, 1985.

[WF94] D Weaire and M A Fortes. Stress and strain in liquid and solid foams. *Adv. Phys.*, 43(6):685–738, 1994.

[YO98] R Yamamoto and A Onuki. Dynamics of highly supercooled liquids: heterogeneity, rheology, and diffusion. *Phys. Rev. E*, 58(3 PtB):3515–3529, 1998.

Aging and rheology in soft materials

S. M. Fielding[a)]

Department of Physics and Astronomy, University of Edinburgh, JCMB, King's Buildings, Mayfield Road, Edinburgh EH9 3JZ, Great Britain

P. Sollich

Department of Mathematics, King's College, University of London, Strand, London WC2R 2LS, Great Britain

M. E. Cates

Department of Physics and Astronomy, University of Edinburgh, JCMB, King's Buildings, Mayfield Road, Edinburgh EH9 3JZ, Great Britain

(Received 7 July 1999; final revision received 18 November 1999)

Synopsis

We study theoretically the role of aging in the rheology of soft materials. We define several generalized rheological response functions suited to aging samples (in which time translation invariance is lost). These are then used to study aging effects within a simple scalar model (the "soft glassy rheology" or SGR model) whose constitutive equations relate shear stress to shear strain among a set of elastic elements, with distributed yield thresholds, undergoing activated dynamics governed by a "noise temperature," x. (Between yields, each element follows affinely the applied shear.) For $1 < x < 2$ there is a power-law fluid regime in which transients occur, but no aging. For $x < 1$, the model has a macroscopic yield stress. So long as this yield stress is not exceeded, aging occurs, with a sample's apparent relaxation time being of order its own age. The (age-dependent) linear viscoelastic loss modulus $G''(\omega,t)$ rises as frequency is *lowered*, but falls with age t, so as to always remain less than $G'(\omega,t)$ (which is nearly constant). Significant aging is also predicted for the stress overshoot in nonlinear shear startup and for the creep compliance. Though obviously oversimplified, the SGR model may provide a valuable paradigm for the experimental and theoretical study of rheological aging phenomena in soft solids. © *2000 The Society of Rheology.* [S0148-6055(00)00102-4]

I. INTRODUCTION

Many soft materials, such as foams, dense emulsions, pastes and slurries, display intriguing features in their low frequency shear rheology. In oscillatory shear, for example, their viscoelastic storage and loss moduli, $G'(\omega)$ and $G''(\omega)$, are often weak power laws of shear frequency [Mackley *et al.* (1994); Ketz *et al.* (1988); Khan *et al.* (1988); Mason *et al.* (1995); Panizza *et al.* (1996); Hoffman and Rauscher (1993); Mason and Weitz (1995)], while their nonlinear stress response σ to shear strain of constant rate $\dot{\gamma}$ is often fit to the form $\sigma = A + B\dot{\gamma}^n$ (known as the Herschel–Bulkley equation, or

a)Author to whom all correspondence should be addressed.

when $A = 0$, the power-law fluid) [Holdsworth (1993); Dickinson (1992); Barnes *et al.* (1989)]. The fact that such a broad family of soft materials exhibits similar rheological anomalies is suggestive of a common cause, and it has been argued that these anomalies are symptomatic of the generic presence in such materials of slow, glassy dynamics [Sollich *et al.* (1997); Sollich (1998)]. Indeed, all the above materials share features of structural disorder and metastability: large energy barriers impede reorganization into states of lower free energy because this would require rearrangement of local structural units, such as the droplets in a dense emulsion. The term "soft glassy materials" (SGMs) has been proposed to describe such materials [Sollich *et al.* (1997); Sollich (1998)].

Glassy dynamics are often studied using hopping (trap) models, in which single particle degrees of freedom hop by an activated dynamics, in an uncorrelated manner, through a random free energy landscape [Bouchaud (1992); Monthus and Bouchaud (1996)]. By incorporating strain degrees of freedom into such a description, Sollich and co-workers [Sollich *et al.* (1997); Sollich (1998)] proposed a minimal model, called the "soft glassy rheology" (SGR) model, which appears to capture several of the rheological properties of SGMs, although (for simplicity) all the tensorial aspects of viscoelasticity are discarded. The model exhibits various regimes depending on a parameter x (discussed in more detail below) representing the "effective temperature" for the hopping process. When this is small ($x \leqslant 1$) the model exhibits a glass phase which shows some interesting properties above and beyond the power-law anomalies in viscoelasticity mentioned above. Specifically, the model shows *aging behavior*: its properties depend on the elapsed time since a sample was prepared. This is because the population of traps visited never achieves a steady state; as time goes by, deeper and deeper traps dominate the behavior (a phenomenon known as "weak ergodicity breaking"). Broadly speaking, the system behaves as though its longest relaxation time is of order its own age.

The success of the SGR model in accounting for some of the generic flow properties of SGMs suggests that a detailed investigation of its aging behavior, and the effect this has on rheology, is now worthwhile. Aging has been intensively studied in the context of spin glasses [Bouchaud and Dean (1995); Cugliandolo and Kurchan (1995); Cugliandolo *et al.* (1997a); Bouchaud *et al.* (1998)], although some of the earliest experimental investigations of it involved rheological studies of glassy polymers [Struik (1978)]. But we know of no previous theoretical work that explores the link between aging phenomena and rheological properties within an explicit constitutive model. Although various kinds of aging effects are often observable experimentally in soft materials, they have rarely been reported in detail. Instead they tend to be regarded as unwanted obstacles to observing the "real" behavior of the system, and not in themselves worthy of study. But this may be illusory: aging, when present, can form an integral part of a sample's rheological response. For example, the literature contains many reports of viscoelastic spectra in which the loss modulus $G''(\omega)$, while remaining less than the (almost constant) storage modulus $G'(\omega)$ in a measured frequency window, appears to be increasing as frequency is lowered (see Fig. 1, bold lines). The usual explanation [e.g., Kossuth *et al.* (1999)] is that some unspecified relaxation process is occurring at a lower frequency still, giving a loss peak (dashed), whose true nature could be elucidated if only the frequency window was extended. This may often be the case, but an alternative explanation, based on our explicit calculations for the SGR model, is shown by the thin solid lines in Fig. 1, representing subsequent observations in a wider frequency window. No oscillatory measurement can probe a frequency far below the reciprocal of the sample's age; yet in aging materials, it is the age itself which sets the relaxation time of whatever slow relaxations are present. Accordingly, the putative loss "peak" can never be observed and is, in fact,

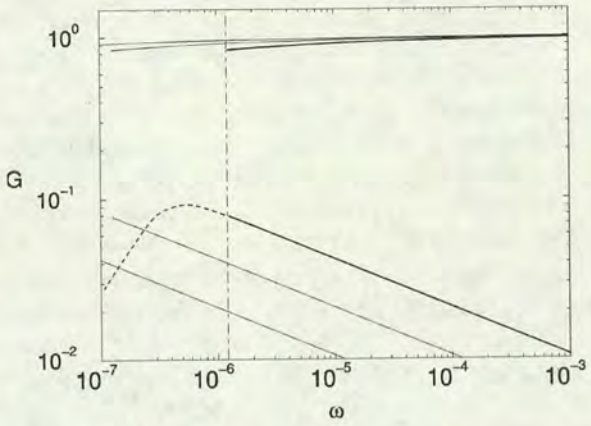

FIG. 1. Sketch of aging scenario for dynamic moduli G' (top) and G'' (bottom). Thick and thin solid lines: initial spectrum and two subsequent ones: (dashed) putative loss peak; (dot-dashed) limit to frequency window set initially by sample age. (In fact, the solid lines are calculated from the SGR model at noise temperature $x = 0.7$; see Sec. VI A 2).

a complete figment of the imagination. Instead, a rising curve in $G''(\omega)$ at low frequencies will *always* be seen, but with an amplitude that decreases as the system gets older [typically ensuring that $G''(\omega)$ never exceeds $G'(\omega)$]. Of course, we do not argue that all published spectra resembling those of Fig. 1 should be interpreted in this way; but we believe that many should be. A reluctance to acknowledge the role of aging effects in parts of the rheological literature suggests that a full discussion of these could now be valuable. An exception has been in the literature on aging in polymeric glasses, especially the monograph by Struik (1978): we return shortly to a brief comparison between that work and ours. In the area of structural glasses, aging effects have also been investigated under the name of "structural relaxation" or "stabilization" [Scherer (1986)]. They have been interpreted mainly using phenomenological "effective time theories," which are likewise discussed below.

The SGR model is simple enough to allow a fairly full exploration of the link between aging and rheology. As well as providing some quantitative predictions of rheological aging, this allows a broader discussion of the conceptual framework within which rheological data for aging systems should be analyzed and interpreted. This conceptual framework is broader than the SGR model itself; for example it is known that aging concepts developed for spin-glass dynamics can also be applied to problems of domain-growth and coarsening [Bouchaud *et al.* (1998)]. Many soft solids, such as polydomain defect textures in ordered mesophases of copolymers or surfactants, may show aging through such coarsening dynamics, or through glassy rearrangement of domains, or both. While the SGR model is intended to address only the second feature, the conceptual framework we present can allow for both mechanisms [in which case a superposition of aging dynamics with different timescales may result; see Eq. (20) below].

Thus we begin in Secs. II and III by briefly introducing rheology and aging respectively. Then in Sec. IV we review the SGR model, and discuss the origin of its glass transition and the nature of the glass phase. We also briefly describe its rheology under nonaging conditions; this is discussed fully elsewhere [Sollich *et al.* (1997); Sollich (1998)]. In Sec. V we give a general discussion of aging within the SGR model, which sets the stage for our new results for the linear and nonlinear rheological response of the SGR model in regimes where aging cannot be neglected. The results for controlled strain

conditions are presented and discussed in Sec. VI; those for controlled stress, in Sec. VII. We close in Sec. VIII with a brief summary and our conclusions.

We now discuss the connection between our work and that of Struik (1978) on polymeric glasses. Struik presented many experimental results for such systems, and gave a coherent qualitative explanation of their aging in terms of a slow relaxation of the free volume in the system below the glass point. However, he did not propose a model constitutive equation for this or any other class of aging material. He argued that the effective relaxation time of a system of age t_w (the "waiting time" since sample preparation) varies as $\tau(t_w) = t_w^{\mu}\tau_0^{1-\mu}$, where τ_0 is a microscopic time and $\mu \simeq 1$; apart from this uniform rescaling of (all) the rheological relaxation time(s), the material properties are almost invariant in time. (This is his "time waiting–time superposition" principle; we show below that the SGR model offers a concrete example of it, with $\mu = 1$.) We do not expect the SGR model, which makes no mention of the free-volume concept, to be particularly relevant to polymeric glasses; nonetheless, various points of contact with Struik's work are indicated below.

As mentioned above, aging effects have also been studied in structural glasses; see Scherer (1986) for a comprehensive review, or Larson (1999) for a more recent summary. In this field, aging is often referred to as structural relaxation or stabilization, and phenomenological theories have been developed to describe this process. A common ingredient is the assumption that deviations from time translation invariance during aging can be captured by replacing time differences $t-t'$ by differences in an "effective time" $\xi(t)$ [Hopkins (1958)]

$$t-t' \rightarrow \xi(t)-\xi(t'), \quad \xi(t) = \int_0^t \frac{dt'}{\tau_r(t')}, \tag{1}$$

where $\tau_r(t)$ is an age-dependent relaxation timescale. An additional hypothesis for the evolution of $\tau_r(t)$ is then needed; a popular approach [Gardon and Narayanaswamy (1970); Narayanaswamy (1971)] is to describe the current state of the sample in terms of a "fictive temperature" T_f and then to postulate coupled dynamical equations for $\tau(t)$ and $T_f(t)$. This procedure appears to be particularly successful in rationalizing the properties of glasses subject to complicated temperature histories involving cooling and heating; for further details, we refer the reader to the book by Scherer (1986). In our general discussion of aging in Sec. III, we will see that the effective time $\xi(t)$ is closely related to what we will there call an aging timescale. Note however that it is different from the effective time *interval* $Z(t,t')$ introduced below in the context of the SGR model.

II. RHEOLOGY

Here we review the basic principles of rheology. Unlike most in the literature, our formulation does not assume time translational invariance (TTI); parts of it may therefore be unfamiliar, even to rheologists. The formalism allows in principle an arbitrary dependence of the material properties on time; we defer to Sec. III a discussion of what form this dependence might take in materials which exhibit aging effects (rather than other, more trivial time dependencies).

A. Constitutive properties

In general, deformation can comprise volume changes, extensional strain, and shear strain; here we consider incompressible materials and assume that only shear strains arise. A system's shear stress $\sigma(t)$ then depends functionally on its strain rate history $\dot{\gamma}(t' < t)$, where $\dot{\gamma}$ is the strain rate. Conversely, $\gamma(t)$ can be expressed as a functional

of the preceding stress history. A specification of either type is referred to as a *constitutive equation*. In general, of course, the constitutive equation is a relationship between stress and strain *tensors*; see Doi and Edwards (1986) for an introduction. We ignore the tensorial aspects here, because the model we describe later is too simple to address them.

B. Step strain

A standard rheological test consists of suddenly straining a previously undeformed material by an amount γ_0. Suppose this to be done at time t_w: then $\gamma(t) = \gamma_0\Theta(t - t_w)$, where Θ is the usual step function. (For the moment, t_w is an arbitrary time label, but later we will take it as the time that the strain is applied, relative to the preparation of the sample in some prescribed state, at time zero.) The subsequent stress can be written

$$\sigma(t) = \gamma_0 G(t-t_w, t_w; \gamma_0) \tag{2}$$

thereby defining the step strain response, $G(t-t_w, t_w; \gamma_0)$.

C. Linearity

In the small deformation limit ($\gamma_0 \to 0$), a regime may exist for which σ is linearly related to γ_0:

$$\lim_{\gamma_0 \to 0} G(t-t_w, t_w; \gamma_0) = G(t-t_w, t_w). \tag{3}$$

The system's stress response is then linearly proportional to strain amplitude, in the sense that doubling the strain at all earlier times will cause the current stress to be doubled. Under these conditions, by decomposing the applied strain $\gamma(t)$ into a series of infinitesimal steps, one finds that

$$\sigma(t) = \int_{-\infty}^{t} G(t-t', t')\dot{\gamma}(t')\, dt', \tag{4}$$

which represents the most general (nontensorial) linearized constitutive equation. Note that there is no unique extension of this to the nonlinear case: the response to an arbitrary flow cannot in general be written solely in terms of $G(t-t_w, t_w; \gamma_0)$, although this is assumed for certain constitutive models [Bernstein *et al.* (1963)].

If the material exhibits TTI, then $G(t-t_w, t_w; \gamma_0)$ can be written $G(t-t_w; \gamma_0)$—it depends only on the elapsed time since the step strain was imposed. Only by assuming *both* linearity and TTI do we obtain

$$\sigma(t) = \int_{-\infty}^{t} G(t-t')\dot{\gamma}(t')\, dt', \tag{5}$$

where $G(t-t_w)$ is the linear step–strain response as usually defined. In the steady state (constant $\dot{\gamma}$) one recovers:

$$\sigma = \dot{\gamma}\int_0^{\infty} G(t'')dt''. \tag{6}$$

The integral, whenever it exists, defines the material's zero-shear viscosity η. For many soft materials, however, $G(t)$ decays to zero so slowly that the integral diverges. In this case, there can be no regime of linear response in steady shear flow, although there may be a linear regime in, say, oscillatory shear.

D. Behavior of the linear response function

The principle of causality demands that the response function $G(t-t_w,t_w)$ is zero for times $t < t_w$. At $t = t_w$, G typically increases very rapidly (in effect discontinuously) to a value G_0, the instantaneous elastic modulus. Thereafter, $G(t-t_w,t_w)$ is (almost always) a decaying function of its first argument. Specializing to the TTI case, we recall that for a purely Newtonian liquid of viscosity η, the function $G(t)$ approaches a delta function $\eta\delta(t)$, whereas an ideally Hookean elastic solid has $G(t) = G_0$. [Note that properly one should write $G(t) = G_0\Theta(t)$; the extra factor of $\Theta(t)$, implied by causality, is omitted here and below.]

Most real materials display intermediate behavior and are thus *viscoelastic*; for the soft materials of interest here, the timescale of the viscoelasticity is readily observable in rheological experiments. The simplest (TTI) example is the Maxwell fluid, which is solid-like at short times and liquid at longer ones, with a simple exponential response function $G(t) = G_0 \exp(-t/\tau)$ connecting the two (so that $\eta = G_0\tau$). This behavior is seen in a few experimental systems [Cates and Candau (1990)], but $G(t)$ is usually not an exponential. In many materials it is possible to identify a longest relaxation time via $\tau_{\max}^{-1} = -\lim_{t\to\infty} \log G(t)/t$. However, in some important cases, for example that of a relaxation which decays asymptotically as a power law, $G(t) \sim t^{-y}$, the required limit does not exist, and the longest relaxation time is infinite.

E. Creep compliance

Arguing along parallel lines to those developed above, we can write the strain response to a step stress $\sigma(t) = \sigma_0\Theta(t-t_w)$ as

$$\gamma(t) = \sigma_0 J(t-t_w,t_w;\sigma_0). \tag{7}$$

The linear creep compliance $J(t-t_w,t_w)$ is then found by letting $\sigma_0 \to 0$ (assuming this limit exists).

For a system exhibiting TTI, the linear compliance reduces to a function of elapsed time, $J(t-t_w)$. (For a viscous liquid, an elastic solid, and a Maxwell material we have $J(t) = t/\eta$, $J(t) = 1/G_0$, and $J(t) = 1/G_0 + t/\eta$, respectively.) The zero-shear viscosity η can then be defined as the limiting ratio of stress to strain rate long after application of an infinitesimal step stress; it therefore obeys $\eta^{-1} = \lim_{t\to\infty} dJ(t)/dt$, which may be shown to be equivalent to Eq. (6) whenever the required limit exists (see also Sec. II G).

F. Viscoelastic spectra

A common experiment is to apply a steady oscillatory strain and measure the resulting stress, or vice versa. For example, suppose that an aging sample is prepared in a known state at time zero. The choice

$$\gamma(t) = \Theta(t-t_s)\mathrm{Re}[\gamma_0 e^{i(\phi+\omega t)}] \tag{8}$$

then describes an oscillatory flow started at time t_s after sample preparation, and continued up to (at least) the time t at which the stress is measured. For small enough γ_0, we can use the linear constitutive equation (4) to obtain

$$\sigma(t) = \mathrm{Re}\left[\gamma_0 i\omega \int_{t_s}^{t} e^{i(\phi+\omega t')} G(t-t',t')\,dt' + \gamma_0 e^{i(\phi+\omega t_s)} G(t-t_s,t_s)\right]$$

$$\equiv \mathrm{Re}[\gamma_0 e^{i(\phi+\omega t)} G^*(\omega,t,t_s)], \tag{9}$$

where the second term in Eq. (9) accounts for any step strain arising at the switch-on time t_s. This procedure defines a *time-varying* viscoelastic spectrum as

$$G^*(\omega,t,t_s) = i\omega \int_{t_s}^{t} e^{-i\omega(t-t')} G(t-t',t')\, dt' + e^{-i\omega(t-t_s)} G(t-t_s,t_s). \tag{10}$$

A similar compliance spectrum, $J^*(\omega,t,t_s)$ can be defined by exchanging stress and strain in this protocol.

Note that in principle, to identify by experiment the real and imaginary parts of G^* for given ω,t,t_s one would require the experiment to be repeated for two different phases ϕ (e.g., pure sine and cosine deformations). A more common procedure for TTI systems is to maintain the oscillatory strain over many cycles and record the "steady state" amplitude and phase response of the stress. However, in systems without TTI this will only give a unique result when material properties vary slowly enough; whenever it does, it will coincide with Eq. (10).

Since it depends on two time arguments as well as frequency, $G^*(\omega,t,t_s)$ is a cumbersome object. However, simplifications arise in the limit $\omega(t-t_s) \gg 1$.

1. Viscoelastic spectra in TTI case

In the TTI case, where $G^*(\omega,t,t_s)$ depends only on the time interval $t-t_s$, the further condition $\omega(t-t_s) \gg 1$ can be used to eliminate simple transients. The stress then settles to a simple harmonic function of time and we can write $\sigma(t) = \mathrm{Re}[G^*(\omega)\gamma(t)]$ where

$$G^*(\omega) = i\omega \int_0^{\infty} e^{-i\omega t} G(t)\, dt. \tag{11}$$

[Note that if $G(t)$ has a nondecaying contribution $G(t \to \infty) > 0$, the form $G^*(\omega) = G(0) + \int_0^{\infty} e^{-i\omega t} G'(t)\, dt$, derived from Eq. (9) by integration by parts, should be used instead of Eq. (11).] Traditionally one writes $G^*(\omega) = G'(\omega) + iG''(\omega)$ where G', G'', the storage and loss moduli, give the in-phase (elastic) and out-of-phase (dissipative) response to an applied strain.

Clearly one can reach an identical steady state by applying a small amplitude oscillatory stress and measuring the resulting strain. This defines, for the TTI case, a complex compliance $J^*(\omega)$ via $\gamma(t) = \mathrm{Re}[J^*(\omega)\sigma(t)]$, which is just the reciprocal of $G^*(\omega)$. But by an argument similar to that given above for Eq. (11) one also has $J^*(\omega) = i\omega \int_0^{\infty} e^{-i\omega t} J(t)\, dt$. Hence, within the linear response regime of a system with TTI, knowledge of any one of $G(t), J(t), G^*(\omega), J^*(\omega)$ is enough to determine the other three.

2. Viscoelastic spectra without TTI

A similar set of simplifications are certainly not guaranteed in the absence of TTI. However, the transient dependence on t_s *may* become negligible when $\omega(t-t_s) \gg 1$, in which case we have

$$G^*(\omega,t,t_s) \to G^*(\omega,t) \tag{12}$$

giving a viscoelastic spectrum that depends only on the measurement time t. If, in addition, the time evolution of the underlying material properties is negligible on the timescale of one oscillation, then $G^*(\omega,t)$ *may* obey the relation

$$G^*(\omega,t) = i\omega \int_0^\infty e^{-i\omega t'} G(t',t)\, dt'. \tag{13}$$

Similarly, for $\omega(t-t_s) \gg 1$ the compliance spectrum *may* become t_s independent, $J^*(\omega,t,t_s) \to J^*(\omega,t)$, and *may* be related to the step stress response via

$$J^*(\omega,t) = i\omega \int_0^\infty e^{-i\omega t'} J(t',t)\, dt'. \tag{14}$$

Finally, $G^*(\omega,t)$ and $J^*(\omega,t)$ *may* obey the usual reciprocal relation $G^*(\omega,t) = 1/J^*(\omega,t)$. Indeed, we shall find that all the above simplifying relationships are true for the SGR model (subject to an additional requirement that $\omega t_s \gg 1$; see Sec. VI A2). As discussed at the end of Sec. III, they may also hold more generally for systems with "weak long term memory." However, we do not have a proof for this; experimenters and theorists alike should beware that, for systems without TTI, such textbook relationships between the oscillatory and step strain response functions cannot be assumed, but should be verified, for each system studied. This *prima facie* breakdown of conventional linear viscoelastic relationships in aging systems was emphasized by Struik (1978), though he argued that they are recovered in sufficiently "short-time" measurements. It does not (as Struik seems to suggest) extend necessarily to breakdown of linear superposition itself, which survives in the form of Eq. (4). In fact, breakdown of TTI is a quite separate issue from nonlinearity; neither implies the other.

G. Steady state response: the flow curve

Consider now the ultimate state of a material, with TTI, long after an infinitesimal step stress of amplitude σ_0 has been applied. The ultimate deformation may involve a limiting strain $\gamma = \sigma_0 J(t \to \infty)$, in which case the steady state elastic modulus is $G_\infty = \sigma_0/\gamma$. Alternatively, it may involve a limiting strain rate, in which case the zero-shear viscosity is $\eta = \sigma_0/\dot{\gamma}$. However, neither outcome need occur. If, for example, one has "power law creep," i.e., $J(t) \sim t^y$ with $0 < y < 1$, the material has both zero modulus (infinite compliance) and infinite viscosity in steady state. (This requires that $\tau_{\max}$ is infinite.)

What if the stress amplitude is larger than infinitesimal? The ultimate steady state can again be that of a solid, a liquid, or something in between. When a liquid-like response is recovered, it is conventional to measure the "flow curve," or steady state relationship between stress and strain rate: $\sigma_{ss} = \sigma(\dot{\gamma})$. In many materials, the following limit, called the yield stress

$$\sigma(\dot{\gamma} \to 0) = \sigma_y \tag{15}$$

is nonzero. (The experimental existence of a true yield stress, in this sense, is debatable [Barnes *et al.* (1989)], although behavior closely approaching it is often reported.)

The presence of nonzero yield stress does not necessarily imply a finite Hookean modulus G_∞: for $\sigma < \sigma_y$, the material could creep forever, but at an ever decreasing rate. (Alternatively, it could reach a steady strain γ that is not linear in σ even as $\sigma \to 0$.) Nor does the *absence* of a finite yield stress imply a finite viscosity; a counter-

example is the power law fluid, for which $\sigma \sim \dot{\gamma}^p$. This has $\sigma_y = 0$ but, for $p < 1$, infinite viscosity $\eta = \lim_{\dot{\gamma} \to 0} \sigma(\dot{\gamma})/\dot{\gamma}$.

What about the flow curve for materials without TTI? For these, no meaningful definition of "steady state response" exists in general. However, in the SGR model considered below, TTI is restored for nonzero $\dot{\gamma}$ [Sollich *et al.* (1997); Sollich (1998)], and this may be generic for certain types of aging [Sollich *et al.* (1997); Sollich (1998); Bouchaud and Dean (1995); Kurchan (1998)]. If so the flow curve, including the value of the yield stress σ_y (but *not* the behavior for $\sigma < \sigma_y$) remains well defined.

III. AGING

So far, we have set up a general framework for describing the rheological properties of systems without TTI. Time translation invariance can be broken, in a trivial sense, by the transients that any system exhibits during equilibration. We now consider how such transients can be distinguished from aging proper. To focus the discussion, we consider the linear step strain response function $G(t-t_w,t_w)$. The other response functions introduced above can be treated similarly. We define aging (of the step strain response) as the property that *a significant part of the stress relaxation takes place on timescales that grow with the age t_w of the system.* If aging is present, then in order to see the full stress relaxation we need to allow the time t at which we observe the stress to be much larger than the time t_w at which the step strain has been applied. Formally, we need to consider

$$\lim_{t \to \infty} G(t-t_w,t_w) \tag{16}$$

at *fixed* t_w. On the other hand, if there is no aging, then the full stress relaxation is "visible" on finite timescales. This means that as long as $\Delta t = t-t_w$ is large enough, we observe the full stress relaxation whatever the age t_w of the system at the time when the strain was applied. Formally, we can take t_w to infinity first, and then make Δt large, which amounts to considering

$$\lim_{\Delta t \to \infty} \lim_{t_w \to \infty} G(\Delta t,t_w). \tag{17}$$

In the absence of aging, the two ways, Eqs. (16) and (17), of measuring the final extent of stress relaxation are equivalent, and we have

$$\lim_{t \to \infty} G(t-t_w,t_w) = \lim_{\Delta t \to \infty} \lim_{t_w \to \infty} G(\Delta t,t_w). \tag{18}$$

If the system ages, on the other hand, this equality will not hold: the right-hand side allows only for the decay of stress by relaxation modes whose timescale does not diverge with the age of the system, and thus attains a limit which includes elastic contributions from all modes that do have age-related timescales. It will be different from the left-hand side, which allows for relaxation processes occurring on all timescales, and thus attains a limit in which only completely nondecaying modes contribute. We therefore adopt the definition that a system *ages* if at least one of its response functions violates Eq. (18). By contrast, we refer to deviations from TTI in other systems (for which all significant relaxation processes can essentially be observed on finite timescales) as *transients*. We discuss this point further in the context of the SGR model in Sec. VI A 1.

Systems that violate Eq. (18) are said to have "long term memory" [Cugliandolo and Kurchan (1995); Bouchaud *et al.* (1998); Cugliandolo and Kurchan (1993)]. They can be further subdivided according to the strength of this memory. To illustrate this distinction,

imagine applying a (small) step strain to a system at time t_0 and switching it off again at some later time t_1. The corresponding stress at time $t > t_1$ is proportional to $G(t-t_0,t_0)-G(t-t_1,t_1)$. If this decays to zero at large times t, that is, if

$$\lim_{t \to \infty} [G(t-t_0,t_0)-G(t-t_1,t_1)] = 0 \tag{19}$$

[and Eq. (18) is violated] then we say that the system has "weak long term memory," otherwise it has "strong long term memory." [There is a slight subtlety with the definition of long term memory for the linear step stress response. Equation (19), applied literally to $J(t-t_w,t_w)$, suggests that even a Newtonian fluid with $J(t-t_w,t_w) \sim t-t_w$ has strong long term memory, because its strain "remembers" stress applications in the arbitrarily distant past. This is clearly undesirable as a definition. The problem can be cured by "regularizing" the step stress response: one simply considers the material in question "in parallel" with an elastic spring with infinitesimal modulus.] Although the weakness condition, Eq. (19), does not hold for all response functions in all aging systems, it seems rather natural to expect it, in the rheological context, for most materials of interest. Indeed, a system with *weak* long term memory eventually forgets any perturbation that was only applied to it during a finite period. Thus, the treatment of a sample directly after it has been prepared (by loading it into the rheometer, preshearing, etc.) will not have a strong impact on the age dependence of its rheological properties. This is the usual experience, and is obviously needed for the reproducibility of experiments results; likewise, it means that one can hope to make theoretical predictions which are not sensitive to minute details of the sample preparation. For the SGR model, any long term memory is indeed weak (as shown in Sec. VI A 1); we consider this an attractive feature. Note in any case that a rheological theory for systems with strong long term memory might look very different from the SGR model.

We have defined aging as the property that a significant part of the stress relaxation $G(t-t_w,t_w)$ takes place on timescales that grow with the age t_w of the system. In the simplest case, there is only one such growing timescale, proportional to the age of the system itself. The (aging part of the) stress relaxation then becomes a function of the scaled time difference $(t-t_w)/t_w$. We will encounter such simple aging behavior in the glass phase of the SGR model, which is discussed below. More complicated aging scenarios are possible, however: There may be several timescales that grow differently with the age of the system. This can be represented as

$$G(t-t_w,t_w) = \sum_i \mathcal{G}_i[h_i(t)/h_i(t_w)], \tag{20}$$

where the functions $h_i(t)$ define the different diverging timescales. If there is only a single term in the sum, with $h(t) = t$, then the simplest aging scenario (shown by the SGR model) is recovered. To see that Eq. (20) also includes TTI and intermediate aging scenarios, it is useful to rewrite it in the form

$$G(t-t_w,t_w) = \sum_i \tilde{\mathcal{G}}_i[\xi_i(t)-\xi_i(t_w)], \tag{21}$$

where $\xi_i = \ln h_i$ and $\tilde{\mathcal{G}}_i(\ln h) = \mathcal{G}_i(h)$. For $\xi(t) = t/\tau_0$, corresponding to $h(t) = \exp(t/\tau_0)$ (where τ_0 is a microscopic time), one has TTI. More generally, $\xi(t) = (t/\tau_0)^{1-\mu}$ interpolates between TTI for $\mu = 0$ and simple aging [$h(t) = t$, $\xi(t)$

$\sim \ln t]$ for $\mu \to 1$. In the regime of short time differences ($t - t_w \ll t_w$), one then finds that the response function depends on

$$\xi(t) - \xi(t_w) = \frac{1-\mu}{\tau_0^{1-\mu}} \frac{t-t_w}{t_w^{\mu}}. \tag{22}$$

Ignoring the irrelevant prefactor, one thus recovers Struik's general "time waiting–time superposition principle" [Struik(1978)].

Equation (21) provides an interesting point of contact with the effective time theories for aging effects that we mentioned briefly in Sec. I. In fact, if we define an age-dependent relaxation timescale by

$$\frac{1}{\tau_r} = \frac{d\xi}{dt} = \frac{d \ln h}{dt},$$

then each term in the sum over i in Eq. (21) has exactly the form postulated by the effectime time approach [compare Eq. (1)]. For simple aging, we have $h(t) = t$ and $\xi(t) = \ln t$, giving $\tau_r(t) = t$ as expected: The relaxation timescale is proportional to the age of the system. For TTI, on the other hand, $\xi(t) = t/\tau_0$ and so $\tau_r(t) = \tau_0$ is independent of time, again as expected. The form $\xi(t) = (t/\tau_0)^{1-\mu}$ interpolates between these limits, with $\tau_r(t) \sim t^{\mu}$. In general, we can interpret Eq. (21) as a generalization of the effective time approach to the case where different effective times $\xi_i(t)$ are needed to describe the aging behavior of the system. This is not merely a phenomenological model, however: Cugliandolo and Kurchan(1994) have shown under fairly mild assumptions that Eq. (20) is the most general representation of the asymptotic behavior of step response and correlation functions in systems with weak long term memory.

To avoid misunderstandings, we emphasize that Eq. (21) only describes how the stress relaxation of the system depends on its age t_w at the time when a step strain is applied. It does not determine the "shape" of the relaxation, which is encoded by the functions $\tilde{\mathcal{G}}_i$. In aging systems, one expects a broad relaxation time spectrum centered around the timescale τ_r, corresponding to nonexponential $\tilde{\mathcal{G}}$. A popular representation is the stretched exponential $\tilde{\mathcal{G}} \sim \exp(-\xi^{\beta})$, which for $\xi(t) = (t/\tau_0)^{1-\mu}$ would correspond to a stress relaxation of the form

$$G(t-t_w, t_w) \sim \exp\left[-\frac{(t^{1-\mu} - t_w^{1-\mu})^{\beta}}{\tau_0^{\beta(1-\mu)}} \right].$$

Looking back at Eq. (22), we see that this would represent a crossover from a stretched exponential in $t - t_w$ with stretching exponent β for short times $t - t_w \ll t_w$ to one with stretching exponent $\beta(1-\mu)$ for long times.

Finally, let us return to the status of Eqs. (12), (13), and (14). [These concern the lack of t_s-dependence in $G^*(\omega, t, t_s)$, the Fourier relationship between frequency and real-time spectra, and the reciprocity between G^* and J^*.] As stated in Sec. II F 2 these equations have no general validity for systems without TTI. Indeed, one can easily construct theoretical model systems with *strong* long term memory which violate them. On the other hand, we speculate that systems with *weak* long term memory will generically have the properties of Eqs. (12), (13) and (14).

IV. THE SGR MODEL

The phenomenological SGR model captures many of the observed rheological properties of soft metastable materials, such as foams, emulsions, slurries and pastes [Mackley *et al.* (1994); Ketz *et al.* (1988); Khan *et al.* (1988); Mason *et al.* (1995); Panizza *et al.* (1996); Hoffmann and Rauscher (1993); Mason and Weitz (1995)]. It is based upon Bouchaud's trap model of glassy dynamics, with the addition of strain degrees of freedom, and the replacement of the thermodynamic temperature by an effective (noise) temperature. It incorporates only those characteristics deemed common to all SGMs, namely structural disorder and metastability. We now review its essential features.

We conceptually divide a macroscopic sample of SGM into many mesoscopic elements. By mesoscopic we mean large enough such that the continuum variables of strain and stress still apply for deformations on the elemental scale, and small enough that any macroscopic sample contains enough elements to allow the computation of meaningful "averages over elements." We then assign to each element a local strain l, and corresponding stress kl, which describe deformation away from some local position of unstressed equilibrium relative to neighboring elements. The macroscopic stress of the sample as a whole is defined to be $\langle kl \rangle$, where $\langle\ \rangle$ denotes averaging over elements. Note that, for simplicity, (shear) stress and strain are treated as scalar properties. The model therefore does not predict, or allow for, the various normal stresses which can arise in real materials undergoing nonlinear shear [Doi and Edwards (1986)].

For a newly prepared, undeformed sample, we make the simplest assumption that $l = 0$ for each element. (Physically, of course, $\langle l \rangle = 0$ would be sufficient and is indeed more plausible.) The subsequent application of a macroscopic strain at rate $\dot{\gamma}$ causes each element to strain relative to its local equilibrium state and acquire a nonzero l. For a given element, this continues up to some maximal strain l_y, at which point that element yields, and rearranges into a new configuration of local equilibrium with local strain $l = 0$. This ignores possible "frustration" effects: an element may not be able to relax to a fully unstrained equilibrium position due to interactions with neighboring elements. (Such effects can be incorporated into the model, but are not expected to affect the results in a qualitative way [Sollich (1998)].) Under continued macroscopic straining, the yielded element now strains relative to its new equilibrium, until it yields again; its local strain (and stress) therefore exhibits a saw-tooth dependence upon time.

The simplest assumption to make for the behavior between yields is that $\dot{\gamma} = \dot{l}$: the material deformation is locally affine [Doi and Edwards (1986)]. Yield events apart, therefore, the SGR model behaves as an elastic solid of spring constant k. Yields confer a degree of liquidity by providing a mechanism of stress relaxation.

Although we have introduced yielding as a purely strain-induced phenomenon, we in fact model it as an "activated" process [Sollich *et al.* (1997); Sollich (1998)]. We assume that an element of yield energy $E = \frac{1}{2}kl_y^2$, strained by an amount l, has a certain probability for yielding in a unit time interval. We write this rate as τ^{-1}, where the characteristic yield time

$$\tau = \tau_0 \exp[(E - \tfrac{1}{2}kl^2)/x] \tag{23}$$

is taken to be the product of an attempt time and an activation factor which is thermal in form. This captures the strain-induced processes described above since any element strained beyond its yield point will yield exponentially quickly; but it also allows even totally unstrained elements to yield by a process of activation over the energy barrier E. These activation events mimic, within our simplified model, nonlinear couplings to other

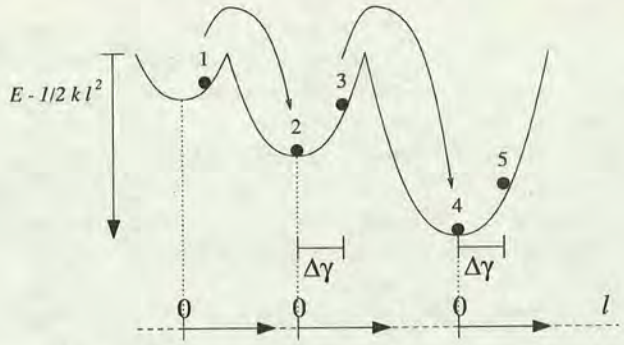

FIG. 2. Dynamics of the SGR model. A representative particle (1) may hop out of its trap by activated hopping ($1 \rightarrow 2$). It enters the new trap in a state of zero local strain ($l = 0$); application of strain $\Delta\gamma$ raises its energy ($2 \rightarrow 3$) making a subsequent hop ($3 \rightarrow 4$) more likely. Note that the horizontal position of the quadratic potential wells (traps) is arbitrary; each has its own independent zero for the scale of the local strain l.

elements (the barrier heights depend on the surroundings, which are altered by yield events elsewhere). A more complete model would treat these couplings explicitly. However, in the SGR model, which does not, x is regarded as an effective "noise" temperature to model the process. (Alternatively, we can think of x as the typical *energy* available for an activated process. We use units in which the Boltzmann constant $k_B = 1$ throughout, so there is no need to distinguish between these two interpretations of x as either a temperature or an energy.) Because the energy barriers are (for typical foams, emulsions, etc.) large compared to the thermal energy k_BT, so are the energy changes caused by these nonlinear couplings, and so to mimic these, one expects to need x of order the mean barrier height $\langle E \rangle$. Whether it is fully consistent to have a noise temperature $x \gg k_BT$ is a debatable feature of the model [Sollich *et al.* (1997); Sollich (1998)]; however, we think the results are sufficiently interesting to justify careful study of the model despite any uncertainty over its interpretation. (It is also intriguing to note that similar "macroscopic" effective temperatures, which remain nonzero even for $k_BT \rightarrow 0$, have recently been found in other theories of out-of-equilibrium systems with slow dynamics [Kurchan (1998); Cugliandolo *et al.* (1997b)].) Note that the SGR model treats "noise-induced" yield events (where the strain is much below the yield strain l_y, i.e., where $\frac{1}{2}kl^2 \ll E$) and "strain-induced" yield events (where $\frac{1}{2}kl^2 \approx E$) in a unified fashion. We will nevertheless find it useful below to distinguish between these two classes occasionally.

The disorder inherent to SGMs is captured by assuming that each element of a macroscopic sample has a different yield energy: a freshly yielded element is assigned a new yield energy selected at random from a "prior" distribution $\rho(E)$. This suggests the following alternative view of the dynamics of the SGR model, which is represented graphically in Fig. 2. Each material element of a SGM can be likened to a particle moving in a landscape of quadratic potential wells or "traps" of depth E. The depths of different traps are uncorrelated with each other and distributed according to $\rho(E)$. The bottom of each trap corresponds to the unstrained state $l = 0$; in straining an element by an amount l, we then effectively drag its representative particle a distance $\frac{1}{2}kl^2$ up the sides of the trap, and reduce the effective yield barrier height ($E \rightarrow E - \frac{1}{2}kl^2$). Once the particle has got sufficiently close to the top of its trap ($E - \frac{1}{2}kl^2 \approx x$), it can hop by activated dynamics to the bottom of another one. This process corresponds to the yielding of the associated material element. In the following, we shall use the terminology of both the "element picture" and the "particle picture" as appropriate. Thus, we will refer to

$\tau = \tau_0 \exp[(E - \frac{1}{2}kl^2)/x]$ as either the yield or relaxation time of an element, or as the lifetime of a (particle in) a trap or element. The inverse of τ is the rate at which an element yields/relaxes or a particle hops. However, we normally reserve the term "yield rate" or "hopping rate" for the *average* of these rates over the whole system, i.e., over all elements or particles. This quantity is denoted Y and will occur frequently below.

A specific choice of $\rho(E)$ is now made: $\rho(E) = (1/x_g)\exp(-E/x_g)$, where $x_g = \langle E \rangle$ is the mean height of a barrier chosen from the prior distribution $\rho(E)$. As shown by Bouchaud (1992), the exponential distribution, combined with the assumed thermal form for the activated hopping, is sufficient to give a glass transition in the model. The transition is at $x = x_g$ and divides the glass phase ($x \leq x_g$), in which weak ergodicity breaking occurs, from a more normal phase ($x > x_g$). In the glass phase, the Boltzmann distribution (which is the only possible steady state for activated hopping dynamics, in the absence of strain),

$$P_{\text{eq}}(E) \propto \rho(E)\exp(E/x) \tag{24}$$

is not normalizable: thus there is no steady state, and the system must age with time. (The converse applies for $x > x_g$: there is then a unique equilibrium state, which is approached at long times. Hence aging does not occur, though there may be transients in the approach to equilibrium.) Apart from our use of an effective temperature x, the only modification to Bouchaud's original model of glasses lies in our introduction of dynamics within traps coupled to strain.

It may appear suspicious that, to obtain a glass transition at all, an exponential form of $\rho(E)$ is required (though strictly, only for large E [Bouchaud (1992)]. In reality, however, the glass transition is certainly a collective phenomenon: the remarkable achievement of Bouchaud's model is to represent this transition within what is, essentially, a single-particle description. Thus the chosen "activated" form for the particle hopping rates, and the exponential form of the trap depth distribution, should not be seen as two independent (and doubtful) physical assumptions, but viewed jointly as a tactic that allows glassy dynamics to be modelled in the simplest possible way [Sollich *et al.* (1997); Sollich (1998)].

From now on, without loss of generality, we choose units so that both $x_g = k = 1$. This means that the strain variable l is defined such that an element, drawn at random from the prior distribution, will yield at strains of order one. Since the actual value of the strain variable can be rescaled within the model (the difference being absorbed in a shift of k), this is purely a matter of convention. But our choice should be borne in mind when interpreting our results for nonlinear strains, given below: where strains "of order unity" arise, these are in fact of order some yield strain l_y, which the model does not specify, but which may in reality be a few percent or less. In addition we choose by convention $\tau_0 = 1$; the timescale in the SGR model is scaled by the mesoscopic "attempt time" for the activated dynamics. The low frequency limit, which is the main regime of interest, is then defined by $\omega\tau_0 = \omega \ll 1$. Note that, with our choice of units, $\langle E \rangle = 1$ so that we expect the interesting physics to involve $x \simeq 1$.

A. Constitutive equation

The SGR model is exactly solved by two coupled constitutive equations [Sollich (1998)], the first of which expresses strain as an integral over stress history, while the second embodies the conservation of probability. We assume that the sample is prepared

(in a known initial state of zero stress and strain) at time zero and that a time dependent macroscopic strain $\gamma(t)$ is applied thereafter, so $\gamma(t) = 0$ for $t \leq 0$. The constitutive equations are then

$$\sigma(t) = \gamma(t)G_0(Z(t,0)) + \int_0^t [\gamma(t) - \gamma(t')]Y(t')G_\rho(Z(t,t'))dt' \tag{25}$$

$$1 = G_0(Z(t,0)) + \int_0^t Y(t')G_\rho(Z(t,t'))dt'. \tag{26}$$

In these equations

$$Z(t,t') = \int_{t'}^t \exp([\gamma(t'') - \gamma(t')]^2/2x)dt'', \tag{27}$$

while $Y(t')$ is the average yield rate at time t'. The functions $G_\rho(Z)$ and $G_0(Z)$ obey

$$G_\rho(Z) = \int_0^\infty \rho(E)\exp(-Ze^{-E/x})dE, \tag{28}$$

$$G_0(Z) = \int_0^\infty P_0(E)\exp(-Ze^{-E/x})dE, \tag{29}$$

where $P_0(E)$ is the probability distribution for the yield energies (or trap depths) in the initial state of preparation of the sample at time $t = 0$. We return below (Sec. V A) to the issue of how to choose this initial state.

These equations can be understood by viewing yielding as a "birth and death" process: each time an element yields it dies and is reborn with zero stress, and with a yield energy selected randomly from the prior distribution $\rho(E)$. The (average) yield rate at time t' is $Y(t')$; the birth rate at time t' of elements of yield energy E is therefore $Y(t')\rho(E)$. The proportion of these which survive without yielding until time t is found as $\exp[-Z(t,t')/\tau(E)]$ where $\tau(E) = \exp(E/x)$ is the (mean) lifetime that an unstrained element of yield energy E would have. The expression, Eq. (27), for $Z(t,t')$ reflects the fact that an element that last yielded at time t' and has a yield energy E will have a yield rate of $\tau(E)^{-1}\exp([\gamma(t'') - \gamma(t')]^2/2x)$ at time t''. Here the exponential factor accounts for the lowering of the yield barrier by strain applied since the element last yielded (see Fig. 2). Note that this factor is unity under conditions where the local strain is everywhere negligible, in which case $Z(t,t') \to t - t'$. More generally, $Z(t,t')$ can be thought of as an effective time interval measured on an "internal clock" within an element, which allows for the effect of local strain on its yield rate, by speeding up the clock. This speeding up effect, which describes strain-induced yielding, is the only source of nonlinearity within the SGR model. Note that this nonlinearity is not of the simple form of a strain-dependent effective time [see, e.g., Hodge (1995) and references therein], as comparison of Eq. (1) with Eq. (27) might at first suggest: The integrand in Eq. (27) is not just a function of the integration variable t'', but also of the inital time t'. More importantly, the nonlinear variation of $Z(t,t')$ with strain feeds back into the average yield rate $Y(t)$, and from there into the stress $\sigma(t)$, in a way that is nonlocal in time. This precludes any simple "effective time" interpretation of the SGR model as a whole: it does *not* obey Eq. (1).

According to the above arguments, the number of elements of yield energy E, present at time t, which were last reborn at time t' is

$$P(E,t,t') = Y(t')\rho(E)\exp[-Z(t,t')/\tau(E)]. \tag{30}$$

Such elements each carry a local strain $\gamma(t)-\gamma(t')$ and so the net contribution they make to the stress at time t is

$$s(E,t,t') = [\gamma(t)-\gamma(t')]Y(t')\rho(E)\exp[-Z(t,t')/\tau(E)]. \tag{31}$$

Integrating these expressions over t' from 0 to t and adding terms representing the contribution from elements which have survived from $t = 0$ without yielding at all, we get respectively the number $P(E,t)dE$ of elements at time t with yield energies between E and $E+dE$:

$$P(E,t) = P_0(E)\exp[-Z(t,0)e^{-E/x}] + \int_0^t P(E,t,t')dt' \tag{32}$$

and the corresponding stress contribution $s(E,t)dE$ at time t from such elements:

$$s(E,t) = \gamma(t)P_0(E)\exp[-Z(t,0)e^{-E/x}] + \int_0^t s(E,t,t')dt'. \tag{33}$$

Integrating Eqs. (32) and (33) over all yield energies E, we finally recover our constitutive equations (25) and (26), respectively. Below we will return to $P(E,t)$ and $s(E,t)$, which will sometimes be expressed instead as a function of the lifetime $\tau(E) = \exp(E/x)$ of an unstrained element with yield energy E, so that $P(\tau,t)d\tau = P(E,t)dE$ and likewise for s. Note that, because $E \geq 0$, these distributions are nonzero only for $\tau \geq 1$. We will not write this restriction explicitly below.

Finally, the following alternative form of the first constitutive equation (25) is sometimes useful:

$$\sigma(t) = \gamma(t) - \int_0^t \gamma(t')Y(t')G_\rho(Z(t,t'))dt'. \tag{34}$$

This is obtained by substituting Eq. (26) into Eq. (25).

B. Rheological properties of the SGR model

Solution of the constitutive equations (25), (26) is relatively straightforward under conditions where TTI applies. Here we recall the main results thereby obtained [Sollich *et al.* (1997); Sollich (1998)].

1. Linear spectra

A regime of linear rheological response arises whenever the effects of strain on the effective time interval $Z(t,t')$ are small. This requires that the local strains in each element remain small; in oscillatory shear, where $\gamma(t) = \gamma_0 e^{i\omega t}$, this is satisfied at low enough strain amplitudes γ_0 for any finite frequency ω. (The same is not true in steady shear flow; we return to this in Sec. IV B 2.) In the linear regime, the model's internal dynamics are independent of the imposed deformation: the elements' lifetimes are, to order γ_0, strain independent. In the constitutive equations, $Z(t,t')$ can then be replaced by the time interval $t-t'$.

As described in Sec. II F, the conventional definition of the linear viscoelastic spectra $G'(\omega),G''(\omega)$ [Eq. (11)], requires not only linearity but also TTI. Thus they are well defined only for an equilibrium state; in the SGR model, the latter exists only for $x > 1$. But even at $x > 1$ these spectra show interesting power law dependencies at low

frequency; these are summarized as follows [the prefactors are omitted, but discussed by Sollich *et al.* (1997); Sollich (1998)]:

$$\begin{aligned} G'' &\propto \omega \quad \text{for } 2 < x, \\ &\propto \omega^{x-1} \quad \text{for } 1 < x < 2, \\ G' &\propto \omega^2 \quad \text{for } 3 < x, \\ &\propto \omega^{x-1} \quad \text{for } 1 < x < 3. \end{aligned} \tag{35}$$

Here and throughout this paper, "low frequency" in the SGR model means $\omega \ll 1$, that is, frequencies small compared to the mesoscopic attempt rate for activated hopping $\tau_0^{-1} = 1$ (in our chosen units).

Throughout its glass phase ($x \leq 1$) where the SGR model violates TTI, we must study instead the time dependent spectra $G^*(\omega,t,t_s)$ as defined in Sec. II F 2 above; this is done in Sec. VI A. An alternative, explored by Sollich *et al.* (1997); Sollich (1998); Evans *et al.* (1999) is to observe that TTI can be restored even for $x \leq 1$ by introducing a cutoff $E_{\max}$ in the trap depth distribution $\rho(E)$. This gives interesting predictions for $x < 1$: for example, one finds $G'(\omega) \sim \omega^{1-x}$, for $\tau^{-1}(E_{\max}) \ll \omega \ll 1$ [Sollich *et al.* (1997); Sollich (1998)]. However, this cutoff brings all aging processes to a halt after a large finite time of order $\tau(E_{\max})$; formally there is no long term memory. Since in the present work we want to study the aging regime itself, we assume instead that $E_{\max}$ is infinite, so that for $x \leq 1$, aging continues indefinitely. [This is mainly a matter of mathematical convenience. Our results would be unchanged if a largest relaxation time $\tau(E_{\max})$ was present, so long as this is much larger than all other timescales of interest.]

2. Flow curve

The flow curve was defined in Sec. II G as the nonlinear stress response $\sigma(\dot{\gamma})$ to a steady strain rate $\dot{\gamma}$. For the SGR model, it shows the following scalings:

$$\begin{aligned} \sigma &\propto \dot{\gamma} \quad \text{for} \quad x > 2 \\ \sigma &\propto \dot{\gamma}^{x-1} \quad \text{for} \quad 1 < x < 2 \\ \sigma - \sigma_y &\propto \dot{\gamma}^{1-x} \quad \text{for} \quad x < 1. \end{aligned} \tag{36}$$

Here $\dot{\gamma} \ll 1$ is assumed; prefactors are discussed by Sollich (1998). The flow curve exhibits two interesting features which are explored more fully in Secs. VI B 2 and VII B 1. First, for $x < 1$ there is a yield stress $\sigma_y(x)$ [whose value is plotted by Sollich (1998)]. A linear response regime exists at $\sigma \ll \sigma_y$; aging can occur for all $\sigma < \sigma_y$. For $\sigma > \sigma_y$ the system achieves a steady state, and aging no longer occurs. This is because any finite flow rate, however small, causes strain-induced yielding of elements even in the deepest traps; the time required to yield, with a steady flow present, is only power law, rather than exponential in E. Thus the aging process is curtailed or "interrupted" by flow [Sollich *et al.* (1997); Sollich (1998)]; the flow curve is well defined even in the glass phase. The second interesting feature is that, for $1 < x < 2$ (where aging is absent) there is no linear response regime at all in steady shear: however small the applied stress, the behavior is dominated by strain-induced yielding. There is an anomalous (power law) relation between stress and strain rate, and an infinite zero-shear viscosity (cf. Sec. II G). This also shows up in Eq. (35), where $\eta = \lim_{\omega \to 0} G''(\omega)/\omega$ is likewise infinite.

V. AGING IN THE SGR MODEL

In this section we discuss some general features of aging in the SGR model; in subsequent ones, we explore the rheological consequences of these phenomena.

A. Initial preparation of sample

As noted above, to solve the constitutive equations (25), (26) the initial distribution $P_0(E)$ of yield energies or trap depths at time zero must be specified. Since we are interested in the rheological properties of the glass phase ($x \leqslant 1$), for which no steady-state distribution of yield energies exists in the absence of flow, we cannot appeal to equilibrium to fix $P_0(E)$. Instead, this should depend explicitly on the way the sample was prepared. For simplicity, we choose the case where $P_0(E) = \rho(E)$; this is equivalent to suddenly "quenching" the noise temperature x, at time zero, from a very large value ($x \gg 1$) to a value within the range of interest. We refer to it as a "deep quench."

The question of whether or not a deep quench is a good model for the sample preparation of a SGM remains open [Sollich *et al.* (1997); Sollich (1998)]; since x is not truly a temperature, it is not clear exactly how one would realize such a quench experimentally. One argument in its favor is that this choice minimizes the information content (maximizes the entropy) of the initial distribution P_0; it is therefore a legitimate default choice when no specific information about the preparation condition is available. In any case, we expect that most interesting aspects of aging behavior are not too sensitive to the initial quench conditions $P_0(E)$, so that a deep quench is indeed an adequate model. A study of the effect of quench depth on the results for the SGR model is summarized in Appendix A 4; we find independence of quench depth so long as the final noise parameter x is not too small. [More precisely, if the "deep quench" specification is altered to one in which, at time zero, the system is quenched from equilibrium at $x_0 > 1$ to its final noise temperature x, the leading results are independent of x_0 so long as the final x value obeys $x > 1/(2-1/x_0)$. Note that this condition is never satisfied for $x < 1/2$.] More generally, a degree of insensitivity to the initial quench conditions is consistent with the weak long term memory scenario; a system whose response decays with a relaxation time of order its age will typically lose its memory of the initial state by a power law decay in time. This can then easily be swamped by larger, P_0-independent contributions, as indeed occurs in most regimes of the SGR model (Appendix A 4).

Following the initial preparation step, subsequent time evolution of the rheological response is, within the glass phase, characterized by aging. To allow comparison with the non-aging (but still slow) dynamics for $1 < x < 2$, below we shall also consider a similar quench from large x to values in this range.

B. Aging of the lifetime distribution

We now [following Bouchaud (1992) and Monthus and Bouchaud (1996)] discuss in detail the way aging affects the lifetime distribution (or equivalently the distribution of particle hopping rates) within the SGR model.

We ignore the presence of a strain; the following results apply when there is no flow, and in the linear response regime, where strain-induced hops can be ignored. Under such conditions, the hopping rate $Y(t)$ is a strain-independent function of time, and is readily found from Eq. (26) by Laplace transform. This is done in Appendix A 2. For the case of a deep quench (as defined above), the exact asymptotic forms of Y are as follows:

$$Y(t) = \frac{x-1}{x} \quad \text{for } x > 1,$$

$$Y(t) = \frac{1}{\ln(t)} \quad \text{for } x = 1, \tag{37}$$

$$Y(t) = \frac{t^{x-1}}{x\Gamma(x)\Gamma(1-x)} \quad \text{for } x < 1,$$

where $\Gamma(x)$ is the usual Gamma function. These results assume $t \gg 1$, which we will usually take to be the case from now on (since timescales of experimental interest greatly exceed the mesoscopic attempt time $\tau_0 = 1$). Note that the late-time asymptotes given here are subject to various subdominant corrections (see Appendix A 2), some of which are sensitive to the initial state of sample preparation. (In fact, for a quench from initial noise temperature x_0, the relative order of the affected subdominant terms becomes $t^{-x(1-1/x_0)}$. Thus, unless one quenches *from* a point that is itself only just above the glass transition, or *to* a point that has x only just above zero, the exact specification of the initial state is unimportant at late times.)

A closely related quantity to the hopping rate Y is the distribution of yield energies $P(E,t)$—which obeys Eq. (32)—or equivalently the lifetime distribution $P(\tau,t)$. As previously pointed out, in the absence of strain, the only candidate for a steady state distribution of yield energies $P_{\rm eq}(E)$ is the Boltzmann distribution: $P_{\rm eq}(E) \propto \rho(E)\exp(E/x)$, which translates to $P_{\rm eq}(\tau) = P_{\rm eq}(E)dE/d\tau \propto \tau^{-x}$; in either language, the distribution is not normalizable for $x < 1$, leading to broken TTI in the model [Bouchaud (1992)].

Let us therefore consider a deep quench at time $t = 0$, and define the probability distribution for trap lifetimes $P(\tau,t_w)$ as a function of the time t_w elapsed since sample preparation. (In Sec. VI, we will identify t_w with the onset of a step strain.) The initial lifetime distribution, $P(\tau,0)$, describes a state in which the trap depths are chosen from the prior distribution $P(E,0) = \rho(E)$; just after a quench to temperature x the distribution of lifetimes is therefore $P(\tau,0) \propto \rho(E)d\tau/dE \propto \tau^{-(1+x)}$. Thereafter, by changing variable from E to τ in Eq. (32), we find the following approximate expressions for $P(\tau,t_w)$:

$$\begin{aligned} P(\tau,t_w) &\simeq xY(t_w)\tau\rho(\tau) \quad \text{for } \tau \ll t_w \text{ and } t_w \gg 1, \\ P(\tau,t_w) &\simeq xY(t_w)t_w\rho(\tau) \quad \text{for } \tau \gg t_w \text{ and } t_w \gg 1. \end{aligned} \tag{38}$$

For a quench temperature above the glass point ($x > 1$), $P(\tau,t_w)$ exhibits a transient decay; as $t_w \to \infty$, we find [using the results in Eq. (37)] that $P(\tau,t) \to P_{\rm eq}(\tau) = (1-x)\tau^{-x}$, as expected. The nature of the approach to the long time limit is illustrated schematically in Fig. 3(a); the final distribution has most of its weight at $\tau = O(1)$, consistent with the fact that the hopping rate, Eq. (37), is itself $O(1)$ in this phase of the model.

For $x < 1$, in contrast, $P(\tau,t_w)$ evolves as in Fig. 3(b); the limit of $P(\tau,t_w)$ is zero for any finite τ as $t_w \to \infty$. Hence, the proportion of elements having yield time of order unity tends to zero as $t_w \to \infty$; the bulk of the distribution's weight is at $\tau \simeq t_w$. [More formally, for $x < 1$, we have $\lim_{t_w \to \infty} \int_1^b P(\tau,t_w)d\tau = 0$ for any $b > 1$, while for any $a < 1 < b$ we have instead $\lim_{t_w \to \infty} \int_{at_w}^{bt_w} P(\tau,t_w)d\tau = O(1)$.] This is consistent with the decay of the hopping rate as a power law of t_w, and with the idea that, in a system undergoing aging, the characteristic relaxation time is typically of the order the age of the system itself.

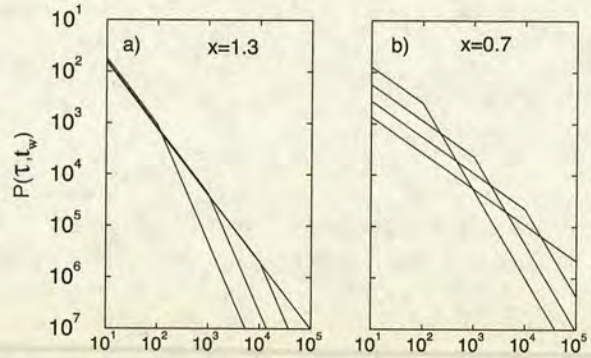

FIG. 3. Schematic evolution of the relaxation time distribution (a) above the glass transition; (b) below it. The first shows a transient decay onto a steady state, the second shows aging behavior. The curves lie in order of increasing t_w at the bottom of each figure.

C. Higher moments

The above analysis focuses on the time evolution of the distribution of elements' lifetimes, which is the usual quantity of interest in the formal analysis of aging effects [Bouchaud and Dean (1995); Bouchaud *et al.* (1998)]. Indeed, the latter are usually attributed to the divergence of the normalization integral, or zeroth moment, of $P_{\rm eq}(\tau)$ (undefined, within the Boltzmann distribution, when $x \leqslant 1$). Formally, however, one can consider a series of critical x values, $x_n = n+1$, below each of which the nth moment of $P_{\rm eq}$ becomes undefined [Evans *et al.* (1999); Odagaki (1995)]. For $n > 0$ this does not lead to aging, in the sense defined in Sec. III, but can lead to anomalous, slow time evolution in any experimental measurement that probes the nth moment. For example, in Sec. VI A 3 below, we discuss the time evolution of the distribution of stresses borne by elements in a steady-shear startup experiment. In steady state, the stress carried by an element whose lifetime is τ is of order $\dot{\gamma}\tau$. If $P(\tau) = P_{\rm eq}(\tau)$ and is unperturbed by flow (as a linear response analysis would assume), then the zero-shear viscosity is of order $\int \tau P_{\rm eq}(\tau) d\tau$, which diverges for $x < 2$ (see Sec. II G).

VI. RHEOLOGICAL AGING: IMPOSED STRAIN

In this and the next sections, we describe our new rheological results for the SGR model. We focus particularly on rheological *aging*, which occurs in the glass phase ($x < 1$); however, several new results for $1 < x < 2$, including anomalous *transient behavior*, are also presented. The case $x = 1$, which divides these regimes, shows its own especially weak (logarithmic) form of aging and is, where necessary, treated separately below.

For simplicity, we consider (for all x values) only the idealized route to sample preparation described in Sec. V A: the system is prepared at time $t = 0$ by means of a deep quench, so that $G_0(Z(t,0)) = G_\rho(Z(t,0))$ in the constitutive equations (25), (26). Note that these constitutive equations for the SGR model are more readily solved to find the stress response to an imposed strain, rather than vice-versa. Accordingly, we focus first on strain-controlled experiments and defer to Sec. VII our analysis of the stress-controlled case.

TABLE I. Stress response to step strain at short and long times ($t-t_w \gg 1$, $t \gg 1$ assumed). $\Gamma(x)$ denotes the usual Gamma function.

	$G(t-t_w,t_w)$ for $t-t_w \ll t_w$	$G(t-t_w,t_w)$ for $t-t_w \gg t_w$
$x > 1$	$\Gamma(x)(t-t_w)^{1-x}$	$(x-1)\Gamma(x)\dfrac{t_w}{(t-t_w)^x}$
$x = 1$	$1-\dfrac{\ln(t-t_w)}{\ln(t_w)}$	$\dfrac{t_w}{t-t_w}\dfrac{1}{\ln(t_w)}$
$x < 1$	$1-\dfrac{1}{\Gamma(2-x)\Gamma(x)}\left(\dfrac{t-t_w}{t_w}\right)^{1-x}$	$\dfrac{1}{\Gamma(1+x)\Gamma(1-x)}\left(\dfrac{t_w}{t-t_w}\right)^{x}$

A. Linear response

As described in Sec. IV B 1, when local strains are negligible, the SGR model displays a linear response regime. The effective time interval $Z(t,t')$ in Eqs. (25), (26) becomes the actual time interval $t-t'$, and the hopping rate $Y(t')$ a strain-independent function of time. For the deep quench considered here, $Y(t')$ assumes the asymptotic forms summarized in Eq. (37). The stress response to any strain history then follows simply from Eq. (25), by integration.

1. Step strain

For a step strain, the amplitude γ_0 gives the maximum local strain experienced by any element. The condition for linearity in this case is therefore simply $\gamma_0 \ll 1$. The linearized step strain response was defined in Eq. (3). It is found for the SGR model using Eq. (34):

$$G(t-t_w,t_w) = 1-\int_{t_w}^{t} Y(t')G_\rho(t-t')dt'. \tag{39}$$

Note that by construction of the SGR model, the linear step strain response is actually identical to the correlation function defined by Bouchaud for his trap model [Bouchaud (1992); Monthus and Bouchaud (1996)].

As outlined in Appendix A 3, analytic limiting forms for $G(t-t_w,t_w)$ can be found when experimental timescales are large on the scale of the mesoscopic attempt time $\tau_0 = 1$, so that $t-t_w \gg 1$ and $t_w \gg 1$. In this limit we identify two distinct regimes: a short time interval regime $t-t_w \ll t_w$ and long time interval regime $t-t_w \gg t_w$ (where the measure of "short" and "long" is not now τ_0 but t_w itself). The limiting forms in each case depend on the value of x; our results are summarized in Table I.

The asymptotic scalings apparent in the various entries of Table I can be physically motivated by the following simple arguments. Upon the application of the strain at time t_w the local strain of each element exactly follows the macroscopic one, and the instantaneous response is elastic: $G(0,t_w) = 1$. (This is a general characteristic of the SGR model: whenever the macroscopic strain changes discontinuously by an amount $\Delta\gamma$, the stress σ also increases by $\Delta\gamma$.) In the time following t_w, elements progressively yield and reset their local stresses l back to zero. The stress remaining at t will be that fraction of elements which has survived from t_w without yielding, and hence roughly that fraction $\int_{t-t_w}^{\infty} P(\tau,t_w)\,d\tau$ which, at time t_w, had time constants greater than $t-t_w$. Hence in

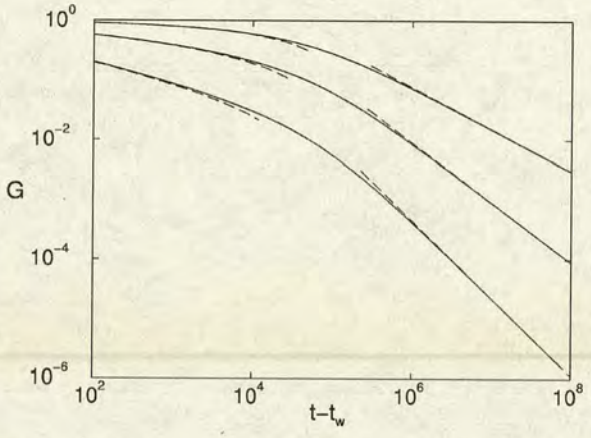

FIG. 4. Approximate curves for $G(t-t_w,t_w)$ generated using the interpolating formulas Eqs. (40), (41) (dashed lines), compared to numerical data for this quantity (solid lines). Solid curves downwards show numerical data for G vs $t-t_w$ at noise temperatures $x = 0.7$, $x = 1.0$ and $x = 1.3$, respectively. The waiting time t_w is 10^5.

measuring the linear response to a step strain we are probing the properties of the system as they were at the time of strain application.

Using the approximate expressions given in Eq. (38), we have $P(\tau,t_w) \propto \tau^{-x}$ for $\tau \ll t_w$ and $P(\tau,t_w) \propto t_w\tau^{-(1+x)}$ for $\tau \gg t_w$. This gives, for short time intervals $(t-t_w \ll t_w)$

$$G(t-t_w,t_w) \simeq 1-\int_1^{t-t_w} P(\tau,t_w)\,d\tau \simeq 1-x\frac{(t-t_w)^{1-x}-1}{t_w^{1-x}-x}$$

and, for long time intervals $(t-t_w \gg t_w)$

$$G(t-t_w,t_w) \simeq \int_{t-t_w}^{\infty} P(\tau,t_w)\,d\tau \simeq \frac{(1-x)t_w(t-t_w)^{-x}}{t_w^{1-x}-x}.$$

In fact these estimates approximate the numerical data already quite well. Even better agreement is obtained by adjusting the prefactors to fit the asymptotic results in Table I:

$$G(t-t_w,t_w) \simeq 1-\frac{\Gamma(x)(t-t_w)^{1-x}-1}{\Gamma^2(x)\Gamma(2-x)t_w^{1-x}-1} \quad \text{for } t-t_w \ll t_w, \tag{40}$$

$$G(t-t_w,t_w) \simeq \frac{(x-1)\Gamma(x)t_w(t-t_w)^{-x}}{1-\Gamma(x)\Gamma(x+1)\Gamma(2-x)t_w^{1-x}} \quad \text{for } t-t_w \gg t_w. \tag{41}$$

In the relevant time regimes, these formulas agree well with our numerical results (see Fig. 4), at least over the noise temperature range 0–2; they could therefore be used in a standard curve fitter for comparison with experimental data. In the limit $t-t_w \to \infty$ and $t_w \to \infty$, they reproduce (by construction) the results shown in Table I for $x > 1$ and $x < 1$. The logarithmic terms at the glass point ($x = 1$) can also be recovered by taking the limit $x \to 1$ first.

Using the forms for $G(t-t_w,t_w)$ as summarized in Table I, and substituting these in Eqs. (18), (19), we see that the SGR model has short term memory for $x > 1$ and weak long term memory for $x \leqslant 1$. Thus we expect transients for $x > 1$ and aging for x

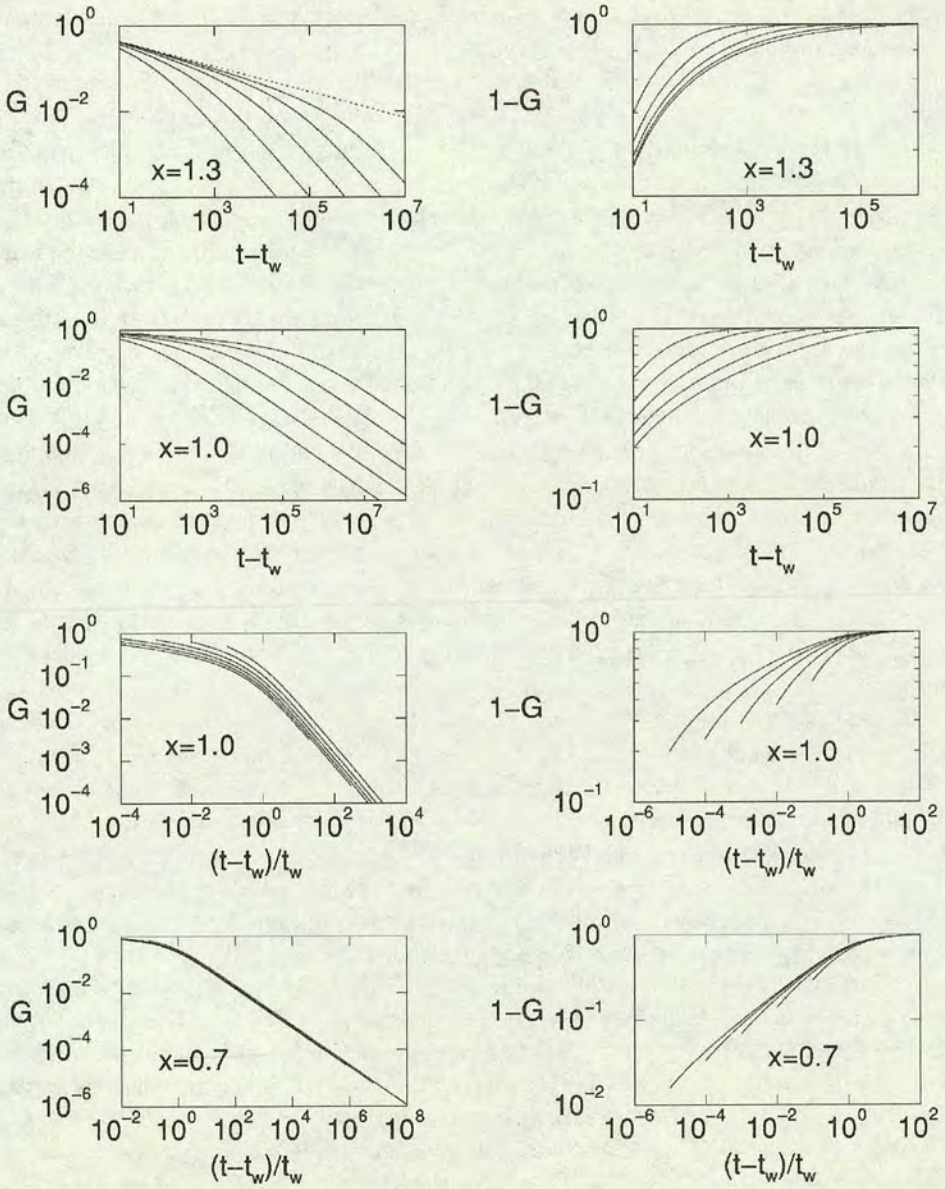

FIG. 5. (Left column) age-dependent stress relaxation modulus $G(t-t_w,t_w)$ against scaled time interval $(t-t_w)/t_w$ (for $x \leqslant 1$) and time interval $t-t_w$ (for $x \geqslant 1$); (Right column) $1-G(t-t_w,t_w)$, plotted similarly. Shown are data for waiting times $t_w = 10^2, 10^3 \ldots 10^6$ (left to right for top four graphs, right to left for bottom four graphs).

$\leqslant 1$. As shown in Fig. 5, this is indeed what we find. Transients are visible in the top left panel: the curves coincide at short time intervals $t-t_w \ll t_w$. At large t_w, this regime accounts for more and more of the decay of G; the remaining t_w dependence is only through an unimportant tail. For $t_w \to \infty$, the "short time" regime extends to all finite values of $t-t_w$; one recovers the equilibrium response (shown as the dotted line) which decays to zero on a t_w-independent timescale. Aging is visible at bottom left, where the

major part of the decay of G occurs on a timescale of order t_w itself, with unimportant corrections to this scaling at early times.

More generally, these step strain results for the SGR model show some interesting features of its rheology. Consider first the behavior above the glass transition ($x > 1$). Here the stress decay at short time intervals ($t-t_w \ll t_w$) depends only upon the time interval between stress imposition and measurement itself ($t-t_w$), and not on the sample age t_w. This is because the traps which contribute to stress decay during this interval are mainly those with lifetimes $\tau < t-t_w$; and the population of these traps has already reached Boltzmann equilibrium before the strain is switched on [see Fig. 3(a)]. Taking the limit $t_w \to \infty$ at constant $t-t_w$ (i.e., letting the system fully equilibrate *before* we apply the strain), we recover a TTI stress relaxation function which decays to zero on timescales of order $\tau_0 = 1$. On the other hand, for any finite waiting time t_w, the stress decay at long enough times ($t-t_w \gg t_w$) violates TTI, since it is controlled by decay out of deep traps ($\tau \gg t_w$) which had not already equilibrated before t_w. Note that even though this feature of the stress relaxation depends explicitly on t_w, it is not an aging effect according to our definition in Sec. III. This is because the deviations from TTI and the dependence on t_w manifest themselves at ever smaller values of G as t_w becomes large. Equivalently, if we assume that $G(t-t_w,t_w)$ can be measured reliably only as long as it remains greater than some specified value [a small fraction ϵ of its initial value $G(0,t_w) = 1$, for example], then the results will become t_w independent for sufficiently large t_w.

Below the glass point ($x \leq 1$) we see true aging, rather than anomalous transient effects: A significant part of the stress relaxation $G(t-t_w,t_w)$ now takes place on timescales that increase with the sample age t_w itself. In fact, in the case of the SGR model, this applies to the *complete* stress relaxation, and t_w itself sets the relevant timescale: for $x < 1$, G-depends on time only through the ratio $(t-t_w)/t_w$. It is still true that stress decay during the interval $t-t_w$ is dominated by traps for which $\tau < t-t_w$, but no longer true that these traps have reached Boltzmann equilibrium by time t_w: in an aging system such equilibrium is never attained, even for a subset of shallow traps [see Fig. 3(b)]. Instead, the population of such traps will gradually deplete with age, as the system explores ever-deeper features in the energy landscape. Decay from these deep traps becomes ever slower; the limit $t_w \to \infty$ (for any finite $t-t_w$) gives completely arrested behavior in which all dynamics has ceased, and the system approaches a state of perfect elasticity ($G = 1$). Even in an experiment that can only resolve values of G above a threshold ϵ (see above), we would detect that the stress relaxation becomes slower and slower as t_w increases.

The fact that G depends on time only through the ratio $(t-t_w)/t_w$ is typical, but not automatic for aging systems; the case $x = 1$, for example, does not have it. It is a simple example of Struik's "time aging-time superposition" principle [Struik (1978)]: the relaxation curves for different t_w can be superposed by a rescaling of the time interval $t-t_w$ by the sample age. However, as mentioned previously, Struik's discussion allows a more general form in which the scale factor varies as t_w^{μ}, with $\mu \leq 1$. Even more generally, the timescale for aging can be any monotonically increasing and unbounded function of t_w. There can also be *parts* of the stress relaxation which still obey TTI. (An example is $G(t-t_w,t_w) = g_1(t-t_w)+g_2[(t-t_w)/t_w]$, which exhibits aging when g_2 is nonzero, but also has a TTI short time part described by g_1.) Superpositions of relaxations with different aging timescales are also possible; compare Eq. (20). The SGR model exemplifies the simplest type of aging behavior only.

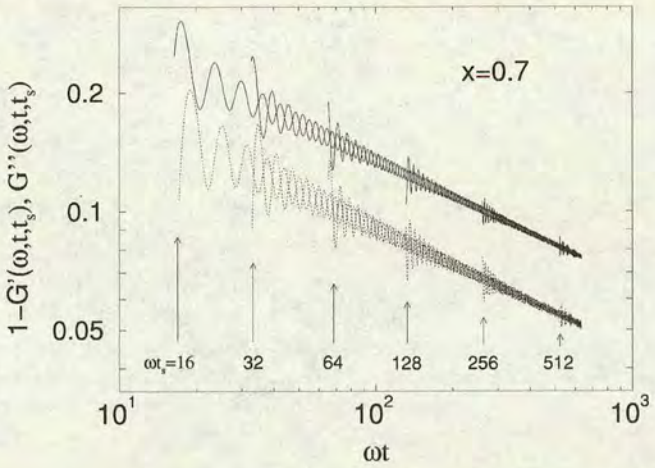

FIG. 6. Demonstration of t_s-independence $G^*(\omega,t,t_s)$ in the glass phase. Shown are $1-G'(\omega,t,t_s)$ (solid lines) and $G''(\omega,t,t_s)$ (dotted lines) against ωt. The noise temperature is $x = 0.7$ and the frequency $\omega = 0.01$. Start-time values t_s obey $\omega t_s = 2^4,2^5,\ldots 2^9$. When $\omega(t-t_s) \gg 1$ (a sufficient number of oscillations after the beginning of each dataset) and $\omega t_s \gg 1$ (datasets beginning further on the right), G^* becomes independent of t_s.

2. Oscillatory strain

In an oscillatory strain, the maximal local strain of any element is γ_0, the strain amplitude. Thus a linear regime in the SGR model is ensured whenever $\gamma_0 \ll 1$. The linear viscoelastic spectrum, as defined in Eq. (10), can be found for the SGR model using Eq. (34)

$$G^*(\omega,t,t_s) = 1-\int_{t_s}^{t} e^{-i\omega(t-t')}Y(t')G_\rho(t-t')dt'. \tag{42}$$

In principle, this quantity depends on t_s, the time when the oscillatory strain was started. However, when the experimental timescales become large, we find (as shown in Appendix B) that this dependence on t_s is weak. In fact, within the SGR model, the conditions needed to make G^* negligibly dependent on t_s (for low frequencies, $\omega \ll 1$) are that $\omega(t-t_s) \gg 1$ and $\omega t_s \gg 1$. The first signifies merely that many cycles of oscillatory strain are performed before the stress is measured; the second ensures that transient contributions from the initial sample preparation stage (the quench at $t = 0$) are negligible. Notably, these criteria do not depend on the noise temperature x, and therefore hold even in the glass phase ($x \leqslant 1$); see Fig. 6. The fact that they are sufficient even in the glass phase is far from obvious physically, and requires a careful discussion: we give this in Appendix B. Broadly speaking, these criteria are satisfied in any experiment that would reliably measure a conventional $G^*(\omega)$ spectrum for systems with TTI.

For the purposes of such experiments, we can therefore drop the t_s argument and define a time-dependent spectrum $G^*(\omega,t)$. Our results for the long-time behavior ($t \gg 1$) of this quantity are as follows (see Appendix A 3)

$$G^*(\omega,t) = \Gamma(x)\Gamma(2-x)(i\omega)^{x-1} \quad \text{for } 1 < x < 2,$$

$$G^*(\omega,t) = 1+\frac{\ln(i\omega)}{\ln(t)} \quad \text{for } x = 1 \tag{43}$$

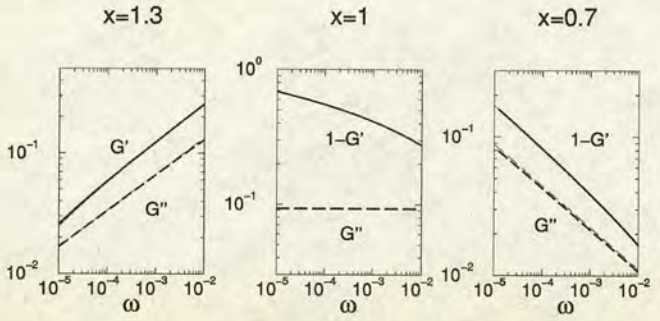

FIG. 7. Approximate curves for $G'(\omega,t)$ and $G''(\omega,t)$ generated using the simple interpolating formula, Eq. (44) (thin lines) compared to the numerical data for these quantities (thick lines), plotted as a function of ω at fixed $t = 10^7$, and $x = 1.3,1,0.7$. Note that the predictions of the interpolating formula are practically indistinguishable from the numerical data over the frequency window shown.

$$G^*(\omega,t) = 1 - \frac{1}{\Gamma(x)}(i\omega t)^{x-1} \quad \text{for } x < 1.$$

For comparison with experimental results, the simple interpolating form

$$G^*(\omega,t) = 1 - \frac{\Gamma(x)\Gamma(2-x)(i\omega)^{x-1} - 1}{\Gamma^2(x)\Gamma(2-x)t^{1-x} - 1} \tag{44}$$

may be useful; we have checked that it provides a good fit to our numerical data, at least over the noise temperature range 0.7 to approximately 1.3 (see Fig. 7).

By measuring $G^*(\omega,t)$ we are directly probing the properties of the system at the time of measurement, t. In light of this, the results of Eq. (43) are easily understood. In the ergodic phase ($x > 1$), $G^*(\omega,t)$ will reach a t-independent value within a time of $O(1/\omega)$ after the quench, as the relevant traps will then have attained their equilibrium population. The relaxation time is then of $O(\tau_0)$ [that is, $O(1)$ in our units] and the response $G^*(\omega,t)$ is a function only of ω. In contrast, below the glass point the characteristic relaxation time at the epoch of measurement is of order t, and the response is a function only of the product ωt. Since the losses in an oscillatory measurement arise from traps with lifetimes less than about $1/\omega$ (elements in deeper traps respond elastically), the overall response becomes more elastic as the system ages into traps with $\tau > 1/\omega$.

Numerical results for the viscoelastic spectrum $G^*(\omega,t)$ at various measurement times t for various x are shown in Fig. 8. These indeed show a characteristic "hardening" of the glassy material as it ages: the storage modulus at low frequencies evolves upwards, and the loss modulus downward [Sollich *et al.* (1997); Sollich (1998)]. There is good data collapse both above and below the glass point (with the appropriate scalings); the data for $x = 1$ do not collapse in either representation due to logarithmic terms. If plotted against ω rather than ωt, the data for $x = 0.7$ would resemble Fig. 1. Each spectrum terminates at frequencies of order $\omega t \simeq 1$. This is because one cannot measure a true oscillatory response for periods *beyond* the age of the system. Therefore, the rise at low frequencies in G' spectra like Fig. 1 represents the ultimate rheological behavior. (Note that this only applies for $\mu = 1$ in Struik's scheme, as exemplified by the SGR model. Whenever $\mu < 1$, the region to the left of the loss peak can, in principle, be accessed eventually.)

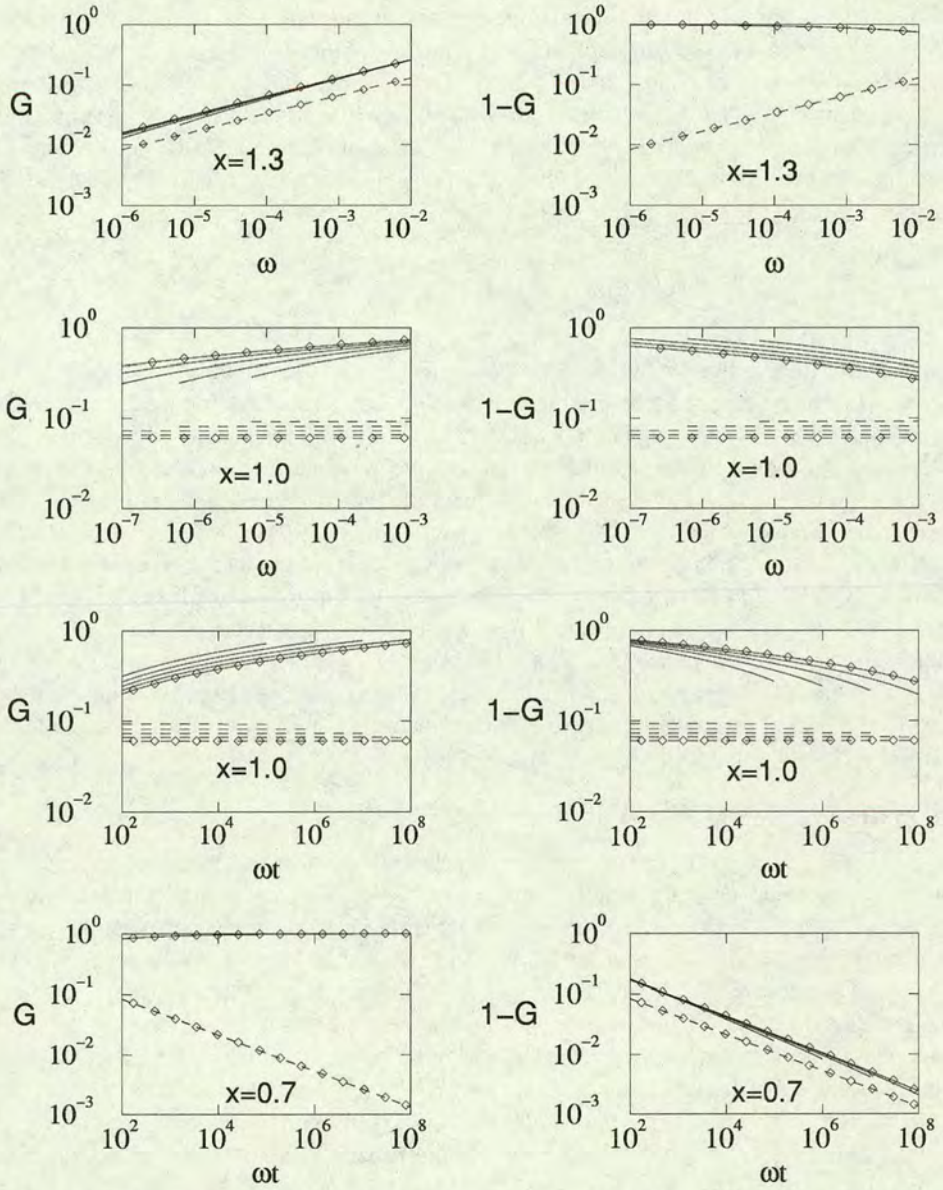

FIG. 8. (Left column) viscoelastic spectra $G'(\omega)$ (solid lines) and $G''(\omega)$ (dashed lines) vs frequency, ω (for $x \geq 1$) or scaled frequency ωt (for $x \leq 1$).(Right column) frequency-dependent corrections to Hookean elasticity, $1-G'$ (solid lines), G'' (dashed lines). Data are shown for systems aged $t = 10^7, 10^8, \ldots 10^{11}$. At any fixed ω the curves lie in order of age; data on the oldest system is marked by the symbols.

It is shown in Appendix B that the insensitivity of $G^*(\omega,t,t_s)$ to t_s in practical measurements of the viscoelastic spectrum (where an oscillatory strain is maintained over many cycles) arises because (even when $x < 1$) the most recently executed strain cycles dominate the stress response at time t. In essence, as long as an oscillatory strain was started many cycles ago, there is no memory of when it was switched on; accordingly (by linearity) an oscillatory strain started in the distant past and then switched off at t_s, will leave a stress that decays on a timescale comparable to the period of the oscillation. This

is markedly different from non-oscillatory stresses, where long term memory implies that the response to a step strain, applied for a long time, persists for a similarly long time after it is removed (see Sec. III). Thus the fact that the SGR glass "forgets" the t_s argument of $G^*(\omega,t,t_s)$, is directly linked to the oscillatory nature of the perturbation. As also shown in Appendix B, this forgetfulness means that, in the SGR model, a Fourier relationship between oscillatory and step strain responses is recovered; to a good approximation, one has the relation, Eq. (13)

$$G^*(\omega,t) = i\omega \int_0^\infty e^{-i\omega t'} G(t',t)\, dt'. \tag{45}$$

Apart from the explicit dependence on the measurement time t, this is the usual (TTI) result. [Formally, t appears as the time at which a step strain was initiated, or an oscillatory measurement ended. Thus $G^*(\omega,t)$ is to within $i\omega$, the Fourier transform of the step strain response function $G(\Delta t,t)$ that would be measured if a step strain were applied immediately *after* the oscillatory measurement had been done.] But here it is nontrivial because of aging effects. As discussed at the end of Sec. III, we speculate that the relation, Eq. (45), holds not only for the SGR model, but in fact for all systems which have only *weak* long term memory. We also note that Eq. (45) can formally be used to *define* $G^*(\omega,t)$ in the range of small frequencies $\omega < 1/t$, where it would reflect the behavior of the step response $G(t',t)$ for long times $t' \gg t$. But in this frequency regime $G^*(\omega,t)$ can no longer be related to a physical measurement of the stress response to an oscillatory strain; as pointed out above, such a measurement always requires at least one period of oscillation and thus $\omega t > 1$.

3. Startup of steady shear

Consider now a startup experiment in which a steady shear of rate $\dot\gamma \ll 1$ begins at time t_w. So long as we restrict attention to times short enough that the total strain remains small [$\dot\gamma(t-t_w) \ll 1$] the system remains in a linear response regime. (This contrasts with the ultimate steady-state behavior which, for $x < 2$, is always nonlinear; the crossover to a nonlinear regime at late times is discussed in Sec. VI B 2.)

Within the regime of linear response, any element's lifetime is independent of strain and obeys $\tau = \exp(E/x)$. As described in Sec. V B above, at a time t after a deep quench, the distribution of lifetimes obeys $P(\tau,t) \sim \tau\rho(\tau)$ for $\tau \ll t$ and $P(\tau,t) \sim t\rho(\tau)$ for $\tau \gg t$. Since the local stress associated with a given trap is of order $\dot\gamma\tau$ for $\tau \ll t - t_w$, and $\dot\gamma(t-t_w)$ for $\tau \gg t-t_w$, we can construct an estimate of the macroscopic stress; for $t-t_w \ll t_w$,

$$\begin{aligned}\sigma(t) &\simeq \frac{\dot\gamma\left[\int_1^{t-t_w}\tau^2\rho(\tau)d\tau+(t-t_w)\int_{t-t_w}^{t}\tau\rho(\tau)d\tau+(t-t_w)t\int_t^\infty\rho(\tau)d\tau\right]}{\int_1^t\tau\rho(\tau)d\tau+t\int_t^\infty\rho(\tau)d\tau} \\ &\simeq \frac{\dot\gamma\left[x(t-t_w)^{2-x}+(x-2)(t-t_w)t^{1-x}+x(1-x)\right]}{(x-2)(t^{1-x}-x)}.\end{aligned} \tag{46}$$

This gives, for long times and in the linear response regime, $\sigma(t) \sim \dot\gamma(t-t_w)$ for $x < 1$ (which is purely elastic behavior), $\sigma(t) \sim \dot\gamma(t-t_w)^{2-x}$ for $1 < x < 2$ (which is an anomalous power law), and $\sigma(x) \sim \dot\gamma$ for $x > 2$; repeating the same calculation with $t \gg t_w$ gives the same asymptotic scaling in each case. An asymptotic analysis of the constitutive equations confirms these scalings, with prefactors as summarized in

TABLE II. Stress response to shear strain of constant rate $\dot{\gamma}$ at short and long times ($t-t_w \gg 1, t \gg 1, \dot{\gamma} \ll 1$ assumed). These results apply to the regime $\dot{\gamma}(t-t_w) \ll 1$, where strain-induced yielding can be neglected, making the response linear.

	$\frac{\sigma(t-t_w,t_w)}{\dot{\gamma}}$ for $t-t_w \ll t_w$	$\frac{\sigma(t-t_w,t_w)}{\dot{\gamma}}$ for $t-t_w \gg t_w$
$2 < x$	$\frac{x-1}{x-2}$	$\frac{x-1}{x-2}$
$1 < x < 2$	$\frac{\Gamma(x)}{2-x}(t-t_w)^{2-x}$	$\frac{(x-1)\Gamma(x)}{2-x}(t-t_w)^{2-x}$
$x < 1$	$(t-t_w)$	$(1-x)(t-t_w)$

Table II. Because the results depend only on $t-t_w$, any explicit dependence on t_w must reside in subdominant corrections to these leading asymptotes. Accordingly, *linear* shear startup is not a good experimental test of aging or slow transient effects. The power law anomaly for $1 < x < 2$ can be understood by examining which traps make dominant contributions to $\sigma(t) = \int s(\tau,t)d\tau$. [Recall that $s(\tau,t)d\tau$ is the stress contribution at time t from elements of lifetime τ, see Sec. IV A.] For $x > 2$, $s(\tau,t)$ is weighted strongly toward traps of lifetime $O(1)$; hence $\sigma(t)$ tends to a finite limit (of order $\dot{\gamma}$) as $t \to \infty$, and the viscosity of the system is finite. For $x < 2$, on the other hand, most of the weight in the $s(\tau,t)$ distribution involves lifetimes of order t. As time passes, stress is carried by deeper and deeper traps, and (in the absence of flow-induced yielding) the mean stress diverges as $t \to \infty$.

In fact, as discussed in Sec. V C, just as the Boltzmann distribution for the relaxation times $P_{eq}(\tau) = P(\tau,\infty) \sim \tau\rho(\tau)$ is non-normalizable for $x \leq 1$ (giving glassiness and aging), so, in the absence of strain-induced yielding, is the ultimate distribution $s(\tau,\infty) \sim \tau^2\rho(\tau)$ of stresses residing in traps of lifetime τ, whenever $x < 2$. The zero shear viscosity η is therefore infinite throughout this regime, as noted previously.

B. Nonlinear response

We now turn to the nonlinear behavior of the SGR model under imposed strain, starting with the step strain case.

1. Step strain

The nonlinear step strain response function was defined in Eq. (3). It is found for the SGR model from Eq. (34)

$$G(t-t_w,t_w;\gamma_0) = G_0(Z(t,0)) + \int_0^{t_w} Y(t')G_\rho(Z(t,t'))dt', \tag{47}$$

where, using Eq. (27)

$$Z(t,t') = (t-t_w)\exp(\gamma_0^2/2x) + (t_w-t'). \tag{48}$$

On the other hand, in the linear regime we have

$$G(t-t_w,t_w,\gamma_0 \to 0) \equiv G(t-t_w,t_w)$$

$$= G_0[(t-t_w)+(t_w-0)] + \int_0^{t_w} Y(t')G_\rho[(t-t_w)+(t_w-t')]dt'. \tag{49}$$

Direct comparison of Eqs. (47) and (49) reveals that

$$G(t-t_w,t_w;\gamma_0) = G[(t-t_w)\exp(\gamma_0^2/2x),t_w]. \quad (50)$$

This result generalizes that of Sollich (1998) for the nonaging case ($x > 1$). It can be understood as follows. Within the SGR model, instantaneous response to a step strain at t_w is always elastic [that is, $G(0,t_w;\gamma_0) = 1$]; the fraction of stress remaining at time $t > t_w$ is the fraction of elements which have survived from t_w to t without yielding (see Sec. VI A 1). The stress decay is therefore determined entirely by the distribution of relaxation times in the system just after the strain is applied at time t_w. The effect of a finite strain is solely to modify the distribution of barrier heights, and hence to modify this distribution of relaxation times τ; in fact (within the model) nonlinear strain reduces the yield time of every element by an identical factor of $\exp(\gamma_0^2/2x)$ [Sollich (1998)]. Thus the relaxation after a nonlinear step strain at t_w is found from the linear case by rescaling the time interval $t-t_w$ using this same factor. Accordingly, the asymptotic results given for $G(t-t_w,t_w)$ in Table I can be converted to those for the nonlinear regime by replacing the time interval $t-t_w$ by a strain-enhanced value $(t-t_w)\exp(\gamma_0^2/2x)$, wherever it appears there.

2. Startup of steady shear

In Sec. VI A 3 we discussed the response to start up of steady shear (with $\dot{\gamma} \ll 1$) at time t_w; we assumed there that a linear response was maintained. Let us now consider the effect of strain-induced yield events, which cause nonlinearity. Consider first what happens for $x > 2$ (where the SGR model predicts Newtonian fluid behavior for $\dot{\gamma} \ll 1$). Here the main stress contribution is from elements which, were they unstrained, would have lifetime $\tau(E) = \exp(E/x)$ of order unity. So, if the strain rate obeys $\dot{\gamma} \ll 1$, these elements will acquire only negligible stress before they yield spontaneously. Hence their lifetimes are not affected by strain, and the stress response remains linear at all times, including the steady state limit: $\sigma(t \to \infty) \to \eta\dot{\gamma}$.

We therefore focus on the case $x < 2$, where nonlinearities do appear. The dominant stress contributions in this regime are from deep traps, i.e., elements with lifetimes of order t. Linearity applies only if such elements are unlikely to undergo strain-induced yielding before they yield spontaneously, after a time of order t. Such elements carry strains of order $\dot{\gamma}t$, which enhances their yield rate by a factor $\exp[(\dot{\gamma}t)^2/2x]$; we require that this is small, which holds only so long as $\dot{\gamma}t \ll 1$. Hence the predictions of the linear theory of Sec. VI A 3 can be maintained to arbitrarily long times only by taking the limit $\dot{\gamma} \to 0$ before one takes the steady state limit of $t \to \infty$. This means that the width of the linear response regime in steady flow is vanishingly small for $x < 2$, as previously discussed.

As mentioned in Sec. VI A 3 throughout the linear period the startup curve shows no strong aging or transient effects, even though the stress is evolving into deeper traps. At finite $\dot{\gamma}$, the linear period ends at $t \simeq \dot{\gamma}^{-1}$ (within logarithmic terms, discussed below); at later times, the main stress-bearing elements will, during their lifetimes, become strongly strained. Indeed, at strain rate $\dot{\gamma}$, an element with yield energy E will be strained to the top of its yield barrier in a time $t_{\rm int} \simeq E^{1/2}/\dot{\gamma} \simeq (\log\tau)^{1/2}/\dot{\gamma}$. The tendency of the stress distribution $s(\tau,t)$ [and also, for any $x < 1$, the lifetime distribution $P(\tau,t)$] to evolve toward deeper and deeper traps is thereby *interrupted*: the lifetime of a deep trap is converted from τ to a much smaller value, of order $(\log\tau)^{1/2}/\dot{\gamma}$ [Sollich *et al.* (1997); Sollich (1998)]. This truncation of the lifetime distribution is enough to ensure that these distributions are never dominated by the deep traps, and a steady state is recovered; accordingly, there are no aging effects at late enough times either.

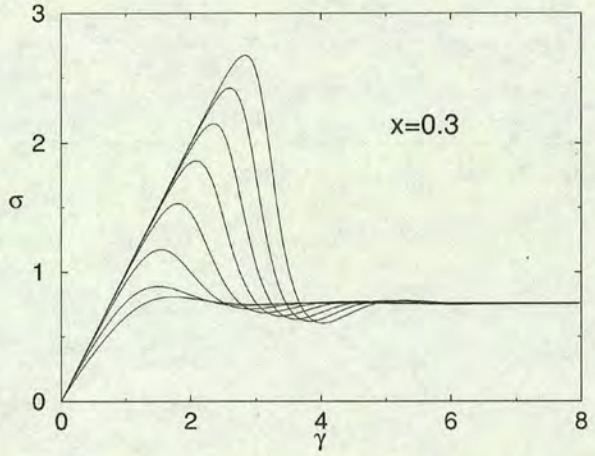

FIG. 9. Stress response σ, in shear startup, vs strain γ at noise temperature $x = 0.3$ and strain rate $\dot{\gamma} = 0.001$. Curves from bottom to top correspond to increasing ages $t_w = 10^2, 10^3 \ldots 10^9$ at time of startup.

Note, however, that the stress at the end of the linear regime can be higher than the steady state value, leading to an overshoot in the startup curve; see Sollich (1998). This overshoot region, unlike the two asymptotes, shows a significant dependence on the system age t_w, as shown in Fig. 9. The physics of this is clear: the extent of the linear regime gets progressively larger as t_w is increased, because the system has aged into deeper traps (and because the SGR model assumes that within each trap the relation between stress and strain is linear). Thus the strain at which strong yielding sets in increases (roughly logarithmically) with t_w; the height of the overshoot is accordingly increased before dropping onto the same, t_w-independent, steady-shear plateau.

VII. RHEOLOGICAL AGING: IMPOSED STRESS

We now analyze the SGR model's predictions for various stress-controlled rheological experiments. (We continue to assume the sample to have been prepared at time $t = 0$ by the idealized ''deep quench'' procedure defined in Sec. V A.) As previously remarked, the structure of the constitutive equations makes the analysis more difficult for imposed stress than for imposed strain. The following discussion is therefore largely based on our numerical results, with asymptotic analysis of a few limiting cases. Our numerical method is outlined in Appendix C 2.

A. Linear response

1. Step stress

The SGR model predicts that upon the application of a step stress there will be an instantaneously elastic response. Elements then progressively yield and reset their local stresses to zero; thus we must apply progressively more strain to maintain the macroscopic stress at a constant value. Strain thus increases with time, but at a rate that could tend to zero at long times. Potentially therefore, individual elements can acquire large local strains and, just as in the shear startup case, linearity of the response need not be maintained at late times. As we did for shear startup, we therefore first proceed by assuming that the response *is* linear; we find the corresponding $\gamma(t)$ and then (in Sec. VII B) consider *a posteriori* up to what time t the linear results remain valid.

TABLE III. Linear creep compliance in the SGR model at long and short times ($t-t_w \gg 1, t_w \gg 1$ assumed). $\Gamma(x)$ denotes the Gamma function, and $\psi(x) = \Gamma'(x)/\Gamma(x)$. The blank entries for $x < 1$ are explained in the text.

	$J(t-t_w,t_w)$ for $t-t_w \ll t_w$	$J(t-t_w,t_w)$ for $t-t_w \gg t_w$
$x > 2$	$\frac{x-2}{x-1}(t-t_w)$	$\frac{x-2}{x-1}(t-t_w)$
$1 < x < 2$	$\frac{(t-t_w)^{x-1}}{\Gamma^2(x)\Gamma(2-x)}$	$\frac{(t-t_w)^{x-1}}{\Gamma^2(x)\Gamma(2-x)-\Gamma(x)}$
$x = 1$	—	$\frac{3}{\pi^2}\ln^2(t-t_w)$
$x < 1$	—	$\frac{1}{\psi(1)-\psi(x)}\ln\left(\frac{t-t_w}{t_w}\right)$

In the linear regime the step stress response is described by the creep compliance $J(t-t_w,t_w)$ which was defined in Sec. II E. We computed this quantity numerically from the linearized form of the constitutive equation (34) for the SGR model, which for step stress may be written

$$1 = J(t-t_w,t_w) - \int_{t_w}^{t} J(t'-t_w,t_w)Y(t')G_\rho(t-t')dt'. \tag{51}$$

In analyzing our numerical results we first identify, as usual, regimes of short and long time interval between stress onset and measurement, $t-t_w \ll t_w$ and $t-t_w \gg t_w$, respectively. (We assume again that $t-t_w \gg 1$ and $t_w \gg 1$.) In these two regimes we find the time dependences summarized in Table III. For the long time interval regime ($t-t_w \gg t_w$), the results were in fact obtained as follows. Curves for $J(t-t_w,t_w)$ were first generated numerically; the observed scalings [for example, $J \sim (t-t_w)^{x-1}$ for $1 < x < 2$] were then taken as ansätze for analytic substitution into the constitutive equation (51). In each case this allowed us to confirm the given functional form, and to compute exactly the x-dependent prefactors shown. These prefactors were cross-checked by comparison with the numerical results; no discrepancies were found.

To obtain results for short time intervals, we proceeded by assuming that the resulting compliance $J(t-t_w,t_w)$ is the same as if we first let $t_w \to \infty$ [the dominant traps are in Boltzmann equilibrium; see Fig. 3(a)]; this limits the analysis to $x > 1$. (For $x < 1$, we find instead $J = 1 + \text{const} \times [(t-t_w)/t_w]^{1-x}$ at very early times; but this breaks down as soon as the second term becomes comparable to the leading, elastic, result.) The resulting prediction of $J(t-t_w,t_w \to \infty)$ was found analytically from $G(t-t_w,t_w \to \infty)$ and the reciprocal relations between the corresponding Fourier transforms (see Sec. II F above); these were again checked numerically.

Further insight into the results of Table III can be gained as follows. In step stress, we need to keep applying larger and larger strains because elements progressively yield and reset their local stresses to zero. To maintain constant stress, the rate at which stress increases due to straining (which in our units is just the strain rate $\dot{\gamma}$) must match the rate at which stress is lost, due to local yielding events. The latter defines a "stress-weighted hopping rate" $Y_s = \int \tau^{-1} s(\tau,t)d\tau$. For $x > 2$, Y_s remains a constant of order σ_0; stress remains in traps of lifetime $\tau = O(1)$ and the creep response is purely viscous. For

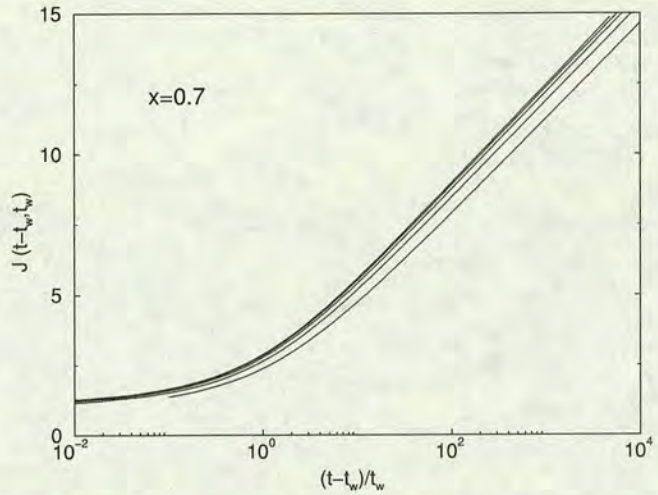

FIG. 10. Linear creep compliance $J(t-t_w,t_w)$ against scaled time interval $(t-t_w)/t_w$ for noise temperature $x = 0.7$. Curves from bottom to top correspond to increasing times $t_w = 10^2,10^3 \ldots 10^6$ of stress onset. Note the approach to a limiting scaling form as t_w becomes very large compared with the microscopic time $\tau_0 = 1$.

$x < 2$, however, Y_s decays as a power law of $(t-t_w)$; the stress distribution $s(\tau,t)$ is dominated at time t by traps with lifetimes τ of order $t-t_w$, the time interval since the stress application. [In fact, $Y_s \sim \dot{\gamma} \sim (t-t_w)^y$ where $y = x-2$ for $1 < x < 2$ and $y = -1$ for $x < 1$.]

For $1 < x < 2$, the scenario given above for the time dependence of Y_s is closely analogous to that given in Sec. V B above for the hopping rate $Y = \int \tau^{-1} P(\tau,t) d\tau$ in systems with $x < 1$. Indeed, the evolution of Y_s following a step stress, at noise temperature x, is closely related to that of Y, following a quench, at noise temperature $x-1$. [More generally one can show for the SGR model that, for an *equilibrium* system whose noise temperature is $x > 1$, the evolution of the stress distribution $s(\tau,t)$ following application of a step stress at $t = 0$ is, at long times, equivalent to that of the probability distribution $P(\tau,t)$, in a system deep-quenched to a noise temperature $x-1$ at $t = 0$. This result is connected with the discussion made in Sec. V C above, of the variation with x of the dynamics of successive moments of the lifetime distribution: at noise temperature $x+n$, the dynamics of the nth moment is like that of the zeroth moment at noise temperature x.]

The aging behavior of the linear creep compliance $J(t-t_w,t_w)$ shows significant differences from the step strain modulus $G(t-t_w,t_w)$ discussed in Sec. VI A 1. In the glass phase ($x < 1$), the strain response to step stress indeed depends on age: it is a function of $(t-t_w)/t_w$ as expected (see Fig. 10). However, the dependence (for long time intervals) is only logarithmic; $J(t-t_w,t_w) \sim \ln[(t-t_w)/t_w] = \ln(t-t_w) - \ln t_w$ (see Table III) which means that in the long time interval limit $(t-t_w \gg t_w)$ the explicit waiting time dependence $(\ln t_w)$ represents formally a "small" correction to the leading behavior $\ln(t-t_w)$. This relatively slight t_w dependence in creep measurements is intuitively reasonable: the strain response at time t to step stress is *not* determined purely by the relaxation spectrum at t_w (as was the case in step strain, Table I), but by the dynamics of the system over the entire interval between t_w and t. This decreases the sensitivity to the time t_w at which the perturbation was switched on. Similar remarks hold above the glass

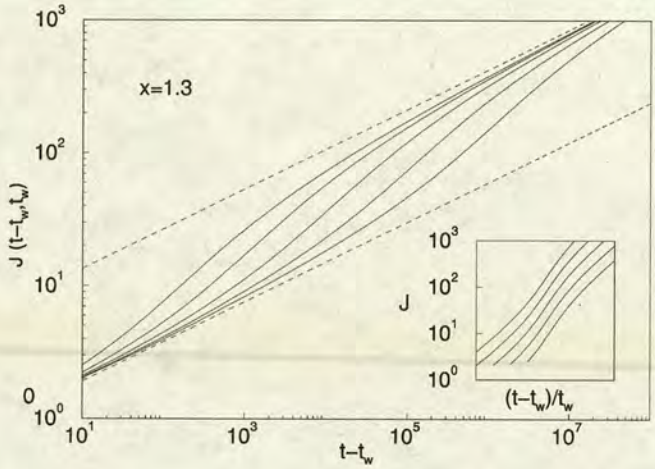

FIG. 11. Linear creep compliance $J(t-t_w,t_w)$ against time interval $t-t_w$ for noise temperature $x = 1.3$ for $t_w = 10^3,10^4 \ldots 10^7$ (solid lines, top to bottom). Lower dashed line: theoretical prediction for the short time regime $t-t_w \ll t_w$. Upper dashed line: asymptote for long time regime $t-t_w \gg t_w$. (Inset) same data plotted against scaled time $(t-t_w)/t_w$; the order of the curves is reversed.

point ($1 < x < 2$): in step strain, we found for $t-t_w \gg t_w$ a slow transient behavior which depended to leading order upon t_w (Table I). For step stress, however, the corresponding t_w dependence is demoted to lower order, and the late-time response is dominated by TTI terms. [We restate here why we call these effects for $x > 1$ transient behavior rather than aging. As explained after Eq. (19), a consistent definition of long term memory and aging for the step stress response function $J(t-t_w,t_w)$ requires a form of "regularization" by considering the material in question in parallel with a spring of infinitesimal modulus g. This effectively puts an upper limit of $J_{\max} = 1/g$ on the observable values of $J(t-t_w,t_w)$. Taking the limit $t_w \to \infty$ for $x > 1$ then results in a fully TTI step stress response, whatever the value of $J_{\max}$. On the other hand, for $x < 1$, the (albeit weak, logarithmic) t_w dependence of the response remains visible even for finite values of $J < J_{\max}$.] This is visible in Fig. 11. Note that short time and long time behaviors are each independent of t_w (as expected for $x > 1$), but that the crossover time between them scales with t_w (as shown in the inset).

2. Oscillatory stress

For the SGR model it was noted in Sec. VI A 2 that: (i) in the oscillatory stress response $G^*(\omega,t,t_s)$, the t_s dependence is negligible for low frequencies ($\omega \ll 1$) whenever $\omega(t-t_s) \gg 1$ and $\omega t_s \gg 1$; (ii) these conditions are satisfied in most conventional rheometrical measurements of the viscoelastic spectrum, where an oscillatory strain is maintained for many cycles; and (iii) perhaps surprisingly, these facts are true even in the glass phase, $x \leqslant 1$, of the SGR model. We also noted that, because response to oscillatory strain is dominated by memory of the few most recent cycles (over which the system has barely aged), $G^*(\omega,t)$ is the Fourier transform (with respect to the time interval Δt) of the step strain response function $G(\Delta t,t)$ that would be measured if a step strain were applied immediately after the oscillatory measurement had been done; see Eq. (45).

We have confirmed numerically that similar remarks apply to the oscillatory stress response function $J^*(\omega,t,t_s)$. (Although unsurprising, this does require explicit confir-

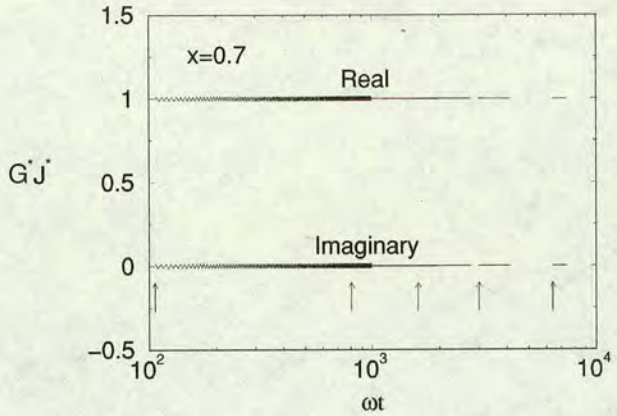

FIG. 12. Real and imaginary parts of the product $G^*(\omega,t)J^*(\omega,t)$ vs ωt at noise temperature $x = 0.7$ and frequency $\omega = 0.01$. The usual reciprocity relation between G^* and J^* is seen to hold to within about 1%. Shown are the results of several runs, each over a different time window. A vertical arrow marks the horizontal coordinate of the start of each data set. In each run shearing was commenced 20 cycles before the start of data output, to ensure that $\omega(t-t_s) \gg 1$ (necessary for t_s independence). The oscillatory deviations, visible for the leftmost data set, arise because the other condition for t_s independence ($\omega t_s \gg 1$) is only just satisfied.

mation since, for example, the transient effects from switching on the perturbation could be different in the two cases.) This was defined in Sec. II F 2 as the strain response, measured at t, to an oscillatory stress initiated at time t_s. Memory of the startup time t_s is indeed small in $J^*(\omega,t,t_s)$ so long as $\omega(t-t_s) \gg 1, \omega t_s \gg 1$ (and $\omega \ll 1$). It appears that, just as in the case of a strain controlled experiment, strain response to oscillatory stress is dominated by memory to the most recent cycles, over which the system has barely aged. We may therefore suppress the t_s parameter, defining a compliance spectrum at time t by $J^*(\omega,t)$. Furthermore, $J^*(\omega,t)$ is found numerically to be the reciprocal of $G^*(\omega,t)$,

$$J^*(\omega,t)G^*(\omega,t) = 1 \tag{52}$$

just as it is (without the t argument) in normal TTI systems. The numerical confirmation of this result is presented in Fig. 12. We emphasize that this result, like the previous one, has been confirmed here specifically for the SGR model; but it may hold more widely for systems with weak long term memory (see Sec. III).

B. Nonlinear response

1. Step stress

In Sec. VII A 1 we argued that a step stress, $\sigma(t) = \sigma_0\Theta(t-t_w)$, of size $\sigma_0 \ll 1$, induces a strain response $\gamma(t)$ which increases over time, but remains linear in σ_0 for at least as long as the linearized constitutive equations predict $\gamma(t) \ll 1$. This is because $\gamma(t)$ provides an upper bound on the local strain of each element. Although sufficient to ensure linearity, this is not always necessary; we require only that the characteristic strain *of those elements which dominate the stress* is small. For $x > 2$ (the Newtonian regime) the dominant elements have lifetimes $O(1)$ and so the response is linear to indefinite times so long as $\sigma_0 \ll 1$ [ensuring $\dot{\gamma}(t) \ll 1$ for all times t]. But, whenever $x < 2$, the linear analysis of Sec. VII A 1 indicates the dominant elements have lifetimes of order $t-t_w$; so a self-consistently linear response is maintained only provided that

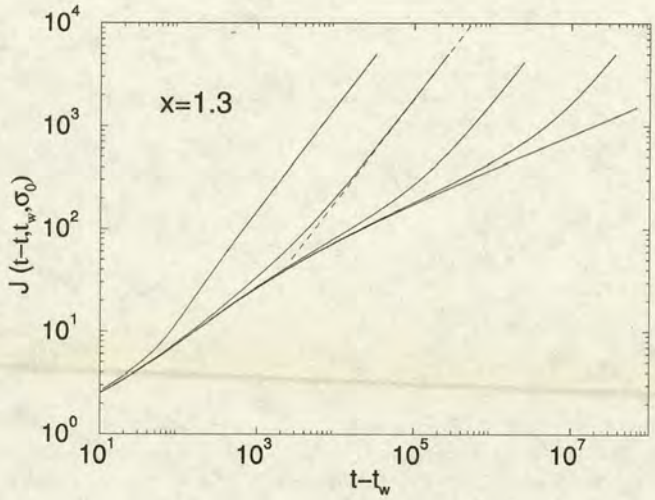

FIG. 13. Nonlinear creep compliance $J(t-t_w,t_w,\sigma_0)$ as a function of time interval $t-t_w$, for a step stress of size σ_0 applied at time $t_w = 100$. The noise temperature is $x = 1.3$. Solid lines, bottom to top: $\sigma_0 = 10^{-3},10^{-2.5},10^{-2},10^{-1.5},10^{-1}$. Over the time intervals shown, the curve for $\sigma_0 = 10^{-3}$ is indistinguishable from the linear compliance (not shown). Dotted line: final flow behavior predicted from steady state flow curve for $\sigma_0 = 10^{-1.5}$.

$\dot{\gamma}(t)(t-t_w) \ll 1$, just as in startup of steady shear (see Sec. VI B 2; here we make the additional assumption that $\dot{\gamma}$ only changes negligibly between t_w and t). Using the forms for $J(t-t_w,t_w)$ as summarized in Table III, we then find that for $1 < x < 2$ the strain response to step stress remains linear only for as long as $t-t_w \ll (1/\sigma_0)^{1/(x-1)}$. Beyond this time we expect strain-induced yielding to become important.

To confirm the predicted linearity at short times, and to extract the long time nonlinear behavior, we numerically solved the nonlinear constitutive equations (25), (26) by an iterative method (see Appendix C 2); this was done first for $1 < x < 2$ (Fig. 13). The results show a linear regime of the expected temporal extent, followed by a crossover into a nonlinear steady-state flow regime, in which $\gamma(t) \propto \sigma_0^{1/(x-1)}t$. The latter is in agreement with the flow curve, Eq. (36).

The same numerical procedure was then used for the glass phase, $x < 1$, for which the flow curve shows a finite yield stress, $\sigma_y(x)$. As expected, the numerical results for step stress of very small amplitude $\sigma_0 \ll \sigma_y$ show no crossover to a steady flow regime at late times. Instead, the system continues to creep logarithmically, according to the linear creep result (Table III)

$$\gamma(t) = \sigma_0 J(t-t_w,t_w) = \sigma_0 \frac{1}{\psi(1)-\psi(x)} \log\left(\frac{t-t_w}{t_w}\right). \tag{53}$$

The resulting value of $\dot{\gamma}(t)(t-t_w)$ never becomes large; so this is self-consistent. Next we studied numerically the case where σ_0 was not small but remained less than the yield stress σ_y. For stresses not too close to the yield stress, we found that the creep was still logarithmic to a good approximation, but now with a nonlinear dependence of its amplitude on stress: $\gamma(t) \approx \sigma_0 A(\sigma_0) J(t-t_w,t_w)$. The prefactor $A(\sigma_0)$ increases rapidly as σ_0 approaches the yield stress σ_y from below. Very close to the yield stress, the creep ceases to be logarithmic; $\gamma(t)$ then grows more quickly, but with a strain rate that still decreases to zero at long times. On the basis of these observations, we suspect that for a

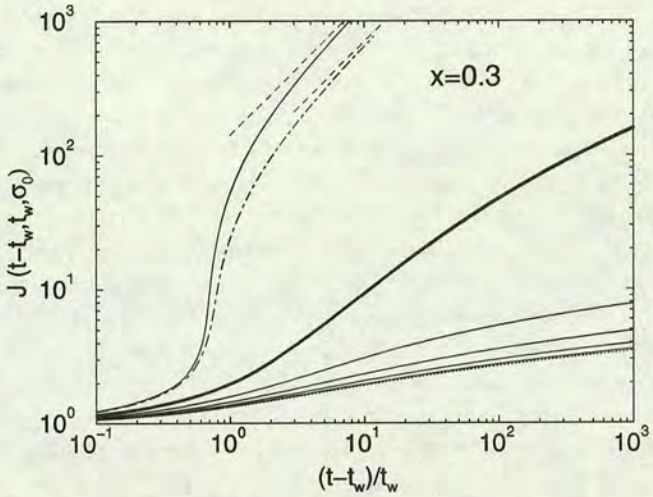

FIG. 14. Nonlinear creep compliance $J(t-t_w, t_w; \sigma_0)$ as a function of scaled time interval $(t-t_w)/t_w$, for a step stress of size σ_0 applied at time t_w. The noise temperature is $x = 0.3$. Solid curves, bottom to top: $\sigma_0/\sigma_y = 0.2, 0.4, \ldots, 1.2$, all for $t_w = 100$. The case $\sigma_0 = \sigma_y$ is shown in bold; the dotted curve is the linear response result ($\sigma_0 \to 0$). The dot-dashed curve shows the effect of decreasing the waiting time to $t_w = 50$, for $\sigma_0/\sigma_y = 1.2$. The dashed lines are the predictions for final flow behavior (for the stress above yield) from the steady state flow curve.

given stress σ_0 the creep will be logarithmic for short times (where "short times" might mean the whole time window which is accessible numerically), but will gradually deviate from this for longer times. The deviation is expected to be noticeable sooner for stress values closer to yield. We attempted to verify this conjecture numerically, but were unable to access a large enough range of values of $\ln[(t-t_w)/t_w]$ to do so. Note that, for any $\sigma_0 < \sigma_y$, the system ages indefinitely, and there is no approach to a regime of steady flow.

Finally, as expected from the flow curve, only for stress amplitudes exceeding the yield stress σ_y (which of course depends on x) did we see an eventual crossover from logarithmic creep to steady flow at long times; when that happened, we recovered numerically the flow-curve result, $\gamma(t) \propto (\sigma_0 - \sigma_y)^{1/(1-x)}(t-t_w)$. Figure 14 shows examples of our numerical results that illustrate the various features of nonlinear creep in the glass phase mentioned above. (Note that whereas for most other shear scenarios we chose to present glass phase results for a noise temperature $x = 0.7$, we here took $x = 0.3$. The yield stress is larger at this value of x, giving us a larger window $0 < \sigma_0 < \sigma_y$ over which we see aging and creep uninterrupted by a crossover into flow.) Comparison of the curves for the two different waiting times for $\sigma_0/\sigma_y = 1.2$ shows that before the crossover into flow, the response scales with $(t-t_w)/t_w$; once ergodicity has been restored and the system flows, on the other hand, scaling with $t-t_w$ is recovered.

VIII. CONCLUSION

In this paper we studied theoretically the role of aging in the rheology of soft materials. We first provided, in Sec. II a general formulation of the linear and nonlinear rheological response functions suited to samples that show aging, in which time translation invariance of material properties is lost. [Our analysis extends and, we hope, clarifies

that of Struik (1978).] This was followed in Sec. III by a review of the concept of aging, formally defined by the presence of long term memory, which can be either weak or strong. We suggested that for many rheological applications the main interest is in systems with weak long term memory: these have properties that are age dependent, but not influenced by perturbations of finite duration that occurred in the distant past. We conjectured that weak long term memory is sufficient to cause the age-dependent linear viscoelastic modulus to become independent of the start time t_s of the oscillatory shear $[G^*(\omega,t,t_s) \rightarrow G^*(\omega,t)]$ while retaining a dependence on system age t; for it to then obey the usual Fourier relation with the linear step strain response (likewise dependent on age t_w); and for it to obey a reciprocal relation $G^*(\omega,t)J^*(\omega,t) = 1$ with the time-varying compliance, similarly defined. Pending a general proof of these conjectures, all such relationships between age-dependent rheological quantities do however require empirical verification for each experimental system, or theoretical model, that one studies.

Within this conceptual framework, we then explored rheological aging effects in detail for the SGR model. After reviewing the basic rheological definition of the model in Sec. IV, we discussed in Sec. V its aging properties from the point of view of the mean jump rate $Y(t)$ whose behavior is radically different in the glass phase (noise temperature $x < 1$) from that in the normal phase ($x > 1$). The glass phase of the SGR model is characterized by "weak ergodicity breaking," which means that the elastic elements that it describes evolve forever towards higher yield thresholds (deeper traps), causing a progression toward more elastic and less lossy behavior. Within the glass phase, there is a yield stress σ_y, and for applied stresses less than this, genuine aging effects arise. These phemonena were explored in depth in Secs. VI and VII for the cases of imposed stress and imposed strain respectively. Aging effects are distinguished from otherwise similar transient phenomena (arising, for example, when $x > 1$) by the criterion that a significant part of the stress relaxation, following infinitesimal step strain, occurs on timescales that diverge with the age of the system at the time of strain application. This rheological definition appears appropriate for most soft materials and follows closely the definition of long-term memory in other areas of physics [Cugliandolo and Kurchan (1995); Bouchaud *et al.* (1998); Cugliandolo and Kurchan (1993)].

In the glass phase of the SGR model, the nature of the aging is relatively simple; for a step strain or stress applied at time t_w, both the linear stress relaxation function $G(t-t_w,t)$ and the linear creep compliance $J(t-t_w,t_w)$ become functions of the scaled time interval $(t-t_w)/t_w$ only. This scaling is a simple example of the time waiting–time superposition principle postulated empirically by Struik (1978) (in the somewhat different context of glassy polymers). The time-dependent viscoelastic spectra $G'(\omega,t)$ and $G''(\omega,t)$ have the characteristic aging behavior shown in Fig. 1: a loss modulus that rises as frequency is *lowered*, but falls with age t, in such a way that it always remains less than $G'(\omega,t)$ (which is almost constant by comparison). For $x < 1$ such spectra collapse to a single curve (see Fig. 8) if ωt, rather than ω, is used as the independent variable. Note that in more complicated systems, Eq. (20) may be required instead, to describe aging on various timescales that show different divergences with the sample age t_w. [Even in simple materials, there may be an additional nonaging contribution to the stress relaxation which the SGR model does not have; this will also interfere with the scaling collapse of both $G(t-t_w,t_w)$ and $G^*(\omega,t)$.] We found that, in its glass phase, the SGR model has weak long term memory, and we confirmed numerically that the conjectured relationships, Eqs. (12), (13), and (14), among age-dependent linear rheological quantities indeed hold in this case.

Significant aging was also found for nonlinear rheological responses of the SGR model. For example the nonlinear step-strain relaxation follows the same aging scenario as the linear one, except that all relaxation rates are speeded up by a single strain-dependent factor [Eq. (50)]. This form of nonlinearity is a characteristic simplification of the SGR model, and would break down if the elastic elements in the model were not perfectly Hookean between yield events. Another interesting case was startup of steady shear; here there is no significant aging in either the initial (elastic) or the ultimate (steady flow) regime; yet, as shown in Fig. 9, the intermediate region shows an overshoot that is dependent on sample age. For an old sample, the elastic elements have higher yield thresholds. The elastic regime therefore extends further before the imposed strain finally causes yielding, followed by a larger drop onto the same steady-shear plateau. The plateau itself is age-independent: the presence of a finite steady flow rate, but not of a finite stress, is always enough to interrupt the aging process within the SGR model. Finally we found that the nonlinear creep compliance (Fig. 14), shows interesting dependence on both the stress level and the age of the sample; for small stresses we found logarithmic creep (for all $x < 1$), crossing over, as the yield stress is approached, to a more rapid creep that nonetheless appears to have zero strain rate in the long time limit. Nonlinear creep gives challenging computational problems in the SGR model, which is otherwise simple enough, as we have shown, that almost all its properties can be calculated either by direct asymptotic analysis or using (relatively) standard numerics. Remaining drawbacks include (from a phenomenological viewpoint) the lack of tensorial elasticity in the model and (from a fundamental one) uncertainty as to the proper physical interpretation, if one indeed exists, of the noise temperature x [Sollich *et al.* (1997); Sollich (1998)].

Though obviously oversimplified, the SGR model as explored in this paper may provide a valuable paradigm for the experimental and theoretical study of rheological aging phenomena in soft solids. More generally, the conceptual framework we have presented, which closely follows that developed to study aging in nonflowing systems such as spin glasses, should facilitate a quantitative analysis of rheological aging phenomena across a wide range of soft materials.

APPENDIX A. CALCULATION OF LINEAR RESPONSE PROPERTIES

1. Initial condition

In discussing the SGR model's nonequilibrium behavior (Secs. VI and VII) we considered for definiteness a system prepared by a quench from an infinite noise temperature (see Sec. V A), i.e., with an initial distribution $P_0(E) = \rho(E)$ of yield energies or trap depths. For our predictions to be easily compared to experimental data, however, they must be largely independent of the details of sample preparation. To test for such independence, we consider the extent to which our results would change if the pre-quench temperature, which we denote by x_0, were finite. This corresponds to an initial trap depth distribution

$$P_0(E) \propto \exp(E/x_0)\rho(E). \tag{A1}$$

In this Appendix, we restrict ourselves to the linear response regime, where the effects of finite x_0 (if any) are expected to be most pronounced; nonlinearity tends to eliminate memory effects. The same is true for high temperatures, and correspondingly we will find that the influence of x_0 on our results is confined mainly to final (postquench) temperatures x within the glass phase ($x < 1$).

2. Yield rate

The yield or hopping rate is the basic quantity from which other linear response properties can be derived; see Eqs. (39), (42), and (51). It can be calculated from the second constitutive equation (26)

$$1 = G_0(t) + \int_0^t Y(t')G_\rho(t-t')dt', \tag{A2}$$

where we have replaced $Z(t,t')$ by $t-t'$, as is appropriate in the linear response regime. The function $G_0(t)$ is defined in Eq. (28); for the initial condition, Eq. (A1), it is related to G_ρ via

$$G_0(t) = G_\rho(t,y), \quad y = x(1-1/x_0),$$

where we have now included explicitly the noise temperature argument (y) in the argument list of G_ρ. Substituting this into Eq. (A2), and taking Laplace transforms with λ as our reciprocal time variable, we get

$$\frac{1}{\lambda} = \bar{G}_\rho(\lambda,y) + \bar{Y}(\lambda)\bar{G}_\rho(\lambda,x), \tag{A3}$$

and hence

$$\bar{Y}(\lambda) = \frac{\frac{1}{\lambda} - \bar{G}_\rho(\lambda,y)}{\bar{G}_\rho(\lambda,x)}, \tag{A4}$$

in which [taking Laplace transforms of Eq. (28)]

$$\bar{G}_\rho(\lambda,x) = x\int_1^\infty \frac{\tau^{-x-1}}{\lambda+\tau^{-1}}d\tau = x\int_1^\infty \frac{\tau^{-x}}{1+\lambda\tau}d\tau. \tag{A5}$$

In its present form, Eq. (A4) cannot be inverted analytically. We will focus on the long time regime, however, where progress can be made by using an alternative expression for $\bar{G}_\rho$. From Eq. (A5), $\bar{G}_\rho(\lambda,x)$ has poles at $\lambda = -\tau^{-1}$. Because of the integration over all $\tau = 1...\infty$, these poles combine into a branch cut singularity on the (negative) real axis between $\lambda = -1$ and $\lambda = 0$. We will now derive an expression for $\bar{G}_\rho$ that is valid near this branch cut. This expression does introduce spurious singularities on the negative real axis for $\lambda < 1$. But after inversion of the Laplace transform these only give contributions to $G_\rho(t)$ decaying exponentially or faster in t; they can therefore be ignored in the long-time limit. We first write Eq. (A5) as

$$\frac{1}{x}\bar{G}_\rho(\lambda,x) = \int_0^\infty \frac{\tau^{-x}}{1+\lambda\tau}d\tau - \int_0^1 \frac{\tau^{-x}}{1+\lambda\tau}d\tau. \tag{A6}$$

After the rescaling $\lambda\tau \to \tau$, the first term becomes a representation of the beta function. [The rescaling can be carried out only when λ is real and positive. But by analytic continuation, the result, Eq. (A7) also holds for complex λ outside the branch cut of λ^{x-1}, i.e., everywhere except on the negative real axis.] In the second term, because now $\tau \leq 1$, we can expand the denominator into a series that is convergent for $|\lambda| < 1$. This gives the desired expression

$$\bar{G}_\rho(\lambda,x) = a(x)\lambda^{x-1} + \sum_{n=0}^{\infty} b_n(x)\lambda^n, \tag{A7}$$

in which

$$a(x) = x\Gamma(x)\Gamma(1-x), \quad b_n(x) = \frac{x(-1)^{n+1}}{n+1-x}. \tag{A8}$$

This is valid for $|\lambda| < 1$ and therefore in particular near the branch cut $\lambda = -1...0$; in the representation, Eq. (A7), this branch cut is apparent in the fractional power of λ in the first term. The above derivation applies a priori only for $x < 1$, because otherwise the integrals in Eq. (A6) diverge at the lower end. However, using the relation

$$\frac{1}{x+1}\bar{G}_\rho(\lambda,x+1) = \frac{1}{x} - \frac{\lambda}{x}\bar{G}_\rho(\lambda,x),$$

which follows directly from Eq. (A5), it can easily be shown that Eq. (A7) holds for all x. (For integer x, there are separate singularities in the first and second term of Eq. (A7), but these just cancel each other.)

We can now substitute Eqs. (A7) and (A8) into Eq. (A4) and expand the denominator to find a readily invertible expression for $\bar{Y}(\lambda)$. Clearly the manner in which we perform the expansion depends on whether $x > 1$ or $x < 1$. Abbreviating $a(x) = a$, $a(y) = a'$, and $b_n(x) = b_n$, we have for $x > 1$:

$$\bar{Y}(\lambda) = \frac{1}{\lambda}\left[\frac{1}{b_0} - \frac{a}{b_0^2}\lambda^{x-1} - \frac{a'}{b_0}\lambda^y + O(\lambda^{2(x-1)},\lambda^{y+x-1},\lambda,...)\right],$$

which, upon inversion of the Laplace transform, gives

$$Y(t) = \frac{1}{b_0} - \frac{1}{\Gamma(2-x)}\frac{a}{b_0^2}t^{1-x} - \frac{1}{\Gamma(1-y)}\frac{a'}{b_0}t^{-y} + O(t^{2(1-x)},t^{1-x-y},...), \tag{A9}$$

the first term of which is the asymptotic expression for $Y(t)$ above the glass point, as in Eq. (37). For $x < 1$ on the other hand, we have

$$\bar{Y}(\lambda) = \frac{1}{\lambda}\left[\frac{\lambda^{1-x}}{a} - \frac{b_0\lambda^{2(1-x)}}{a^2} - \frac{a'}{a}\lambda^{y+1-x} + O(\lambda^{3(1-x)},\lambda^{y+2(1-x)},...)\right], \tag{A10}$$

which can be inverted to give

$$Y(t) = \frac{1}{\Gamma(x)}\frac{t^{x-1}}{a} - \frac{1}{\Gamma[1+2(x-1)]}\frac{b_0 t^{2(x-1)}}{a^2} - \frac{a'}{a\Gamma(x-y)}t^{x-1-y} + O(t^{3(x-1)},t^{2(x-1)-y},...) \tag{A11}$$

the first term again being in agreement with Eq. (37). Finally, to obtain $Y(t)$ *at* the glass point $x = 1$ we rewrite Eq. (A10) as

$$\bar{Y}(\lambda) = -\frac{1}{b_0\lambda}\left[\sum_{n=1}^{p} z^n(\lambda) + O(\lambda^y,\lambda,\lambda^{(p+1)(1-x)}...)\right]$$

in which $z(\lambda) = -b_0\lambda^{1-x}/a$ and p is the largest integer which is less than $1/(1-x)$. Inversion of the Laplace transform gives

$$Y(t) = \frac{-1}{b_0} \sum_{n=1}^{p} \frac{z^n(t)}{\Gamma[1+n(x-1)]} + O(t^{-y}, t^{(p+1)(x-1)}, \ldots)$$

in which $z(t) = -b_0 t^{x-1}/a$. The gamma function can now be expanded around $\Delta = 1-x = 0$; the sum over p can be performed explicitly for each term in this expansion. Retaining only the dominant terms for small Δ, and also taking the limit $\Delta \to 0$ of the quantities $z(t)$, a and b_0, one finds eventually

$$\lim_{x \to 1} Y(t) = \frac{1}{\ln(t)} + \frac{\Gamma'(1)}{\ln^2(t)} + O\left(\frac{1}{\ln^3(t)}\right)$$

as stated in Eq. (37).

Consider now the effect of the prequench temperature x_0 on the above results for the asymptotic behavior of the hopping rate $Y(t)$. We note first that all the leading terms are independent of y and hence of x_0. For $x > 1$, the largest y-dependent subleading term (t^{-y}) in Eq. (A9) becomes more important for smaller prequench temperatures x_0. However, provided we restrict ourselves to the regime $x_0 > x$ (i.e., to a nonequilibrium situation in which a quench is actually performed; $x = x_0$ corresponds to equilibrium conditions), we see that $y > x-1$ and that, even to subleading order, $Y(t)$ is independent of x_0. (We note furthermore that in the case of the deep quench defined in Sec. V A, $y = x$ and the term t^{-y} is very small.) For $x < 1$, in Eq. (A11), the relative importance of the largest y-dependent term (t^{x-1-y}) again depends upon the relative values of the pre- and postquench temperatures. For a high enough prequench temperature [specifically, provided $y > 1-x$, i.e., provided $x_0 > x/(2x-1)$] the leading and subleading terms of $Y(t)$ are independent of x_0. For any postquench temperature $x < 1/2$, the subleading term necessarily depends upon x_0 since the condition defined above for independence cannot be satisfied. Intuitively this is physically reasonable, since in general we expect a system at a lower temperature to remember its initial condition more strongly.

3. Step strain and oscillatory strain response

Once the yield rate $Y(t)$ is known, the linear stress response $G(t-t_w, t_w)$ to a step strain can be calculated from Eq. (39). To get its asymptotic behavior for $t-t_w \gg 1$, $t_w \gg 1$, the two regimes in which the time interval $t-t_w$ is much less and much greater than the age at the time of stress application t_w have to be considered separately. In the first regime ($t-t_w \ll t_w$), one can Taylor expand the hopping rate Y around its value at time t. In the second regime, we rewrite Eq. (39) as

$$G(t-t_w, t_w) = G_0(t) + \int_0^{t_w} Y(t') G_p(t-t') dt'. \tag{A12}$$

The first term on the right-hand side can then be shown to be subdominant (at least for $x_0 \to \infty$; see Appendix A 4), and the second can be treated by expanding $G_p(t-t')$ around $t' = 0$. To leading order, one then finds the results in Table I. The asymptotic behavior of the stress response to oscillatory strain, $G^*(\omega, t, t_s)$, is obtained in a similar manner from Eq. (42).

4. Rheological irrelevance of initial condition

In Appendix A 2 we discussed the influence of the initial state of the sample, as parameterized by the "prequench" temperature x_0, on the yield rate $Y(t)$. Now we consider the effects of x_0 on the various (linear) rheological observables, concentrating on the regime $x < 1$ where such effects are expected to be most pronounced. We begin with the response to a step strain, $G(t-t_w,t_w)$. In the short time regime $t-t_w \ll t_w$, it follows directly from Eq. (39) that x_0 affects only subdominant terms [through its effect on $Y(t)$]. In the long time regime $t-t_w \gg t_w$, we see similarly from Eq. (A12) that any effect on the leading behavior can only be through the first term on the right-hand side, $G_0(t) = G_\rho(t,y) \sim t^{-y}$. Comparing this with the second term, which from Table I is of order $(t_w/t)^x$ (note that $t \approx t-t_w$ in the long time regime), and using $y = x(1-1/x_0)$, one finds that the effect of x_0 is negligible up to $t \approx t_w^{x_0}$. For larger t, $G(t-t_w,t_w) \approx G_0(t) \approx G_0(t-t_w)$ and the response is TTI to leading order. An intuitive explanation for this behavior can be found by analyzing the evolution of the relaxation time distribution $P(\tau,t_w)$ with t_w. It can be shown that the initial condition $P(\tau,0)$ is remembered in the long time tail of this distribution, $\tau \gg t_w^{x_0}$. For times $t \gg t_w^{x_0}$, these long relaxation times dominate the behavior of $G(t-t_w,t_w)$ and cause the observed x_0-dependence.

For the step stress response $J(t-t_w,t_w)$, we found in Sec. VII A 1 that memory effects are rather weaker than for the step strain response. This is because J is sensitive to the average behavior of the relaxation time distribution $P(\tau,t')$ over the time interval $t' = t_w \ldots t$, while G depends on $P(\tau,t_w)$ only. Correspondingly, we also find that $J(t-t_w,t_w)$ is affected only weakly by the initial preparation of the system and hence by x_0. All effects are in subdominant terms; for the long time behavior in the glass phase, for example, one finds that the asymptotic behavior $J(t-t_w,t_w) \sim \ln[(t-t_w)/t_w]$ is only changed by an x_0-dependent constant offset.

Finally, consider the oscillatory response functions $G^*(\omega,t,t_s)$ and $J(\omega,t,t_s)$. Any linear oscillatory perturbation effectively probes only those traps which have a relaxation time $\tau < 1/\omega$. Provided such traps have attained an x_0-independent distribution by the time the perturbation is switched on at t_s, $G^*(\omega,t,t_s)$ and $J^*(\omega,t,t_s)$ will be insensitive to x_0. It can be shown that the requirement for this is $\tau \ll t_s^{x0}$ for all $\tau < 1/\omega$ and hence $\omega t_s^{x0} \gg 1$. We argue in Appendix B, however, that in order to get a sensible measurement of G^* (and J^*) which is independent of *start time* t_s, we must ensure $\omega t_s \gg 1$. This condition then automatically guarantees that the results are independent of x_0.

In summary, the only significant effects of the initial sample preparation appear in the step strain response at long times ($t \gg t_w^{x0}$). In the other linear response properties that we studied, the initial condition only affects subdominant terms. We reiterate our earlier statement that for nonlinear response, the initial sample condition should be even less important, because nonlinearities tend to wipe out memory effects. Finally, we mention the work of Kob and Barrat (1997), who investigated the effects of pre-quench temperature in a Lennard-Jones glass using computer simulations. They rationalized their data by the hypothesis that different prequench temperatures introduce different offsets in the effective age of the sample. Since these offsets are finite, this suggests asymptotic behavior for large t_w which is independent of pre-quench temperature, in qualitative agreement with our findings for the SGR model.

APPENDIX B. IRRELEVANCE OF SWITCH-ON TIME IN THE GLASS PHASE

It was stated in Sec. VI A 2 that $G^*(\omega,t,t_s)$ does not depend on t_s so long as $\omega(t-t_s) \gg 1$ and $\omega t_s \gg 1$. These criteria do not depend on the noise temperature x, and therefore hold even in the glass phase, $x \leqslant 1$, where aging occurs.

This behavior can be understood as follows. Consider a material which has not been strained since preparation except during a time window of duration t^* before the present time t. First write the linearized constitutive equation as

$$\sigma(t) = -\int_{t-t^*}^{t} \gamma(t') \frac{dG(t-t',t')}{dt'} dt', \tag{B1}$$

where for the SGR model

$$\frac{dG(t-t',t')}{dt'} = -\delta(t-t') + Y(t')G_\rho(t-t') \tag{B2}$$

with $G_\rho(t-t') \sim (t-t')^{-x}$. This result follows by differentiation of Eq. (39), respecting the fact that $G(t-t_w,t_w)$ vanishes for negative $t-t_w$ [that is, it contains a factor $\Theta(t-t_w)$ which is conventionally suppressed].

Now consider the case of a step strain imposed at $t-t^*$, so that $\gamma(t)$ is constant in Eq. (B1). Because dG/dt' contains a contribution of order $(t-t')^{-x}$, the integral has significant contributions from t' near $t-t^*$ whenever $x \leqslant 1$; in fact in the absence of the factor $Y(t')$ the integral would not even converge to a finite limit as t^* becomes large. This is a signature of long-term memory: Even the strain history in the distant past has an effect on the stress at time t. On the other hand, for an oscillatory strain (likewise switched on at $t-t^*$) one has Eq. (B1) with $\gamma(t) = \gamma_0 e^{i\omega t}$, and even without the factor $Y(t')$ the integral would now converge to a finite limit so long as ωt^* is large. The convergence of the oscillatory integral follows from the mathematical result known as Jordan's lemma [Copson (1962)] which, crudely speaking, states that inserting the oscillatory factor $e^{i\omega t'}$ has a similar effect to converting the integrand dG/dt' to $\omega d^2G/dt'^2$. (Physically, this extra time derivative arises since the stress at t due to any previously executed strain cycle must involve the change in dG/dt' over the cycle: if this change is small, the response to positive and negative strains will cancel.) Accounting for this extra time derivative, it is simple to check that the most recently executed strain cycles indeed dominate the response at time t, in contrast to the nonoscillatory case where the entire strain history contributes.

This observation allows us to simplify Eq. (B1) further by setting $G(\Delta t,t') \rightarrow G(\Delta t,t)$ where $\Delta t = t-t'$ (we assume $\omega t \gg 1$, so that the variation in the stress response function over a fixed number of recent cycles is negligible). Likewise, the limit of integration can safely be set to $\Delta t = \infty$. Thus we have

$$G^*(\omega,t) = \int_0^\infty e^{-i\omega\Delta t} \frac{dG(\Delta t,t)}{d\Delta t} d\Delta t. \tag{B3}$$

This can be integrated by parts to give Eq. (45) as required.

APPENDIX C. NUMERICAL METHODS

1. Yield rate in the linear regime

To obtain numerical results for the linear response properties of the SGR model, the yield rate $Y(t)$ has to be calculated first. A convenient starting point for this can be obtained by differentiating Eq. (A2)

$$Y(t) = -G_0'(t) - \int_0^t Y(t')G_\rho'(t-t')\,dt'. \tag{C1}$$

This is a Volterra integral equation of the second kind, which can in principle be solved by standard numerical algorithms [Press *et al.* (1992)]. Such algorithms are based on discretizing the time domain into a grid $t_0 = 0, t_1 \ldots t_n$; the values $Y_n = Y(t_n)$ are then calculated successively, starting from the known value of Y_0. The subtlety in our case is the choice of the grid: Because for times $t \gg 1$ we expect the hopping rate to be a power law, we expect relative discretization errors given a time step Δt to scale as $\Delta t/t_n$. Once we have chosen an acceptable (constant) value for the discretization error we are therefore at liberty to increase the time step Δt linearly with the time t_n, which corresponds to using a geometric time grid. This allows us to generate data over many decades without too much computational effort. To improve accuracy, we also used a spline interpolation between the known points $(t_0, Y_0), (t_1, Y_1) \ldots (t_{n-1}, Y_{n-1})$ when determining the next value Y_n.

2. Strain response to finite step stress

The numerical scheme used to solve Eqs. (25) and (26) in the case of an imposed step stress $\sigma(t) = \sigma_0 \Theta(t - t_w)$ is rather more complicated. This is because both the strain and the hopping rate, which are coupled through nonlinear integral equations, have to be calculated as functions of time. Again, we discretize time into a grid $t_0, t_1 \ldots t_n$, where $t_0 = t_w^+$, and proceed along the grid calculating the strain γ_n and the hopping rate Y_n for successive values of the index n. [Note that the integral form of the constitutive equations renders the strain and the hopping rate at any time step t_n dependent upon the values of these quantities at all previous times-even times prior to stress application ($0 < t' < t_w$). However, for such times the strain is clearly zero and the hopping rate is identical to that in the linear response regime, calculated previously.] The first data point $\gamma_0 = \gamma(t_w^+)$ and $Y_0 = Y(t_w^+)$ on this grid is obtained directly by treating the discontinuity at t_w "by hand." At any subsequent time step the two nonlinear constitutive equations (25) and (26) are solved simultaneously. The first is essentially of the form:

$$0 = f(\gamma_n, Y_n, \{\gamma_{n'}\}, \{Y_{n'}\}, t_w, \sigma_0) \quad \text{for} \quad 0 \leq n' < n, \tag{C2}$$

while the second can be differentiated and rearranged to give

$$Y_n = g(\gamma_n, \{\gamma_{n'}\}, \{Y_{n'}\}, t_w, \sigma_0) \quad \text{for } 0 \leq n' < n. \tag{C3}$$

Because Eq. (C2) cannot be solved explicitly for γ_n, we use an iterative process. At each time-step we start by placing sensible upper and lower bounds on γ_n, derived from physical expectations about the time dependence of the strain $\gamma(t)$. Each bound in turn is substituted into Eq. (C3) (to find the corresponding value of Y_n) and (with its Y_n) into the function f of the right hand side of Eq. (C2). The secant method [Press *et al.* (1992)] is then used to update one of the bounds, and the new bound used to calculate a new Y_n

and f. This process is repeated until we obtain a sufficiently small value of f ($|f| < 10^{-8}$). The current values of γ_n and Y_n are then accepted and we proceed to the next time step.

We initially chose a geometric grid of time values $t_0, t_1 \ldots$, but this led to numerical instabilities. We therefore switched to an adaptive procedure which chooses time-steps such that the strain always increases by approximately the same amount in a given time step.

Finally, note that at each iteration loop of each time step we in principle need to evaluate double integrals of the form $I = \int_0^t h[Z(t,t')]dt'$ in which

$$Z(t,t') = \int_{t'}^{t} dt'' \exp\{[\gamma(t'') - \gamma(t')]^2/2x\}. \tag{C4}$$

Because this is very costly computationally, we first calculate at each loop $Z(t,t')$ on a grid of t' values ranging from 0 to t and set up an interpolation over the calculated points. We are then left with single integrals of the same form as I, and look up the value of Z whenever the integrand is called.

References

Barnes, H. A., J. F. Hutton, and K. Walters, *An Introduction to Rheology* (Elsevier, Amsterdam, 1989).

Bernstein, B., E. A. Kearsley, and L. J. Zapas, "A study of stress relaxation with finite strain," Trans. Soc. Rheol. **7**, 391–410 (1963).

Bouchaud, J. P., "Weak ergodicity breaking and aging in disordered-systems," J. Phys. I **2**, 1705–1713 (1992).

Bouchaud, J. P., L. F. Cugliandolo, J. Kurchan, and M. Mézard, "Out of equilibrium dynamics in spin-glasses and other glassy systems," in *Spin Glasses and Random Fields*, edited by A. P. Young (World Scientific, Singapore, 1998).

Bouchaud, J. P. and D. S. Dean, "Aging on Parisi's tree," J. Phys. I **5**, 265–286 (1995).

Cates, M. E. and S. J. Candau, "Statics and dynamics of wormlike surfactant micelles," J. Phys.: Condens. Matter **2**, 6869–6892 (1990).

Copson, E. T., *An Introduction to the Theory of Functions of a Complex Variable* (Oxford University Press, New York, 1962).

Cugliandolo, L. F. and J. Kurchan, "Analytical solution of the off-equilibrium dynamics of a long-range spin-glass model," Phys. Rev. Lett. **71**, 173–176 (1993).

Cugliandolo, L. F. and J. Kurchan, "On the out-of-equilibrium relaxation of the Sherrington-Kirkpatrick model," J. Phys. A **27**, 5749–5772 (1994).

Cugliandolo, L. F. and J. Kurchan, "Weak ergodicity breaking in mean-field spin-glass models," Philos. Mag. B **71**, 501–514 (1995).

Cugliandolo, L. F., J. Kurchan, P. LeDoussal, and L. Peliti, "Glassy behaviour in disordered systems with nonrelaxational dynamics," Phys. Rev. Lett. **78**, 350–353 (1997a).

Cugliandolo, L. F., J. Kurchan, and L. Peliti, "Energy flow, partial equilibration, and effective temperatures in systems with slow dynamics," Phys. Rev. E **55**, 3898–3914 (1997b).

Dickinson, E., *An Introduction to Food Colloids* (Oxford University Press, Oxford, 1992).

Doi, M. and S. F. Edwards, *The Theory of Polymer Dynamics* (Clarendon, Oxford, 1986).

Evans, R. M. L., M. E. Cates, and P. Sollich, "Diffusion and rheology in a model of glassy materials," Eur. Phys. J. B **10**, 705–718 (1999).

Gardon, R. and O. S. Narayanaswamy, "Stress and volume relaxation in annealing flat glass," J. Am. Ceram. Soc. **53**, 380–385 (1970).

Hodge, I. M., "Physical aging in polymer glasses," Science **267**, 1945–1947 (1995).

Hoffmann, H. and A. Rauscher, "Aggregating systems with a yield stress value," Colloid Polym. Sci. **271**, 390–395 (1993).

Holdsworth, S. D., "Rheological models used for the prediction of the flow properties of food products," Trans. Inst. Chem. Eng. **71**, 139–179 (1993).

Hopkins, L. L., "Stress relaxation or creep of linear viscoelastic substances under varying temperature," J. Polym. Sci. **28**, 631–633 (1958).

Ketz, R. J., R. K. Prudhomme, and W. W. Graessley, "Rheology of concentrated microgel solutions," Rheol. Acta **27**, 531–539 (1988).

Khan, S. A., C. A. Schnepper, and R. C. Armstrong, "Foam rheology. 3: Measurement of shear-flow properties," J. Rheol. **32**, 69–92 (1988).

Kob, W. and J. L. Barrat, "Aging effects in a Lennard-Jones glass," Phys. Rev. Lett. **78**, 4581–4584 (1997).

Kossuth, M. B., D. C. Morse, and F. S. Bates, "Viscoelastic behavior of cubic phases in block copolymer melts," J. Rheol. **43**, 167–196 (1999).

Kurchan, J., "Rheology, and how to stop aging," Preprint cond-mat/9812347 (1998); Proceedings of *Jamming and Rheology: Constrained Dynamics on Microscopic and Macroscopic Scales*, workshop at ITP, Santa Barbara, 1997 (to be published).

Larson, R. G., *The Structure and Rheology of Complex Fluids* (Oxford University Press, Oxford, 1999).

Mackley, M. R., R. T. J. Marshall, J. B. A. F Smeulders, and F. D. Zhao, "The rheological characterization of polymeric and colloidal fluids," Chem. Eng. Sci. **49**, 2551–2565 (1994).

Mason, T. G. and D. A. Weitz, "Linear viscoelasticity of colloidal hard-sphere suspensions near the glass-transition," Phys. Rev. Lett. **75**, 2770–2773 (1995).

Mason, T. G., J. Bibette, and D. A. Weitz, "Elasticity of compressed emulsions," Phys. Rev. Lett. **75**, 2051–2054 (1995).

Monthus, C. and J. P. Bouchaud, "Models of traps and glass phenomenology," J. Phys. A **29**, 3847–3869 (1996).

Narayanaswamy, O. S., "Model of structural relaxation in a glass," J. Am. Ceram. Soc. **54**, 491–498 (1971).

Odagaki, T., "Glass-transition singularities," Phys. Rev. Lett. **75**, 3701–3704 (1995).

Panizza, P., D. Roux, V. Vuillaume, C. Y. D. Lu, and M. E. Cates, "Viscoelasticity of the onion phase," Langmuir **12**, 248–252 (1996).

Press, W. H., S. A. Teukolsky, W. T. Vetterling, and B. P. Flannery, *Numerical Recipes in C*, 2nd ed. (Cambridge University Press, Cambridge, 1992).

Scherer, G. W., *Relaxation in Glass and Composites* (Wiley, New York, 1986).

Sollich, P., "Rheological constitutive equation for a model of soft glassy materials," Phys. Rev. E **58**, 738–759 (1998).

Sollich, P., F. Lequeux, P. Hébraud, and M. E. Cates, "Rheology of soft glassy materials," Phys. Rev. Lett. **78**, 2020–2023 (1997).

Struik, L. C. E., *Physical Aging in Amorphous Polymers and Other Materials* (Elsevier, Houston, 1978).